**Eunice Margarida Santos Costa**

Licenciada em Engenharia Biológica

# Bioactive Beads for Local Sensing of Proteases in 3D Engineered Tissues

Dissertação para obtenção do Grau de Doutor em
Bioengenharia (MIT)

Orientador: Profª Doutora Ana Isabel Nobre Martins Aguiar Oliveira Ricardo
Co-orientador: Profª Doutora Paula Theresa Hammond
Profª Doutora Linda G. Griffith

FACULDADE DE CIÊNCIAS E TECNOLOGIA
UNIVERSIDADE NOVA DE LISBOA

**Setembro de 2011**

*To my sister Ana Lúcia*

# Acknowledgments

The conclusion of such an adventure would only be possible with the guidance, support, encouragement and friendship of so many wonderful people that I had the pleasure to share these last 4 years with. First of all I want to say a sincere and wholehearted thank you to my advisors, for trusting me with a challenging, exciting and so diverse project. To Ana Isabel for opening the doors to the exciting and special world of supercritical fluids. Indeed it is a very special lab, like no other I had seen before. She has always pushed me to excel, gave me the opportunity to pursuit my own ideas while critically questioning my hypothesis. Most of all, she champions her students like no other and is always supportive. To Paula for welcoming me at MIT, always with a comforting smile and a word of encouragement, even when the data looked puzzling! She is an inspiration in her ability to critically assess such diverse subjects, pointing new directions and opportunities, but above all in her constant positive attitude! To Linda, for her scientific excitement in the proteases project. Her enthusiasm was key on the last yards of the PhD marathon. It was great to feel I was part of a great scientific dream! Above all I have to thank you all for your kindness and for providing me with such an excellent learning experience.

I also want to thank Prof Manuel Nunes da Ponte. I remember very clearly my first contact with him as part of the MIT-Portugal Program interviewer's panel, since he was the one making the tough questions. Thank you for welcoming me on the program, for being our mentor at Bioengineering Systems and your constant support all the way through!

And to my colleagues for making the lab such an enjoyable place to work in! In the "Polymer Synthesis and Processing in supercritical $CO_2$" lab at FCT, I want to thank Teresa Casimiro for teaching me all about the supercritical fluids apparatus. For always being patient in guiding me through the process of learning with my mistakes and, most importantly, in calming me down when I needed the most! To Margarida Coelho: you were there when we needed to work side by side for long hours, you were my teacher in the spectral analysis and, most of all, a great friend that was always there to help me and give me energy! To Mara, Raquel, Rita, Telma, Vasco and Vanessa for being such great colleagues, always helpful and kind and even appreciative of my lab "dancing" moves. To Lígia and Márcio for being there when I first contacted with the supercritical fluids. Also at FCT, I want to thank Dona Idalina and Dona Conceição for their help. A huge thank you to the Hammond and Griffith labs at MIT, most especially the Proteases team: Abby, Caroline, Grinia and Megan! Caroline I do miss working together with you at the lab and I would have not reached thus far in the

project without your creativity, insight and hard work! You are a great friend that taught me the nuts and bolts of chemical synthesis. Go proteases! To Margaret, my UROP student, thanks for your hard work. Grinia thanks for teaching me different techniques and for speaking Portuguese (our secret language) with me. Miles and Rachel thank you for helping with the cell cultures. I also want to thank Anita, Edgar, Hsinhwa, Linda S., Matthew, Nate and Ta for your support and for making me feel welcome to the labs. And to Prof Beyong-Su for introducing me to the characterization techniques for LbL on particles.

I thank Prof Joaquim Sampaio Cabral and Prof Cláudia Lobato da Silva for allowing me to do the cytoxicity tests at their lab. I want to especially thank Prof Laura Ilharco for her hard work on the spectral analysis and kindness. Also to Prof Teresa Cidade for the rheology assays and overall insights.

I also want to acknowledge the funding from Fundação de Ciências e Tecnologia and the support of all the people that make the MIT-Portugal Program possible both in Portugal and at the MIT.

Finally, I want to thank the people outside the labs whose friendship and love were life-savers. To my parents for your unconditional love and support, and all the time spent on the phone that lighted up my days. To my beloved big brother Nuno, for simply knowing me better than anybody else on the planet! To Ana, for being the rock ‘n roll sister in law and at heart. To Xavier: it is nice to be back in Portugal to watch you grow. To mighty Kate, my dearest friend that always managed to bring out the best in people and from any new expedition. To Tushar, for our wholehearted conversations and all the new comedians I got to know. To my colleagues at the MIT-Portugal program for sharing the Cambridge adventure, especially Daniela for her friendship when most needed. To Miguel, for believing. To Daniel, for the flying pigs!

# Abstract

Metalloproteinases are endopeptidases involved in mediating interactions between cells and the extracellular microenvironment, being ascribed to several cellular processes and signaling events. The dysregulation of protease activity has been correlated with several diseased states, such as cancer and arthritis; hence metalloproteinases constitute potential therapeutic targets. However, these therapies have thus far shown little success due to an ill-defined knowledge of the complex regulatory network dictating protease activity. The availability of 3D *in vitro* tissues in which cells are able to closely recapitulate native physiological behavior, has been essential for studying tissue physiology and for drug development. Therefore, the design of real-time specific protease activity sensors amenable to 3D tissue constructs would be a valuable tool for understanding fundamental aspects of protease biology as well as monitor drug activity towards proteases. Herein, bio-friendly technologies were combined for the preparation of cell-interactive hydrogel particles functionalized with metalloproteinase fluorogenic sensors to monitor local protease activity in 3D cell cultures. Well-defined and cell-sized smart microgels were prepared by synthesis in supercritical carbon dioxide, a green chemistry approach that enables pure and biocompatible materials, without extensive purification steps. Further aqueous complexation of macromolecules or layer-by-layer assembly of polyelectrolytes was used for the preparation of cell-interactive coatings and for fine-tuning the microbeads physical properties of swelling, stimuli-responsive behavior and overall net charge; being a potential strategy to adjust microbead differential permeability to proteases and thus the sensing construct specificity. The impact of the macromolecules deposition on the smart microbeads behavior was assessed by FT-IR spectroscopy analysis. Finally, protease sensing function was conferred to the microbeads by complexation of a modified polymer or by directly tethering probes on the native microbead. The successful activation of the microbeads by a model protease constitutes a significant step towards the validation of this technological basis for preparing local protease probes for 3D engineered tissues.

**Keywords:** Layer-by-layer assembly of polyelectrolytes; Metalloproteinases; Poly(*N*-isopropylacrylamide); Microbeads; Supercritical carbon dioxide;

# Resumo

As metaloproteinases são endopeptidases envolvidas em vários processos celulares e de sinalização, que mediam a interacção entre células e a matriz extracelular envolvente. A desregulação da sua actividade está subjacente a várias doenças, tais como o cancro e artrites. Embora as metaloproteinases tenham sido propostas como alvos terapêuticos no tratamento destas patologias, ensaios clínicos não revelaram melhorias significativas dos pacientes, o que pode ser devido em parte ao desconhecimento de toda a complexidade de eventos regulatórios a que está submetida a actividade de proteases. O estudo de metaloproteinases em tecidos 3D *in vitro* poderá possibilitar uma forma fidedigna de responder a várias destas questões biológicas e de testar potenciais drogas, já que configurações de células em 3D mimetizam de forma mais semelhante o comportamento nativo de tecidos vivos. Para esse efeito, neste trabalho desenvolveram-se micropartículas para monitorizar *in situ* a actividade de proteases em tecidos 3D *in vitro*, recorrendo a tecnologias limpas que asseguram a obtenção de materiais puros e adequados ao contacto com culturas celulares. Inicialmente, sintetizaram-se microgéis inteligentes em dióxido de carbono supercrítico, com uma morfologia bem definida e tamanho semelhante ao de células animais. Posteriormente, as propriedades destas micropartículas em termos de conteúdo em água, capacidade de resposta a estímulos e carga foram sistematicamente modificadas por complexação de macromóleculas ou deposição camada-a-camada de polielectrólitos; esta deposição foi seguida por espectroscopia de infravermelhos. Estas estratégias podem possibilitar a formação de filmes adesivos para células e ao mesmo tempo o controlo do transporte de proteases através das partículas, importante para o controlo da especificidade do sensor. Finalmente, foram incorporados substratos fluorogénicos sintéticos nos microgéis por conjugação em polímeros complexados nas partículas ou directamente nas micropartículas. Estes sensores foram activados com sucesso por uma protease modelo, demonstrando o potencial desta plataforma tecnológica no desenvolvimento de sensores locais para tecidos celulares 3D.

**Palavras-chave:** Deposição camadas-a-camada de polielectrólitos; Metaloproteinases; Poli(*N*-isopropilacrilamida); Micropartículas; Dióxido de carbono supercrítico.

# List of Contents

# List of Figures

# List of Tables

# List of Abreviations

ADAM – A disintegrin

ATR – attenuated total reflectance

$\bar{d}$ – average diameter (sanple population mean)

Dabcyl – 4-(4-dimethylaminophenylazo)benzoic acid

DEGDMA – diethylene glycol dimethacrylate

DRIFT – diffuse reflectance infrared spectroscopy

DSC – differential scanning calorimetry

EDC – 1-1-ethyl-3-[3-dimethylaminopropyl]carbodiimide hydrochloride

FAM – 5(6)-carboxyfluorescein

FBS – Fetal Bovine Serum

FITC – fluorescein isothiocyanate

FRET – Förster resonance energy transfer

FT-IR – Fourier transform infrared spectroscopy

$G^*$ – dynamic complex modulus

$G'$ – dynamic storage modulus

$G''$ – dynamic loss modulus

GDMA – glycerol dimethacrylate

LbL – layer-by-layer

MBAm – *N,N'*-methylenebisacrylamide

MAA – methacrylic acid

Mal – maleimide

MMP – matrix metalloproteinase

MP – metalloproteinase

$M_w$ – molecular weight

MWCO – molecular weight cut-off

NIPAAm – *N*-isopropylacrylamide

PAA – poly(acrylic acid)

PAH – poly(allylamine hydrochloride)

PAH-RhoB – Rhodamine B-labeled poly(allylamine hydrochloride)

PBS – phosphate buffer saline (150 mM of salts)

PDAC – poly(diallyldimethylammonium chloride)

PE – polyelectrolyte

PEGa – poly(ethylene glycol) acrylate macromonomer

PLGA – poly(L-glutamic acid)

PLL – poly(L-lysine)

PNIPAAm – poly(*N*-isopropylacrylamide)

p(NIPAAm-co-MAA) – poly(*N*-isopropylacrylamide-co-methacrylic acid)

PNIPAAm-*g*-PEG – poly(*N*-isopropylacrylamide)-*graft*-poly(ethylene glycol)

PSS – poly(styrene sulfonate)

PZLL – poly(Z-L-lysine)

Q – volumetric swelling ratio

$R_g$ – radius of gyration (Å)

RhoB – Rhodamine B

RhoCOOH – carboxyrhodamine

*s* – sample standard deviation

$scCO_2$ – supercritical carbon dioxide

SCF – supercritical fluid

*SE* – sample standard error of the mean

SEM – Scanning Electron Microscopy

TA – tannic acid

$\xi$ – hydrogel mesh size

# CHAPTER 1:

# Introduction

# 1 Introduction

## 1.1 Aim of the Thesis

The PhD thesis focus on the development of cell-sized hydrogel microbeads with defined mechanical properties and cell-interactive surface properties, for monitoring cell secreted proteases in 3D tissue models, while providing physiological relevant local mechanics. Beads were prepared using a green chemistry synthesis approach that enables highly pure materials ideal for use in sensitive cell cultures. To detect local cell responses, different strategies were developed for the incorporation of fluorogenic proteases substrates into the beads. Layer-by-layer assembly of polymeric coatings on the hydrogel beads was proposed as a method to potentially render the beads cell-adhesive and create diffusion barriers to protease permeation in order to increase the sensitivity of the overall sensing construct. Finally, the applicability of the protease sensing construct in terms of reporter activation and microbead integration within 3D cell cultures was assessed. The specific goals of the thesis are described below.

### 1.1.1 Preparation of well-defined hydrogel beads

The first goal of the thesis is the preparation of hydrogel microbeads with well-defined physical properties, namely in terms of size and mechanical modulus. Tissue cells range in size from 8- 20 μm. In order to deploy a protease sensing bead in cell cultures, beads should be within this size range and as close to monodisperse as possible, so that interaction with cells is promoted and regular cell culture lab techniques can be used to monitor their activation, such as confocal microscopy or flow cytometry. As illustrated in Figure 1.1, it is anticipated that beads matching normal tissue compliance will result in physiological tissue function (e.g., in the case of liver, secretion of serum proteins), whereas beads that are relatively stiff will result in pathophysiological function, including abnormal cell morphology, cell proliferation, and loss of key physiological functions. Using mammary gland as a representative epithelial tissue, the target elastic modulus for the beads should be in the range 0.1-5 kPa.[1]

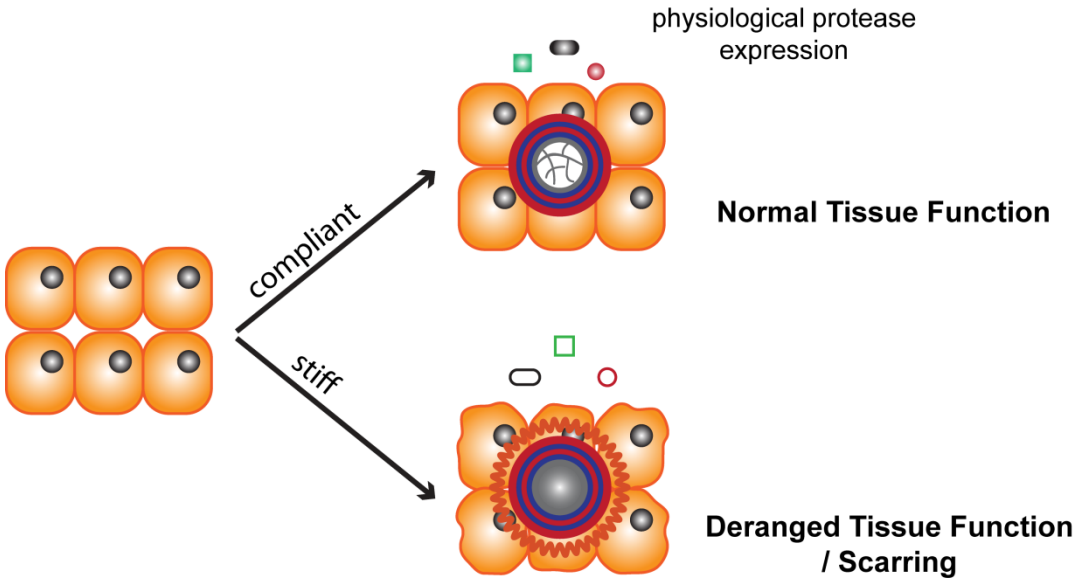


**Figure 1.1** Effect of the bead mechanical properties on the tissue behavior and protease secretion.

### 1.1.2 Tuning surface chemistry and permeability

For optimal activation of the sensing construct it is advantageous to promote a direct contact between the microbead and surrounding cells so that (i) secreted proteases are not diluted to the media and (ii) some level of spatial resolution of cell protease activity is obtained. Thus, the second goal of the thesis is to modify the surface chemistry of the hydrogel microbeads to promote cell interaction, through layer-by-layer assembly of polyelectrolytes, as shown in Figure 1.2. Polymers to be used in this project have been shown to facilitate protein adsorption and cell adhesion. In addition, multilayered films with different porosity, cross-linking and transport properties can be prepared by LbL, depending on the type of polyelectrolytes used and assembly conditions. Hence, this technique has the potential to create diffusion barriers for selective permeation of macromolecules such as proteases according to their size and charge, as outlined in Figure 1.3, being a possible strategy to tune the microbead sensitivity to a specific protease. During multilayers assembly on soft porous substrates, dynamic interactions are established between the coating and the hydrogel, being an atypical LbL system. It is anticipated that LbL will impact the hydrogel native properties, being a flexible approach to manipulate the overall construct performance.

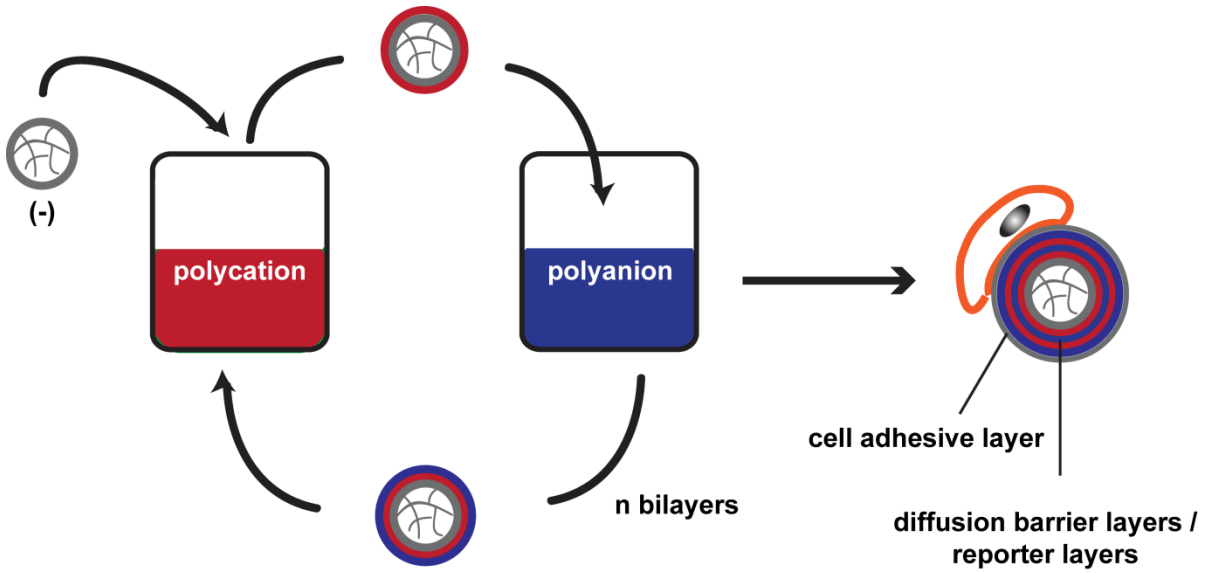


**Figure 1.2** Layer-by-layer assembly of polyelectrolytes as a method to tune microgel surface chemistry and create diffusion barriers to increase specificity for protease monitoring.

### 1.1.3 Incorporate a protease sensing function

The final goal of this project is to incorporate protease reactive moieties into the microbeads in order to monitor protease activity at a cellular level. Focus will be given to cell secreted proteases known to be differentially expressed in healthy or diseased tissues. There are several classes of such proteases, including matrix metalloproteinases which have been described as an interesting therapeutical target for the treatment of a vast array of diseases. Furthermore, fluorogenic synthetic substrates have been prepared for monitoring and imaging metalloproteinases activity. Herein, those substrates will be incorporated within the construct, so that the amount of substrate cleaved serves as a record of protease activity.

## 1.2. Matrix Metalloproteinases and the Cellular Microenvironment

Individual cells in tissue structures integrate many external cues arising from interactions with the surrounding microenvironment to maintain their basal phenotype and respond to changes in physiological conditions. Most cells require inputs from a truly 3D environment to recapitulate physiological or pathophysiological processes *in vitro*, which has sprung intense research on the development of synthetic biomaterials and scaffold fabrication techniques for preparing extracellular microenvironments that mimic the structural, mechanical, transport and regulatory characteristics of

natural extracellular matrices (ECM), both for therapeutic applications and fundamental biological studies.[2,3] The natural extracellular matrix comprises a scaffold of structural biomacromolecules, such as collagens and elastins, intertwined with proteoglycans (PGs), providing mechanical support and elasticity to tissues as well as resistance against compression forces. The overall ECM architecture, composition and cross-linking dictates not only the mechanical properties of the cellular microenvironment, but also several processes such as cell adhesion, migration, and matrix remodeling capability. Indeed, many growth and adhesion factors, chemokines and other signaling proteins are secreted in matrix-binding forms, and the ECM is involved in establishing local gradients of factors which are released upon proteolytic degradation.

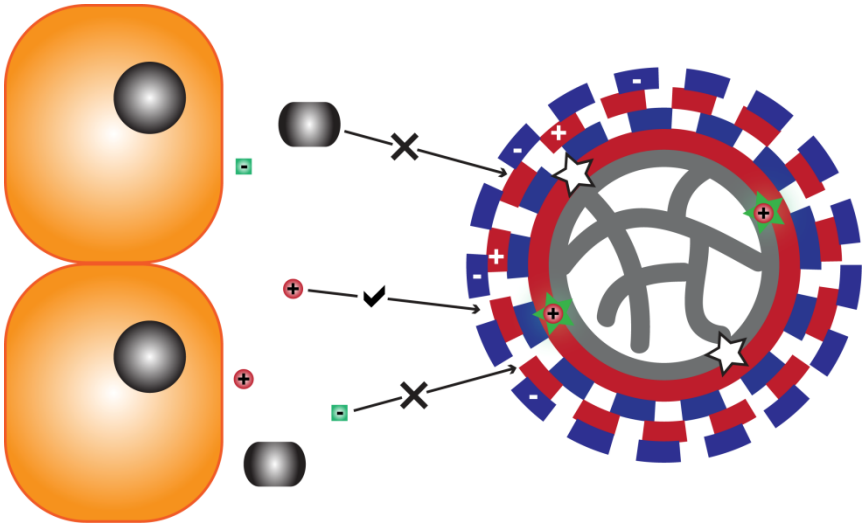

**Figure 1.3** Permeation selectivity of the LbL assembled films to protease charge and size. It is hypothesized that larger secreted proteases or with the same charge as the outermost layer do not permeate as much into the protease sensing construct, whereas smaller proteases with opposite charge can permeate and activate the protease sensing element.

Extracellular proteases are key regulators of tissue homeostasis.[4] The matrix metalloproteinases (MMPs), of which 23 have currently been identified in humans, are a family of structurally related zinc endopeptidases that require activation of their latent zymogen forms prior to exerting their enzymatic functions, generally near or at the cell surface.[5] MMPs exhibit varied substrate specificity, ranging from multiple ECM components, to signaling molecules (cytokines, chemokines, and growth factors), and adhesion molecules. The MMP family comprises the collagenases (MMP-1, 8 and 13) which degrade collagen, the stromelysins (MMP-3, 7, 10 and 11) which have a broad substrate specificity (PGs, laminin, fibronectin), the gelatinases (MMP-2 and 9) which degrade denaturated collagen, and the membrane-tethered MMPs, which activate other MMPs. MMPs and the closely related ADAM (A Disintegrin and Metalloproteinase) and ADAMTS (A Disintegrin and Metalloproteinase with ThromboSpondin motifs) proteases regulate a variety of physiological

processes and signaling events, being key players in the dynamic interplay between the cells and surrounding matrix. In fact metalloproteinases (MP) have been associated with cellular processes such as migration,[6] differentiation,[7] tissue remodeling,[8] inflammation,[9] wound healing,[10] angiogenesis[11] and morphogenesis.[1] In normal functioning tissues, a tight regulation of the MMPs activity is assured at multiple levels, including: (i) gene expression;[12] (ii) synthesis of inactive zymogen; (iii) compartmentalization; (iv) conversion of the pro-enzyme to the active form;[13] (v) presence of tissue inhibitors of MMPs (TIMP), which also regulate proteolytic activity of ADAMs; and (vi) mechanical load.[1,14] On the other hand, the dysregulation of the MPs activity has been associated with a wide range of pathologies, such as cancer[4] and tumor metastasis,[15] arthritis,[16] neurodegenerative diseases[17] or endometriosis.[18] Better understanding of the proteolytic activity profiles and regulatory networks at the cellular level would be of great importance for both fundamental biology studies and diagnosis and treatment of various diseases. However, for retrieving physiologically relevant information from *in vitro* models, sensing constructs amenable to incorporation in 3D engineered tissues need to be developed.

### 1.2.1. Therapeutic relevance of metalloproteinases

The association of MPs activity with several diseases has prompted researchers to consider MPs as targets for the diagnosis, prognosis and treatment of several diseases. In general, increased expression of proteinases occurs in tumors and other diseased tissues, but the particular circumstances is key, namely if endogenous inhibitors or activating enzymes are present. In cancer treatment, the first drug development approaches were based on the preparation of small-molecule MP inhibitors for blocking MMP-mediated angiogenesis and metastasis. The effects of these inhibitors in phase III clinical trials turned out to be disappointing as they failed to increase patient survival rates.[19] MPs are involved on the modulation of the tumor microenvironment at virtually every process: growth, survival, invasion, etc. However, MPs exhibit opposing effects on tumorigenesis with some MPs actively promoting it while others exhibiting protective action, or even acting independently of their proteolytic activity,[4,13] in a process-dependent way: MMP-3 exhibits activity against tumor cell survival while promoting establishment of metastatic niches in another phase of the disease. In arthritis, characterized by the progressive degradation of articular cartilage matrix components, while ADAMTS-4 (aggrecanase-1) and ADAMTS-5 (aggrecanase-2) proteolytic activity inhibition has been proposed as a therapeutical strategy for the disease treatment,[16] inhibiting MMP-3 actually exacerbates the disease rather than showing any chondroprotective effect.[20] In addition, inhibiting specific proteases activity may have potential side-effects, as the same MPs are expressed in different tissues and their biology has not been totally characterized. Indeed, the redundancy on the MPs activity makes the effort of unveiling a specific MP function quite challenging. Overall, the success of therapies targeting MPs has been

hindered by an ill-defined knowledge on the integrated actions of the several MPs engaged at different stages of the disease and on the complex regulatory networks determining protease activity. Studies on understanding these processes will hopefully lead to a more rational approach towards reducing or entirely alleviating the ill effects of MPs in diseased states while maintaining their necessary and beneficial functions.

### 1.2.2. Development of biosensors to monitor metalloproteinases: FRET probes

The availability of tools for determining protease activity in physiological relevant settings is crucial not only for understanding the fundamental MP biology but also to facilitate MP-targeting therapies optimization and monitoring.

Several methods are available to gather information on MPs biology and function under certain biological contexts. At the transcriptional level, DNA microarrays or real-time PCR can provide data on the expression patterns of MPs and inhibitors. A DNA microarray was indeed specifically developed for addressing the proteases transcriptome.[21] Other common methods used to assess protein function, such as ELISAs, western blotting, immunohystochemistry and genetic manipulation have been also used for determining the presence and relative levels of proteases.[21-23] However, these assays are limited in their ability to clearly distinguish active from inactive forms and do not take into account the post-translational modifications and regulatory mechanisms that actually dictate proteolytic activity. There are also available techniques based on the proteolytic cleavage of endogenous substrates to derive information on protease activity, namely mass spectrometry based methods[21] and zymography (electrophoretic separation of MPs in gels containing a proteolytic substrate such as gelatin).[24] But the variety of endogenous substrates that are cleaved by a certain MP[13], the context dependency of such cleavage,[25] and the partial overlapping of substrate specificity among closely related MPs hinders the interpretation and matching of the global substrate degradation to the activity of specific proteases.

In order to capture MPs spatial and temporal dynamics in a non-invasive manner, Förster Resonance Energy Transfer (FRET) synthetic polypeptide protease substrates have been extensively developed, allowing the assessment of MP activity by an increase in fluorescence upon hydrolysis.[26,27] These substrates typically consist of a fluorescent donor group and a quenching acceptor fluorophore that are separated by a 3-10 aminoacid residues containing a protease cleavage motif – Figure 1.4. Resonance energy transfer occurs when the donor and acceptor are within a specified distance estimated by the pair's Förster radius ($R_0$). Upon cleavage of the peptide linker, energy transfer is eliminated and fluorescence appears. For the design of a FRET activity probe, it is important to consider (i) a FRET pair with highly efficient energy transfer (donor with high quantum yield ($\Phi_F$) and acceptor that absorbs at the donor emission wavelength) and (ii) a specific protease cleavage motif. Fields recently

compiled a series of efficient fluorogenic substrates for MMPs and ADAMs monitoring, namely utilizing 5-carboxyfluorescein (FAM) as a fluorophore and 4-(4-dimethylaminophenylazo)benzoic acid (Dabcyl) as a quencher.[28]

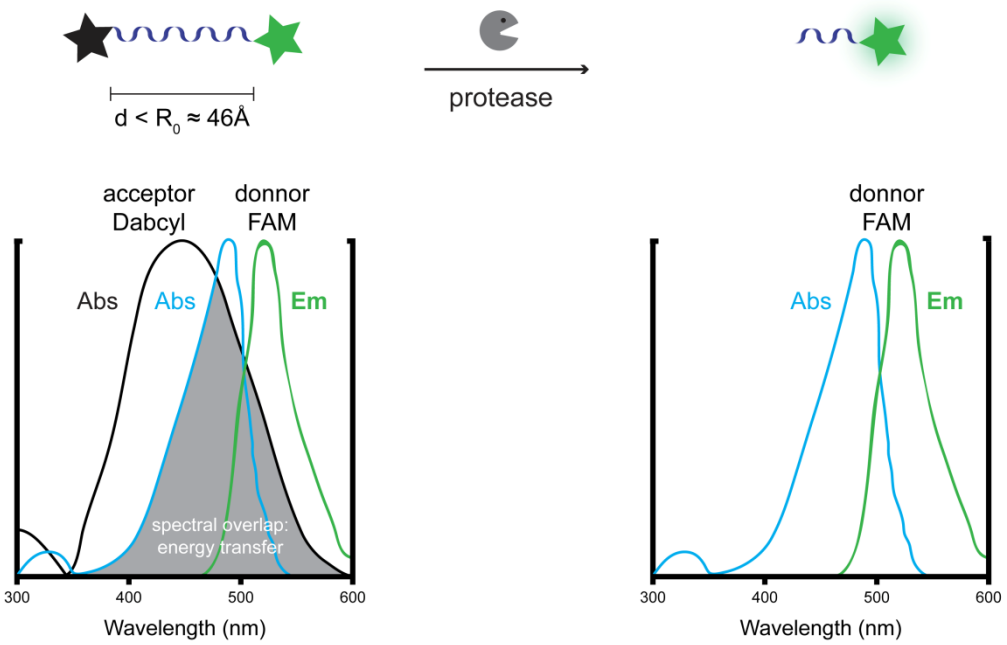


**Figure 1.4** Schematic representation of a FRET protease substrate before and after activation by enzymatic cleavage of the peptidic linker: 5-carboxyfluorescein as a FRET donor and Dabcyl as an acceptor (quencher).

Similarly to many endogenous substrates, MP FRET probes are generally cleaved by multiple proteases.[29] Improving the specificity of the substrate sequence has been performed using peptides based on protein sequences surrounding MPs cleavage sites,[30] synthetic peptide libraries,[31] and phage substrate-mapping experiments.[32] Combination of a number of protease substrates and inhibitors has also been deployed as a strategy to fingerprint specific protease activity, but cross-reactivity remains nonetheless problematic.[29,32] Nevertheless, these FRET-substrates have been successfully deployed *in vivo* for tumor detection and inhibitor efficacy assessment on MMP activity.[26,33] In addition, such probes have been incorporated in synthetic ECM networks to monitor MMP activity with cellular resolution during cell migration[6] or elastase activity in a biomimetic drug delivery platform.[34]

The secreted MMPs differ significantly among themselves in terms of molecular weight, size and charge in physiological conditions, as shown in the Table 1.1. Indeed these are the properties that dictate protease separation during analysis by zymography.[24] The approach proposed in this thesis would explore an increase in specificity of the existing fluorogenic substrates by using sieving strategies for selective proteases permeation, according to size and charge, prior to reaching the sensing moiety.

**Table 1.1** Physiochemical properties of some secreted matrix metalloproteinases.

| Protease | Type | Molecular Weight[30] | | Radius of Gyration ($R_g$; Å)[b] | pI[g] |
|---|---|---|---|---|---|
| | | precursor | active | | |
| MMP-1 | collagenase | 52,000; 56,000[a] | 41,000; 45,000[a] | 28.3[c, 35] | 6.5 |
| MMP-2 | gelatinase | 72,000 | 67,000 | 25.9[d, 36] | 5.3 |
| MMP-3 | stromelysin | 57,000; 59,000[a] | 28,000 - 45,000 | -[e] | 5.8 |
| MMP-7 | matrilysin | 28,000 | 19,000 | 15.1[c, 37] | 7.7 |
| MMP-8 | collagenase | 75,000[a] | 65,000[a] | -[e] | 6.4 |
| MMP-9 | gelatinase | 92,000[a] | 84,000[a] | 49.2[d, 38] | 5.7 |
| MMP-10 | stromelysin | 57,000 | 28,000 - 45,000 | -[e] | 5.9 |
| MMP-12 | metalloelastase | 53,000 | 22,000 - 45,000 | 26.0[c, 39] | 8.8 |
| MMP-13 | collagenase | 65,000 | 55,000 | -[e] | 5.3 |

[a] Glycosylated

[b] Radius of gyration was determined directly from the X-ray crystal structure of MMPs stored in the Protein Data Bank (http://www.pdb.org/pdb/home/home.do), using the following equation:

$$\boldsymbol{R_g}^2 = \frac{1}{n}\sum[(\boldsymbol{x_i} - \bar{\boldsymbol{x}}_n)^2 + (\boldsymbol{y_i} - \bar{\boldsymbol{y}}_n)^2 + (\boldsymbol{z_i} - \bar{\boldsymbol{z}}_n)^2] \quad \text{(Equation 1.1)}$$

in which $(x_i, y_i, z_i)$ refers to the spatial coordinates of each aminoacid residue and $(\bar{x}_n, \bar{y}_n, \bar{z}_n)$ refers to the average coordinates of all the residues.

[c] $R_g$ for the active form.

[d] $R_g$ for the precursor form.

[e] No crystal structure available for the uncomplexed complete MP.

[f] Basal isoelectric point (without modifications) from PhosphosSitePlus protein database: http://www.phosphosite.org/homeAction.do

## 1.3 Strategies for the Preparation of Hydrogel Microbeads

The development of biomaterials for biological applications has focused on promoting physiological interactions between the foreign material and cells. Although naturally-derived biomacromolecules, such as collagens, fibronectins, etc., have the intrinsic potential of closely mimicking the natural ECM surrounding cells, concerns regarding their immunogenicity hinder their applicability. As the gel-like character of most ECMs is one of its key features, researchers have proposed hydrogels as synthetic

mimics of the ECM and as backbones for scaffolds, drug carriers or sensors. Hydrogels are tri-dimensional cross-linked polymer networks, characterized by a high water content, potential biocompatibility and suitable mechanical properties.[3] Several synthesis and processing approaches and chemistries are currently available to enable biological characteristics to hydrogels, such as incorporation of cell-adhesion ligands,[40] proteolytic susceptibility recapitulating natural matrix remodeling[41] and biological relevant properties in terms of water content, mesh size and mechanical modulus.[42] In regards to the latter parameter, the precise modulation of the mechanical properties of the hydrogel is essential as each cell type is physiologically tuned to the mechanical properties of their matrix, with mammary epithelial cells growth, survival and morphogenesis favored by compliant matrices, while osteoblast differentiation and survival being optimal on matrices more similar to bone.[1] Furthermore, a seminal work by Engler *et al.* showed that mesenchemycal stem cell differentiation into the different lineages is to some extent dictated by substrate elasticity.[43] The synthetic hydrogels physical properties can be systematically varied through the choice of the polymers, the polymer fraction within the gel, the extent of cross-linking (either physical or chemical), and the experimental conditions under which the hydrogel is prepared.[42,44]

Hydrogel microparticles, also denominated as microgels,[45] are typically prepared by heterogeneous free-radical polymerization by dispersion, precipitation or emulsion polymerization.[46] If carried out carefully, narrow size distributions are possible to obtain following a polymerization strategy. However, for most monomers this approach involves the use of surfactants and also hazardous organic solvents during the reaction and subsequent purification steps, and extensive removal of contaminants and unreacted monomers needs to be performed to render pure materials. Alternative techniques such as photolitography or micromolding and microfluidics have also been proposed to fabricate microgels with a fine control over their aspect ratio, but they require costly equipment and yield very small amounts of microgels.[44,46] Hydrogel particles can also be formed by self-assembly of block copolymers, in which the shell and core chemistries and size are controlled by the copolymer composition and assembly conditions. In general, block copolymers are formed by the combination of a hydrophobic and a hydrophilic segment and therefore naturally form micelles in aqueous environment. In some cases, these micelles can be further cross-linked to form stable particles. Nevertheless, only particles in the nanometer range are obtained through this method.

In the thesis, a polymerization strategy is followed for the preparation of large hydrogel microbeads with a narrow size distribution and well-defined physical properties. A green chemistry approach, by synthesis in supercritical carbon dioxide, will lead to the facile preparation of the particles free from contaminants, being especially suitable for biological applications.

### 1.3.1 Preparation of microbeads in supercritical carbon dioxide

A supercritical fluid can be defined as any substance for which both the temperature and pressure are above the thermodynamical critical values[47] – Figure 1.5.

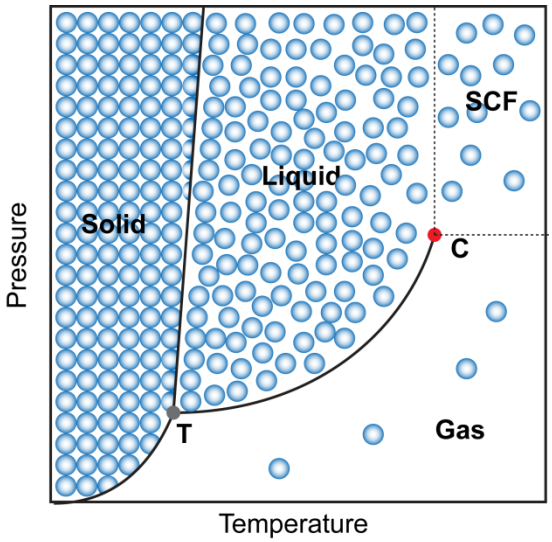


**Figure 1.5** Schematic pressure-temperature phase diagram for a pure component, highlighting the supercritical fluid (SCF) region, the triple point (T) and the critical point (C). The blue circles illustrate the fine tuning of the density at the SCF region, demonstrating a continuous variation from the liquid to the SCF phase if the liquid-gas equilibrium line is not crossed. Adapted from the literature.[47]

Above the critical point, a pure component exhibits properties that are to some degree in between those characteristic of a gas and a liquid, specifically liquid-like densities (0.3 – 1 g/cm$^3$) and gas-like diffusivities (0.01 – 0.1 mm$^2$/s) and viscosities (0.05 – 0.1 cP). In addition, supercritical fluids are highly compressible allowing the fine tuning of the density (thus their solvent power) by variations in pressure. From the accessible supercritical fluids, carbon dioxide has been the most widely explored fluid, as supercritical conditions are easily achieved ($T_c$ = 31.1 $^o$C; $P_c$ = 73.8 bar). Furthermore, it is considered a sustainable solvent, being relatively non-toxic, non-flammable, chemically inert, and naturally abundant. Since $CO_2$ is a gas at atmospheric pressure, it can be removed after processing simply by depressurization, yielding pure and dry products. The advantages of supercritical $CO_2$ ($scCO_2$) have been widely explored in applications particularly interesting for the biomedical field, such as preparation of porous scaffolds for cell culture/controlled-release of factors,[48-50] synthesis of polymers with well-defined architectures,[51,52] drug impregnation,[53] and particle design through synthesis[54-56] or polymer processing.[57]

While most non-polar small molecules are soluble in $CO_2$, polymers are in general poorly solubilized in $CO_2$ at accessible experimental conditions (T < 100 °C, P < 350 bar), with the exception of fluoropolymers or silicones; hence precipitating out of the supercritical phase at small conversions.[47] There are only limited reports on the preparation of hydrocarbon polymeric particles with controlled

morphology by precipitation polymerization in $CO_2$,[58] as this strategy could not be easily extended to other monomers. The exceptional solubility of fluorinated and siloxane compounds in $scCO_2$ prompted researchers to develop the first amphiphilic stabilizers for free-radical dispersion, and emulsion / suspension polymerizations, enabling the preparation of well-defined particles from a vast array of monomers in good yields.[54-56,59,60] These stabilizers are typically copolymers including a $CO_2$-philic moiety that extends to the $scCO_2$ continuous phase and a $CO_2$-phobic group with high affinity to the growing polymer chain.[60] A few examples on the preparation of polymeric particles in $scCO_2$ are shown in Table 1.2, in which it is also possible to infer that there are only few examples of monodisperse spherical polymeric particles above the micrometer range. The use of stabilizers to obtain improved molecular weights and yields, as well as some degree of control over particle morphology, has some considerable disadvantages. The majority of the stabilizers contain a hydrocarbon backbone, leading to its covalent binding or "entrapment" within the polymer, and contamination of the final product. Finally, the developed stabilizers are usually expensive, hindering the overall commercial application of polymerizations in $scCO_2$. However, a commercially available perfluoropolyether was shown to effectively stabilize methyl methacrylate (PMMA) and diethylene glycol dimethacrylate (DEGDMA) by reversible H-bonding interactions, providing a clean polymer synthesis route.[54,56,61] The use of this stabilizer for preparing microbeads becomes a reasonable strategy for applications with high added value, as in the biomedical field.

There are alternative strategies for the preparation of polymer microbeads, taking advantage of $scCO_2$ as a solvent, an anti-solvent or a polymer plasticizer. Briefly, for the limited range of $CO_2$-soluble polymers, particles may be created from an initial homogenous polymer solution in SCF (and possibly a co-solvent mixed) which is then rapidly expanded to form precipitated particles – a process called rapid expansion of a supercritical fluid (RESS).[68] In other techniques, SCF is used as an anti-solvent that causes precipitation of polymers initially dissolved in a liquid solvent, and thus can be applied for the micronization of a larger range of polymers. The gas or supercritical anti-solvent (GAS/SAS) process encompass the injection of $CO_2$ into an initially homogenous mixture, leading to polymer supersaturation and subsequent precipitation, while in aerosol solvent extraction system (ASES) or solution enhanced dispersion by supercritical fluids (SEDS), the polymer solution is sprayed into or co-injected with dense $CO_2$. A similar experimental set-up is used for particle formation from gas-saturated solutions (PGSS).[57] The solubility of compressed gases in polymers is usually quite high and thus dense or $scCO_2$ may be used as a plasticizer, by swelling and/or lowering the polymer melting temperature. Polymer melts can then be expanded through a nozzle leading to particle formation.
These described micronization techniques present several advantages interesting for biological applications, namely the possibility of processing a vast array of materials; a control over particle morphology and size by manipulation of the experimental conditions; preparation of composite particles by co-dissolution of drugs, dyes, etc.; processing of shear-sensitive compounds such as

proteins; and specifically for PGSS low processing temperatures, important for sensitive active moieties. However, in comparison with polymer strategies in $scCO_2$, obtaining truly monodisperse populations of particles with well-defined morphologies via $scCO_2$ assisted polymer micronization remains quite challenging.[57,68,69]

**Table 1.2** Microbeads prepared by polymerization in supercritical carbon dioxide: parameters shown for the best performing experimental conditions balancing morphology, size and yield.

| **Monomer** | **stabilizer** | **polymerization** | **yield (%)** | **size (μm)** | **morphology** | **reference** |
|---|---|---|---|---|---|---|
| acrylic acid | - | precipitation | 81 | 10 – 100 | spherical particles | 58 |
| *N*-isopropylacryl-amide | | | 90 | - | aggregated spherical particles | 62 |
| methyl methacrylate | poly(1,1-dihydroperfluorooctyl acrylate) (PFOA) | free-radical dispersion | 92 | 2.44 | monodispersed spherical particles | 63 |
| | perfluoropolyether (PFPE) | | >95 | 2.5 | monodispersed spherical particles | 54 |
| styrene | poly(styrene)-*b*-poly(dimethylsilo-xane) | | 96 | 0.85 | spherical particles | 64 |
| diethyleneglycol dimethacrylate | PFPE | | 90 | 1.73 | monodispersed spherical particles | 56 |
| glycidyl methacrylate | polystyrene-*b*-PFOA | | >90 | 0.28; 4.78 | monodispersed spherical particles | 59 |
| vinyl pyrrolidone | PFOA | | 82 | 1.00 | monodispersed spherical particles | 65 |
| *N*-ethylacrylamide | poly(3-*O*-methacryloyl-d-glucopyronose)-*b*-poly(1,1-dihydroperfluoro-octyl methacrylate) | emulsion $scCO_2/H_2O$ | 100 | 0.19 | monodispersed spherical particles | 66 |
| trimethylolpro-pane trimethacrylate | poly(vinyl alcohol) | suspension $scCO_2/H_2O$ | 90 | 114 | porous spherical particles | 67 |

### 1.3.2 Smart hydrogels: temperature and pH responsive

Stimuli-responsive hydrogels, have been subject of a lot research, due to the possibility of controlling their swelling by small changes in the surrounding environment; and thus have been proposed for a diverse range of applications, including drug delivery,[70,71] bioseparation,[72,73] sensors,[74-76] smart cell culture systems[77] and biocatalysis.[78] Different materials have been explored to render hydrogels responsive to temperature,[79] pH,[80] light,[81] electric field,[82] the presence of biomolecules[74] or other stimuli.[83]

Temperature-responsive hydrogels are the most commonly studied environmental-switchable soft materials. There is a variety of polymers with temperature-dependent phase transitions in aqueous solutions, being poly(*N*-isopropylacrylamide) (PNIPAAm) and poly(*N*,*N*-diethylacrylamide) (PDEAm) well-characterized examples,[84] as both exhibit a native low critical solution temperature (LCST) close to body temperature (25 – 32 °C). The nature of the thermo-responsive behavior arises from the balance between polymer-polymer, polymer-water and water-water interactions. It has been thoroughly described for PNIPAAm that below the LCST interactions between the amide group and surrounding water are thermodynamically more favorable; the polymer adopts a random coil conformation and is soluble. However, with increasing temperature, an entropy-driven weakening of the polymer hydration leads to the preferential establishment of polymer-polymer hydrophobic interactions, leading to the formation of a globular polymer conformation and subsequent phase separation.[79,85] For cross-linked polymeric networks, this thermodynamic behavior translates into the reversible swelling and collapse of the hydrogel with temperature, as illustrated in Figure 1.6.

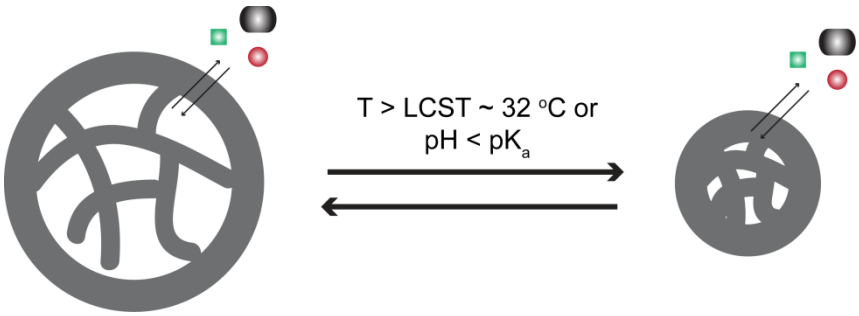


**Figure 1.6** Volume phase transition of a temperature and/or pH responsive polymer. Also illustrated is the impact of the hydrogel swelling on the permeation/release of other molecules.

Thermoresponsive polymers such as PNIPAAm can be further tuned in terms of their LCST behavior or environmental sensitivity by copolymerization with other monomers. It has been shown that incorporation of additional hydrophobic groups, as through copolymerization with butyl methacrylate, decreases the LCST, while copolymerization with hydrophilic monomers such as acrylamide results in polymers with higher LCST and increased swelling.[86] In addition, multi-sensitive systems can be created by copolymerization with other stimuli responsive moieties. Specifically, copolymers of

NIPAAm with polyacids, such as acrylic, methacrylic acid or valeric acid (AA, MAA, VA), exhibit a pH-dependent thermoresponsive behavior and thus have a broader range of applicability.[87,88] Homopolymeric polyacid hydrogels exhibit sharp volume phase transitions with pH, swelling to high degrees above the polyacid $pK_a$ and collapsing upon protonation of the carboxylic group. This behavior is due to contributions of Couloumbic repulsions among charged carboxylate groups and also to the transport of mobile counterions inside the polymer mesh to neutralize charge.[89] The presence of polyacids copolymerized with NIPAAm has been shown to increase the copolymer LCST in comparison with PNIPAAm homopolymers and to contribute for overall swelling of cross-linked networks, especially at physiological or basic conditions. The swelling ability of PNIPAAm-based hydrogels also depends on the ionic strength of the aqueous media. In addition, it was shown that complexation of molecules as different as phenols[90] or charged polyelectrolytes[91] on PNIPAAm hydrogels have a significant impact on the swelling and overall thermoresponsive behavior. These observations open a possible route to further modulate the behavior of "smart" microgels.
Cross-linked PNIPAAm polymer has already been synthesized in $scCO_2$.[62] Therefore, this green and clean synthesis approach may be a possible route to prepare stimuli-responsive microbeads with well-defined morphology for monitoring sensitive cell cultures.

## 1.4 Layer-by-Layer Coating of Hydrogel Microbeads

The control of surface properties of materials is a possible route to positively impact the materials' performance and interaction with cells. Several techniques of nanofabrication can be applied to modify the surface properties of materials, such as chemical vapor or Langmuir-Blodgett deposition. These techniques usually require sophisticated equipments and are limited in the range of materials that can be processed.[91] Since it was first proposed by Decher *et al.* in 1997, layer-by-layer assembly (LbL) has emerged as a facile and versatile technique to tailor and functionalize surfaces ranging from flat substrates[92] to living cells.[93] LbL method refers to the sequential deposition of polymers (and other macromolecules) with opposite interacting chemistries for the preparation of nanostructured thin films, as illustrated in Figure 1.2. Over the past two decades, a diverse range of synthetic or naturally-derived polymers were used to prepare multilayered films, exploring electrostatics, van der Waals interactions, hydrogen bonding, etc.; and producing coatings with nanometer to micrometer range thicknesses. Through the LbL technique, a wide variety of surface physical properties such as charge, mechanical properties, hydrophilicity, and functionality can be modulated with high precision through assembly sequence, number of depositing layers, chemical compositions, and deposition conditions. Being generally performed in aqueous solutions, LbL is particularly suitable for processing sensitive biomolecules and fabrication of coatings for biological applications, as demonstrated for drug delivery

thin films, antimicrobial coatings, cell culture surfaces, and biosensing devices.[95] Thorough reviews were recently published on LbL films for drug delivery[96] and control of cellular processes.[97]

Although the LbL technique was initially developed for planar surfaces, research has expanded for the multilayer assembly of polyelectrolytes on microparticles, specifically colloidal substrates as sacrificial templates for the preparation of hollow capsules.[98,99] The size of the hollow capsules is determined by the template diameter, while the capsule wall thickness and permeability is controlled by the LbL assembled film; systems have been fabricated for drug delivery, sensing, and catalysis applications, among others.[99,100] On the other hand, very limited examples of LbL assembly on soft porous substrates, such as hydrogels or microgels, are found in the literature. For macroscopic hydrogels, LbL technique has been recently employed for enabling sustained protein release[101] or cell adhesive properties.[102] Richtering *et al.* have demonstrated for PNIPAAm-based microgels that the adsorbed polyelectrolyte (PE) layers can modify not only the microgel surface properties, but also penetrate the hydrogel mesh.[103] In addition, the native responsive behavior of these microgels was modified depending on the initial microgel architecture, the polyelectrolyte pairs used, the assembly sequence and ultimately the experimental conditions.[103-106] Nevertheless, the design principles on modulation of the LbL film architecture, permeability, and cell-interactive properties in other substrates may be informative for the rational modification of microgels properties.

### 1.4.1 LbL as a tool for tuning hydrogel microbead properties: cell adhesion and permeability

Modulation of protein deposition and ultimately cell adhesion to substrates is of tremendous importance for biosensing applications, as direct interaction with cells allows the straight monitoring of cell-secreted and possibly membrane-tethered factors. Several studies have shown that LbL film assembly allows the preparation of cell adhesive surfaces by tweaking the films hydrophilicity, and ultimately their mechanical properties. The important parameters that dictate cell adhesion to PE films are (i) the multilayer assembly conditions such as pH and ionic strength (ii) the intrinsic characteristics of the PEs and (iii) subsequent cross-linking between constituent PEs.

A significant contribution for the rational design of cell adhesive films was described by Rubner *et al*, using synthetic PE pairs.[107] In this report, adhesion of murine fibroblasts was controlled by the architecture of the weak polyelectrolytes (poly(acrylic acid) (PAA) and poly(allylamine) (PAH)) films, which is strongly dependent on the assembly pH, with negligible differences between their protein adsorption or wettability characteristics. Overall, under pH conditions where both PEs are ionized (e.g. pH 7.5/3.5 PAH/PAA), thin and highly ionically cross-linked films are obtained and cell adhesion is observed (at a same extent as in tissue culture polystyrene). On the other hand, cytophobic surfaces are characterized by few ionic cross-links (thus being more enriched in one of the PEs), and

exhibit increased swellability under physiological conditions. Further mechanical characterization of PAH/PAA multilayers showed that adhesion of human microvascular endothelial cells can be correlated with the film elastic moduli in proportion to its swellability.[108] For this cell line, cell density was dependent on the outermost layer, showing that the film mechanical properties and interfacial chemistry can be independently changed to modulate cell attachment and proliferation.

The modulation of the LbL films thickness, mechanical properties and surface chemistry, as design parameters for creating cell-adhesive coatings, still holds for polysaccharide and polypeptide films. The assembly of these PEs is generally characterized by an exponential film growth regime in mass and thickness, yielding thicker and more hydrated coatings than synthetic-based nanoassemblies, at comparable experimental conditions.[97] For poly(L-lysine)/poly(L-glutamic acid) (PLL/PLGA) and collagen-coated poly(L-lysine)/hyaluronan (PLL/HA) films, cell adhesion[109] and spreading[110] was greater on thinner and stiffer films. The thickness of PLL/PLGA films can be systematically tuned depending on the deposition pH.[111] In addition, depending on the cell line and experimental conditions, initial attachment was dependent on the outermost layer composition.[110,111] On the whole, these studies also show that anchorage-response of cells to LbL films is dependent on the specific cell type and might be related to the physical properties of their natural ECM. Indeed photoreceptor cells were shown to adhere and maintain their viability on PLL/HA films, which, without post-assembly modifications, are generally perceived as bioinert.[112] Alternative methods available to tune the films mechanical properties include the incorporation of nanometer-sized colloids such as clays or using polyelectrolytes bearing cross-linkable antagonist moieties through carbodiimide coupling[109] or, alternatively, through biorthogonal azide-alkyne cycloaddition.[113] Another strategy to promote cell adhesion to assembled films encompasses the grafting of pro-adhesive RGD peptide sequences[113] or subsequent coating with cell matrix biomacromolecules such as fibronectin.[114] A recent example on the successful modification of bulk hydrogel cell adhesive properties by LbL assembly of thin films was the PLL/HA films deposition on otherwise bioinert HA hydrogels. In this study, polyelectrolyte diffusion inside the pores was observed, with an impact on the hydrophobic character of the surface, a reduction on the equilibrium swelling, an enhanced failure stress/strain properties, and most importantly, an improved cell attachment and spreading.[102]

The strategies outlined for tuning cell adhesion are quite similar to those used for controlling LbL film permeability, as the diffusion transport properties are also closely related to (i) the inherent characteristics of the PEs; (ii) assembly conditions; (iii) cross-linking (either physical and covalent); and (iv) post-assembly processing. Several studies have shown that the permeability of PE multilayers is extremely dependent on their composition. In general, greater charge density of the polyelectrolytes results in more ionic cross-linking, less swelling, and lower permeabilities.[92,115] Indeed nanofiltration studies across PE multilayers has shown that rejection of neutral molecules increases with the constituent PEs charge density, allowing the tuning of the multilayer molecular weight cut-off (MWCO) from 100 for poly(styrene sulfonate)/poly(allylamine hydrochloride) (PSS/PAH) films to >

20,000 Da for the weak natural PEs HA/chitosan (HA/CHI).[116] These observations were further correlated with the films swelling, as synthetic PE films with lower thicknesses presented overall higher solute rejections in water.[117] Early studies on hollow capsules assembled from PSS/PAH and sodium alginate/CHI had also shown that the natural composed capsules were permeable to a dye-labeled dextran ($M_w$ ~ 70,000) at physiological pH, while the synthetic PE capsules were not. In addition the capsule thickness was large in the first case.[98] When the formation of both films and hollow capsules is based on electrostatic interactions, changes in pH (for weak PEs) and/or ionic strength (especially for strong PE) can alter interactions between the successive layers, and thus impact permeability. As a consequence the swelling and permeability of PSS/PAH and PSS/poly(diallyldimethylammonium chloride) (PSS/PDAC) films increases with ionic strength.[116,117] Not surprisingly, it was shown for PSS/PAH hollow capsules (which contain a pH-sensitive PE) that pH could be used as an external stimuli post-assembly to modulate the capsules permeability.[118] For the PAH/PAA system thoroughly characterized by Rubner *et al.* the post-assembly immersion of such multilayers in a medium of different pH results in a substantial and irreversible change on the film morphology, yielding microporous thin films (with pores up to 100 nm) and increasing overall thickness.[119]

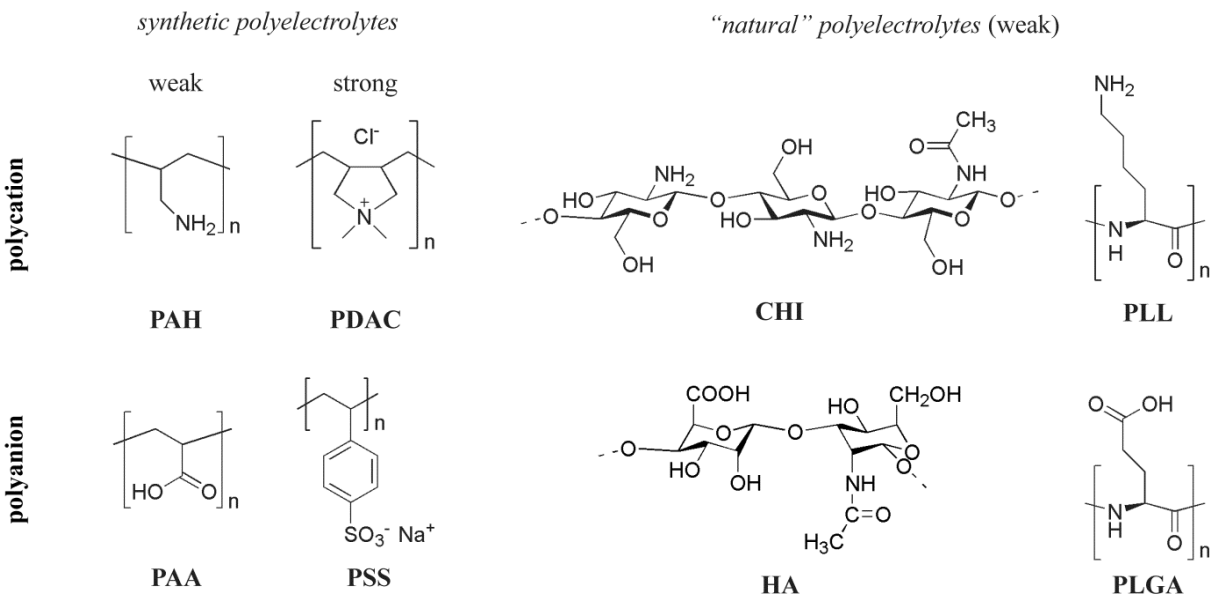


**Figure 1.7** Common polyelectrolytes used for LbL assembly. Synthetic PEs: poly(diallyldimethylammonium chloride), PDAC, and poly(sodium styrene sulfonate), PSS, both have a permanent charge, being designated as strong PEs; poly(allylamine hydrochloride), PAH, and poly(acrylic acid), PAA, both have a pH-dependent charge, being designated as weak PEs. Naturally-derived PEs: chitosan, CHI, and hyaluronic acid, HA; poly(L-lysine), PLL, and poly(L-glutamic acid), PLGA, are also considered weak PEs.

The different characteristics of the nanoassemblies obtained from natural weak PEs or synthetic PEs has prompted researchers to create multicomponent, stratified thin films. In fact, the polypeptide/polysaccharide films are particularly suitable for the loading of large amounts of sensitive

biomolecules, without compromising their free diffusion within the film nor their activity. The capping of these hydrated films with dense linearly growing synthetic PE coatings has been shown to create a barrier to polyelectrolyte diffusion and to slow down proton transport in HA/PLL and PSS/PAH composite films in a study by Lavalle *et al.*[120] A different study by Hammond *et al.*, using different polysaccharides as PEs, showed that effective separation of the film composite components was only achieved by covalent cross-linking of the barrier layers, assuring sequential release of biomacromolecules.[121] These flexible approaches for creating multiple functionalized coatings can potentially be explored to tune permeation of biomolecules to embedded target sensing moieties.
The above design parameters for the modulation of cell adhesion and overall permeability of LbL systems could potentially be used as guidelines for tuning the microbead-based protease sensor properties, according to the desired features.

## 1.5 Outline of the Thesis

The thesis is organized in the following chapters:
Chapter 1 – Introduction. The aim of the PhD project as well as the biological motivation is discussed. A brief review on the technologies used for fabricating a protease sensor is also compiled.
Chapter 2 – Synthesis of Well-Defined Stimuli-Responsive Microbeads in Supercritical $CO_2$. This chapter discusses the strategies pursued to obtain the hydrogel microbead core of the protease sensing construct according to the specified design constrains. Part of this work was included on a published paper.[122*]
Chapter 3 – Tuning Smart Microbeads Properties by Macromolecules Assembly. In this chapter the impact of macromolecule complexation and multilayer assembly on tuning the properties of the synthesized smart microbeads is discussed. The complexation of a polyphenol on thermoresponsive particles was subject of a published paper.[123*] Another paper is under preparation on the multilayer assembly of polyelectrolytes on pH and temperature-responsive microbeads.
Chapter 4 – Development of a Microbead Biosensor. Herein, strategies to incorporate a protease sensing function on the synthesized microbeads are explored. Proof-of-concept with a model protease of sensor activation is shown.
Chapter 5 – Conclusions and Future Directions.
Chapter 6 – Annexes.

---

[*] Reproduced with the authorization of the editor and subjected to the copyrights imposed

## 1.6 References


1. Butcher, D.T., Alliston, T. & Weaver, V.M. A tense situation: forcing tumour progression. *Nat. Rev. Cancer* **9**, 108-22 (2009).

2. Langer, R. & Peppas, N.A. Advances in biomaterials, drug delivery, and bionanotechnology. *AIChE Journal* **49**, 2990-3006 (2003).

3. Lutolf, M.P. & Hubbell, J.A. Synthetic biomaterials as instructive extracellular microenvironments for morphogenesis in tissue engineering. *Nat. Biotechnol.* **23**, 47-55 (2005).

4. Kessenbrock, K., Plaks, V. & Werb, Z. Matrix metalloproteinases: regulators of the tumor microenvironment. *Cell* **141**, 52-67 (2010).

5. López-Otín, C. & Matrisian, L.M. Emerging roles of proteases in tumour suppression. *Nat. Rev. Cancer* **7**, 800-8 (2007).

6. Packard, B.Z., Artym, V.V., Komoriya, A. & Yamada, K.M. Direct visualization of protease activity on cells migrating in three-dimensions. *Matrix Biol.* **28**, 3-10 (2009).

7. Mannello, F. Multipotent mesenchymal stromal cell recruitment, migration, and differentiation: what have matrix metalloproteinases got to do with it? *Stem Cells* **24**, 1904-7 (2006).

8. Page-McCaw, A., Ewald, A.J. & Werb, Z. Matrix metalloproteinases and the regulation of tissue remodelling. *Nat. Rev. Mol. Cell Biol.* **8**, 221-33 (2007).

9. Parks, W.C., Wilson, C.L. & López-Boado, Y.S. Matrix metalloproteinases as modulators of inflammation and innate immunity. *Nat. Rev. Immunol.* **4**, 617-29 (2004).

10. Eming, S.A., Krieg, T. & Davidson, J.M. Inflammation in wound repair: molecular and cellular mechanisms. *J. Invest. Dermatol.* **127**, 514-25 (2007).

11. Handsley, M.M. & Edwards, D.R. Metalloproteinases and their inhibitors in tumor angiogenesis. *Int. J. Cancer* **115**, 849-60 (2005).

12. Banu, S.K., Lee, J., Starzinski-Powitz, A. & Arosh, J.A. Gene expression profiles and functional characterization of human immortalized endometriotic epithelial and stromal cells. *Fertil. Steril.* **90**, 972-87 (2008).

13. Sternlicht, M.D. & Werb, Z. How Matrix Metalloproteinases Regulate Cell Behavior. *Annu Rev Cell Dev Biol* **17**, 463-516 (2001).

14. Blain, E. Mechanical regulation of matrix metalloproteinases. *Front Biosci* **12**, 507-527 (2007).

15. Deryugina, E.I. & Quigley, J.P. Pleiotropic Roles of Matrix Metalloproteinases in Tumor Angiogenesis: Contrasting, Overlapping and Compensatory Functions. *Biochim. Biophys. Acta* **1803**, 103-120 (2010).

16. Huang, K. & Wu, L.D. Aggrecanase and aggrecan degradation in osteoarthritis: a review. *J. Int. Med. Res.* **36**, 1149-60 (2008).

17. Rosenberg, G.A. Matrix metalloproteinases and their multiple roles in neurodegenerative diseases. *The Lancet Neurology* **8**, 205-216 (2009).

18. Osteen, K.G., Ph, D., Yeaman, G.R. & Bruner-tran, K.L. Matrix Metalloproteinases and Endometriosis. *Semin. Reprod. Med.* **21**, 155-164 (2003).

19. Coussens, L.M., Fingleton, B. & Matrisian, L.M. Matrix metalloproteinase inhibitors and cancer: trials and tribulations. *Science* **295**, 2387-92 (2002).

20. Mudgett, J.S. *et al.* Collagen-induced Arthritis and Cartilage Destruction. *Rheumatism* **41**, 110-121 (1998).

21. Overall, C.M. *et al.* Protease degradomics: mass spectrometry discovery of protease substrates and the CLIP-CHIP, a dedicated DNA microarray of all human proteases and inhibitors. *Biol. Chem.* **385**, 493-504 (2004).

22. Horiuchi, K. *et al.* Substrate Selectivity of Epidermal Growth Factor-Receptor Ligand Sheddases and their Regulation by Phorbol Esters and Calcium Influx. *Mol. Biol. Cell* **18**, 176-188 (2007).

23. Pillinger, M.H. *et al.* Matrix metalloproteinase secretion by gastric epithelial cells is regulated by E prostaglandins and MAPKs. *J. Biol. Chem.* **280**, 9973-9 (2005).

24. Hawkes, S.P., Li, H. & Taniguchi, G.T. Matrix Metalloproteinase Protocols. *Methods Mol. Biol.* **622**, 257-269 (2010).

25. Herrlich, A., Klinman, E., Fu, J., Sadegh, C. & Lodish, H. Ectodomain cleavage of the EGF ligands HB-EGF, neuregulin1-beta, and TGF-alpha is specifically triggered by different stimuli and involves different PKC isoenzymes. *FASEB J.* **22**, 4281-95 (2008).

26. Bremer, C., Tung, C.H. & Weissleder, R. In vivo molecular target assessment of matrix metalloproteinase inhibition. *Nat. Med.* **7**, 743-8 (2001).

27. Ryu, J.H. *et al.* "One-step" detection of matrix metalloproteinase activity using a fluorogenic Peptide probe-immobilized diagnostic kit. *Bioconjug. Chem.* **21**, 1378-84 (2010).

28. Fields, G.B. Matrix Metalloproteinase Protocols. *Methods Mol. Biol.* **622**, 393-423.

29. Miller, M.A., Barkal, L., Jeng, K., Herrlich, A., Moss, M., Griffith, L.G. & Lauffenburger, D.A. Proteolytic Activity Matrix Analysis (PrAMA) for simultaneous determination of multiple protease activities. *Integr. Biol.***3**, 422-438 (2011).

30. Nagase, H. & Fields, G.B. Human matrix metalloproteinase specificity studies using collagen sequence-based synthetic peptides. *Biopolymers* **40**, 399-416 (1996).

31. Caescu, C.I., Jeschke, G.R. & Turk, B.E. Active-site determinants of substrate recognition by the metalloproteinases TACE and ADAM10. *Biochem. J.* **424**, 79-88 (2009).

32. Rasmussen, F.H. *et al.* Use of a Multiple-Enzyme/Multiple-Reagent Assay System To Quantify Activity Levels in Samples Containing Mixtures of Matrix Metalloproteinases. *Biochemistry* **43**, 2987-2995 (2004).

33. Scherer, R.L., McIntyre, J.O. & Matrisian, L.M. Imaging matrix metalloproteinases in cancer. *Cancer Metastasis Rev.* **27**, 679-90 (2008).

34. Aimetti, A.A., Tibbitt, M.W. & Anseth, K.S. Human Neutrophil Elastase Responsive Delivery from Poly(ethylene glycol) Hydrogels. *Biomacromolecules* **10**, 1484-1489 (2009).

35. Iyer, S., Visse, R., Nagase, H. & Acharya, K.R. Crystal Structure of an Active Form of Human MMP-1. *J. Mol. Biol.* **362**, 78-88 (2006).

36. Morgunova, E. *et al.* Structure of human pro-matrix metalloproteinase-2: activation mechanism revealed. *Science* **284**, 1667-1670 (1999).

37. Edman, K. *et al.* The Discovery of MMP7 Inhibitors Exploiting a Novel Selectivity Trigger. *ChemMedChem* **6**, 769-773 (2011).

38. Rosenblum, G. *et al.* Insights into the structure and domain flexibility of full-length pro-matrix metalloproteinase-9/gelatinase B. *Structure* **15**, 1227-36 (2007).

39. Bertini, I. *et al.* Evidence of Reciprocal Reorientation of the Catalytic and Hemopexin-Like Domains of Full-Length MMP-12. *J. Am. Chem. Soc.* **130**, 7011-7021 (2008).

40. Griffith, L.G. Emerging Design Principles in Biomaterials and Scaffolds for Tissue Engineering. *Ann. N. Y. Acad. Sci.* **961**, 83-95 (2002).

41. Lutolf, M.P., Lauer-Fields, J.L., Schmoekel, H.G., Metters, A.T., Weber, F.E., Fields, G.B., Hubbell, J.A. Synthetic matrix metalloproteinase-sensitive hydrogels for the conduction of tissue regeneration: engineering cell-invasion characteristics. *Proc. Natl. Acad. Sci. U.S.A.* **100**, 5413-8 (2003).

42. Anseth, K.S., Bowman, C.N. & Brannon-Peppas, L. Mechanical properties of hydrogels and their experimental determination. *Biomaterials* **17**, 1647-1657 (1996).

43. Engler, A.J., Sen, S., Sweeney, H.L. & Discher, D.E. Matrix elasticity directs stem cell lineage specification. *Cell* **126**, 677-89 (2006).

44. Nayak, S. & Lyon, L.A. Soft nanotechnology with soft nanoparticles. *Angew. Chem., Int. Ed.* **44**, 7686-708 (2005).

45. Jones, C.D. & Lyon, L.A. Synthesis and Characterization of Multiresponsive Core−Shell Microgels. *Macromolecules* **33**, 8301-8306 (2000).

46. Oh, J.K., Drumright, R., Siegwart, D.J. & Matyjaszewski, K. The development of microgels/nanogels for drug delivery applications. *Prog. Polym. Sci.* **33**, 448-477 (2008).

47. Cooper, A.I. Polymer synthesis and processing using supercritical carbon dioxide. *J. Mater. Chem.* **10**, 207-234 (2000).

48. Mooney, D.J., Baldwin, D.F., Suh, N.P., Vacanti, J.P. & Langer, R. Novel approach to fabricate porous sponges of poly(D,L-lactic-co-glycolic acid) without the use of organic solvents. *Biomaterials* **17**, 1417-22 (1996).

49. Barry, J.J.A., Gidda, H.S., Scotchford, C.A. & Howdle, S.M. Porous methacrylate scaffolds: supercritical fluid fabrication and in vitro chondrocyte responses. *Biomaterials* **25**, 3559-68 (2004).

50. Watson, M.S., Whitaker, M.J., Howdle, S.M. & Shakesheff, K.M. Incorporation of Proteins into Polymer Materials by a Novel Supercritical Fluid Processing Method. *Adv. Mater.* **14**, 1802-1804 (2002).

51. Villarroya, S., Thurecht, K.J., Heise, A. & Howdle, S.M. Supercritical CO2: an effective medium for the chemo-enzymatic synthesis of block copolymers? *Chem. Commun.* 3805 (2007).doi:10.1039/b701128h

52. Grignard, B., Jérôme, C., Calberg, C., Jérôme, R., Wang, W., Howdle, S.M., Detrembleur, C. Dispersion Atom Transfer Radical Polymerization of Vinyl Monomers in Supercritical Carbon Dioxide. *Macromolecules* **41**, 8575-8583 (2008).

53. Kikic, I. & Vecchione, F. Supercritical impregnation of polymers. *Curr. Opin. Solid State Mater. Sci.* **7**, 399-405 (2003).

54. Christian, P., Howdle, S.M. & Irvine, D.J. Dispersion Polymerization of Methyl Methacrylate in Supercritical Carbon Dioxide with a Monofunctional Pseudo-Graft Stabilizer. *Macromolecules* **33**, 237-239 (2000).

55. Desimone, J.M. *et al.* Dispersion Polymerizations in Supercritical Carbon Dioxide. *Science* **265**, 356-359 (1994).

56. Casimiro, T., Banetosuna, A., Ramos, A., Da Ponte, M. & Aguiar-Ricardo, A. Synthesis of highly cross-linked poly(diethylene glycol dimethacrylate) microparticles in supercritical carbon dioxide. *Eur. Polym. J.* **41**, 1947-1953 (2005).

57. Knez, Z. & Weidner, E. Particles formation and particle design using supercritical fluids. *Curr. Opin. Solid State Mater. Sci.* **7**, 353-361 (2003).

58. Liu, T., Garner, P., DeSimone, J.M., Roberts, G.W. & Bothun, G.D. Particle Formation in Precipitation Polymerization: Continuous Precipitation Polymerization of Acrylic Acid in Supercritical Carbon Dioxide. *Macromolecules* **39**, 6489-6494 (2006).

59. Shiho, H. & DeSimone, J.M. Dispersion Polymerization of Glycidyl Methacrylate in Supercritical Carbon Dioxide. *Macromolecules* **34**, 1198-1203 (2001).

60. Woods, H.M., Silva, M.M.C.G., Nouvel, C., Shakesheff, K.M. & Howdle, S.M. Materials processing in supercritical carbon dioxide: surfactants, polymers and biomaterials. *Journal of Materials Chemistry* **14**, 1663 (2004).

61. Temtem, M., Casimiro, T., Santos, A.G., Macedo, A.L., Cabrita, E.J., Aguiar-Ricardo, A. Molecular Interactions and $CO_2$-Philicity in Supercritical $CO_2$ . A High-Pressure NMR and Molecular Modeling Study of a Perfluorinated Polymer in scCO2. *J. Phys. Chem. B* **111**, 1318-1326 (2007).

62. Temtem, M., Casimiro, T., Mano, J.F. & Aguiar-Ricardo, A. Green synthesis of a temperature sensitive hydrogel. *Green Chem.* **9**, 75 (2007).

63. Hsiao, Y.-ling, Maury, E.E. & DeSimone, J.M. Dispersion Polymerization of Methyl Methacrylate Stabilized with Poly(1,1-dihydroperfluorooctyl acrylate) in Supercritical Carbon Dioxide. *Macromolecules* **28**, 8159-8166 (1995).

64. Canelas, D.A. & DeSimone, J.M. Dispersion Polymerizations of Styrene in Carbon Dioxide Stabilized with Poly(styrene-b-dimethylsiloxane). *Macromolecules* **30**, 5673-5682 (1997).

65. Carson, T., Lizotte, J. & DeSimone, J.M. Dispersion Polymerization of 1-Vinyl-2-pyrrolidone in Supercritical Carbon Dioxide. *Macromolecules* **33**, 1917-1920 (2000).

66. Ye, W. & DeSimone, J.M. Emulsion Polymerization of *N*-Ethylacrylamide in Supercritical Carbon Dioxide. *Macromolecules* **38**, 2180-2190 (2005).

67. Wood, C.D. & Cooper, A.I. Synthesis of Macroporous Polymer Beads by Suspension Polymerization Using Supercritical Carbon Dioxide as a Pressure-Adjustable Porogen. *Macromolecules* **34**, 5-8 (2001).

68. Jung, J. & Perrut, M. Particle design using supercritical fluids: Literature and patent survey. *J. Supercrit. Fluids* **20**, 179-219 (2001).

69. Martín, Á., Pham, H.M., Kilzer, A., Kareth, S. & Weidner, E. Micronization of polyethylene glycol by PGSS (Particles from Gas Saturated Solutions)-drying of aqueous solutions. *Chem. Eng. Process.: Process Intensification* **49**, 1259-1266 (2010).

70. Brazel, C.S. & Peppas, N.A. Pulsatile local delivery of thrombolytic and antithrombotic agents using poly(N-isopropylacrylamide-co-methacrylic acid) hydrogels. *J. Controlled Release* **39**, 57-64 (1996).

71. Torres-Lugo, M. & Peppas, N.A. Molecular Design and in Vitro Studies of Novel pH-Sensitive Hydrogels for the Oral Delivery of Calcitonin. *Macromolecules* **32**, 6646-6651 (1999).

72. Temtem, M., Pompeu, D., Barroso, T., Fernandes, J., Simões, P.C., Casimiro, T., Aguiar-Ricardo, A. Development and characterization of a thermoresponsive polysulfone membrane using an environmental friendly technology. *Green Chem.* **11**, 638 (2009).

73. Barroso, T., Temtem, M., Casimiro, T. & Aguiar-Ricardo, A. Development of pH-responsive poly(methylmethacrylate-co-methacrylic acid) membranes using $scCO_2$ technology. Application to protein permeation. *J. Supercrit. Fluids* **51**, 57-66 (2009).

74. Suzuki, H. & Kumagai, A. A disposable biosensor employing a glucose-sensitive biochemomechanical gel. *Biosens. Bioelectron.* **18**, 1289-1297 (2003).

75. Kim, J., Singh, N. & Lyon, L.A. Label-free biosensing with hydrogel microlenses. *Angew. Chem., Int. Ed.* **45**, 1446-1449 (2006).

76. Lapeyre, V., Gosse, I., Chevreux, S. & Ravaine, V. Monodispersed glucose-responsive microgels operating at physiological salinity. *Biomacromolecules* **7**, 3356-3363 (2006).

77. Okano, T., Yamada, N., Sakai, H. & Sakurai, Y. A novel recovery system for cultured cells using plasma-treated polystyrene dishes grafted with poly(N-isopropylacrylamide). *J. Biomed. Mater. Res.* **27**, 1243-51 (1993).

78. Ogawa, K., Wang, B. & Kokufuta, E. Enzyme-Regulated Microgel Collapse for Controlled Membrane Permeability. *Langmuir* **17**, 4704-4707 (2001).

79. Schild, H.G. Poly(*N*-isopropylacrylamide) - Experiment, Theory and Application. *Prog. Polym. Sci.* **17**, 163-249 (1992).

80. Garcia, D. *et al.* Synthesis and characterization of poly(methacrylic acid) hydrogels for metoclopramide delivery. *Eur. Polym. J.* **40**, 1637-1643 (2004).

81. Suzuki, A. & Tanaka, T. Phase transition in polymer gels induced by visible light. *Nature* **346**, 345 (1990).

82. Tanaka, T., Nishio, I., Shao-Tang, S. & Ueno-Nishio, S. Collapse of Gels in an Electric Field. *Science* **218**, 467-469 (1982).

83. Traitel, T., Cohen, Y. & Kost, J. Characterization of glucose-sensitive insulin release systems in simulated in vivo conditions. *Biomaterials* **21**, 1679-87 (2000).

84. Qiu, Y. & Park, K. Environment-sensitive hydrogels for drug delivery. *Adv. Drug Deliv. Rev.* **53**, 321-39 (2001).

85. Heskins, M. & Guillet, J.E. Solution Properties of Poly(*N*-isopropylacrylamide). *J. Macromol. Sci. A - Chem.* **2**, 37-41 (1968).

86. Kaneko, Y., Yoshida, R., Sakai, K., Sakurai, Y. & Okano, T. Temperature-responsive shrinking kinetics of poly (N-isopropylacrylamide) copolymer gels with hydrophilic and hydrophobic comonomers. *J. Membr. Sci.* **101**, 13-22 (1995).

87. Hoare, T. & Pelton, R. Highly pH and Temperature Responsive Microgels Functionalized with Vinylacetic Acid. *Macromolecules* **37**, 2544-2550 (2004).

88. Brazel, C.S. & Peppas, N.A. Synthesis and Characterization of Thermo- and Chemomechanically Responsive Poly(N-isopropylacrylamide-co-methacrylic acid) Hydrogels. *Macromolecules* **28**, 8016-8020 (1995).

89. Flory, P.J. *Principles of Polymer Chemistry*. (Cornell University, London, 1986).

90. Kosik, K., Wilk, E., Geissler, E. & László, K. Distribution of Phenols in Thermoresponsive Hydrogels. *Macromolecules* **40**, 2141-2147 (2007).

91. Greinert, N. & Richtering, W. Influence of polyelectrolyte multilayer adsorption on the temperature sensitivity of poly(N-isopropylacrylamide) (PNiPAM) microgels. *Colloid Polym. Sci.* **282**, 1146-1149 (2004).

92. Hammond, P.T. Form and Function in Multilayer Assembly: New Applications at the Nanoscale. *Adv. Mater.* **16**, 1271-1293 (2004).

93. Decher, G. Fuzzy Nanoassemblies: Toward Layered Polymeric Multicomposites. *Science* **277**, 1232-1237 (1997).

94. Swiston, A., Cheng, C., Um, S., Irvine, D., Cohen, R.E., Rubner, M.F. Surface functionalization of living cells with multilayer patches. *Nano Lett.* **8**, 24-29 (2008).

95. Mertz, D., Vogt, C., Hemmerlé, J., Mutterer, J., Ball, V., Voegel, J.-C., Schaaf, P., Lavalle, P. Mechanotransductive surfaces for reversible biocatalysis activation. *Nat. Mater.* **8**, 731-736 (2009).

96. Zelikin, A.N. Drug releasing polymer thin films: new era of surface-mediated drug delivery. *ACS Nano* **4**, 2494-509 (2010).

97. Picart, C. Polyelectrolyte multilayer films: from physico-chemical properties to the control of cellular processes. *Curr. Med. Chem.* **15**, 685-97 (2008).

98. Shenoy, D.B., Antipov, A.A., Sukhorukov, G.B. & Möhwald, H. Layer-by-layer engineering of biocompatible, decomposable core-shell structures. *Biomacromolecules* **4**, 265-72 (2003).

99. Johnston, A.P.R., Cortez, C., Angelatos, A.S. & Caruso, F. Layer-by-layer engineered capsules and their applications. *Curr. Opin. Colloid Interface Sci.* **11**, 203-209 (2006).

100. Stubbe, B.G., Gevaert, K., Derveaux, S., Braeckmans, K., De Geest, B.G., Goethals, M., Vandekerckhove, J., Demeester, J. Evaluation of Encoded Layer-By-Layer Coated Microparticles As Protease Sensors. *Adv. Funct. Mater.* **18**, 1624-1631 (2008).

101. Mehrotra, S. *et al.* Time Controlled Protein Release from Layer-by-Layer Assembled Multilayer Functionalized Agarose Hydrogels. *Adv Funct Mater* **20**, 247-258 (2010).

102. Yamanlar, S., Sant, S., Boudou, T., Picart, C. & Khademhosseini, A. Surface functionalization of hyaluronic acid hydrogels by polyelectrolyte multilayer films. *Biomaterials* **32**, 5590-9 (2011).

103. Kleinen, J., Klee, A. & Richtering, W. Influence of architecture on the interaction of negatively charged multisensitive poly(*N*-isopropylacrylamide-co-methacrylic acid) microgels with oppositely charged polyelectrolyte: absorption vs adsorption. *Langmuir* **26**, 11258-65 (2010).

104. Wong, J.E. & Richtering, W. Surface Modification of Thermoresponsive Microgels via Layer-by-Layer Assembly of Polyelectrolyte Multilayers. *Prog. Coll. Polym. Sci.* **133**, 45-51 (2006).

105. Wong, J.E., Díez-Pascual, A.M. & Richtering, W. Layer-by-Layer Assembly of Polyelectrolyte Multilayers on Thermoresponsive P(NiPAM-co-MAA) Microgel: Effect of Ionic Strength and Molecular Weight. *Macromolecules* **42**, 1229-1238 (2009).

106. Díez-Pascual, A.M. & Wong, J.E. Effect of layer-by-layer confinement of polypeptides and polysaccharides onto thermoresponsive microgels: a comparative study. *J. Colloid Interface Sci.* **347**, 79-89 (2010).

107. Mendelsohn, J.D., Yang, S.Y., Hiller, J., Hochbaum, A.I. & Rubner, M.F. Rational design of cytophilic and cytophobic polyelectrolyte multilayer thin films. *Biomacromolecules* **4**, 96-106 (2003).

108. Thompson, M.T., Berg, M.C., Tobias, I.S., Rubner, M.F. & Van Vliet, K.J. Tuning compliance of nanoscale polyelectrolyte multilayers to modulate cell adhesion. *Biomaterials* **26**, 6836-45 (2005).

109. Richert, L., Engler, A.J., Discher, D.E. & Picart, C. Elasticity of native and cross-linked polyelectrolyte multilayer films. *Biomacromolecules* **5**, 1908-16 (2004).

110. Richert, L., Lavalle, P., Vautier, D., Senger, B., Stoltz, J.-F., Schaaf, P., Voegel, J.-C., Picart, C. Cell interactions with polyelectrolyte multilayer films. *Biomacromolecules* **3**, 1170-8 (2002).

111. Richert, L., Arntz, Y., Schaaf, P., Voegel, J. & Picart, C. pH dependent growth of poly(L-lysine)/poly(L-glutamic) acid multilayer films and their cell adhesion properties. *Surf. Sci.* **570**, 13-29 (2004).

112. Tezcaner, A., Hicks, D., Bouldmedais, F., Sahel, J., Schaaf, P., Voegel, J.-C., Lavalle, P. Polyelectrolyte multilayer films as substrates for photoreceptor cells. *Biomacromolecules* **7**, 86-94 (2006).

113. Kinnane, C.R., Wark, K., Such, G.K., Johnston, A.P.R. & Caruso, F. Peptide-functionalized, low-biofouling click multilayers for promoting cell adhesion and growth. *Small* **5**, 444-8 (2009).

114. Wittmer, C.R., Phelps, J.A., Saltzman, W.M. & Van Tassel, P.R. Fibronectin terminated multilayer films: protein adsorption and cell attachment studies. *Biomaterials* **28**, 851-60 (2007).

115. De Cock, L.J. *et al.* Polymeric multilayer capsules in drug delivery. *Angew. Chem,. Int. Ed.* **49**, 6954-73 (2010).

116. Miller, M.D. & Bruening, M.L. Controlling the nanofiltration properties of multilayer polyelectrolyte membranes through variation of film composition. *Langmuir* **20**, 11545-51 (2004).

117. Miller, M.D. & Bruening, M.L. Correlation of the Swelling and Permeability of Polyelectrolyte Multilayer Films. *Chem. Mater.* **17**, 5375-5381 (2005).

118. Antipov, A.A. *et al.* Polyelectrolyte multilayer capsule permeability control. *Colloids Surf., A* **198-200**, 535-541 (2002).

119. Mendelsohn, J.D., Barrett, C.J., Chan, V.V., Pal, A.J., Mayes, A.M., Rubner, M.F. Fabrication of Microporous Thin Films from Polyelectrolyte Multilayers. *Langmuir* **16**, 5017-5023 (2000).

120. Schaaf, P., Muller, S., Ball, V., Stoltz, J.-F., Voegel, J.-C., Lavalle, P. Multicompartment Films Made of Alternate Polyelectrolyte Multilayers of Exponential and Linear Growth. *Langmuir* **20**, 7298-7302 (2004).

121. Wood, K.C., Chuang, H.F., Batten, R.D., Lynn, D.M. & Hammond, P.T. Controlling interlayer diffusion to achieve sustained, multiagent delivery from layer-by-layer thin films. *Proc. Natl. Acad. Sci. U.S.A.* **103**, 10207-12 (2006).

122. Costa, E., de-Carvalho, J., Lobato da Silva, C., Cidade, M.T., Aguiar-Ricardo, A. Tailoring thermoresponsive microbeads in supercritical carbon dioxide for biomedical applications. *J. Supercrit. Fluids* **56**, 292-298 (2011).

123. Costa, E., Coelho, M., Ilharco, L.M., Aguiar-Ricardo, A. & Hammond, P.T. Tannic Acid Mediated Suppression of PNIPAAm Microgels Thermoresponsive Behavior. *Macromolecules* **44**, 612-621 (2011).

# CHAPTER 2:

## Synthesis of Well-defined Stimuli-responsive Microbeads in Supercritical $CO_2$

# 2 Synthesis of Well-defined Stimuli-responsive Microbeads in Supercritical $CO_2$

The initial goal of this project was the development of well-defined cell-sized hydrogel microbeads. The preparation of polymeric particles in supercritical carbon dioxide ($scCO_2$) presents many advantages for the biomedical field over conventional processes due to the easy elimination of trace contaminants, rendering biocompatible pure particles. The use of smart polymers facilitates further tuning of the microbead properties, according to the specific application. Herein the optimization of the poly(*N*-isopropylacrylamide) (PNIPAAm) synthesis strategy, the effect of using different cross-linkers, cross-linking densities and co-monomers is described for obtaining hydrogel microbeads with tailored swelling, responsive behavior, permeability and rheological/mechanical properties. The microbeads obtained with well-defined morphology and "cell-like" size (under physiological conditions), with potential for the aimed biosensing application, were characterized thoroughly.

## 2.1 Experimental Section

### 2.1.1 Materials

*N*-isopropylacrylamide (NIPAAm; 97 % purity), *N,N'*-methylenebisacrylamide (MBAm; 99 % purity), di(ethyleneglycol) dimethacrylate (DEGDMA, 95% purity), glycerol dimethacrylate (GDMA; mixture of isomers 85 %), poly(ethylene glycol) acrylate (PEGa, average $M_n \approx 375$), methacrylic acid (MAA, ≥ 98.0% purity), 2,2' -azobis(isobutyronitrile) (AIBN, 98 % purity) and phosphate buffer saline (PBS; 10 mM pH 7.4), AccutaseTM, MTT formazan and MTT solvent (0.1 N HCl in anhydrous isopropanol) were purchased from Sigma-Aldrich. Acetic acid glacial (99.7% purity) was obtained from Panreac and sodium acetate trihydrate (99.5% purity) from Riedel-de Haën. Krytox 157 FSL was purchased from DuPont. Carbon dioxide was obtained from Air Liquide with 99.998 % purity. RPMI-1640 (a Roswell Park Memorial Institute medium), trypan blue and fetal bovine serum (FBS) used in cell culture were purchased from Invitrogen. L929 cells were obtained from DSMZ, Germany. All materials were used without any further purification. The deionized water was purified through a Milli-Q system and had a resistivity greater than 18 MΩ.cm.

### 2.1.2 Preparation of PNIPAAm hydrogel beads

Synthesis of cross-linked PNIPAAm particles was carried out on a high-pressure apparatus already described in literature.[1] In a typical procedure, monomer, initiator (2 wt% relative to monomer amount), cross-linker (0.74 mol% relative to the amount of monomers) and stabilizer (Krytox) were loaded into a high-pressure cell (33 mL volume), which was then sealed, purged and tested for leakage. Liquid $CO_2$ was added to the cell using a high-pressure compressor. The cell was immersed in a thermostatized water bath and additional $CO_2$ was added to top up the pressure until the desired set point.

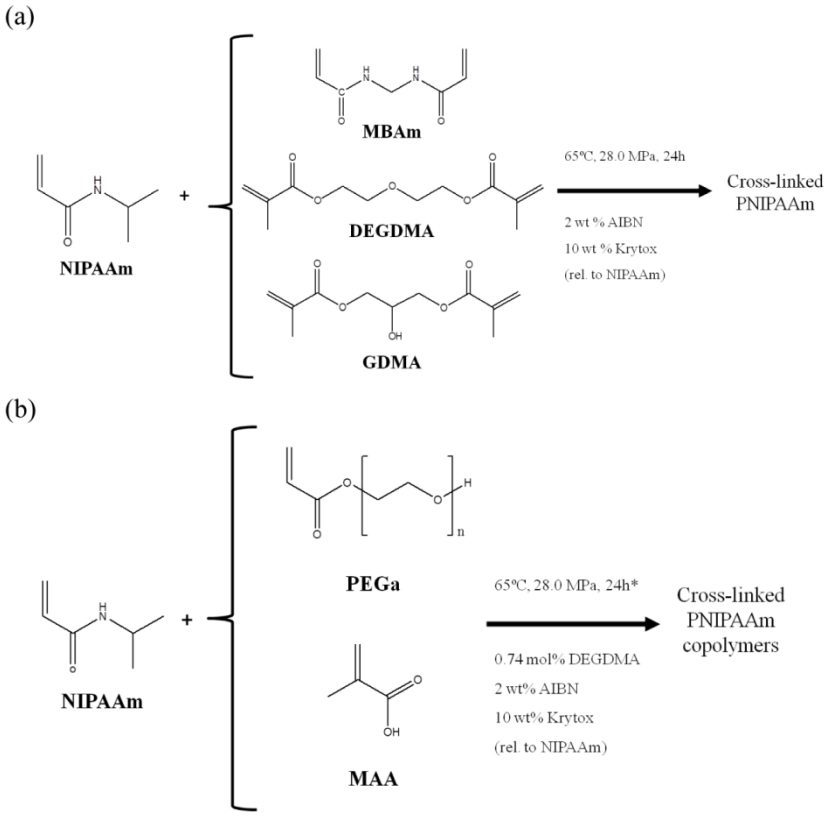


**Figure 2.1** Synthesis of (a) cross-linked PNIPAAm homopolymer hydrogels; and of (b) cross-linked PNIPAAm copolymer hydrogels in $scCO_2$ (*reaction progressed until 36 and 48 hours for poly(NIPAAm-co-MAA) 85:15 and 80:20 copolymers, respectively).

All polymerization reactions were conducted at 65 ºC and 28.0 MPa for 24 hours using different cross-linkers for the PNIPAAm homopolymer microbeads, as outlined in Figure 2.1a, and with different relative molar fractions of PEGa and MAA for the PNIPAAm copolymeric microbeads (for the poly(NIPAAm-co-MAA) 85:15 and 80:20 the reaction was performed for 36 and 48 hours, respectively), as outlined in Figure 2.1b. As the reaction progressed white particles began precipitating inside the cell. The obtained polymer was washed continuously with fresh $CO_2$ for 1

hour to remove the stabilizer and any residual monomer or cross-linker since all the reactants are soluble in $CO_2$ in those conditions. After venting the $CO_2$ the resulting polymer was a white, dry, free flowing powder.

### 2.1.3 Cloud-point determination of the polymerization initial feed

In order to optimize the preparation of PNIPAAm cross-linked microbeads, cloud point measurements were performed to determine the experimental conditions at which a homogeneous initial mixture would be obtained for the homopolymers.[2] The cloud point measurements were performed in a high-pressure variable volume steel cell with a front sapphire window and a bottom screw-tap connected to a Teflon piston that can be moved by pressurizing water (Figure 2.2).

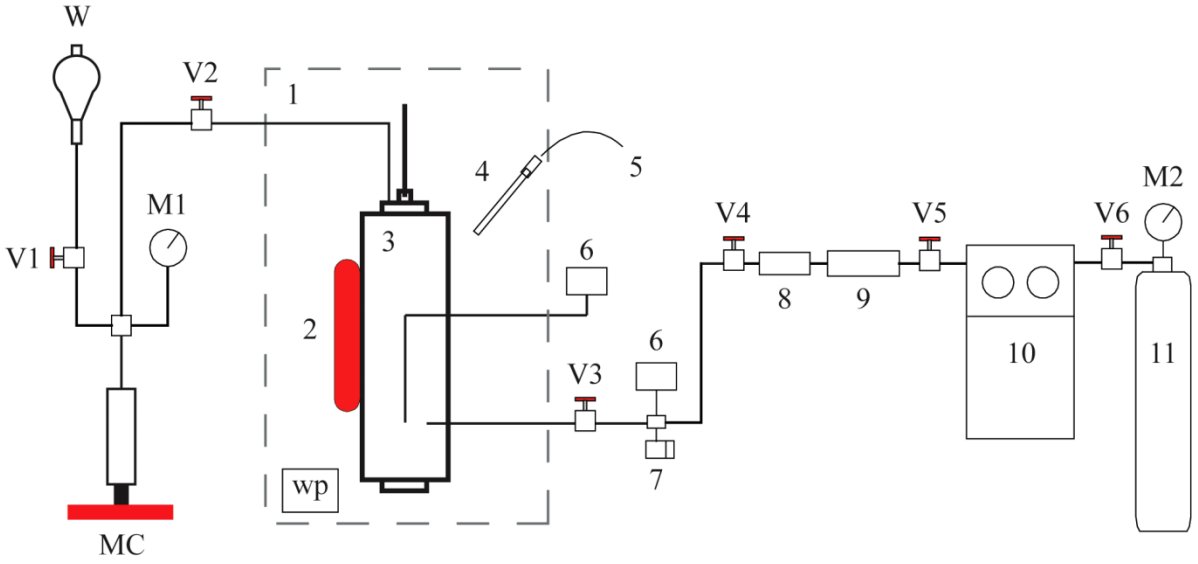


**Figure 2.2** Schematic representation of the apparatus used for cloud point determination: 1 - water bath; 2 - immersible stirrer; 3 - high-pressure variable volume cell; 4 - thermocouple; 5 - temperature controller; 6 - high-pressure manometer; 7 - rupture disk; 8 - check valve; 9 - line filter; 10 - high-pressure pneumatic compressor; 11 - $CO_2$ cylinder; W - water separatory funnel; MC - manual compressor; wp - water recirculation pump; M1, M2 - Bourdon manometer.

Pressure was generated via a hand pump (High-Pressure Equipment Co., model 87-6-5) and monitored with a Bourdon manometer. The monomer, cross-linker and polymerization stabilizer were introduced into the high-pressure cell at the same proportions as used for the polymerization reactions (initiator was not introduced to prevent polymerization). The high pressure cell was immersed in a thermostated water bath at 65 °C and carbon dioxide was introduced into the cell using a high-pressure compressor (NWA PM-101), being monitored using a pressure manometer (Keller, model Leo 2). Carbon dioxide was slowly added to the cell until a homogenous phase was observed. After

each carbon dioxide addition the Teflon piston was moved back to its original position by pressurizing water with the hand pump. The system was allowed to equilibrate for 10 min. Stirring was provided by means of a magnetic stir bar. Afterwards the pressure was slowly decreased until two phases appeared. The cloud point pressure recorded was the pressure at which the cell became cloudy. The cell volume for the cloud point was determined by measuring the piston movement. Cloud points were measured and reproduced five times.

### 2.1.4 Polymers and microbeads characterization

Polymer morphology was evaluated using scanning electron microscopy (SEM) in Hitachi S-2400 for the PNIPAAm homopolymers and a JEOL JSM-7001F for the copolymers, with an accelerating voltage set to 15 kV. All samples were gold coated before analysis. For the polymers with a well-defined morphology, particle size of dry dispersions was measured by image analysis using a Malvern G3 automated optical microscopy system (Malvern Instruments, UK). The particle size distribution was calculated using descriptive statistics from OriginPro 8.04 software, for a total population above 1500 particles. The values presented are relative to the average diameter, $\bar{d}$ (sample population mean) and the sample standard deviation, *s*.

Particle size distribution in aqueous environments can typically be determined through dynamic light scattering (DLS) or using a Coulter counter. However particle diameter was too large for DLS or too water swollen for the latter method, giving rise to unreliable measurements. For the PNIPAAm homopolymers and copolymeric microbeads, aqueous dispersions of the beads were observed using a Zeiss Axioskop 2 optical microscope (OM) at 400× magnification with temperature control (THMS 600 hot stage, Linkam Scientific Instruments, UK). Bead size was evaluated from 22 to 40 ºC in Milli-Q water and 10 mM PBS buffer (the latter for selected microbeads), by image analysis of more than 100 different particles using Image J software, NIH. For the pH-sensitive PNIPAAm copolymers the swelling behavior was also assessed in 10 mM acetate pH 4 buffer with the same salt composition as the commercial PBS (150 mM of salts). The error presented for these values is relative to the sample standard error of the mean $SE_{\bar{d}}$, which is calculated according to equation 2.1:

$$\boldsymbol{SE_{\bar{d}} = \frac{s}{\sqrt{n}}} \qquad \text{(Equation 2.1)}$$

in which *n* refers to the analyzed sample size.

The cross-linked polymers were insoluble, thus making impossible to determine the molecular weight of the obtained samples. Polymers were analyzed using Fourier Transform Infrared Spectroscopy (FT-IR) in a Thermo Nicolet 6700 FT-IR equipped with a Germanium ATR, using a DTGS/KBr detector (256 scans, 4 $cm^{-1}$ resolution). Polymer samples were partially solubilized in deuterated chloroform

($CDCl_3$) to perform nuclear magnetic resonance (NMR) on a Bruker ARX 400 MHz spectrometer. $^{1}H$, $^{13}C$ and $^{19}F$ NMR spectra were recorded demonstrating the synthesis of PNIPAAm with high purity as no residual monomer was detected (data not shown). Polymer yield was determined gravimetrically. The thermal features of the hydrogel particles were further investigated through differential scanning calorimetry (DSC). Analysis was performed in a TA Instruments Q1000 DSC from 15 to 40 ºC at a 2 ºC.min$^{-1}$ rate under a dry nitrogen atmosphere (50 mL.min$^{-1}$ flow rate). Calibration for the temperature and heat flow ranges was carried out using a pure indium standard ($T_m$ = 156.6 ºC and $\Delta H_m$ = 28.4 J.mol$^{-1}$). For pH-sensitive poly(NIPAAm-co-MAA) polymers DSC is not a suitable method to determine LCST. Therefore samples were dispersed at a concentration of 0.2 mg/mL in 10 mM acetate buffer pH 4 and 10 mM PBS buffer pH 7.4 and turbidimetric analysis was performed using a UV/VIS spectrometer PerkinElmer Lambda 35 (PerkinElmer Inc., USA), equipped with a water-jacketed cell holder coupled to a temperature-controlled circulating bath. Measurements were performed at 600 nm where the copolymer has no absorption bands. Turbidity was recorded upon heating from 24 $^{o}$C up to a temperature at which an absorbance plateau was clearly defined (after 5 min of equilibration for each temperature step) and cooling back to 24 $^{o}$C. The temperature of the sample dispersion was continuously monitored by a thermocouple inside the cuvette. The increase in turbidity with increasing temperature is a result of the volume phase transition. The LCST for the thermoresponsive samples was calculated as the inflexion point of the normalized absorbance to temperature curve using OriginPro 8.04 software.

For the rheological characterization of the microbeads, all samples were left in equilibrium in 10 mM PBS buffer pH 7.4 overnight at 20 $^{o}$C. Rheological measurements were performed on a Bohlin Gemini HR$^{nano}$ rotational rheometer (Malvern Instruments, UK). Firstly, a strain amplitude sweep was performed to determine the linear viscoelastic behavior region. Oscillatory measurements, at 20 $^{o}$C, were then performed at frequencies ranging from 1 to 100 Hz and 1 % strain (within the linear viscoelastic range) to determine the complex dynamic modulus $G^*$ at these conditions. $G^*$ consists of a real component, the storage modulus $G'$, related to the elastic behavior of the material, and an imaginary component, the loss modulus $G''$, that translates the viscous component.

PNIPAAm hydrogels were tested for cytotoxicity following the ISO 10993-5 guidelines. For that purpose, triplicates of the polymers were placed in polystyrene tubes at a concentration of 10 mg/mL in RPMI – 1640 media with 10 vol % of FSB and kept in an incubator (37 ºC, 5 % $CO_2$, fully humidified) for 1 day. The liquid extracts were further diluted to 1 mg/mL and 0.1 mg/mL concentration. After sterile filtration, the media conditioned with the polymers was used to culture L929 mouse fibroblasts (initial density $10\times10^4$ cells/mL) in 24-well plates for 36 hours. The cell metabolic activity was determined by analyzing the conversion of MTT (yellowish color) to its formazan derivative (purple – absorbance at 570 nm after a 3 hour incubation at 37 ºC) using a MTT-based cell growth determination kit. The results were normalized to the negative control for cytotoxicity (fresh RPMI medium).

## 2.2 Poly(*N*-isopropylacrylamide) Hydrogel Microbeads

Smart hydrogel particles are three dimensional cross-linked polymer networks exhibiting reversible swelling responses to external stimuli, namely changes in temperature, pH and ionic strength, and have been explored for a diverse range of biotechnological applications.[3] Poly(*N*-isopropylacrylamide) (PNIPAAm) is a well-known thermosensitive polymer in which the volume phase transition occurs at a lower critical solution temperature (LCST) of about 30-32 $^{o}$C.[4] The microgel collapse above the LCST is characterized by an entropy-driven weakening of the water-amide hydrogen bonds and increasing hydrophobic interactions among isopropyl groups, leading to water expulsion.[4,5] Different strategies may be pursued to control the water uptake and mechanical properties of hydrogels: altering the co-monomer composition and/or cross-linking density, and changing the experimental conditions under which the polymer is formed.[6] In this work, cell-sized PNIPAAm microgels with well-defined morphology and mechanical properties were prepared for their application on the development of biosensing platforms to assess cell microenvironments in tissue cultures. Studies have demonstrated that the particle size plays a key role in their adhesion to and interaction with biological cells. While nanoparticles are suitable for drug delivery applications, cell-sensing applications require particle sizes higher than 0.5 – 1 μm to prevent cellular uptake through endocytosis[7] and to be observed using conventional cell culture tools: confocal laser scanning microscopy, flow cytometry, etc. PNIPAAm-containing microgels have been proposed as building blocks for different sensing devices in which a physicochemical change in the hydrogel is monitored and related to antigen/antibody interactions,[8] an immobilized enzyme reaction[9] or ligand-binding event[10]. Furthermore PNIPAAm may be used to minimize biofouling of devices through adherent cells release upon thermal cycling, thus extending lifetime and efficiency of implantable biosensors.[11]
Synthesis of PNIPAAm cross-linked polymers in scCO$_2$ has already been reported in literature.[1] The authors prepared sub-micron PNIPAAm particles using *N,N'*-methylenebisacrylamide (MBAm) as cross-linker through free radical polymerization in scCO$_2$. There are a great number of publications describing the preparation of sub-micrometer polymer and composite particles in scCO$_2$.[12-15] By contrast, there are very few reports on the synthesis of spherical particles with diameters above the micrometer range.[16,17] In this work, an improved strategy for the polymerization of PNIPAAm that enables the preparation of biocompatible cell-sized particles with defined morphology and tuned rheological behavior is described. Previous studies on PNIPAAm nanogels have shown the influence of cross-linking density on the rheological behavior of concentrated nanogel suspensions.[18] In fact when the microgel particles are densely packed elastic properties arise which are dependent on cross-linking. The cross-linking agent was used to control the elastic modulus of the micron-sized beads. Elastic modulus determined from rheological measurements has been correlated with sample stiffness in several studies.[19,20] In this chapter the impact of the specific composition of the cross-linkers used

on the structural, morphological, rheological and thermal features of the microgels was assessed. Finally, cytotoxicity tests on the obtained smart microgels were conducted to assess their biomedical applicability.

### 2.2.1 Results and discussion

PNIPAAm hydrogels cross-linked with MBAm had already been prepared through precipitation polymerization in supercritical $CO_2$, yielding defined particles although aggregated.[1] In precipitation polymerizations, both monomer and initiator are soluble in the continuous supercritical phase, but as the polymer grows the insoluble polymer chains precipitate and the particles tend to form an agglomerated powder.[15] A possible strategy to further improve the PNIPAAm polymer morphology and obtain large particles is to both follow a dispersion polymerization approach, through the addition of a stabilizer, and increase the initial monomer concentration – Figure 2.3.

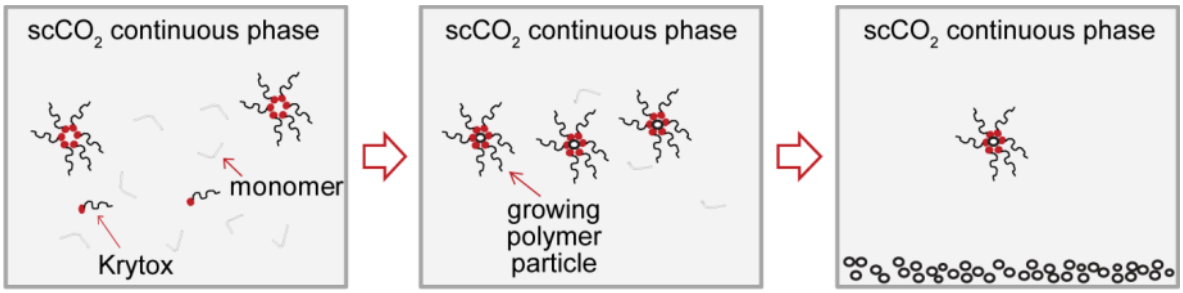


**Figure 2.3** Dispersion polymerization in $scCO_2$ with Krytox as a stabilizer.

The successful polymerization stabilizers in $scCO_2$ media combine polymer- and $CO_2$-philic moieties, enabling polymer chain growth in the continuous phase to higher degrees of polymerization and providing some degree of control over the polymer morphology[21] – Figure 2.2. In the literature, polymeric microbeads with controlled morphology prepared from methylmethacrylate[16] and diethyleneglycol dimethacrylate[22] were obtained by dispersion polymerization in $scCO_2$ using a commercially available carboxylic acid terminated perfluoropolyether, Krytox 157 FSL (DuPont) – Figure 2.4. This stabilizer has many advantages over other available siloxane, fluorinated or carboxylic acid based block copolymers, as it is inexpensive and easily removed from the obtained polymer by washing with fresh $CO_2$.[16] In both referred literature examples, it was suggested that Krytox, as a pseudo-graft stabilizer, stabilized the growing polymer chain through H-bonding between Krytox carboxylic terminal group and the carbonyl of the ester group of either methylmethacrylate[16] or diethyleneglycol dimethacrylate[22]. The same mechanism can be foreseen for the stabilization of NIPAAm polymerization, involving the NIPAAm amide group. As for the contribution of the initial monomer concentration, larger particles are typically obtained by increasing the initial monomer feed,

since the presence of more monomer leads to a higher solvency of the medium for the growing polymer and stabilizer, enabling higher degrees of polymerization.[17,23]

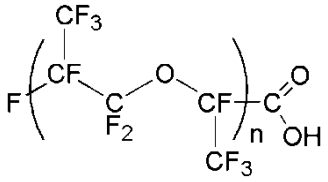

**Figure 2.4** Krytox 157 FSL (DuPont): carboxylic acid terminated perfluoropolyether ($M_n$~2500).

Using the low cross-linking density of 0.74 mol% of cross-linker to NIPAAm amount in the initial feed as a benchmark for the optimization of PNIPAAm microbeads synthesis (corresponding to 1 wt% of MBAm relative to the amount of NIPAAm described by Temtem *et al.*), the solubility of NIPAAm mixed with different cross-linkers and 10 wt% of Krytox in supercritical $CO_2$ was assessed through cloud point determination, mimicking polymerization initial conditions – Table 2.1. From the collected data it is possible to observe that the mixture solubility is quite similar irrespective of the cross-linker as the latter was maintained at a very low concentration.

**Table 2.1** Cloud points for the mixture of NIPAAm, cross-linker (0.74 mol% relative to NIPAAm) and Krytox (10 wt% relative to NIPAAm) at 65 $^{o}$C.

| **Cross-linker** | ***w* mixture (wt% relative to $CO_2$)** | **Cloud-point p (MPa)** |
|---|---|---|
| MBAm | 5.2 | 25.0 |
| DEGDMA | 5.3 | 23.8 |
| GDMA | 4.7 | 24.7 |

Initially, polymerizations using MBAm as a cross-linker, were performed below and above the initial feed solubility limit. Well-defined and monodisperse particles were obtained for an initial feed of 7.7 wt% NIPAAm to $CO_2$ and 10 wt% Krytox relative to the monomer, when compared with the initial benchmark composition described by Temtem *et al.* (3.8 wt% NIPAAm to $CO_2$) plus a small amount of stabilizer added (3 wt% of Krytox to monomer) - Figure 2.5.

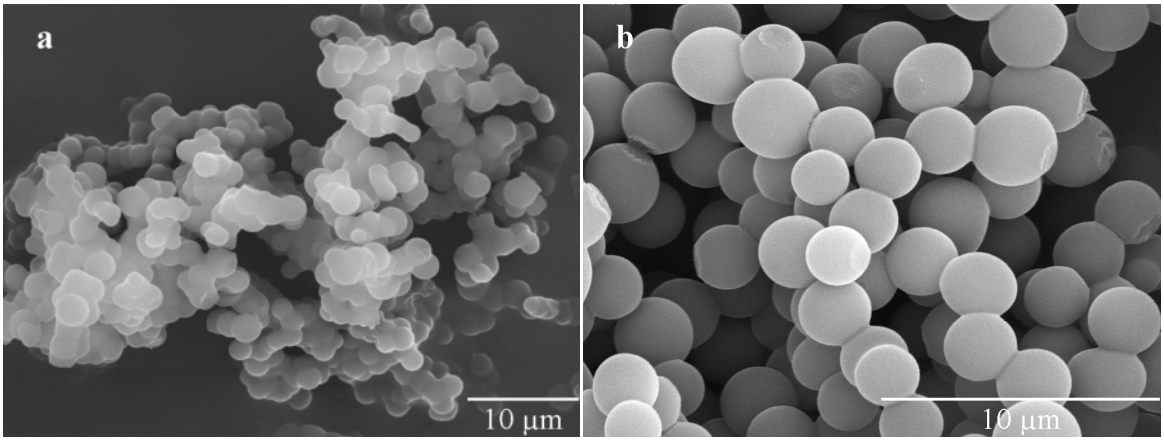


**Figure 2.5** Scanning electron microscopy (SEM) images of PNIPAAm microbeads cross-linked with 0.74 mol% of MBAm (relative to NIPAAm amount) prepared under different conditions: (a) 3.8 wt% monomer relative to $CO_2$ amount (conditions described in Temtem *et al.*) and 3 wt% stabilizer relative to monomer amount; (b) 7.7 wt% monomer relative to $CO_2$ amount and 10 wt% stabilizer relative to monomer amount.

On the above SEM micrographs the stabilizing effect of Krytox on controlling polymer morphology becomes evident as well as the contribution of larger initial amounts of monomer in obtaining larger beads. Although these optimized conditions yielded an improved morphology, the polymerization was carried out in heterogeneous conditions, as the initial feed concentration was above the determined solubility limit by cloud point measurements (Table 2.1). Indeed during the polymerization a liquid phase dispersed in the supercritical phase was observed and a white hard deposit was formed at the bottom of the high-pressure vessel in the end of the polymerization. Consequently, the polymerization yield for MBAm cross-linked PNIPAAm microbeads was lower than literature values for other polymers synthesized by dispersion polymerization with Krytox in scCO$_2$[16,22], as shown in Table 2.2.

**Table 2.2** Effect of the cross-linker on the preparation of NIPAAm in supercritical carbon dioxide: 7.7 wt% NIPAAm (relative to $CO_2$), 10 wt% of Krytox (relative to monomer) and 2 wt% of AIBN.

| cross-linker | molar fraction (mol%) | yield (%) | diameter, $\bar{d}$ (μm)[a] | LCST (ºC)[b] |
|---|---|---|---|---|
| MBAm | 0.74 | 72 | 3.2±0.4 | 30.1±0.1 |
| DEGDMA | 0.74 | 59 | 3.8±0.3 | 30.6±0.0 |
| | 1.4 | 64 | 3.6±0.4 | 30.2±0.2 |
| GDMA | 0.74 | 72 | 3.8±0.6 | 30.4±0.1 |

[a] determined from particle analysis in an automated optical microscope: $\bar{d} \pm s$.
[b] as determined from DSC analysis.

Having optimized the PNIPAAm synthesis with MBAm to obtain large spherical microbeads, polymerizations of NIPAAm with more hydrophilic cross-linkers were carried out. The impact of cross-linker hydrophilicity on PNIPAAm physical and thermal features was assessed, as shown in Table 2.2. In fact the cross-linkers GDMA and DEGDMA may be considered more hydrophilic than MBAm due to the presence of a hydroxyl group for GDMA and of ethylene glycol for DEGDMA

(Figure 2.1a).[24] The initial feed was maintained at 7.7 wt% NIPAAm relative to $CO_2$ and 0.74 mol% cross-linker relative to monomer, respectively, as the compliance, swellability and thermoresponsiveness of PNIPAAm hydrogels was shown to decrease with cross-linking density, since cross-linked regions do not participate in the conformational transitions.[1,25] The polymerization reactions were again carried out under heterogeneous conditions, impairing polymerization yield.

Figure 2.6 shows the FT-IR spectra in the region 1400-1800 $cm^{-1}$ for the synthesized PNIPAAm cross-linked polymers, in which the characteristic PNIPAAm Amide I at 1643 $cm^{-1}$ and the Amide II at 1540 $cm^{-1}$ bands may be observed.[26] All spectra are similar with respect to composition and peak intensities with the exception of the PNIPAAm polymer cross-linked with DEGDMA, in which the strong stretch vibration of the cross-linker free carbonyl groups may be observed as a shoulder at 1725 $cm^{-1}$. This vibration becomes more intense for the PNIPAAm with 1.4 mol% DEGDMA, being an indication of successful incorporation of increasing cross-linker.

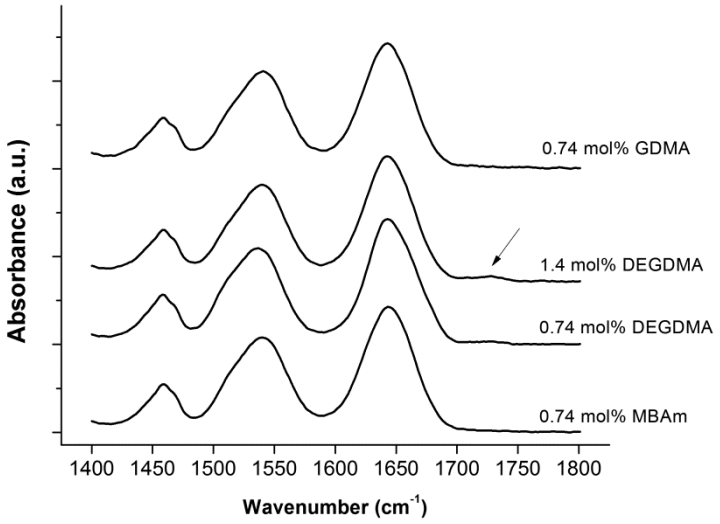


**Figure 2.6** (a) FT-IR spectra for PNIPAAm cross-linked with 0.74 mol% MBAm, DEGDMA and GDMA and 1.4 mol% DEGDMA (relative to NIPAAm amount). The arrow highlights the υC=O of DEGDMA.

In regards to the microgels morphology, well-defined spherical particles with a smooth surface were obtained for both PNIPAAm cross-linked with DEGDMA and GDMA, as shown in Figure 2.7. Table 2.2 presents the average diameter of the microbeads. As it can be seen the average diameter for the microbeads cross-linked with DEGDMA and GDMA is higher than with MBAm. Furthermore, an increase in the amount of DEGDMA leads to the formation of smaller particles, as the number of nuclei generated in the reaction increases, which is in agreement to literature.[1]

Figure 2.8 presents the particle size distribution for the obtained polymers with the same initial molar fraction of cross-linker. Although they have similar average diameters, particles cross-linked with

GDMA present a broader size distribution, as illustrated by the SEM micrograph as well. Particles cross-linked with DEGDMA presented the narrowest particle size distribution.

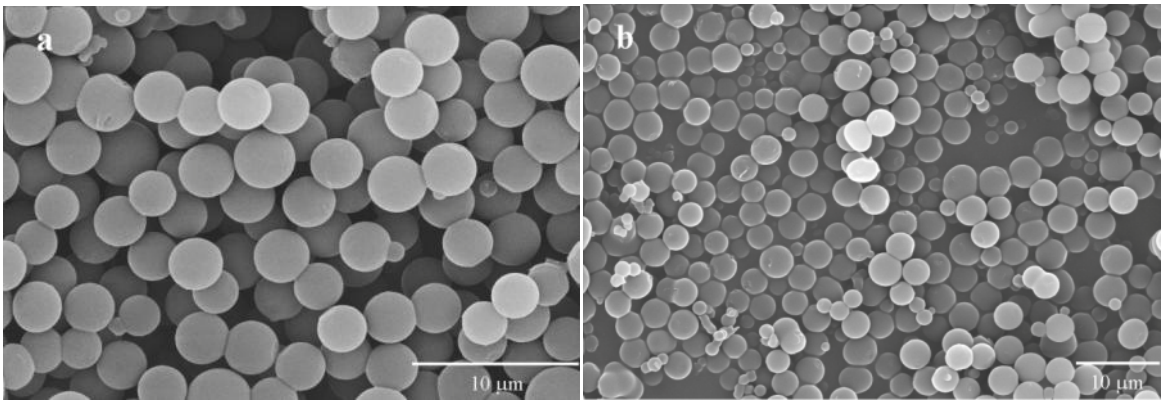


**Figure 2.7** Scanning electron microscopy images of PNIPAAm microbeads prepared from an initial feed containing 7.7 wt% monomer relative to $CO_2$ amount and 10 wt% stabilizer relative to monomer amount and using 0.74 mol% of (a) DEGDMA and (b) GDMA (relative to NIPAAm) as cross-linkers.

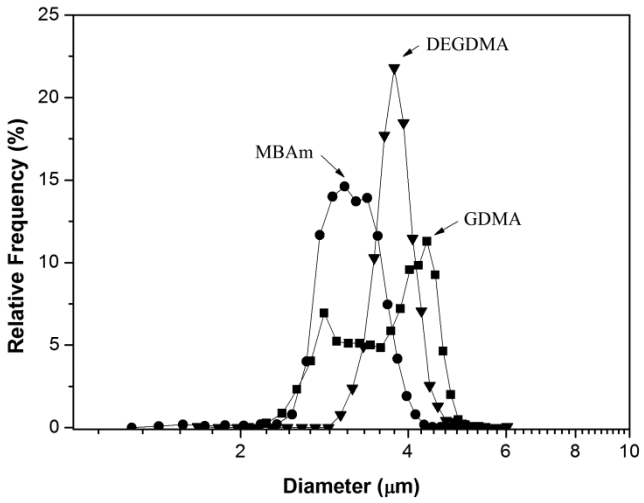


**Figure 2.8** Particle size distribution of PNIPAAm microbeads prepared using 0.74 mol% (relative to NIPAAm) of MBAm (●); DEGDMA ( ▼) and GDMA (■). Particle size was determined using an automated optical microscope for particle characterization.

Since the largest particles with narrower size distribution were prepared with 0.74 mol% DEGDMA cross-linker, the synthesis was further investigated, by performing a polymerization close to the solubility limit of the initial mixture in $CO_2$ at 65 $^oC$ and 28.0 MPa: initial NIPAAm concentration of 4.8 wt% relative to $CO_2$. The polymerization yield increased to 91 % in comparison with the previous polymerizations and no deposit was obtained. SEM micrographs showed that the morphology of these PNIPAAm particles was totally similar to the described beforehand, but the average particle diameter decreased from 3.8±0.3 μm to 3.6±0.7 μm (as determined by particles analysis with an automated optical microscope). These observations indicate that particle size can be possibly fine tuned by

changing the initial mixture concentration, while maintaining well-defined and monodisperse particle morphology, allowing the design of thermoresponsive microgels in $scCO_2$ according to the desired application.

Aqueous dispersions of PNIPAAm microbeads were observed under an optical microscope with temperature control. The PNIPAAm microbeads thermoresponsive behavior can be clearly observed in Figure 2.9. Bead diameter decreased with increasing temperature, presenting a sharp collapse in diameter around the LCST. Below the LCST, PNIPAAm is able to uptake water due to hydrogen-bonding between water molecules and the PNIPAAm hydrophilic amide group, leading to microgel swelling. Above the LCST, PNIPAAm polymer chains shift to a hydrophobic conformation and the microgels collapse, releasing water.[5] Moreover, PNIPAAm microbeads cross-linked with the hydrophilic GDMA and DEGDMA cross-linkers have larger diameters when dispersed in water, especially at temperatures below the LCST. For PNIPAAm particles cross-linked with 1.4 mol % of DEGMA the diameter was lower than with 0.74 mol%, as expected. When dispersing the PNIPAAm 0.74 mol% DEGDMA in PBS buffer, the variations in size with temperature are much less significant and the diameters are overall smaller, since the presence of salts screen the polymer-water interactions.

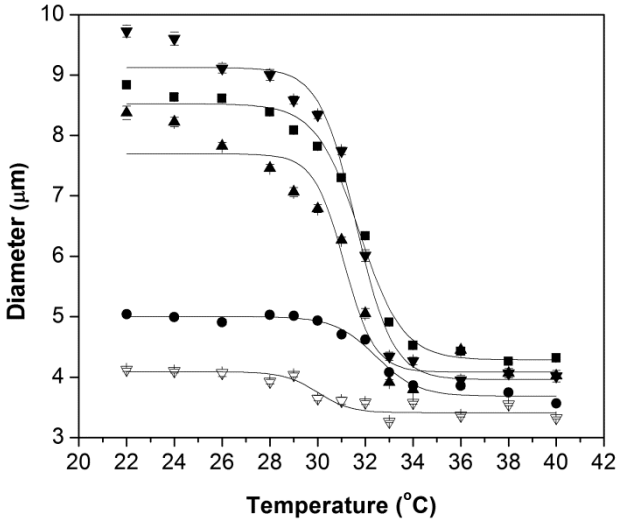


**Figure 2.9** Diameter of PNIPAAm microgels with different cross-linkers ($\bar{d} \pm SE_{\bar{d}}$), as determined from optical micrographs after equilibrium swelling from 22 to 40 °C in Milli Q water: 0.74 mol% MBAm (♦); 0.74 mol% DEGDMA (▼); 1.4 mol% DEGDMA (▲) and 0.74 mol% GDMA (■). The diameter for the PNIPAAm 0.74 mol% DEGDMA sample dispersed in PBS (▽) is also depicted, as reference for the ionic strength impact on microgel swelling. The lines refer to sigmoidal curve fittings of the data, represented herein just to facilitate interpretation.

The volume swelling ratio ($Q$) of the PNIPAAm particles was evaluated from the increase in particle volume when aqueous dispersions of the beads were equilibrated at 24 ºC and 40 ºC, as described in equation 2.2:

$$\boldsymbol{Q = \frac{V_{aq,T(°C)}}{V_{dry}}} \qquad \text{(Equation 2.2)}$$

where $V_{aq,T(\,^oC)}$ refers to the average volume of beads in aqueous solution and $V_{dry}$ is the volume of a dry bead calculated from the determined size distribution.

The determination of the microgel swelling is important not only to characterize the microbeads in terms of water content, but also to estimate their mesh size ($\xi$), or the linear distance between two cross-links, through the Flory and Rehner equilibrium swelling theory[27] – equation 2.3:

$$\boldsymbol{\xi = \alpha r_0 = Q^{1/3}\left[2C_n\left(\frac{\overline{M_c}}{\overline{M_r}}\right)\right]^{1/2} l} \qquad \text{(Equation 2.3)}$$

in which the end-to-end distance in the unperturbed state ($r_0$) was calculated as shown in the above equation. In equation 2.3, $C_n$ refers to the polymer characteristic ratio, $\overline{M_c}$ is the molecular weight between consecutive cross-links, $l$ is the carbon-carbon bond length (1.54 Å), and $\overline{M_r}$ is the molecular weight of the repeating unit. The values for $C_n$ used for each polymer and copolymer are outlined in Table 2.3. The molecular weight between cross-links was assumed as the theoretical one – equation 2.4.

$$\boldsymbol{\overline{M_c} = \frac{\overline{M_r}}{2X}} \qquad \text{(Equation 2.4)}$$

where $X$ refers to the cross-linking ratio.

**Table 2.3** Parameters for the calculation of microgels mesh size of PNIPAAm microbeads.

| Parameters | values |
|---|---|
| $C_n$ | 10.6*[29] |
| $\overline{M_r}$ (g/mol) | 113.16 |
| $\overline{M_c}$ (g/mol) | 7646 ($X$ = 0.74 mol%) |
| | 3823 ($X$ = 1.4 mol%) |

* value for PNIPAAm in water at 20 $^o$C; herein it was used for the estimation of the mesh size at all conditions.

The mesh size may be regarded as a measure of the microgel porosity in aqueous environment, being a theoretical prediction of the microgel permeability. Table 2.4 contains the calculated swelling and mesh size for the cross-linked microgels dispersed in water (and in physiological PBS buffer for the optimal PNIPAAm 0.74 mol% DEGDMA beads).

**Table 2.4** Volume swelling ratio and mesh size for PNIPAAm microbeads dispersed in water below (24 °C) and above the LCST (37 °C).

| Monomer | | diameter, $\bar{d}$ (μm)[ǂ] | | swelling ratio, $Q$[ǂ] | | mesh size, $\xi$ (nm)[ǂ] | |
|---|---|---|---|---|---|---|---|
| | | **24 °C** | **40 °C** | **24 °C** | **40 °C** | **24 °C** | **40 °C** |
| $MBA_m$ | | 5.0 ± 0.0 | 3.6 ± 0.0 | 3.8 ± 0.2 | 1.4 ± 0.1 | 9.1 ± 0.0 | 6.5 ± 0.0 |
| DEGDMA | 0.74 mol% | 9.6 ± 0.1 | 4.0 ± 0.1 | 16 ± 0.7 | 1.2 ± 0.1 | 15 ± 0.1 | 6.2 ± 0.1 |
| | | 4.1 ± 0.0* | 3.3 ± 0.0* | 1.3 ± 0.0* | 0.67±0.02* | 6.3 ± 0.0* | 5.1±0.0* |
| | 1.4 mol% | 8.2 ± 0.1 | 4.0 ± 0.1 | 11.9 ± 0.5 | 1.4 ± 0.1 | 9.4 ± 0.1 | 4.6 ± 0.0 |
| GDMA | | 8.6 ± 0.1 | 4.3 ± 0.0 | 11.7 ± 0.6 | 0.6 ± 0.1 | 13 ± 0.1 | 6.6 ± 0.0 |

[ǂ] average ± standard error of the mean for diameter ($SE_{\bar{d}}$), swelling ratio ($SE_Q$) and mesh size ($SE_\xi$).
* dispersed in PBS.

The swelling of hydrogel networks depends on the balance between the gain in entropy from water incorporation and the elastic retractive forces of the elongated polymer chains. From the above table, the contribution of cross-linker hydrophilicity and lower cross-linking densities for larger swelling degrees becomes clearer. The microbeads cross-linked with DEGDMA and GDMA present higher swelling ratios than the MBAm cross-linked PNIPAAm particles. Thus, the larger observed swollen particle sizes are mostly due to increased water uptake and stabilization when PNIPAAm was cross-linked with DEGDMA or GDMA. These observations may also be correlated with the DSC results in Table 2.2, in which a slight increase in LCST was observed for PNIPAAm samples with DEGDMA and GDMA cross-linkers, showing that polymer-water interactions are more favorable when these hydrophilic moieties were present. The increase in DEGDMA cross-linking or the presence of salts, leads to a decrease in swelling below LCST, as expected. Another interesting observation is the ability of PNIPAAm in retaining water even above the LCST, despite the hydrophobic conformation of the polymer chains, which agrees with previous reports and theoretical predictions.[29]
From the estimated values for microgel mesh size, it is possible to infer that the microgels have the potential for differential permeation of biomacromolecules, according to changes on environmental temperature. This feature could be explored for the targeted protease sensor in this project. For example, a metalloproteinase such as MMP-1, with a diameter around 5.7 nm (*vide* Chapter 1), could theoretically permeate across a PNIPAAm 0.74 mol% DEGDMA microgel below the polymer LCST in physiological salt conditions, while above the LCST it could not.

When placing the synthesized PNIPAAm polymers under equilibrium swelling, a weak macroscopic gel is formed by aggregation of the microgel particles, as indeed observed in previous studies with PNIPAAm colloids.[18] This allows the determination of the viscoelastic properties of the PNIPAAm microbeads as a bulk under equilibrium swelling by oscillatory measurements at 20 °C, below the

LCST. The effect of cross-linker content on the gels rheological behavior is more important when the polymer is fully swollen at a temperature below the LCST. In the swollen state physical entanglements are nearly nonexistent and the mechanical properties of the material are strongly dependent on the network cross-linking.[6] The gels exhibited a typical gel-like behavior with a high degree of elasticity as the dynamic elastic modulus, *G'*, was weakly dependent on frequency and much higher than the loss modulus, *G''*, over the entire frequency range (*vide* Figure 2.10). Microgels cross-linked with hydrophilic cross-linkers had lower elastic modulus, *G*', exhibiting a more compliant mechanical behavior, in agreement with a larger water uptake shown on the equilibrium swelling studies. In fact the elastic moduli of PNIPAAm microgels cross-linked with DEGDMA and GDMA were about two to three-fold lower than for PNIPAAm microgels containing MBAm, enabling the possibility of fine tuning microgel mechanical properties by varying the cross-linker. It would be interesting to assess the rheological behavior of these microgels at a physiological temperature for potential biological applications. However at temperatures above the LCST the microgels suspensions flocculate, thus making impossible to perform measurements with this technique, as already observed in previous rheological studies with PNIPAAm nanogels.[18] Other alternative advanced techniques such as atomic force microscopy indentation could be used for PNIPAAm gels above the LCST.[19]

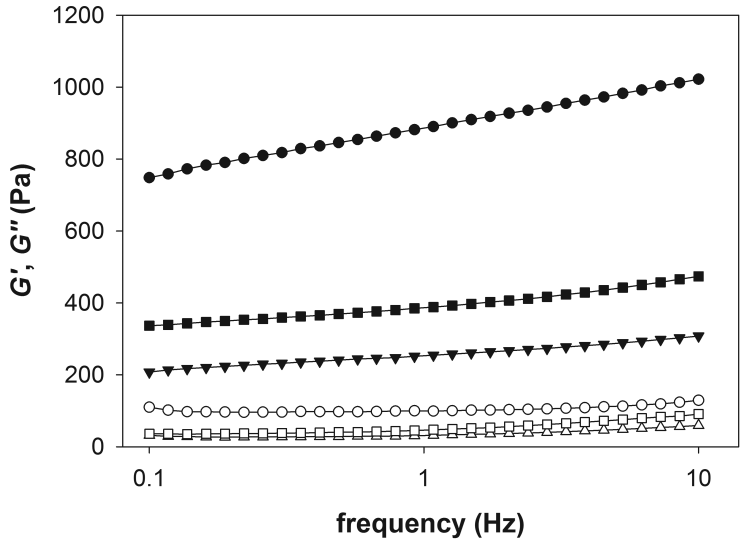


**Figure 2.10** Rheological characterization of PNIPAAm microgels cross-linked with 0.74 mol% relative to NIPAAm in equilibrium swelling at 20 °C: MBAm (●,○); DEGDMA (▼,▽); GDMA (■,□) – elastic modulus, *G'* (filled symbols), and viscous modulus, *G''* (open symbols).

The use of PNIPAAm microparticles in biomedical applications requires a previous evaluation of their cytotoxicity. Figure 2.11 presents the metabolic activity of L929 cells (normalized to control) after 36 hours of culture with medium conditioned with polymer extracts at an initial concentration of

0.1 mg/mL and 1 mg/mL. No cytotoxic effect was observed for any of the PNIPAAm samples prepared, when compared to non-conditioned RPMI media. These results are in agreement with previously reported data for PNIPAAm cross-linked particles prepared using a conventional method followed by extensive and time-consuming purification steps.[30] Furthermore, the data emphasizes the ability of $scCO_2$ in removing any residual monomers that might be present, since especially NIPAAm would be toxic for mammalian cell cultures even at very low concentrations.[30] Therefore, the preparation of smart microgels in supercritical carbon dioxide rendered highly pure polymers without any need of further treatment before their application, enabling their potential use in biomedical devices.

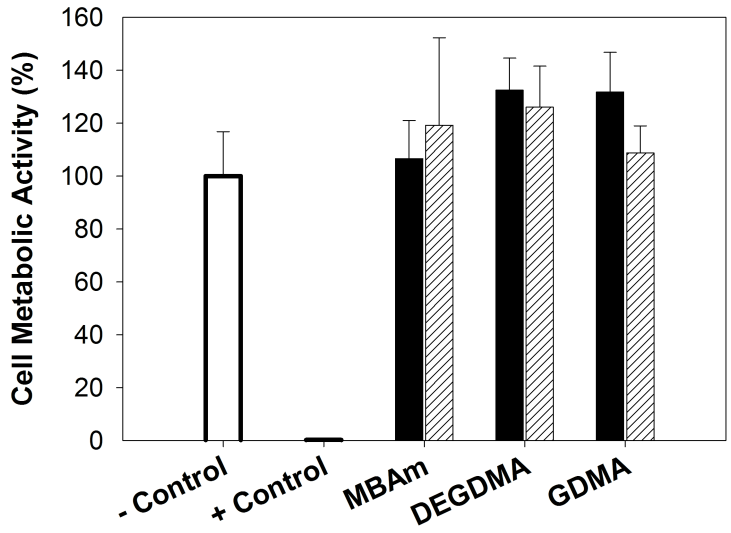


**Figure 2.11** Cytotoxicity assays for PNIPAAm microbeads cross-linked with 0.74 mol% of MBAm, DEGDMA and GDMA. L929 fibroblast cells were incubated with media previously conditioned with PNIPAAm polymer samples at two polymer concentrations: ( ▬ ) 0.1 mg/mL and ( ▨ ) 1 mg/mL. Cell metabolic activity after 36 hours was assessed using an MTT-based cell growth determination kit (measurements were normalized to negative control).

## 2.3 Poly(*N*-isopropylacrylamide)-based Copolymers: Microbeads with Additional Functionality

Copolymerization of NIPAAm with hydrophilic monomers is a possible route to fine tune swelling degree, the thermal and mechanical features of the polymer as well as introducing additional functionalities. Poly(ethylene glycol) (PEG) is a FDA approved biocompatible hydrophilic polymer that has been widely explored for different biomedical applications due to its resistance to protein adsorption and cell adhesion.[31] Conventional synthesis of PNIPAAm-PEG nanoparticles for drug delivery applications has already been reported in literature, in which the presence of PEG contributes for higher LCST and equilibrium swelling. In principle, that behavior facilitates the incorporation of drugs into the nanoparticles.[32] Poly(methacrylic acid) (PMAA) is a biocompatible weak polyelectrolyte with a $pK_a$ ~ 5-6. When cross-linked, PMAA hydrogels exhibit sharp pH sensitivity, swelling to high degrees in basic solutions and collapsing upon protonation of the carboxylic group. This behavior is due to contributions of Couloumbic repulsions among charged carboxylate groups and of Donnan osmotic pressure driven transport of mobile counterions to maintain electroneutrality inside the microgel.[23] At high pH values, the hydrogel mesh expands to minimize charge concentration. NIPAAm and MAA copolymers create systems that exhibit reversible swelling responses to both temperature and pH stimuli. The functionalization of NIPAAm with MAA provides a functional group for chemical modification, and, when ionized, increases or even suppresses the LCST behavior and contributes to microgel swelling for MAA fractions below 30 mol%.[33,34] Nano-sized poly(NIPAAm-co-MAA), p(NIPAAm-co-MAA), microgels have already been prepared through conventional synthesis and thoroughly studied in their ability to uptake and release different drugs[35] and also in their interaction with macromolecules[36]. The preparation of PNIPAAm-based hydrogel particles using supercritical fluid technology offers many advantages over conventional synthesis methods, as biocompatible beads with well-defined morphology and physical properties are readily obtained without the need of extensive purification or further processing, being especially suitable for sensitive biological applications.[1,37]

Herein, the preparation of PNIPAAm-*graft*-PEG (PNIPAAm-*g*-PEG) and p(NIPAAm-co-MAA) copolymers by free-radical dispersion polymerization is described. The impact of the different co-monomers on the morphological properties of the hydrogels was evaluated with the main goal of obtaining defined microbeads for a protease sensing application.

### 2.3.1 Results and discussion

From the previous experiments with PNIPAAm homopolymers, it was clear that larger particles were obtained for initial polymerization conditions close to or above the solubility limit determined by cloud point assessment. For PNIPAAm-*g*-PEG synthesis, polymerizations were performed mimicking the experimental conditions previously optimized for the largest particles: NIPAAm initial concentration of 7.7 wt% relative to $CO_2$, 10 wt% Krytox relative to the monomers, and increasing molar fraction of PEGa macromonomer relative to NIPAAm (5-15 mol%). Once again, the initial feed was not totally homogeneous at 65 ºC and 28.0 MPa, which impaired polymerization yield and lead to a final molar composition different from the initial mixture (Table 2.5). On the other hand, p(NIPAAm-co-MAA) copolymer was synthesized slightly below NIPAAm solubility limit: NIPAAm initial concentration of 4.8 wt% (relative to $CO_2$) and increasing molar fractions of MAA (10-20 mol%). The initial feed was totally soluble at 65ºC and 28.0 MPa and therefore higher yields were obtained when compared with the PNIPAAm-*g*-PEG reaction. The polymers were characterized in their monomer composition, size distribution for monodisperse beads, and thermal features (LCST).

The copolymerization of PEG and MAA with NIPAAm was confirmed by elemental analysis and by FT-IR spectroscopy (Figure 2.12). Comparing with the spectra of the DEGDMA cross-linked PNIPAAm homopolymer, the PNIPAAm-*g*-PEG copolymer showed a characteristic peak corresponding to the carbonyl stretch mode ($\upsilon$(C=O) at 1725 cm$^{-1}$) of the macromonomer, overlapping the vibration previously assigned to DEGDMA. Whereas, p(NIPAAm-co-MAA) exhibited an additional band corresponding to the carbonyl stretch mode ($\upsilon$(C=O) at 1705 cm$^{-1}$) of protonated carboxylic groups.[38] Both the characteristic comonomer band intensities increased for copolymers with higher content in PEGa or MAA. In addition, the peaks relative to the Amide I and Amide II for both copolymeric systems can be found at around 1544-1549 cm$^{-1}$ and 1648-1650 cm$^{-1}$, respectively, being both at higher wavenumbers when compared to the FT-IR spectra of the PNIPAAm homopolymers. This significant shift is characteristic of H-bonding interactions being established between NIPAAm and co-monomer segments, as shown for other acrylamide copolymer systems.[39] Details regarding the infrared spectra of the p(NIPAAm-co-MAA) 90:10 copolymer will be subject of Chapter 3.

**Table 2.5** Effect of the initial co-monomer molar fraction on the obtained PNIPAAm copolymers.

| Polymer | | *x* co-monomer[a] | yield (%) | diameter, $\bar{d}$ (μm) | LCST (ºC)[c] pH 4 | pH7.4 |
|---|---|---|---|---|---|---|
| PNIPAAm-*g*-PEG | 95:5 | 4 | 69 | 2.70±0.37[b] | 31.5 | |
| | 90:10 | 15 | 89 | 1.87±0.30[b] | 33.3 | |
| | 85:15 | 17 | 93 | 1.43±0.39[b] | 34.5 | |
| p(NIPAAm-co-MAA) | 90:10 | 8 | 92 | 4.0±0.4 | 30.1 | none |
| | 85:15 | 14 | 98 | n.a. | none | none |
| | 80:20 | 17 | 98 | n.a. | none | none |

[a] determined through elemental analysis.

[b] the particle size for individual particles was determined from image analysis of SEM micrographs: $\bar{d} \pm s$ for 100 particles.

[c] determined from DSC analysis for PNIPAAm-*g*-PEG copolymers; the LCST of pH-sensitive p(NIPAAm-co-MAA) is pH-dependent and therefore was determined through turbidimetry.

The successful copolymerization of NIPAAm with both hydrophilic co-monomers had also a significant impact on the determined LCST. As the amount of PEGa macromonomer increases the LCST shifts to higher values, as the water and NIPAAm interactions are stabilized by the presence of hydrophilic ethyleneglycol segments to higher temperatures.[32] The incorporation of MAA lead to a pH-dependent thermoresponsive behavior of the copolymer. Above the MAA $pK_a$ (~5-6), no LCST was observed by turbidimetric analysis, as the carboxylic groups of MAA are fully deprotonated, stabilizing water within the hydrogel and preventing the entropy-driven collapse of PNIPAAm.[34] In addition, as the composition in MAA increases there is no observed LCST at any pH which may be due not only to the hydrophilic character of the carboxylic group but possibly to intermolecular interactions among NIPAAm and MAA segments that impair NIPAAm native interaction with water, in agreement with previous reports.[34]

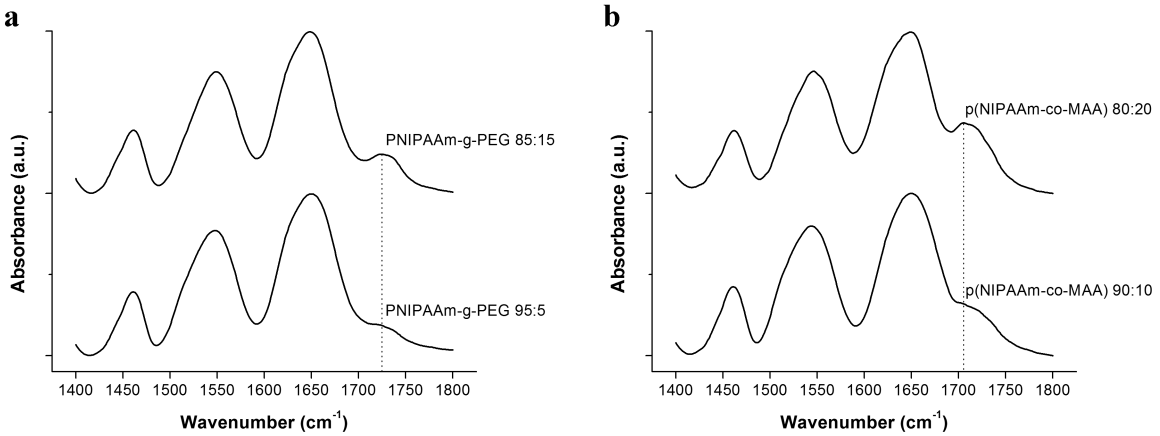


**Figure 2.12** FT-IR spectra in the region between 1400-1800 $cm^{-1}$ for (a) PNIPAAm-g-PEG 95:5 and 85:15 showing an increase in the intensity of the shoulder at 1725 $cm^{-1}$ (highlighted by the dotted line) characteristic of free υC=O vibration of the PEGa macromonomer in copolymers with higher content in PEGa; (b) p(NIPAAm-co-MAA) 90:10 and 80:20 demonstrating higher incorporation of MAA for higher initial feeds by an increase in the intensity of the shoulder corresponding to protonated carboxylic υC=O ~ 1705 $cm^{-1}$ (highlighted by the dotted line).

In regards to the copolymers morphology it was clear that the dispersion polymerization approach lead to the *in situ* formation of well defined PNIPAAm-*g*-PEG and p(NIPAAm-co-MAA) microbeads, as shown by the SEM micrographs in Figure 2.13 and 2.14. It is possible to observe for both systems that incorporation of larger amounts of the co-monomer lead to poor morphological definition, especially for the MAA copolymerizations. For the p(NIPAAm-co-MAA) 85:15 and 80:20 copolymers, the reactions were allowed to proceed for more than 24 hours to obtain the more defined morphology shown in the SEM micrographs. Indeed shorter polymerization times lead to more aggregated particles (data not shown).

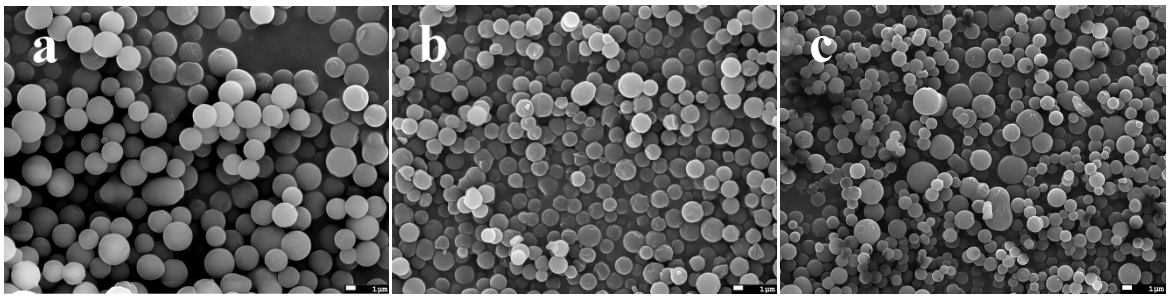


**Figure 2.13** Scanning electron microscopy images of PNIPAAm-*g*-PEG copolymers with increasing PEG content: (a) 95:5; (b) 90:10; (c) 85:15. Scale bar: 1 μm.

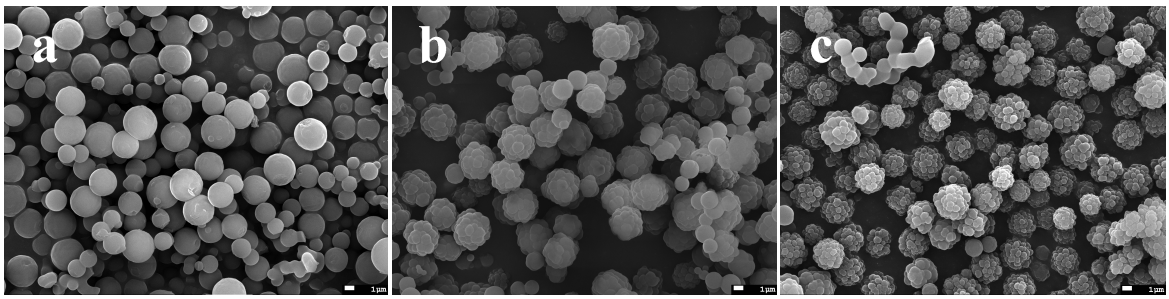


**Figure 2.14** Scanning electron microscopy images of p(NIPAAm-co-MAA) copolymers with increasing MAA content: (a) 90:10; (b) 85:15; (c) 80:20. Scale bar: 1 μm.

The particles with more potential for the proposed biosensing application are the PNIPAAm-*g*-PEG 95:5 and the p(NIPAAm-co-MAA) 90:10 microbeads, as they exhibit a well-defined morphology, as shown on the SEM micrographs, and a larger size (Table 2.5). The particle diameters when dispersed in Milli-Q water (at different pH for the MAA containing polymer) and 10 mM PBS buffer pH 7.4 is shown in Figure 2.15 (as well as 10 mM acetate buffer pH 4 for the p(NIPAAm-co-MAA)).

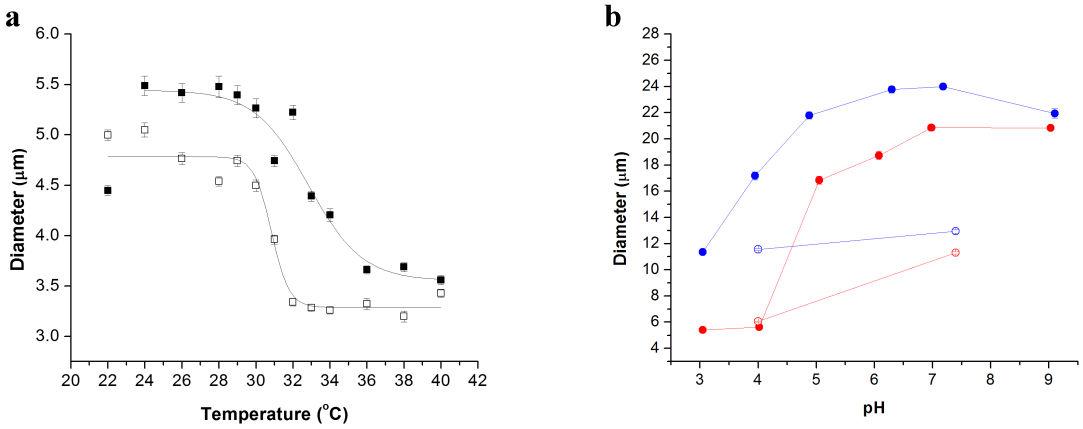


**Figure 2.15** (a) Diameter ($\bar{d} \pm SE_{\bar{d}}$) of PNIPAAm-*g*-PEG 95:5 microparticles dispersed in water (■) and 10 mM PBS buffer (□) from 22 to 40 °C (the depicted curves are a Boltzmann sigmoidal fit to the data to illustrate the observed tendency). (b) Diameter of p(NIPAAm-co-MAA) 90:10 microbeads variation with solution pH and ionic strength at 24 °C (—) and 37 °C (—): closed symbols when dispersed in Milli-Q water with negligible ionic strength and open symbols when dispersed in 10 mM PBS buffer pH 7.4 (I = 160 mM) and 10 mM acetate buffer pH 4 (I = 160 mM).

The variation of PNIPAAm-*g*-PEG 95:5 microbeads diameter with temperature is quite similar to the observed for the homopolymeric beads, in which the microgel collapse is clearly observed above the LCST, though the presence of PEG introduces a larger lag in temperature between the fully swollen and collapsed states. The microbeads were smaller than the DEGDMA crosslinked PNIPAAm particles when dispersed in Milli Q water. However, their deswelling in the physiological buffer is not as significant as in the homopolymeric beads, which is particularly relevant for the targeted biosensing application. The p(NIPAAm-co-MAA) 90:10 microbeads diameter is both dependent on temperature and the solution pH, as expected from the LCST measurements. Below the MAA $pK_a$, the microbeads size is comparable to PNIPAAm 0.74 mol% DEGDMA homopolymer particles. However at physiological pH the p(NIPAAm-co-MAA) 90:10 microbeads present large diameters around the target cell-size of 10 μm in 10 mM PBS buffer pH 7.4. As mentioned before, MAA's carboxylic groups above their $pK_a$ contribute to the overall microgel swelling and minimize the polymeric network collapse even at temperatures above native PNIPAAm LCST. In solutions with higher ionic strength the swelling is less significant in agreement with overall charge shielding of the co-polymers.[33,34,40]

The volume swelling ratio (Q) at 24 and 37 °C and mesh size ($\xi$) of the copolymeric microgels were determined using the equations 2.1 and 2.2 previously described. The values for $C_n$, $\overline{M_c}$ and $\overline{M_r}$ used for copolymers are presented in Table 2.6. Since these are copolymeric systems, the values were calculated for the PNIPAAm-*g*-PEG 95:5 and p(NIPAAm-co-MAA) 90:10 assuming average contributions of each of the co-monomers based on the determined elemental analysis compositions.

For the MAA containing polymers, characteristic ratios for ionized and non-ionized polymer were taken into account, as shown in Table 2.6.

**Table 2.6** Parameters for the calculation of the mesh size for the PNIPAAm-*g*-PEG 95:5 and p(NIPAAm-co-MAA) 90:10 microgels.[41,42]

| Parameters | PNIPAAm-*g*-PEG 95:5 | p(NIPAAm-co-MAA) 90:10 |
|---|---|---|
| $C_n$ | $C_{n,PEG}$ = 4.1<br>$C_{n,copolymer}$ = 10.3 | $C_{n,MAA\ non-ionized}$ = 7.5<br>$C_{n,MAA\ ionized}$ = 14.6<br>$C_{n,copolymer\ non-ionized}$ = 10.4<br>$C_{n,copolymer\ non-ionized}$ = 10.9 |
| $\overline{M_r}$ (g/mol) | $\overline{M_r}_{PEG}$ = 375<br>$\overline{M_r}_{copolymer}$ = 124 | $\overline{M_r}_{MAA}$ = 86.09<br>$\overline{M_r}_{copolymer}$ = 111 |
| $\overline{M_c}$ (g/mol) | 8354 | 7509 |

In Table 2.7, it is possible to infer that the incorporation of hydrophilic co-monomers lead to larger overall swelling and mesh sizes, most importantly under physiological conditions, emphasizing the contribution of the hydrophilic moieties to water uptake and stabilization. For the particular case of p(NIPAAM-co-MAA) 90:10, the microgels could actually be theoretically permeated by large biomacromolecules, such as extracellular matrix components as fibrinogen[43] or the large metalloproteinase MMP-9 (with a diameter around 10 nm; *vide* Chapter 1) under physiological conditions.

**Table 2.7** Volume swelling ratio and mesh size for PNIPAAm-*g*-PEG 95:5 and p(NIPAAm-co-MAA) 90:10 microgels dispersed in water and buffers below (24 °C) and above the LCST (37 °C).

| Monomer | | | diameter, $\bar{d}$ (μm)[ʃ] | | swelling ratio, Q[ʃ] | | mesh size, $\xi$ (nm)[ʃ] | |
|---|---|---|---|---|---|---|---|---|
| | | | 24 °C | 37 °C | 24 °C | 37 °C | 24 °C | 37 °C |
| PNIPAAm-g-PEG 95:5 | water | | 5.5 ± 0.1 | 3.7 ± 0.0 | 7.4 ± 0.6 | 1.5 ± 0.1 | 11 ± 0.2 | 6.7 ± 0.0 |
| | buffer | pH 7.4 | 5.1 ± 0.1 | 3.2 ± 0.1 | 5.5 ± 0.4 | 0.7 ± 0.1 | 10 ± 0.1 | 5.0 ± 0.0 |
| P(NIPAAm-co-MAA) 90:10 | water | pH 4 | 17 ± 0.3 | 5.6 ± 0.1 | 79 ± 5 | 2.8 ± 0.1 | 25 ± 2 | 7.0 ± 0.0 |
| | | pH 7.4 | 24 ± 0.2 | 21 ± 0.2 | 216 ± 8 | 141 ± 6 | 35 ± 4 | 31 ± 3 |
| | buffer | pH 4* | 12 ± 0.1 | 6.1 ± 0.0 | 24 ± 1 | 3.5 ± 0.1 | 17 ± 0 | 8.7 ± 0 |
| | | pH 7.4[§] | 13 ± 0.2 | 11 ± 0.1 | 34 ± 2 | 23 ± 1 | 19 ± 1 | 17 ± 0 |

[ʃ] average ± standard error of the mean for diameter ($SE_{\bar{d}}$), swelling ratio ($SE_Q$) and mesh size ($SE_\xi$).

* dispersed in 10 mM acetate buffer (I = 160 mM).

[§] dispersed in PBS buffer (I = 160 mM).

The copolymeric microbeads as a bulk were further characterized in terms of their viscoelastic properties by dynamic oscillatory measurements in equilibrium swelling conditions below the LCST, where both samples are fully swollen. Both copolymeric microbeads presented a high degree of elasticity, as the elastic modulus is higher than the loss modulus in the linear viscoelastic regime and weakly dependent on frequency – Figure 2.16. In agreement with the higher water content determined by particle analysis of the swollen microbeads, the p(NIPAAm-co-MAA) presented a lower moduli when compared to the PNIPAAm-*g*-PEG 95:5 or the homopolymeric microbeads. Furthermore, since there is no significant temperature-driven volume transition of the microgels in physiological salt and pH conditions, probably the rheological properties of these microbeads are close to what would be observed at 37 $^{o}$C, being in the order of magnitude of soft compliant tissues (Young's modulus from 0.1-10 kPa): the target of the present project.[44]

However, it should be noted that the rheological properties of the bulk p(NIPAAm-co-MAA) 90:10 aggregated particles do not directly translate the mechanical properties at the particle level and should just be regarded as an approximation. Furthermore, the fragile gels formed by aggregated soft polymer colloids in equilibrium swelling have been shown to form percolated structures with large voids containing water.[45] Therefore, the determined values for dynamic elastic modulus are probably an underestimation.

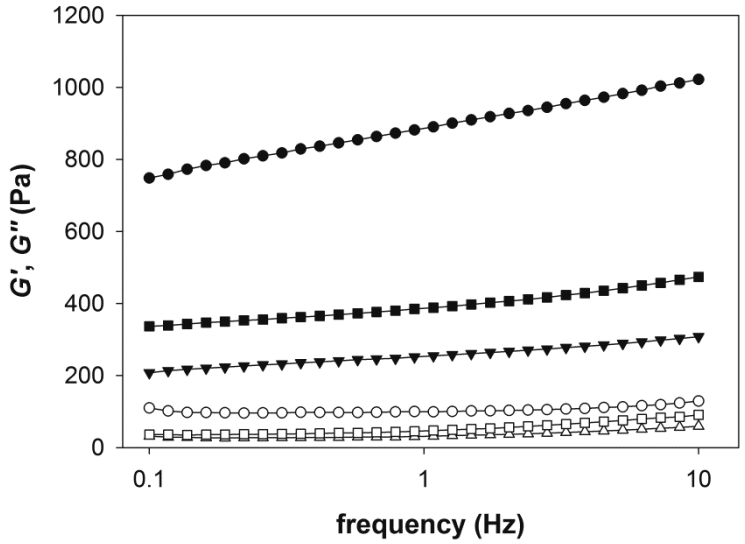


**Figure 2.16** Rheological characterization of copolymeric PNIPAAm-based microbeads in 10 mM PBS pH 7.4 at equilibrium swelling and 20$^{o}$C: PNIPAAm-*g*-PEG 95:5 (●,○); and p(NIPAAm -co-MAA) 90:10 (▼,△) – elastic modulus, *G'* (filled symbols), and viscous modulus, *G''* (open symbols).

The synthesized monodisperse microbeads were also tested for their biocompatibility. Figure 2.17 presents the metabolic activity of L929 fibroblast cells (normalized to control) after 36 hours of culture with liquid extracts of the copolymers. No considerable cytotoxic effect is observed for any

polymer nor any trend in terms of the concentrations of polymers extracts present in the media. Therefore these copolymers may potentially be used in biomedical settings.

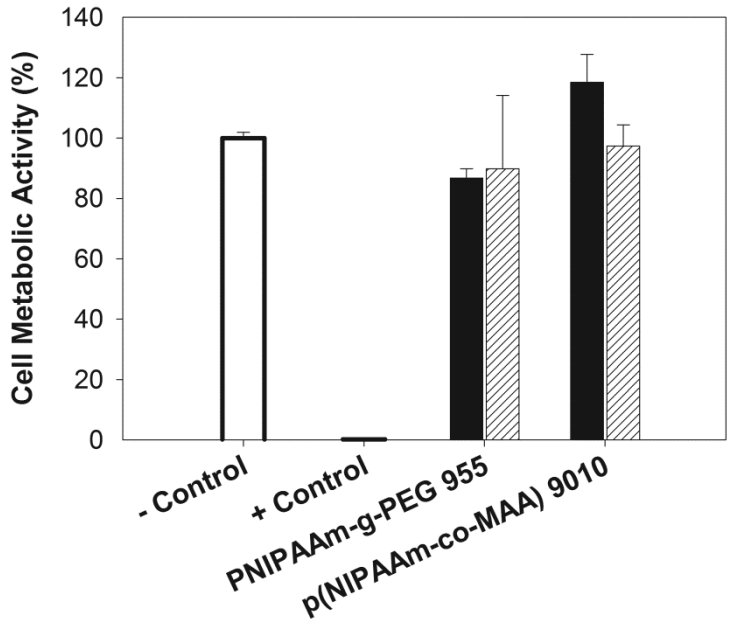


**Figure 2.17** Citotoxicity assays of PNIPAAm-*g*-PEG 95:5 and p(NIPAAm-co-MAA) 90:10 microgels according to the ISO standards for biomaterials. L929 fibroblast cells were incubated with media previously conditioned with the copolymer samples at two polymer concentrations: (▬) 0.1 mg/mL and (▨) 1 mg/mL. Cell metabolic activity after 36 hours was assessed using an MTT-based cell growth determination kit (measurements were normalized to negative control).

## 2.4 Conclusions

Synthesis of thermoresponsive PNIPAAm particles in supercritical $CO_2$ was successfully optimized to yield large spherical monodisperse beads by following a dispersion polymerization strategy using a commercial perfluoropolyether as a stabilizer, Krytox, and using large initial concentrations of monomer. The physical, thermal and viscoelastic properties of PNIPAAm microgels could be tuned by changing cross-linker species, the cross-linking degree or the co-monomer composition. The microbeads with more potential for the aimed biosensing application are the DEGDMA cross-linked homopolymeric and the p(NIPAAm-co-MAA) 90:10 particles. The PNIPAAm 0.74 mol% DEGDMA microbeads have an average diameter under physiological salt conditions of about 3.3 μm, below the aimed cell-like size. However, by changing the environmental temperature, these particles enable a theoretical on-off permeation behavior to biomacromolecules within the range size of relevant metalloproteinases. The copolymerization of NIPAAm with MAA conferred pH-sensitivity to the

native thermoresponsive microbeads, expanding the range of application of these beads. Moreover, these microbeads exhibit reactive groups that may be chemically modified or that can interact with macromolecules through electrostatics, determinant for stable layer-by-layer assembly. In addition, these particles exhibit a mammalian cell-like size of about 11 μm in physiological pH, temperature and salt conditions. The mesh size of these microgel particles is large enough to allow the permeation of bulky proteases such as MMP-9. Although no rheological data was determined at 37 $^{o}$C, this study shows that the mechanical properties of the prepared microbeads may be manipulated in agreement with the mechanical behavior of a target tissue to promote a physiological sustainable interaction between the material and surrounding cells. However, for the latter p(NIPAAm-co-MAA) 90:10 microbeads the determined viscoelastic properties of the microbeads are probably maintained at 37 $^{o}$C as the microgel water content does not vary significantly with temperature at physiological pH and salt conditions, and are within the targeted range. The obtained polymers had no toxic effect over fibroblast cell cultures, thus enabling their potential use within biomedical devices. This strategy offers a new route for the design of smart particles in supercritical $CO_2$ according to the desired biomedical application: by manipulating the experimental condition in scCO$_2$ in terms of cross-linking species, cross-linking degree, co-monomer, stabilizer and concentrations, it is possible to prepare sub-micron particles for drug delivery applications or microbeads with cell-like size and stiffness for probing tissue microenvironments.

## 2.5 References

1. Temtem, M., Casimiro, T., Mano, J.F. & Aguiar-Ricardo, A. Green synthesis of a temperature sensitive hydrogel. *Green Chem.* **9**, 75 (2007).

2. Soares da Silva, M., Temtem, M., Henriques, S., Casimiro, T. & Aguiar-Ricardo, A. Phase Behavior Studies of 2-Hydroxyethyl Methacrylate and Methyl Methacrylate in High-Pressure Carbon Dioxide. *J. Chem. Eng. Data* **52**, 1970-1974 (2007).

3. Nayak, S. & Lyon, L.A. Soft nanotechnology with soft nanoparticles. *Angew. Chem., Int. Ed.* **44**, 7686-708 (2005).

4. Heskins, M. & Guillet, J.E. Solution Properties of Poly (*N*-isopropylacrylamide). *J. Macromol. Sci. A* **2**, 37-41 (1968).

5. Schild, H.G. Poly(*N*-isopropylacrylamide) - Experiment, Theory and Application. *Prog. Polym. Sci.* **17**, 163-249 (1992).

6. Anseth, K.S., Bowman, C.N. & Brannon-Peppas, L. Mechanical properties of hydrogels and their experimental determination. *Biomaterials* **17**, 1647-1657 (1996).

7. Win, K.Y. & Feng, S.-S. Effects of particle size and surface coating on cellular uptake of polymeric nanoparticles for oral delivery of anticancer drugs. *Biomaterials* **26**, 2713-2722 (2005).

8. Kim, J., Singh, N. & Lyon, L.A. Label-free biosensing with hydrogel microlenses. *Angew. Chem., Int. Ed.* **45**, 1446-1449 (2006).

9. Ogawa, K., Wang, B. & Kokufuta, E. Enzyme-Regulated Microgel Collapse for Controlled Membrane Permeability. *Langmuir* **17**, 4704-4707 (2001).

10. Lapeyre, V., Gosse, I., Chevreux, S. & Ravaine, V. Monodispersed glucose-responsive microgels operating at physiological salinity. *Biomacromolecules* **7**, 3356-3363 (2006).

11. Gant, R.M. et al. Design of a self-cleaning thermoresponsive nanocomposite hydrogel membrane for implantable biosensors. *Acta Biomater.* **6**, 2903-10 (2010).

12. Shiho, H. & Desimone, J.M. Dispersion Polymerization of Glycidyl Methacrylate in Supercritical Carbon Dioxide. *Macromolecules* **34**, 1198-1203 (2001).

13. Wang, W. et al. The homo and copolymerisation of 2-(dimethylamino)ethyl methacrylate in supercritical carbon dioxide. *Polymer* **44**, 3803-3809 (2003).

14. Wang, W., Howdle, S.M. & Yan, D. One-step seed dispersion polymerization in supercritical carbon dioxide. *Chem. Commun.* 3939-41 (2005).

15. Cooper, A.I., Hems, W.P. & Holmes, A.B. Synthesis of Highly Cross-Linked Polymers in Supercritical Carbon Dioxide by Heterogeneous Polymerization. *Macromolecules* **32**, 2156-2166 (1999).

16. Christian, P., Howdle, S.M. & Irvine, D.J. Dispersion Polymerization of Methyl Methacrylate in Supercritical Carbon Dioxide with a Monofunctional Pseudo-Graft Stabilizer. *Macromolecules* **33**, 237-239 (2000).

17. Liu, T., Garner, P., DeSimone, J.M., Roberts, G.W. & Bothun, G.D. Particle Formation in Precipitation Polymerization: Continuous Precipitation Polymerization of Acrylic Acid in Supercritical Carbon Dioxide. *Macromolecules* **39**, 6489-6494 (2006).

18. Senff, H. & Richtering, W. Temperature sensitive microgel suspensions: Colloidal phase behavior and rheology of soft spheres. *J. Chem. Phys.* **111**, 1705 (1999).

19. Constantinides, G., Kalcioglu, Z.I., McFarland, M., Smith, J.F. & Van Vliet, K.J. Probing mechanical properties of fully hydrated gels and biological tissues. *J. Biomech.* **41**, 3285-9 (2008).

20. Yeung, T. et al. Effects of substrate stiffness on cell morphology, cytoskeletal structure, and adhesion. *Cell Motil. Cytoskeleton* **60**, 24-34 (2005).

21. Desimone, J.M. et al. Dispersion Polymerizations in Supercritical Carbon Dioxide. *Science* **265**, 356-359 (1994).

22. Casimiro, T., Banet-Osuna, A.M., Ramos, A., Nunes da Ponte, M. & Aguiar-Ricardo, A. Synthesis of highly cross-linked poly(diethylene glycol dimethacrylate) microparticles in supercritical carbon dioxide. *Eur. Polym. J.* **41**, 1947-1953 (2005).

23. Flory, P.J. *Principles of Polymer Chemistry*. (Cornell University, London, 1986).

24. Elmas, B., Tuncel, M., Senel, S., Patir, S. & Tuncel, A. Hydroxyl functionalized thermosensitive microgels with quadratic crosslinking density distribution. *J. Colloid Interface Sci.* **313**, 174-83 (2007).

25. Matzelle, T.R., Geuskens, G. & Kruse, N. Elastic Properties of Poly(*N*-isopropylacrylamide) and Poly(acrylamide) Hydrogels Studied by Scanning Force Microscopy. *Macromolecules* **36**, 2926-2931 (2003).

26. Sun, B., Lin, Y. & Wu, P. Structure Analysis of Poly(*N*-isopropylacrylamide) Using Near-Infrared Spectroscopy and Generalized Two-Dimensional Correlation Infrared Spectroscopy. *Appl. Spectrosc.* **61**, (2007).

27. Flory, P.J. & Rehner, J. Statistical Mechanics of Cross-Linked Polymer Networks I. Rubberlike Elasticity. *J. Chem. Phys.* **11**, 512 (1943).

28. Kubota, K., Fujishige, S. & Ando, I. Solution properties of Poly (*N*-isopropylacrylamide) in water. *Polym. J.* **22**, 15-20 (1990).

29. Lele, A.K., Hirve, M.M., Badiger, M.V. & Mashelkar, R.A. Predictions of Bound Water Content in Poly(*N*-isopropylacrylamide) Gel. *Macromolecules* **30**, 157-159 (1997).

30. Wadajkar, A.S., Koppolu, B., Rahimi, M. & Nguyen, K.T. Cytotoxic evaluation of N-isopropylacrylamide monomers and temperature-sensitive poly(*N*-isopropylacrylamide) nanoparticles. *J. Nanopart. Res.* **11**, 1375-1382 (2008).

31. Krishnan, S., Weinman, C.J. & Ober, C.K. Advances in polymers for anti-biofouling surfaces. *J. Mater. Chem.* **18**, 3405 (2008).

32. Leobandung, W., Ichikawa, H., Fukumori, Y. & Peppas, N.A. Monodisperse nanoparticles of poly(ethylene glycol) macromers and N-isopropyl acrylamide for biomedical applications. *J. Appl. Polym. Sci.* **87**, 1678-1684 (2003).

33. Hoare, T. & Pelton, R. Highly pH and Temperature Responsive Microgels Functionalized with Vinylacetic Acid. *Macromolecules* **37**, 2544-2550 (2004).

34. Brazel, C.S. & Peppas, N.A. Synthesis and Characterization of Thermo- and Chemomechanically Responsive Poly(N-isopropylacrylamide-co-methacrylic acid) Hydrogels. *Macromolecules* **28**, 8016-8020 (1995).

35. Hoare, T. & Pelton, R. Impact of Microgel Morphology on Functionalized Microgel-Drug Interactions. *Langmuir* **24**, 1005-1012 (2008).

36. Kleinen, J., Klee, A. & Richtering, W. Influence of architecture on the interaction of negatively charged multisensitive poly(*N*-isopropylacrylamide-co-methacrylic acid) microgels with oppositely charged polyelectrolyte: absorption vs adsorption. *Langmuir* **26**, 11258-65 (2010).

37. Costa, E. et al. Tailoring thermoresponsive microbeads in supercritical carbon dioxide for biomedical applications. *The Journal of Supercritical Fluids* **56**, 292-298 (2011).

38. Choi, J. & Rubner, M.F. Influence of the Degree of Ionization on Weak Polyelectrolyte Multilayer Assembly. *Macromolecules* **38**, 116-124 (2005).

39. Shibanuma, T. *et al.* Thermosensitive Phase-Separation Behavior of Poly(acrylic acid)-graft-poly(N, N-dimethylacrylamide) Aqueous Solution. *Macromolecules* **33**, 444-450 (2000).

40. Canal, T. & Peppas, N.A. Correlation between mesh size and equilibrium degree of swelling of polymeric networks. *J. Biomed. Mater. Res.* **23**, 1183-93 (1989).

41. Horský, J., Petrus, V. & Bohdanecký, M. The characteristic ratio of poly (methacrylic acid) in organic solvents. *Makromol. Chem.* **187**, 2621 -2628 (1986).

42. Torres-Lugo, M. & Peppas, N. a Molecular Design and in Vitro Studies of Novel pH-Sensitive Hydrogels for the Oral Delivery of Calcitonin. *Macromolecules* **32**, 6646-6651 (1999).

43. Tyn, M.T. & Gusek, T.W. Prediction of diffusion coefficients of proteins. *Biotechnol. Bioeng.* **35**, 327-38 (1990).

44. Butcher, D.T., Alliston, T. & Weaver, V.M. A tense situation: forcing tumour progression. *Nat. Rev. Cancer* **9**, 108-22 (2009).

45. Lattuada, M., Wu, H. & Morbidelli, M. Experimental investigation of colloidal gel structures. *Langmuir* **20**, 4355-62 (2004).

# CHAPTER 3:

## Tuning Smart Microbead Properties by Macromolecules Assembly

# 3 Tuning Smart Microbeads Properties by Macromolecules Assembly

In the development of smart hydrogel devices for biosensing, the interactions between macromolecules and the polymeric hydrogels can significantly alter their native expected performance. In fact, the complexation of large macromolecules is a possible strategy to fine tune the swelling, morphology, responsive behavior, and surface chemistry of soft porous microbeads; thus potentially adjust their permeability and/or create cell adhesive coatings. This chapter focus on the impact of the complexation of a polyphenol via H-bonding on the optimized PNIPAAm homopolymer microbeads and of the layer-by-layer assembly of polyelectrolytes on the p(NIPAAm-co-MAA) microbeads properties. In addition, the molecular mechanisms of interaction between the assembled macromolecules and the microbeads were thoroughly investigated by FT-IR spectroscopy analysis.

## 3.1 Tannic Acid Complexation on PNIPAAm Microbeads and Modification of their Responsive Behavior

Tannic acid (TA) is a water-soluble high molecular weight polyphenolic compound containing a central carbohydrate (glucose) core, which is esterified by phenols (gallic acid) (Figure 3.1B). TA is a natural hydrolysable tannin, mostly extracted from plants and microorganisms, and hence it is fully biodegradable. The high biological activity of TA as an antimutagenic, anticarcinogenic, antimicrobial, antioxidant and antibacterial agent prompted researchers to further investigate its potential especially in the biomedical field.[1,2] In fact, several studies have been performed on the association of TA with biopolymers such as collagen, gelatin, albumin and some polysaccharides through non-covalent interactions.[3-6] Polyphenols such as tannic acid appear to associate with macromolecules by H-bonding through donating and accepting groups,[7] and by hydrophobic interactions with the aromatic rings on its galloyl phenols[8]. Ionic interactions with positively charged aminoacids and polyelectrolytes have also been reported.[9]

A previous study confirmed the presence of specific intermolecular H-bonding interactions between the carbonyl groups of polyesters and the phenolic hydroxyl groups of TA.[10] Recently, there has been increasing interest on using TA as an H-bond donor/acceptor for layer-by-layer assembly with several neutral polymers such as poly(*N*-vinylcaprolactam), poly(*N*-vinylpyrrolidone), poly(ethylene oxide) and poly(*N*-isopropylacrylamide) (PNIPAAm) for the development of physiologically stable thin films[11] and hollow capsules[12] for controlled drug release[13] and other biotechnology applications[14].

Specifically, Sukhisvili *et al.* have demonstrated the formation of TA and PNIPAAm multilayers through H-bonding that remained stable up to the critical dissolution pH of about 8.[11]

Therefore, TA stands as a suitable candidate for association to PNIPAAm microbeads, as an approach to systematically adjust the microgel properties. Despite the development of the devices combining both macromolecules, little is known about the real impact of TA interactions on PNIPAAm properties. It has been shown that the presence of macromolecules such as polyelectrolytes within the hydrogel network can change the PNIPAAm microgel phase transition behavior.[15,16] Therefore, it is essential to fully understand the interactions and dynamics between PNIPAAm and complexed molecules, and its relation with environmental conditions such as pH, for the rational design and application of this responsive system for biosensing. Studies concerning the effect of phenols on the PNIPAAm phase transition in aqueous solutions have shown that the LCST decreases in the presence of phenols by reducing thermodynamic interactions between the polymer and water. Furthermore, at a constant temperature, the PNIPAAm phase transition can also be induced when the concentration of phenols is above a certain threshold. The threshold concentration decreases with increasing hydroxyl substitution in the aromatic molecules.[17] On the other hand this trend cannot be generalized for complex polyphenolic compounds as shown in a recent study on the phase transition behavior of PNIPAAm cross-linked microgels in TA solutions. For TA concentrations in solution lower than $10^{-2}$ mM, the LCST of PNIPAAm microgels with mean diameters of ~233 μm shifts slightly to higher temperatures and, above that critical TA concentration, the thermoresponsive behavior of PNIPAAm microgels is inhibited.[18]

In the present work, the effect of tannic acid complexation on the PNIPAAm homopolymeric microgels morphology and thermoresponsive behavior was evaluated as a function of initial TA concentration and solution pH. Monodisperse and well-defined DEGDMA cross-linked PNIPAAm microgels were prepared as described in the previous chapter. The interactions between TA and PNIPAAm in the microgels were thoroughly assessed by analysis of their diffuse reflectance infrared Fourier transform (DRIFT) spectra.

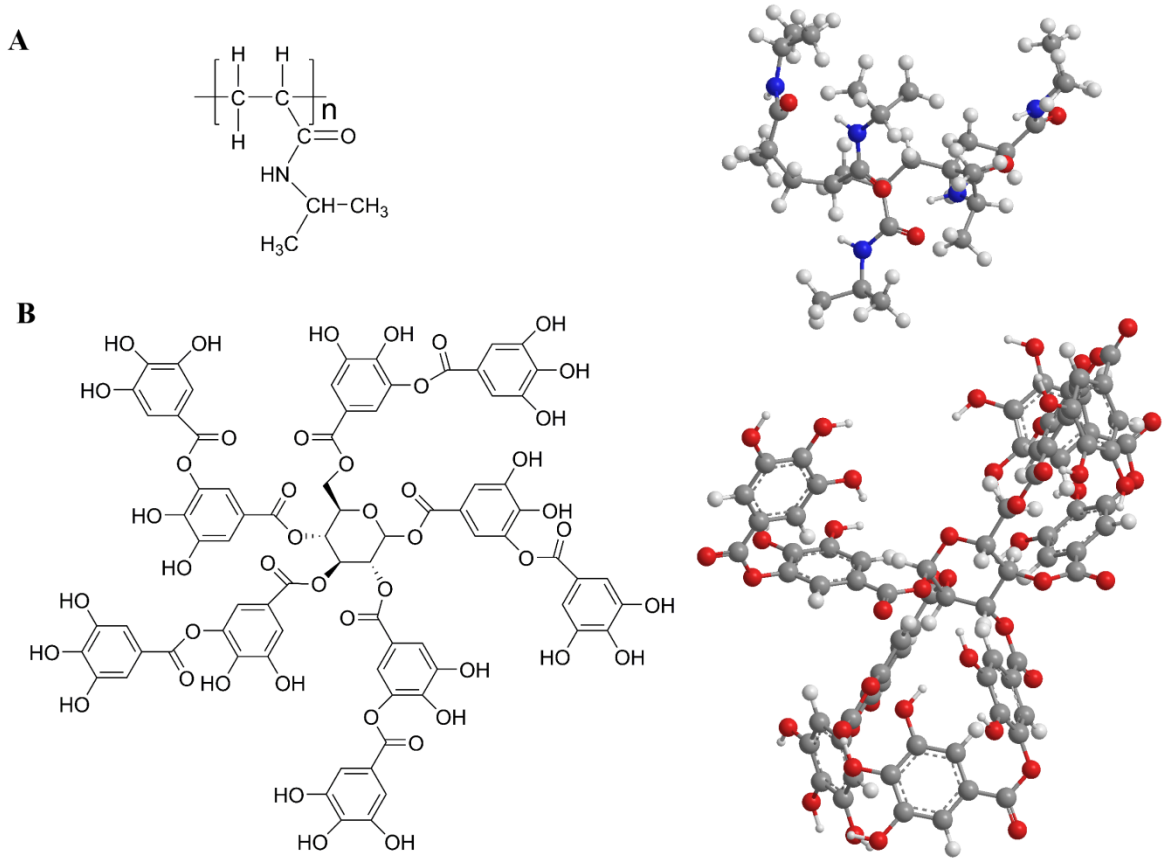


**Figure 3.1** Chemical structure and ball and stick models of PNIPAAm with n = 5 (A) and Tannic Acid (B), in the minimum energy conformation optimized by the MM2 module of Chem 3D Ultra 10.0.

## 3.1.1 Experimental section

### 3.1.1.1 Materials and complexes preparation

Tannic acid (TA; $M_w$ 1701.2), hydrochloric acid (HCl, 37 % purity) and potassium bromide (KBr; FTIR grade) were purchased from Sigma-Aldrich. Sodium phosphate dibasic dihydrate (99.5 % purity), sodium phosphate monobasic dihydrate (> 98 % purity) and sodium hydroxide (NaOH) were obtained from Riedel-de Haën. All the materials were used without any further purification. Deionized water was purified through a Milli-Q system and had a resistivity greater than 18 MΩ.cm. PNIPAAm microbeads cross-linked with 0.74 mol% DEGDMA were prepared as described in Chapter 2.

Complexation experiments between TA and PNIPAAm microgels were performed in 10 mM phosphate buffer at pH 4 and pH 7 at increasing TA to PNIPAAm weight ratios: 1, 5, 50, 100 and 500 wt%. Dispersions of PNIPAAm microgels were added drop-wise to TA solutions to a final PNIPAAm concentration of 1 mg/mL, and were stirred for 20 minutes. All solutions were freshly prepared beforehand. Afterwards the obtained microgels were collected by centrifuging the dispersions for 10

min at 7800 × *g*. Microgels were further rinsed in the respective buffer by at least 3 centrifugation and re-suspension cycles to remove all non-adsorbed TA (as monitored by absorption measurements in a UV/VIS spectrometer). All supernatants were collected for further analysis. A similar experiment was conducted between gallic acid (tannic acid structural unit) and PNIPAAm microgels at pH 7 using an initial concentration of 46 wt% in GA, in order to have the same amount of hydroxyl groups as those found in TA at 50 wt%. At pH 7 the contributions from GA carboxylic acid for H-bonding may be neglected as it is mostly ionized (GA -COOH $pK_a$ ~ 4.3 and -OH $pK_a$ ~ 8.7).[19] PNIPAAm microgels complexed with TA (PNIPAAm-TA) and GA were lyophilized for 3 hours before further analysis. Lyophilization did not compromise microgel structure.

#### 3.1.1.2 Determination of the amount of complexed TA.

The UV/VIS absorption spectrum of TA depends on the degree of ionization of the molecule.[11] The absorbance spectra of the TA solutions in 10 mM phosphate buffer at pH 4 and pH 7 were determined using a UV/VIS spectrometer PerkinElmer Lambda 35 (PerkinElmer Inc., USA). TA solutions at pH 4 exhibited two absorption peaks at 213 nm and 275 nm, while at pH 7 the peaks shift to 211 nm and 276 nm. Therefore, the amount of TA present in the collected supernatants ($m_{TA,supernatant}$) was calculated by comparison with calibration curves established for each pH. The amount of complexed TA ($q$) was determined as in equation 3.1:

$$\boldsymbol{q(wt\,\%) = \frac{m_{TA,initial} - \sum m_{TA,supernatant}}{m_{PNIPAAm}} \times 100} \qquad \text{(Equation 3.1)}$$

where $m_{TA,initial}$ and $m_{PNIPAAm}$ refer to the initial amount of TA and PNIPAAm in solution, respectively. TA complexation on PNIPAAm was described using Langmuir isotherms. The model can be represented by the following linear form – equation 3.2:[20]

$$\boldsymbol{\frac{C}{q} = \frac{1}{Q_{max}K_d} + \frac{C}{Q_{max}}} \qquad \text{(Equation 3.2)}$$

where $C$ is the equilibrium concentration (mg/mL) of tannic acid in solution in the preparation of the PNIPAAm-TA complexes, $Q_{max}$ is the Langmuir constant describing the maximum attainable amount of TA complexed with PNIPAAm (wt%), and $K_d$ is the Langmuir affinity constant (mL/mg). The essential characteristics of the Langmuir isotherm can be expressed as a dimensionless separation factor or equilibrium parameter, $R_L$, defined by equation 3.3:

$$\boldsymbol{R_L = \frac{1}{1 + K_d C_0}} \qquad \text{(Equation 3.3)}$$

where $C_0$ is the initial tannic acid concentration (mg/mL).

#### 3.1.1.3 Analysis of the complexes thermoresponsive behavior

Turbidity of PNIPAAm and PNIPAAm-TA aqueous buffered microgels dispersions at a concentration of 0.2 mg/mL was measured using a UV/VIS spectrometer PerkinElmer Lambda 35 (PerkinElmer Inc., USA), equipped with a water-jacketed cell holder coupled to a temperature-controlled circulating bath. Measurements were performed at 600 nm where both individual PNIPAAm and TA or PNIPAAm-TA microgels have no absorption bands. Turbidity was recorded upon heating from 24 $^{o}$C up to a temperature at which an absorbance plateau was clearly defined (after 5 min of equilibration for each temperature step) and cooling back to 24 $^{o}$C. The temperature of the sample dispersion was continuously monitored by a thermocouple inside the cuvette. The increase in turbidity with increasing temperature is a result of the volume phase transition, both in individual PNIPAAm and PNIPAAm-TA complexes. The LCST for the thermoresponsive samples was calculated as the inflexion point of the normalized absorbance to temperature curve using OriginPro 8.04 software.

Optical micrographs of prepared PNIPAAm and PNIPAAm-TA microgels were obtained with an automatic Malvern Morphologi G3 optical microscope (Malvern Inc., UK) kept inside a temperature-controlled chamber with an infrared lamp coupled to a PID temperature controller. PNIPAAm-TA complexes were dispersed in phosphate buffer (according to the pH at which they were initially prepared) and observed at 24, 32 and 37 $^{o}$C. Furthermore samples were titrated up to pH 9 and down to the initial complexation pH using 1 M NaOH and HCl solutions to assess TA complexation and decomplexation reversibility and its effects on PNIPAAm microgels morphology and thermoresponsive behavior. Particle morphology of PNIPAAm microgels and lyophilized PNIPAAm-TA complexes was assessed using scanning electron microscopy (SEM) in a Hitachi S-2400, with an accelerating voltage set to 15 kV. All samples were gold coated before analysis.

#### 3.1.1.4 DRIFT spectra analysis of the complexes

PNIPAAm, TA and lyophilized PNIPAAm-TA complexes were analyzed by diffuse reflectance infrared Fourier transform spectroscopy (DRIFT). Sample preparation consisted in grinding a mixture of KBr and each sample in appropriate weight proportions in order to obtain spectral absorbance in the range of applicability of the Kubelka-Munk transformation.[21] The amount of sample was sufficient to be considered of infinite thickness. The DRIFT spectra were measured in a Mattson Research Series 1 FTIR spectrometer, equipped with a wide-band MCT detector (4000-400 $cm^{-1}$) and a Graseby/Specac Selector (with specular reflection blocker). A total of 500 scans were performed with 4 $cm^{-1}$ resolution. No baseline corrections were made. The diffuse reflectance spectra were transformed to Kubelka-Munk units using the FIRST software.

The specific interactions between TA molecules and PNIPAAm chains were not always inferred directly from the complexes spectra, due to partial band overlaps. In order to clarify those interactions, and when necessary, a detailed spectral analysis was made by deconvolution to identify

the constituent components of relevant bands, using OriginPro 8.04 software. A non-linear least-squares fitting method was used, assuming Gaussian and Lorentzian band profiles for the components. No baseline corrections were made, and no restrictions were imposed on the band positions and widths. The best fits were obtained with reduced $\chi^2 \approx 10^{-6}$ and a correlation coefficient of≈ 0.999. Upon deconvolution the intensity of the methyl vibrations of PNIPAAm isopropyl group ($\nu_s CH_3$ and $\nu_{as} CH_3$ at 2878 and 2972 $cm^{-1}$, respectively) relative to the methylene groups ($\nu_{as} CH_2$ at 2933 $cm^{-1}$) on the polymer backbone ($I_{rel}$) in both the pure component and prepared PNIPAAm-TA complexes was determined using equation 3.4:

$$\boldsymbol{I_{rel} = 100 \times \left[\frac{Area(\upsilon_{as}CH_3 + \upsilon_s CH_3)}{Area(\upsilon_{as}CH_2)}\right]} \qquad \text{(Equation 3.4)}$$

### 3.1.2 Results and discussion

#### 3.1.2.1 PNIPAAm-TA complexes

The influence of tannic acid concentration and of solution pH on TA complexation with PNIPAAm lightly cross-linked microgels was assessed. Tannic acid assembly on PNIPAAm microgels was performed at pH 4 and pH 7 (below the TA $pK_a$ of about 8.5)[11] in increasing TA to PNIPAAm weight ratios. The amounts of tannic acid effectively complexed with PNIPAAm microgels are shown in Table 3.1. PNIPAAm-TA complexes content in TA increased with increasing initial concentration of TA, as expected. Nevertheless, the increase in TA content from the experiments performed at initial TA weight ratio of 100 wt% to 500 wt% (relative to PNIPAAm amount at a concentration of 1 mg/mL in PNIPAAm) was much less than five times, indicating that all available interactive PNIPAAm moieties may have reached saturation in between these concentrations. Overall, a higher amount of TA was present on PNIPAAm microgels at pH 4 than at pH 7, indicating that TA complexation is dependent on its protonation.

The complexation of TA with PNIPAAm can be described through a Langmuir isotherm as shown by the correlation factor values in Table 1. Overall, the obtained $R_L$ values were between 0 and 1, indicating that the complexation of tannic acid with PNIPAAm is a thermodynamically favorable process at both pH. However at pH 4, the binding capacity of PNIPAAm, $Q_{max}$, was higher and the affinity constant $K_d$ was lower, clearly emphasizing that the complexation process was more favorable when TA was more protonated at acidic pH.

**Table 3.1** Langmuir isotherm parameters for Tannic Acid complexation with PNIPAAm microgels and LCST of obtained PNIPAAm-TA complexes.

| pH | Langmuir isotherm | | | | | | LCST, |
|---|---|---|---|---|---|---|---|
| | $C_0$, wt% [a] | $q$, wt% [b] | $R_L$ | $Q_{max}$, wt% | $K_d$, mL/mg | $R^2$ | °C |
| 4 | 0 | - | - | 68 | 9.2 | 0.998 | 31.5±0.07 |
| | 1 | 0.7±0.2 | 0.92 | | | | 34.6±0.18 |
| | 5 | 4.2±0.2 | 0.68 | | | | - |
| | 50 | 42±1 | 0.18 | | | | - |
| | 100 | 62±1 | 0.10 | | | | - |
| | 500 | 66±5 | 0.021 | | | | - |
| 7 | 0 | - | - | 66 | 6.2 | 0.997 | 31.7±0.12 |
| | 1 | 0.4±0.1 | 0.94 | | | | 31.4±0.06 |
| | 5 | 3.4±0.1 | 0.76 | | | | 34.4±0.60 |
| | 50 | 43±0.2 | 0.24 | | | | - |
| | 100 | 56±0.4 | 0.14 | | | | - |
| | 500 | 63±1 | 0.031 | | | | - |

[a] initial TA concentration in solution in wt% relative to PNIPAAm.

[b] $q$ is the amount of complexed TA in wt% relative to PNIPAAm (± standard deviation for a 95 % confidence interval; assembly performed in solution to a final PNIPAAm concentration of 1 mg/mL).

The lower critical solution temperature (LCST) behavior of the synthesized PNIPAAm microgels and PNIPAAm-TA complexes was investigated in aqueous dispersions by turbidity measurements, as shown in Figure 3.2. For that purpose, turbidity measurements were performed at 600 nm on particles dispersed in 10 mM phosphate buffer at the initial assembly pH. Absorbance was recorded upon heating from 24 °C up to a temperature at which an absorbance plateau was clearly defined. Microgel thermoresponsive behavior was dependent on the initial assembly conditions in terms of TA concentration and pH. When heating PNIPAAm microgel dispersions, turbidity increased with temperature, exhibiting a sharp slope at the LCST. The derived values for the LCST are in agreement with previous reports on PNIPAAm and close to the values determined by DSC in Chapter 2. The observed thermoresponsive behavior is totally reversible upon cooling, as no hysteresis was observed (data not shown). In general, no cloud points were observed for PNIPAAm-TA microgels complexed at pH 4 and a TA weight ratio above 5 wt% (relative to PNIPAAm amount at a concentration of 1 mg/mL in PNIPAAm); and at pH 7 above 50 wt% - Table 3.1 and Figure 3.2. For lower TA concentrations, the complexes prepared with an initial ratio of 1 wt% at pH 4 and of 1 and 5 wt% at pH 7 exhibited a volume phase transition with temperature. However, the LCST increased about 3 °C for PNIPAAm-TA 1 wt% pH 4 and 5 wt% pH 7, in comparison with pure PNIPAAm, and the

transition was not as sharp. A similar trend was described recently in a paper by Chen *et al.* for the behavior of PNIPAAm microgels dispersed in solutions of tannic acid. The PNIPAAm volume phase transition was suppressed in solutions with concentrations above 0.02 mg/mL.[18] Below that critical concentration, the LCST of PNIPAAm microgels also exhibited a slight shift to higher values. Nevertheless, it is not possible to directly compare this report with the results described above, as they refer to distinct systems. Herein, the behavior of PNIPAAm microgels effectively complexed with a defined amount of TA is analyzed, while Chen *et al* refers to the behavior of PNIPAAm microgels dispersed in solutions of tannic acid. Furthermore the effect of TA protonation on the interactions with PNIPAAm is not analyzed in the latter.

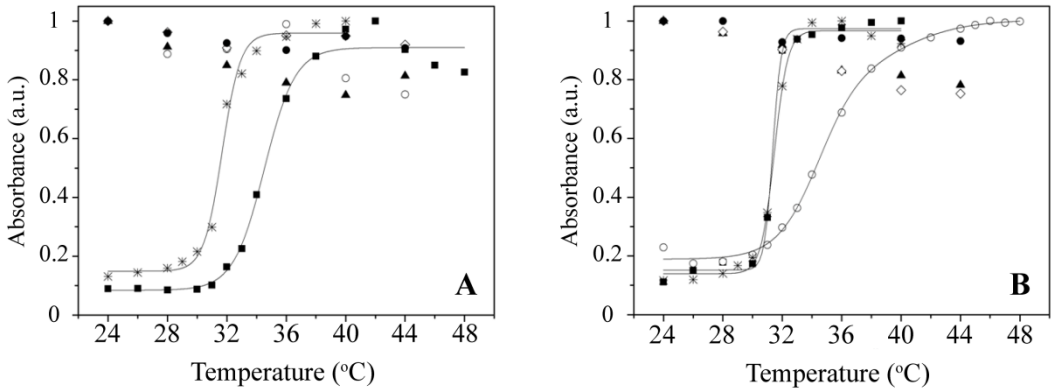


**Figure 3.2** Turbidimetry analysis of PNIPAAm-TA complexes assembled in 10 mM phosphate buffer at pH 4 (A) and pH 7 (B): (■) TA 1 wt%; (○) TA 5 wt%; (▲) TA 50 wt%; (◊) TA 100 wt%; (●) TA 500 wt% and (*) PNIPAAm. Data shown was obtained upon heating from 24 °C up to a temperature at which an absorbance plateau was clearly defined. A similar profile was obtained upon cooling with no significant hysteresis.

Optical micrographs of the PNIPAAm-TA complexes dispersed in 10 mM phosphate buffer solutions at pH 4 and pH 7 are shown in Figure 3.3 at increasing temperature. Volume phase transition was clearly observed for microgels prepared with TA to PNIPAAm ratios of 1 wt% when complexed at pH 4 and 1 wt% and 5 wt% at pH 7; while no thermoresponsive behavior was obtained for higher TA ratios, further emphasizing the results obtained from the turbidimetric analysis. The assembly of tannic acid on the prepared PNIPAAm microparticles had a dramatic impact on the microgel morphology. For low TA to PNIPAAm ratios, the microgels maintain a spherical morphology. As the amount of TA is increased the particles become more deformed. The effect of TA on PNIPAAm microparticles morphology can also be clearly observed in the SEM micrograph shown in Figure 3.4 depicting PNIPAAm-TA complexes prepared at an initial TA concentration of 50 wt% at pH 4, when compared to the SEM micrographs of PNIPAAm microbeads in Chapter 2. In fact, it seems that the increasing interactions between TA and lightly cross-linked PNIPAAm microparticles lead to physical cross-linking of the polymeric network and therefore to microparticle collapse.

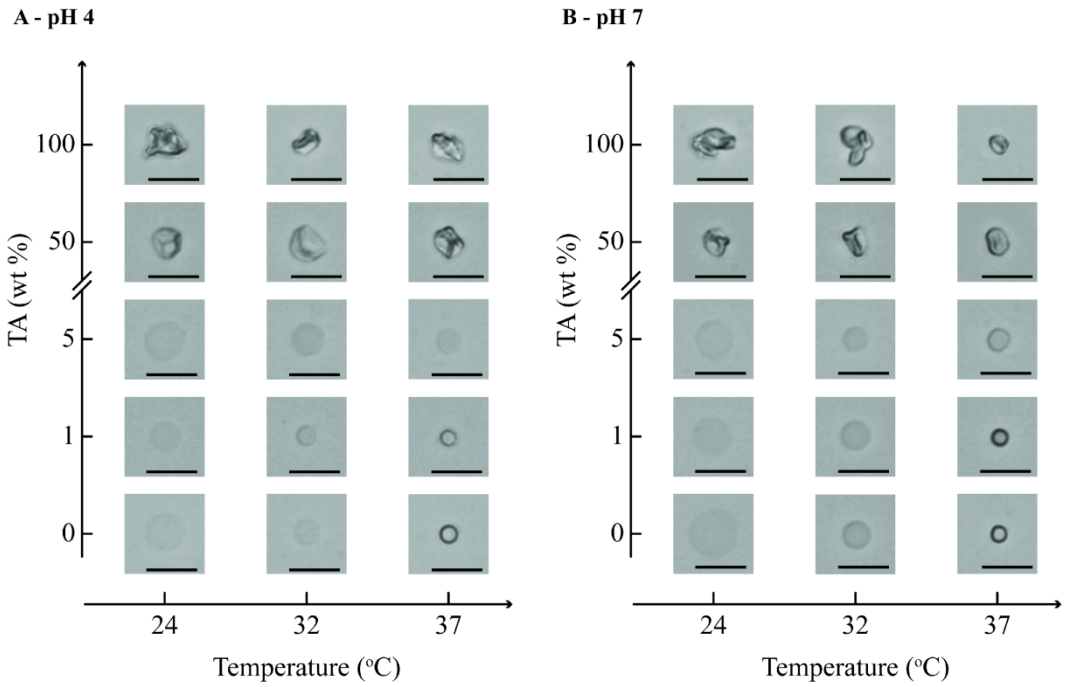


**Figure 3.3** Optical micrograms showing the response to solution temperature of PNIPAAm-TA complexes dispersed in 10 mM phosphate buffer at pH 4 (A) and pH 7 (B). Data shown refers to observed behavior upon heating since similar response is observed when cooling. Scale bar: 10 μm.

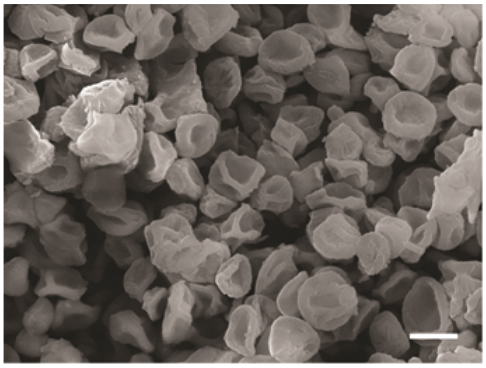

**Figure 3.4** SEM micrographs of PNIPAAm-TA complexes after complexation with TA at an initial concentration of 50 wt% (relative to PNIPAAm amount at 1 mg/mL final concentration) in 10 mM phosphate buffer at pH 4 (B). Scale bar: 2 μm.

#### 3.1.2.2 Reversibility of PNIPAAm-TA thermoresponsive behavior with pH

PNIPAAm-TA complexes prepared at an initial TA ratio of 1 wt% were dispersed in 10 mM phosphate buffer pH 4 or 7, according to the complexation pH. These dispersions were titrated up to pH 9, above the tannic acid $pK_a$, equilibrated for 10 min, and then titrated down to the initial pH; the microgels were observed under an optical microscope from 24 to 37 ºC at each titration step, as shown in Figure 3.5. For particles prepared at both of these TA complexation pH, it can be observed that they

regain their spherical shape at pH 9 regardless of temperature. Furthermore, as temperature was increased, it was clear that at pH 9, PNIPAAm microgels recovered their thermoresponsive behavior as a deswelling of the microgels above the LCST temperature is observed. As the pH was titrated back down to the original complexation pH, we see that at 37 ºC the particle swells a small amount rather than retaining the more compact size of the gel that is anticipated at this temperature. On the other hand, at 32 and 24 ºC, the microgels actually contract and release water rather than exhibiting the highly swollen state characteristic of PNIPAAm microgels at these temperatures. At all three temperatures, it appears that the native condition of the thermoresponsive polymer has been suppressed, and the microgel particles are all very close to the same size. This on-off suppression of the thermoresponsive behavior in response to pH for the PNIPAAm-TA complexes is probably due to the reversible complexation and decomplexation of TA on PNIPAAm at pH values below and above the TA $pK_a$. Indeed, infrared spectra analysis confirmed that TA was partly retained in PNIPAAm-TA microgels after successive rinses using 10 mM phosphate buffer at pH 9 (data not shown), further supporting the quasi-reversible nature of this process.

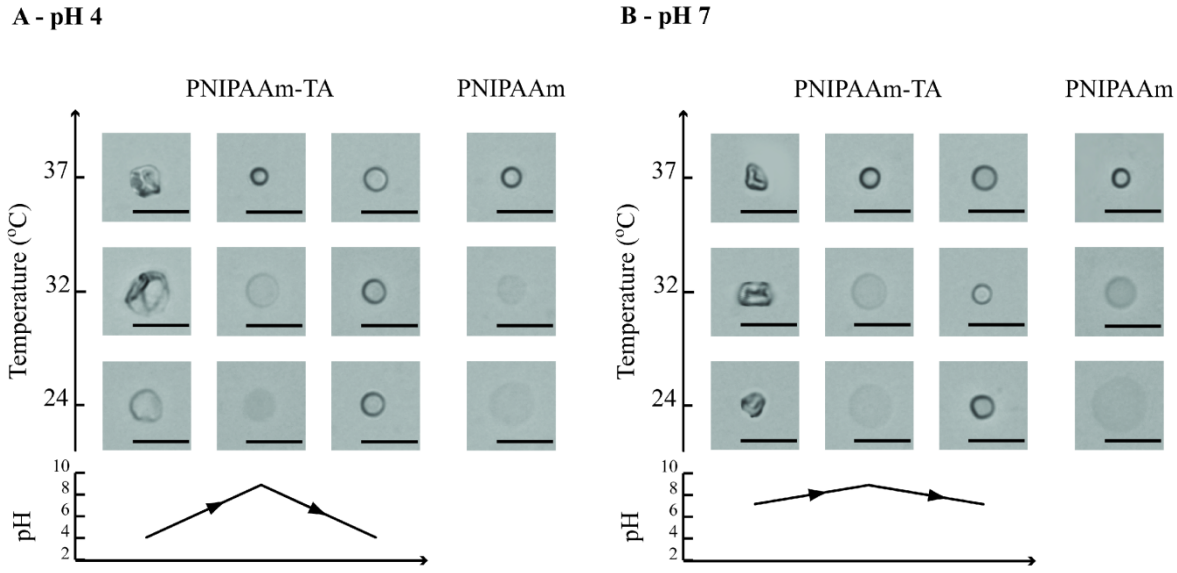


**Figure 3.5** Optical micrographs showing PNIPAAm-TA complexes response to temperature when titrated up to pH 9 and down to original assembly pH. Complexes were initially prepared with 100 wt% TA (relative to PNIPAAm amount at 1 mg/mL final concentration) in (A) 10 mM phosphate buffer pH 4 and (B) in 10 mM phosphate buffer at pH 7. Micrographs shown were obtained upon heating from 24 to 37 °C; micrographs obtained upon cooling demonstrated a similar behavior (data not shown). Scale bar: 10 μm.

For the target biosensing application, TA complexation on the synthesized PNIPAAm microbeads can be used to systematically manipulate the size, water content, morphology and responsiveness at physiological conditions simply by adjusting initial assembly conditions. This feature may be explored to fine tune the permeability by changes in mesh size and overall microgel chemistry.

The mechanisms underlining PNIPAAm and TA complexation and the modification or suppression of the complexes thermoresponsive behavior at different pH and TA concentration were elucidated through the analysis of the infrared spectra of the different complexes, as described in the next section.

#### 3.1.2.3 DRIFT spectroscopy analysis of PNIPAAm-TA complexes

In order to avoid the overlapping of water characteristic bands, the vibrational study was executed with dry microgels, in diffuse reflectance infrared Fourier transform mode (DRIFT). For the purpose of this study, the DRIFT spectra will be discussed in the wavenumber regions of interest for describing the interactions between tannic acid and PNIPAAm within the complexes. A more detailed spectral analysis for all components can be found in Annex I.

The deconvoluted DRIFT spectra of pure PNIPAAm, TA and dry PNIPAAm-TA complexes with increasing TA contents, prepared at pH 4 and pH 7, are shown in Figure 3.6 and 3.7 for the spectral regions 900-1400 $cm^{-1}$ and 1400-1800 $cm^{-1}$, respectively. A summary of the proposed band assignment and deconvolution results as well as the relative contributions of each component to the bands of the pure PNIPAAm and TA and microgel complexes are shown in Table 3.2.

**i)DRIFT analysis of the 900-1420 $cm^{-1}$ spectral region.** The analysis of the complexes DRIFT spectra required a previous assignment of the pure components bands. The spectrum of tannic acid was in good agreement with those collected by Cowen *et al*. above 1000 $cm^{-1}$ in diffuse reflectance mode,[22] and by Jastrzebska *et al.* in transmission[23] (Annex I). Their partial analysis and, in some cases, comparison with gallic acid allowed band assignments.[19,22,24,25] In the low wavenumber region, several bands from C-O stretching modes in different TA functional groups are observed, namely the carbohydrate νC-OC mode at 1089 $cm^{-1}$ and the phenolic νC-OH mode at 1027 $cm^{-1}$.

The DRIFT spectra of the PNIPAAm-TA complexes (Figure 3.6) prepared with the lowest TA concentration, 1 wt%, were very similar to those of PNIPAAm in the 900-1400 $cm^{-1}$ region for both pH values. However, for the microgels prepared with 5 wt% in TA at pH 7, the main bands of TA can already be observed as shoulders, with the phenolic νC-OH shifted to 1038 $cm^{-1}$. For the same TA initial content at pH 4, the phenolic νC-OH shoulder is better defined and shifted to higher wavenumbers (~1040 $cm^{-1}$) and the νC-OC mode of the carbohydrate moiety has higher relative intensity and shifts to 1099 $cm^{-1}$. Similar shifts to higher energy states in the νC-O modes were observed for TA-hydrates and other carbohydrates.[22]

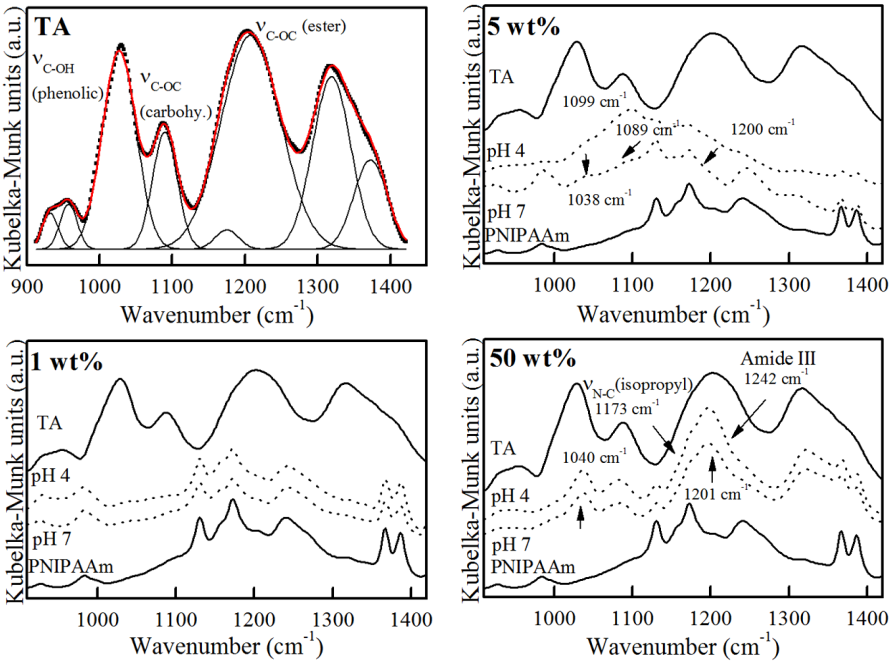


**Figure 3.6** DRIFT spectra from 900-1420 $cm^{-1}$ of TA, PNIPAAm-TA complexes and PNIPAAm: deconvoluted TA spectra (TA); PNIPAAm-TA complexes prepared with: 1 wt% TA at pH 4 and pH 7 (1 wt%); 5 wt% at pH 4 and pH 7 (5 wt%); 50 wt% at pH 4 and pH 7 (50 wt%).

Similar shifts to higher energy states in the νC-O modes were observed for TA-hydrates and other carbohydrates.[22] Therefore, it is proposed that at both pH PNIPAAm and TA interactions involved TA phenolic groups and that at pH 4 the carbohydrate oxygen of TA was additionally engaged in H-bonding (which can act as charge donors in H-bonding with the NH groups of PNIPAAm). When increasing TA initial amount to 50 wt% at both pH values, TA bands became dominant and the phenolic νC-OH mode remained shifted to 1040 $cm^{-1}$. In the 1150-1250 $cm^{-1}$ region, the two PNIPAAm bands (isopropyl νN-C at 1173 $cm^{-1}$ and Amide III at 1242 $cm^{-1}$) appeared as shoulders of the strong νC-O (ester) of TA at 1201 $cm^{-1}$. Surprisingly, this band became much narrower than in pure TA, suggesting that TA ester moieties were involved in more specific interactions when complexed with PNIPAAm, or that a more isotropic microenvironment was obtained.

**ii) DRIFT analysis of the 1400-1800 $cm^{-1}$ spectral region.** The near and mid infrared spectra of PNIPAAm have received considerable attention due to efforts to understand the changes in conformation, interactions and microenvironment of the individual chemical groups that occur upon its coil-to-globule transition.[26,27] In the 1400-1800 $cm^{-1}$ spectral region, the dominant bands in the PNIPAAm spectrum, at 1646 and 1540 $cm^{-1}$, are assigned to Amide I and Amide II vibrations, respectively.

**Table 3.2** Summary of the deconvolution results (positions and relative areas of the components) for the DRIFT spectra of pure TA, pure PNIPAAm and PNIPAAm-TA complexes prepared at pH 4 and pH 7.

| | **Wavenumber ($cm^{-1}$) (%Area)** | | | | | | | |
|---|---|---|---|---|---|---|---|---|
| **Tannic Acid** | | | | | | | | |
| Assignments | 932 (1.7) | 957 (2.3) | 1027 (19.9) | 1090 (8.6) | 1175 (1.4) | 1208 (37.7) | 1319 (19.5) | 1373 (8.9) |
| | νC-OH (phenolic) | | | νC-OC (carbohy) | νC-OC (ester) | | δCH | νC-O / δCOH |
| | 1447 (12.7) | 1469 (2.3) | 1512 (1.9) | 1534 (10.8) | 1608 (20.2) | 1629 (2.0) | 1701 (42.4) | 1728 (7.7) |
| | νC-C, aromatic | | | | νC=O, HB | | | νC=O, free |
| **PNIPAAm** | | | | | | | | |
| Assigments $I_{rel}$=110 | 1446 (5.7) $\delta CH_2$ gauche | 1461 (7.3) $\delta_{as}CH_3$ | 1509 (7.2) δNH free | 1529 (16.0) δNH intra HB | 1548 (17.7) δNH inter HB | 1607 (5.0) νC=O inter HB | 1644 (32.0) νC=O intra HB | 1669 (9.1) νC=O "freer" |
| **PNIPAAm-TA complexes** | | | | | | | | |
| 1 wt% pH 4 $I_{rel}$=115 | 1446 (5.6) | 1463 (7.9) | 1513 (14.3) | - | 1549 (28.2) | 1640 (36.0) | 1654 (3.6) | 1674 (4.1) |
| 1 wt% pH 7 $I_{rel}$=110 | 1448 (10) | 1462 (6.1) | 1510 (10.9) | - | 1544 (29.1) | 1611 (8.0) | 1644 (26.4) | 1667 (9.6) |
| 5 wt% pH 4 $I_{rel}$=130 | 1450 (10.6) | 1463 (4.6) | 1511 (8.2) | - | 1542 (29.2) | 1617 (15.9) | 1647 (24.2) | 1670 (7.3) |
| 5 wt% pH 7 $I_{rel}$=115 | 1443 (3.2) | 1461 (8.8) | 1509 (8.3) | - | 1539 (32.5) | 1605 (4.2) | 1649 (37.8) | 1674 (5.2) |
| 50 wt% pH 4 $I_{rel}$=140 | 1442 (4.8) | 1461 (8.8) | 1515 (11.0) | 1534 (3.9)* | 1545 (23.7) | 1598 (3.9) | 1624 (22.2) | 1654 (21.7) |
| 50 wt% pH 7 $I_{rel}$=130 | 1444 (7.2) | 1463 (7.4) | 1513 (4.6) | 1530 (0.5)* | 1536 (34.4) | 1603 (10.9) | 1643 (26.2) | 1662 (8.8) |

*overlapping of TA νC-C modes of aromatic rings; HB: Hydrogen bonded.

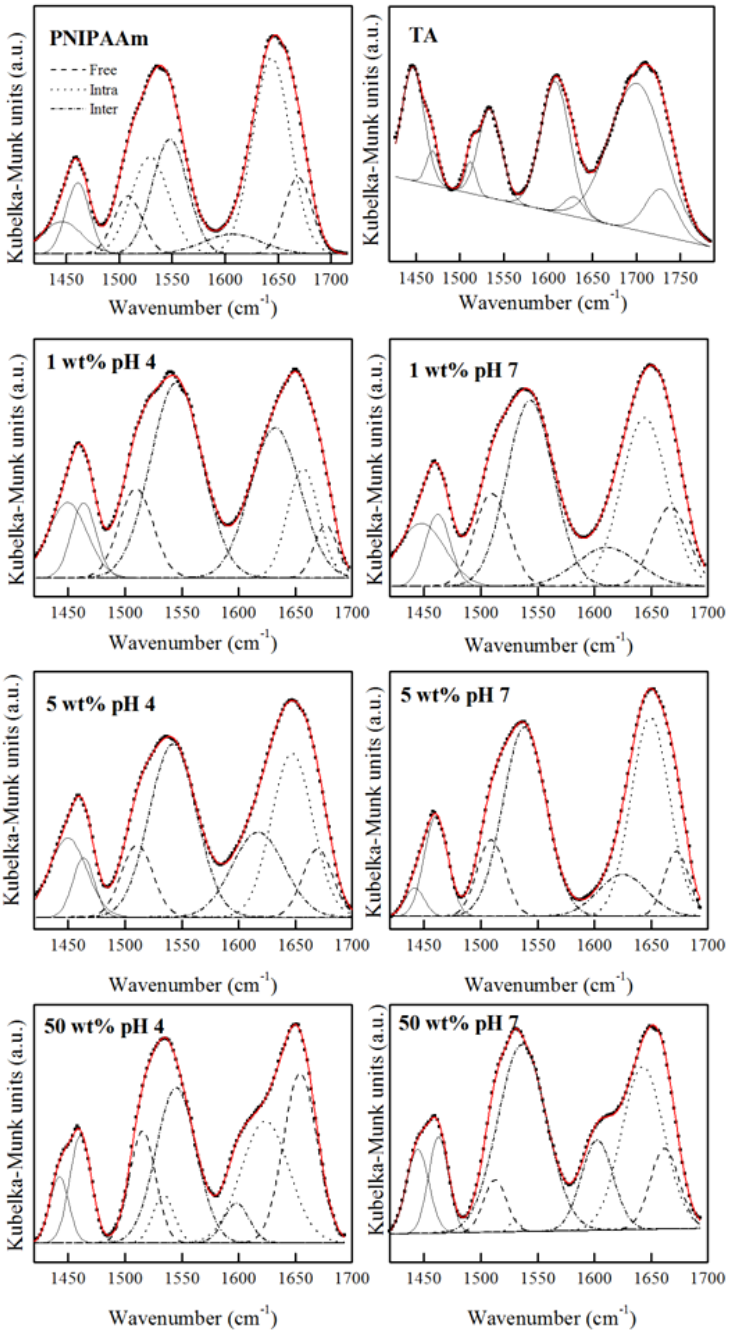


**Figure 3.7** Deconvoluted DRIFT spectra from 1400-1800 $cm^{-1}$ of PNIPAAm, TA and PNIPAAm-TA complexes prepared with: 1 wt% TA at pH 4 (1 wt% pH 4) and pH 7 (1 wt% pH 7); 5 wt% TA at pH 4 (5 wt% pH 4) and pH 7 (5 wt% pH 7); and 50 wt% TA at pH 4 (50 wt% pH 4) and pH 7 (50 wt% pH 7).

The main contribution to the Amide I band is the carbonyl stretching mode, whereas the Amide II is mainly due to the in-plane N-H bending. The spectral deconvolution in the Amide I band revealed the presence of three components at 1607, 1644 and 1669 $cm^{-1}$ that were assigned to intermolecular, intramolecular H-bonded and free or freer C=O groups, respectively, with the majority involved in intramolecular interactions (Figure 3.7 and Table 3.2).[28] Similarly, in the Amide II band, H-bonded N-

H groups originated the components at 1529 and 1548 $cm^{-1}$ (intra and intermolecularly, respectively),[29] with similar relative intensities, plus a minority of free or freer N-H groups appearing at 1509 $cm^{-1}$. In the DRIFT spectra of PNIPAAm-TA complexes prepared with 1 wt% and 5 wt% of TA, the component related with the intramolecularly H-bonded NH groups in the Amide II band was absent and the fractions of the freer ones and of those involved in intermolecular bonds increased significantly for both pH. For pH 7, the Amide I band is similar to pure PNIPAAm. On the other hand, at pH 4, all the carbonyl components in the Amide I band shift to higher wavenumbers, indicating that all the intermolecular H-bonds have been replaced by less strong ones with TA molecules (in spite of the overlapping with the TA band at 1608 $cm^{-1}$). Upon increasing the initial TA concentration to 50 wt% a component previouslty assigned to intramolecular H-bonded NH appeared at ~1530 $cm^{-1}$ (Table 3.2). The latter is due to the overlap of TA νC-C modes of aromatic rings that became more significant with increasing TA content in the complexes. Therefore, the relative contribution of the constituent components of the δNH band cannot be evaluated in complexes prepared with 50 wt% TA initial concentration and above.

**iii) DRIFT analysis of the 2400-3800 $cm^{-1}$ spectral region.** For all the PNIPAAm-TA complexes (in Annex I), there were neither observable changes nor shifts in the C-H stretching modes ($\nu_{as}CH_3$ at 2972 $cm^{-1}$ and $\nu_sCH_3$ at 2878 $cm^{-1}$), when compared with pure PNIPAAm, suggesting that there are no hydrophobic interactions between TA and PNIPAAm, as proposed in previous studies.[18] A deconvolution in this region allowed estimating the relative intensities of the $\nu CH_3$ using $\nu_{as}CH_2$ modes (2933 $cm^{-1}$) as a reference ($I_{rel}$), since it can be assumed that the methylene groups on the polymer backbone are not affected by TA complexation. The $I_{rel}$ of the PNIPAAm-TA complexes prepared with the lowest TA concentration at pH 7 was similar to that of pure PNIPAAm (~110), increasing for the complexes prepared with higher TA amount and protonation. These observations suggest that not only PNIPAAm and TA show no hydrophobic interactions but also that PNIPAAm isopropyl groups are freer in the complexes than in the pure polymer. The 2400-3800 $cm^{-1}$ spectral region of PNIPAAm also included the strong N-H stretching modes (as a broad band with maximum at 3294 $cm^{-1}$ and shoulders at higher wavenumbers) – in Annex I. In the PNIPAAm-TA complexes, the νNH band broadened with increasing TA concentration due to the superposition of the νOH band of TA. Nevertheless, it did not reach the full width at half height of this band for pure TA. This means that the diversity of hydrogen bonds in which the hydroxyl groups of TA are involved was much reduced, as H-bonding preferentially occurred with PNIPAAm moieties.

The information derived from the DRIFT spectra was consistent across the analyzed spectral regions and clearly indicated that TA complexation on PNIPAAm microgels was a consequence of preferential hydrogen bonding between the polymer and TA molecules: both C=O···HO (phenolic), NH···OH and NH···O-C (ester), at the expense of intra and intermolecular interactions between

identical species. At pH 4, TA is more protonated and H-bonding with PNIPAAm is more favorable than pH 7, as demonstrated by the higher diversity of TA and PNIPAAm functional groups involved in the interactions. As a consequence, a higher TA amount was effectively complexed at pH 4 than at pH 7 and a smaller amount of TA is necessary for increasing the LCST or for suppressing PNIPAAm-TA complexes thermosensitivity. Specifically, for the complexes prepared at 1 wt% TA, more TA was complexed at pH 4 because PNIPAAm carbonyl groups were additional engaged in H-bonding (besides the NH groups at both pHs). The thermodynamically driven coil-globule transition of PNIPAAm was shifted to higher temperatures in the complexes at pH 4 (Table 3.1, Figures 3.2A and 3.3A), possibly due to the presence of free TA hydrophilic hydroxyl groups. However, the phase transition was not as sharp as in pure PNIPAAm, since interactions with TA may have displaced water from their adsorption sites on PNIPAAm. The increasing amount of TA in the complexes prepared with 5 wt% lead to an upper shift on the LCST at pH 7 and to the inhibition of the thermoresponsive behavior at pH 4. At these concentrations the involvement of TA phenolic moieties in the TA interaction with PNIPAAm became visible on the DRIFT spectra. Furthermore, TA complexation on the microgels at pH 4 additionally included the carbohydrate oxygen of TA. As the amount of TA increases in the complexes, extensive H-bonding also involving TA ester moieties lead to physical cross-linking and a non-spherical morphology of the microgels. Above an initial TA concentration of 100 wt% there were no significant changes in the complexes DRIFT spectra at both pH (data not shown), which confirms that a saturation occurred between 100 and 500 wt%.

The 3D molecular structure of TA (Figure 3.1B) is responsible for the extension and diversity of interactions that enabled the preparation of PNIPAAm-TA complexes. Indeed, a similar complexation experiment with gallic acid (tannic acid structural unit) at equivalent conditions as those used for TA at a initial concentration of 50 wt% in pH 7 was performed and no gallic acid remained complexed, as confirmed from absorbance measurements and DRIFT spectra (data not shown). The different complexation behaviors should be related to the different entropic terms contributions. While the gallic acid complexation on PNIPAAm involves an enormous entropy drop, the much larger and constrained TA molecule has a smaller entropy variation when changes from the initial hydrated state to the PNIPAAm-TA complex.

### 3.1.3 Conclusions

The complexation of tannic acid with cross-linked PNIPAAm microgels is a thermodynamically favorable process that can be explored for the systematic adjustment of the microgel thermoresponsive behavior, water content and size depending on the initial amount of TA and pH. This process may be explored for the purposed biosensing application to the extent that the modification of PNIPAAm microgel properties can impact its permeability to proteases while the presence of TA confers a beneficial bioactivity to the microbead. PNIPAAm-TA complexes with a low content on TA exhibited a LCST shifted to higher temperatures due to the hydrophilic character of the complexed tannic acid. However, above a critical concentration, TA physically cross-links the polymer chains due to extensive H-bonding between PNIPAAm and TA and displaces water from the polymeric network, inhibiting the temperature driven coil-to-globule transition of PNIPAAm. PNIPAAm-TA thermoresponsive behavior depends also on the assembly pH: for complexes assembled at pH 7, closer to TA $pK_a$, a larger amount of TA is required for altering or suppressing response to temperature stimuli than at pH 4. Furthermore upon titration of PNIPAAm-TA aqueous dispersions to a pH above tannic acid $pK_a$ (pH 9), interactions between PNIPAAm and TA within the microgels were destabilized and the microgels totally recover the ability to respond to temperature stimuli. Nevertheless, tannic acid is still partly retained within the polymeric network assuring the quasi-reversibility of the process. The mechanism of pH-dependent PNIPAAm-TA microgels temperature response was elucidated using a DRIFT analysis approach. It has been shown that PNIPAAm and TA interact through hydrogen bonding between PNIPAAm amide groups and hydroxyl and ester groups of TA. At acidic pH, H-bonding is more diverse, as the carbohydrate oxygen of TA is also clearly engaged, leading to stronger interactions between the species. Moreover, the PNIPAAm isopropyl groups are not involved in any hydrophobic interactions with TA aromatic rings.

This study clearly underlines how the expected performance of smart devices designed for biosensing, controlled drug release, or other applications, can be modified by complexation of macromolecules, depending on the experimental conditions. Herein, the prepared PNIPAAm-TA complexes may potentially be used for others applications besides the target biosensor, such as pH on-off switches in microfluidic devices or pH and temperature-driven drug delivery platforms. Furthermore, since TA can successfully complex a diversity of macromolecules, these PNIPAAm-TA microgels could be further functionalized with other guest molecules of interest.

## 3.2 Layer-by-Layer Assembly of Polyelectrolytes on Stimuli-responsive p(NIPAAm-co-MAA) Microbeads

Increasing research on the design and nanoengineering of microparticles has enabled the preparation of highly functional materials with specific and customized properties. First reported by Decher [30] for the modification of planar surfaces, the layer-by-layer (LbL) assembly method has been thoroughly applied to microparticles for a diverse range of applications, such as biosensing,[31,32] controlled delivery of therapeutics,[33] optical sensing,[34] and materials encapsulation[35]. This approach is based on the consecutive adsorption of materials containing complementary charged or functional groups onto a surface, yielding nanoscaled thin films.[30,36] The LbL method renders a precise control over the surface interfacial properties by varying the specific complementary materials being used, the build-up conditions and/or post-assembly modification. Extensive reports may be found on the influence of the salt concentration, ionic strength and pH on the growth and morphology of LbL multilayers to achieve different functionalities. Strong polyelectrolyte (PE) pairs such as poly(diallyldimethylammonium chloride) / poly(sodium styrene sulfonate) (PDAC/PSS) form thin, fully charged and highly ionically cross-linked multilayers, in which the swelling, hydrophobicity and ion transport is dependent on the presence of salts and the ionic strength.[37-40] On the other hand, for weak polyelectrolytes in which the charge density is pH-dependent, the deposition pH is a key parameter that can be systematically varied to tune the film structure, thickness and hydration, as shown for poly(allylamine hydrochloride) / poly(acrylic acid) (PAH/PAA).[37,41] This strategy has been explored to control cell adhesion,[42] film porosity[43] or to develop nanoreaction schemes[44]. Biologically active films with cell adhesive,[45] pro- and anticoagulant[46] or antifouling[47] properties have been mostly prepared from synthetic polypeptides, such as poly(L-lysine) / poly(L-glutamic acid) (PLL/PLGA), polyssacharides or naturally derived materials. These biocompatible films are generally more hydrated than synthetic polyelectrolytes multilayers (at comparable ionic strength) and exhibit an exponential growth regime characterized by a high interdiffusion between PE layers.[48,49]

The vast majority of the literature reports regarding the LbL thin film assembly on particles concern the use of colloidal substrates as sacrificial cores for the preparation of hollow capsules.[50,51] More recently, studies concerning soft and porous beads have been developed,[31,52] in which the film morphology, the mechanism of multilayer growth and molecular conformation of the assembled polyelectrolytes is closely related to the interactions with the underlying substrate, as interpenetration of the polymer chains within the hydrogel mesh may occur. Specifically for smart carboxylic acid copolymerized PNIPAAm nanogels, it has been shown by Richtering *et al.* that the LbL assembly of polyelectrolytes modifies their physical properties and responsive behavior, depending on the location of the charges within the microgel,[15,53] the specific polyelectrolyte pair used,[54,55] the polyelectrolyte molecular weight[53] as well as the processing conditions such as ionic strength and salt concentration.[55]

Herein, the impact of the LbL assembly of polyelectrolytes pairs with distinct intrinsic charge densities and mobility characteristics on the properties of temperature and pH-responsive p(NIPAAm-co-MAA) micron-sized hydrogel beads synthesized in supercritical carbon dioxide ($scCO_2$) is described. Furthermore, this work aims at understanding the mechanisms of interaction between the LbL multilayers and the microgels through and FT-IR spectral analysis. The combination of the $scCO_2$ microbeads synthesis with the versatile LbL assembly technique may enable tailored microgel systems with potential for controlled drug delivery or biomacromolecules recovery applications.

## 3.2.1 Experimental section

### 3.2.1.1 Materials and sample preparation

Methacrylic acid (MAA; 98 % purity), poly(sodium styrene sulfonate) (PSS; $M_w$ 70,000), poly(acrylic acid) (PAA; $M_w$ 100,000, 35 wt% in water, $pK_a \sim 6.5$[41]), poly(L-lysine) (PLL; $M_w$ 30,000 – 70,000, $pK_a \sim 9$), poly(L-lysine) fluorescein isothiocyanate (PLL-FITC; $M_w$ 30,000 – 70,000), poly(L-glutamic acid) (PLGA; $M_w$ 50,000 – 70,000, $pK_a \sim 7.4$), Rhodamine B (RhoB) isothiocyanate, and dimethylformamide (DMF) were purchased from Sigma-Aldrich. Poly(diallyldimethylammonium chloride) (PDAC; $M_w$ 240,000; 28 wt% in water) and poly(allylamine) hydrochloride (PAH; $M_w$ 120,000, $pK_a \sim 8\text{-}9$[41]) were purchased from Polysciences, Inc. Cascade blue ethylenediamine trisodium salt was purchased from Invitrogen. All the materials were used without any further purification. Deionized water was purified through a Milli-Q system and had a resistivity greater than 18 MΩ.cm. Poly(NIPAAm-co-MAA) 90:10, PP9010, microbeads were prepared as described in Chapter 2.

LbL sequential deposition of the polyelectrolyte pairs was performed by adding a PP9010 microgels aqueous dispersion (pH ~ 5) to a polyelectrolyte solution to a final concentration of 0.5 mg/mL in microgels and 10 mM in polyelectrolyte (based on the repeating unit) and stirring for 15 min. Since the microgels were negatively charged the first layer was always a polycation (PDAC, PAH or PLL) – *vide* Figure 3.8. For the strong polyelectrolyte pair (PDAC and PSS) the pH was adjusted to 7.4 by adding NaOH and HCl solutions; whereas for the weak polyelectrolytes the solutions pH was adjusted to a value at which the polyelectrolytes were mostly ionized: pH 6 for PAH and 9 for PAA; and pH 7.4 for both PLL and PLGA. Afterwards the obtained layered microgels were collected by centrifuging the dispersions for 30 min at 4500 × *g*. Microgels were further rinsed in Milli-Q water at the respective polyelectrolyte pH by at least 3 centrifugation and re-suspension cycles to remove all non-adsorbed polyelectrolyte. All solutions were freshly prepared. For the infrared spectroscopy analysis all samples were lyophilized overnight.

#### 3.2.1.2 Microgel characterization

The zeta potential of the native PP9010 microgels was initially determined as a function of pH at 24 $^{o}$C when dispersed in Milli Q water in a ZetaPALS analyzer (Brookhaven Instruments Corp). For the assembled microgels the zeta potential measurements were performed at assembly pH as a function of the number of layers. Each point is the average of ten independent measurements. The microgels size upon heating from 24 to 37 $^{o}$C was determined using a Zeiss Axioskop 2 optical microscope at 400 × magnification with temperature control (THMS 600 hot stage, Linkam Scientific Instruments) as a function of the layer number for LbL assembled microgels at assembly pH. Each point is the average of at least 100 different microgels. The microgel size was also qualitatively assessed upon cooling and no significant differences were observed.

#### 3.2.1.3 Fluorescent-labeled polyelectrolytes preparation and analysis

Rhodamine B-labeled PAH (PAH-RhoB) and cascade blue-labeled PAA (PAA-Cascade Blue) were prepared by modifying the protocols outlined in the literature,[56,57] and used for the LbL assembly of PP9010 microgels. Briefly, a solution of RhoB isothiocyanate in methanol was prepared at 1 mg/mL and added drop-wise to a solution of 2 mg/mL PAH in 0.1 M sodium carbonate buffer at pH 9.0 (2 vol% dye to polymer solution). The reaction was performed at room temperature under stirring for 6 hours. The dye-conjugated polymer was purified by dialysis ($M_WCO$~10,000) until no fluorescence was detected in the wash Milli-Q water by spectroscopy (about 3 days). The dialyzed polymer solution was then lyophilized. In regards to PAA, 10 equivalents of 1-1-ethyl-3-[3-dimethylaminopropyl]carbodiimide hydrochloride (EDC; 1.92 mg, 10 μmol) and *N*-hydroxybenzotriazole (HOBt; 1.35 mg; 10 μmol) were added to a solution of PAA (120 mg, 1 μmol) in anhydrous DMF (3 ml) and the mixture was stirred under argon for 1 hour. A solution of cascade blue ethylenediamine was prepared separately in anhydrous DMF (3 ml) and added to the reaction. The reaction proceeded for 24 hours. The labeled polymer was purified by dialysis ($M_WCO$~10,000) against Milli-Q water (about 4 days) and lyophilized. The conjugation was assessed by thin layer chromatography using methanol as mobile phase. LbL assembly of dye-labeled polymers was performed as described previously. The microgels were observed when dispersed in PBS buffer on a CARV II spinning disk confocal system equipped with an environmental chamber and a Zeiss inverted microscope.

PP9010 microgels assembled with dye-labeled polyelectrolytes were also analyzed for fluorescence intensity up to 4 bilayers by flow cytometry using a LSR Fortessa HTS (BD Biosciences) and processed using the FlowJo software (Tree Star). Microgels layered with $(PLL\text{-}FITC/PLGA)_n$ were excited at 488 nm and monitored at 530/30 nm and those layered with $(PAH\text{-}RhoB/PAA)_n$ were excited at 561 nm and monitored at 610/20 nm. Preliminary gating isolated events having fluorescence greater than 500 and 2500 for FITC and RhoB labeled microgels, respectively. To limit

assay interference from debris, the "autogating tool" (http://www.flowjo.com/v8/html/autogate.html) was applied to select 75-85 % of the remaining events having the most clustered density on a FSC × SSC (forward by side scattering) plot. Reported values are the median fluorescence of this subpopulation.

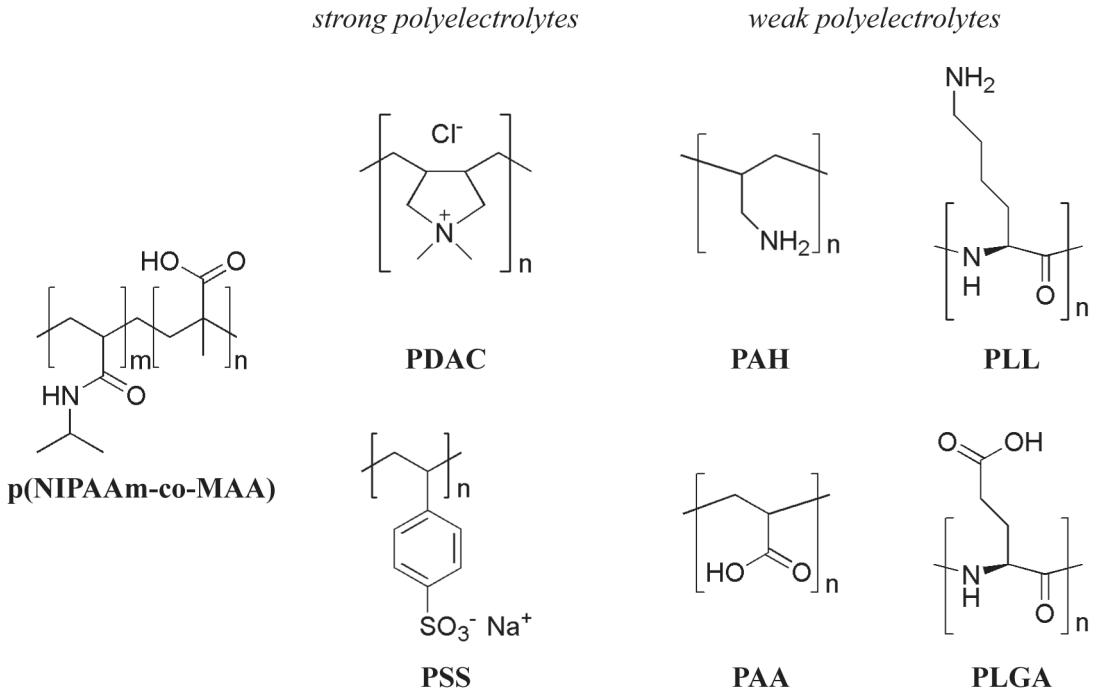


**Figure 3.8** Chemical structure of the p(NIPAAm-co-MAA) microgels used as well as the assembled polyelectrolyte pairs: poly(diallyldimethylammonium chloride), PDAC, and poly(sodium styrene sulfonate), PSS; poly(allylamine hydrochloride), PAH, and poly(acrylic acid), PAA; poly(L-lysine), PLL, and poly(L-glutamic acid), PLGA.

#### 3.2.1.4 ATR FT-IR spectra analysis

PP9010 microgels, the dry pure polyelectrolytes and the LbL assembled microgels were analyzed by Atenuated Total Reflection Fourier Transform Infrared (ATR FT-IR) in a Thermo Nicolet 6700 FT-IR equipped with a Nicolet Continuμm infrared microscope and a MCTA detector. A total of 256 scans were performed with a 4 $cm^{-1}$ resolution and no baseline corrections were performed. The specific interactions in pure PP9010 microgels and between the PP9010 microgels and assembled polyelectrolytes were not always inferred directly from the infrared spectra, because of band overlaps. In order to clarify those interactions, when necessary, a detailed spectral analysis was made by deconvolution to identify the constituent components of relevant bands, using OriginPro 8.04 software. A non-linear least-squares fitting method was used, assuming Gaussian band profiles for the components. No baseline corrections were made, and no restrictions were imposed on the band positions and widths. The best fits were obtained with reduced $\chi^2 \approx 10^{-6}$ and a correlation coefficient of ≈ 0.999.

## 3.2.2 Results and discussion

### 3.2.2.1 LbL polyelectrolytes assembly on PP9010 microgels

As described in Chapter 2 well-defined, monodisperse, pH and temperature responsive p(NIPAAm-co-MAA) 90:10 microbeads, PP9010, were successfully synthesized in $scCO_2$. The presence of the carboxylic acid groups enables a pH-dependent negative charge on the microgels that can be explored for the electrostatic-driven multilayer assembly of PEs. In order to optimize the LbL conditions on PP9010 microgels, the zeta potential of the native microgels was initially determined as a function of solution pH, as shown in Figure 3.9. The obtained zeta potential results from the application of hard-sphere colloid equations to electrophoretic mobility measurements and can only be considered as approximate values for soft microgels; nevertheless they can be used for establishing comparisons among similar systems.[58] The zeta potential is a measure of the potential difference between the dispersion medium and the stationary layer of fluid surrounding the particle and thus can be related to the stability of the colloidal dispersion: particles with high zeta potential (> ± 30 mV) have higher surface charge and tend to repel each other, preventing aggregation. In order to obtain defined multilayers on single particles, the LbL assembly of the different polyelectrolyte pairs on PP9010 microgels was therefore performed at pH in which not only the microgels are more charged (pH ≥ 6) but also the polyelectrolytes are mostly ionized and without added salts, in order to maintain high microgel surface charge during the process. From the Figure 3.9 it is also possible to infer a striking pH-dependence of the surface charge. This observation together with the observed microgel swelling variation depicted in Chapter 2, points out to a "core-shell"-like microstructure where possibly there is a higher local concentration of carboxylic groups on the microgel outer shell, as it was described that charged groups located in loosely cross-linked shells enable larger surface charge and swelling degree variations with pH when compared to charged groups in the core.[53,59,60] Depending on the polymerization conditions, examples of proposed "core-shell" microstructures in p(NIPAAm-co-MAA) nanogels are found in the literature.[59,61] In aqueous bulk polymerizations it was found that methacrylic acid exhibits a much lower reactivity than NIPAAm, suggesting a higher probability for NIPAAm homopolymerization, with MAA monomers more prone to react at higher NIPAAm conversions.[62] Thus, the formation of MAA-rich chains late in the polymerization reaction appears to be likely, consistent with the outlined "core-shell" hypothesis, which may even be more significant in the microscale than in nanoscaled systems. Unfortunately no polymerization kinetics data is available in $scCO_2$. A radial distribution of the cross-linker may also contribute for the formation of more dense cores decorated by loosely cross-linked outer shells, as shown for MBAm cross-linked PNIPAAm nanogels.[63] Further experiments would be required to directly assess carboxylic groups' localization within the microgels, such electron microscopic analysis of stained carboxylic groups in dry

microgels or potentiometric titrations to establish correlations between ionization and electrophoretic mobility.

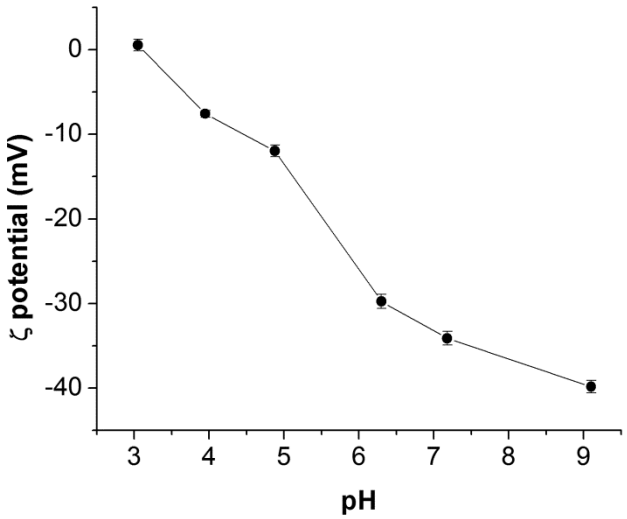


**Figure 3.9** Zeta potential of PP9010 microgels dispersed in Milli-Q water at different pH.

The LbL assembly of the different polyelectrolyte pairs on PP9010 microgels had an impact not only on the native microgel's size but also on the thermoresponsiveness – Figure 3.10. For all the samples dispersed in Milli-Q water at assembly pH, the initial complexation of a polycation led to a contraction of the microgel, followed by a recovery in size to values close to the native PP9010 microgel upon sequential assembly of the polyanion. In the PP9010/$(PDAC/PSS)_n$ system, the microgels kept their size unchanged, over the value at the first bilayer, upon further LbL assembly. On the other hand, for both the weak polyelectrolyte pairs the sequential complexation of the polycation on the first bilayer led again to microgel contraction, followed by swelling upon polyanion deposition, being a trend sustained across the analyzed layer number range. Moreover, the microgels exhibited thermoresponsive collapse when a polycation was the outermost layer (except for the PP9010/$(PDAC/PSS)_n$ system after the first bilayer); while that behavior is suppressed when a polyanion was the last assembled layer (a reversibility on the thermoresponsiveness was qualitatively observed under the microscope – data not shown).

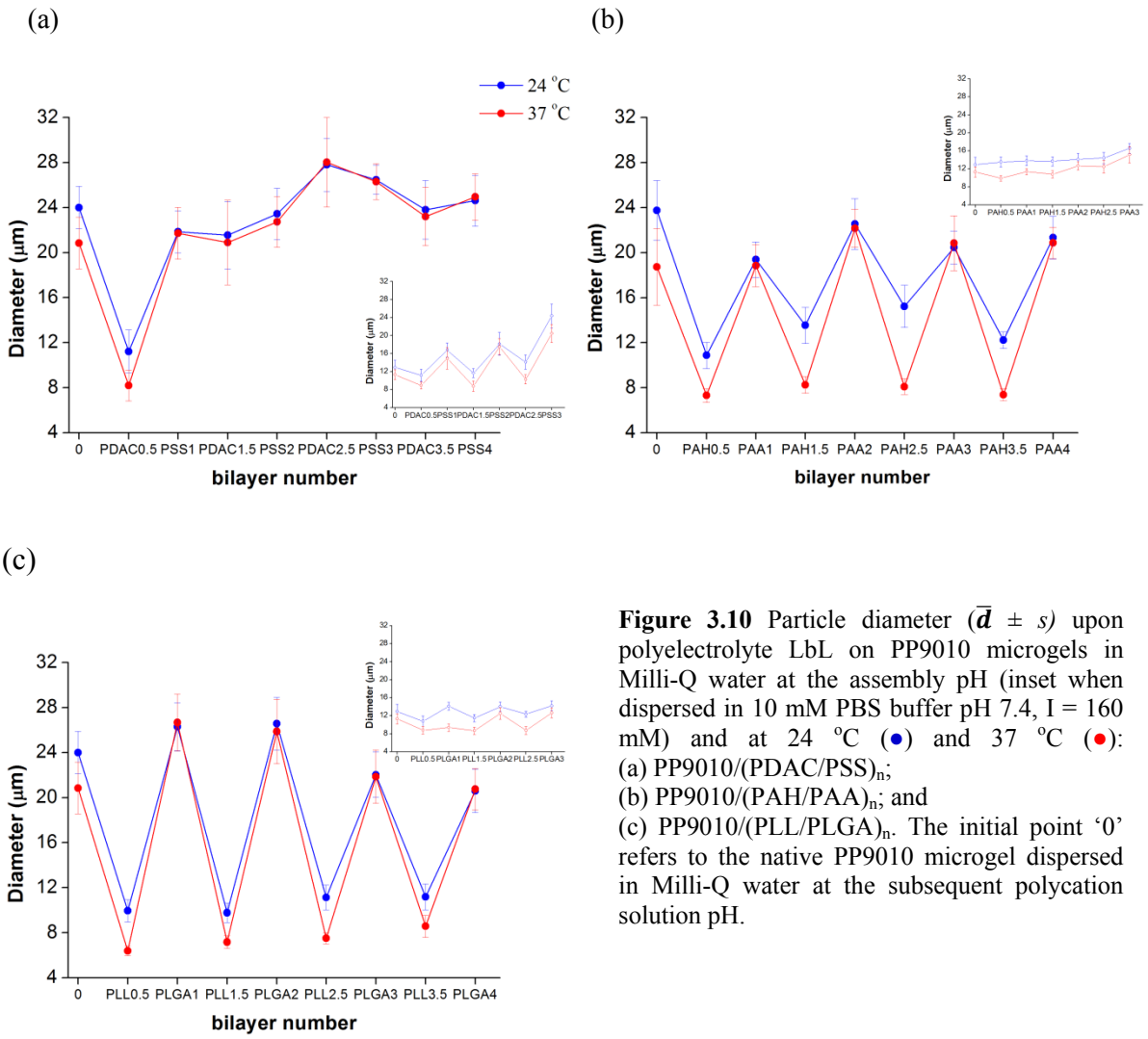


**Figure 3.10** Particle diameter ($\bar{d} \pm s$) upon polyelectrolyte LbL on PP9010 microgels in Milli-Q water at the assembly pH (inset when dispersed in 10 mM PBS buffer pH 7.4, I = 160 mM) and at 24 °C (●) and 37 °C (●): (a) PP9010/(PDAC/PSS)$_n$; (b) PP9010/(PAH/PAA)$_n$; and (c) PP9010/(PLL/PLGA)$_n$. The initial point '0' refers to the native PP9010 microgel dispersed in Milli-Q water at the subsequent polycation solution pH.

The polycation probably complexes on the PP9010 microgel mostly through ionic interactions with the available carboxylic groups, therefore decreasing the electrostatic contribution of the carboxylate groups for swelling; as a consequence the microgel contracted and the entropy-driven collapse of the microgel occurred when increasing the temperature, even at pH values above PMAA p$K_a$ for which the native microbeads collapse is less significant (pH 7.4 for the PP9010/(PDAC/PSS)$_n$ and PP9010/(PLL/PLGA)$_n$ and pH 6 for the PP9010/(PAH/PAA)$_n$). The subsequent polyanion complexation occurs via interactions with the underlying polycationic layer at the expense of existing contacts between the polycation and the PP9010 microgel. Therefore, the MAA groups were again freer to stabilize water within the microgel, similarly to the native PP9010, the swelling was recovered and the thermoresponsive behavior was suppressed at pH above PMAA p$K_a$. However, the subsequent PDAC deposition on the PP9010/(PDAC/PSS)$_n$ microgels did not change the microgel responsiveness significantly. Possibly, the high degree of ionic cross-links within the first PDAC/PSS bilayer coupled with a lower intrinsic interdiffusion of the polyelectrolytes impairs any effect of further layers on the overall responsiveness of the LbL assembled microgel. The magnitude of the outermost layer "odd-even" effect on the size and thermoresponsive behavior was larger for the PP9010/(PLL/PLGA)$_n$

microgels than it is for PP9010/$(PAH/PAA)_n$. Although both systems were assembled in conditions where all polyelectrolytes were mostly ionized, interdiffusion in polypeptide systems is generally more significant[48,49] and the polycation/polyanion specific effect on the microgels behavior may be more easily reversed than in synthetic multilayer films. Consistent with the behavior of native PP9010 microgels, when LbL assembled microgels were buffer exchanged to solutions with physiological ionic strength, the presence of salts shields electrostatic repulsions within the microgels and assembled polyelectrolyte pairs, weakening their interactions. For the strong polyelectrolyte system, the presence of salts yielded PDAC-terminated microgels able to respond to temperature stimuli for all bilayer numbers; and for the weak polyelectrolytes there were less sharp differences in size and thermoresponsiveness among polycation and polyanion-terminated microgels (insets in Figure 3.10). On the latter case, the microgel size is within the targeted cell-size under physiological conditions at the analyzed bilayer number.

These results are not totally in agreement with other studies performed using p(NIPAAm-co-MAA) microgels with hydrodynamic radius between ~ 200-360 nm and approximately the same MAA content and cross-linking degree,[15,54] as in the latter the polyanion terminated microgels retained the thermoresponsive behavior presenting the higher swelling degree. This disparity may be due to different charge distributions within the microgels, which was shown to impact the thermoresponsive behavior[15] and localization of complexed polyelectrolytes;[53] and/or larger mesh sizes for the microgels used in this study that might allow further interpenetration of the polyelectrolytes contributing to enhance water stabilization within the hydrogel in the polyanion-terminated systems.

Evidence of the sequential deposition of the different polyelectrolytes on PP9010 microgels can be assessed using zeta potential measurements as a function of layer number, at the conditions used during assembly. In Figure 3.11 it is clear that the surface charge of the microgel was reversed with each assembly step, suggesting that the polyelectrolytes were sequentially complexed. However, in terms of absolute value, the surface charge was not totally reversed upon sequential layering, differing from what is observed for LbL assembly on flat surfaces or rigid particles.[34,37] This behavior is an indication that interactions between the soft and porous microgel substrate and the LbL films are occurring and may be due to incomplete coverage of the microgel surface and/or interpenetration of the polyelectrolytes throughout the microgel mesh.

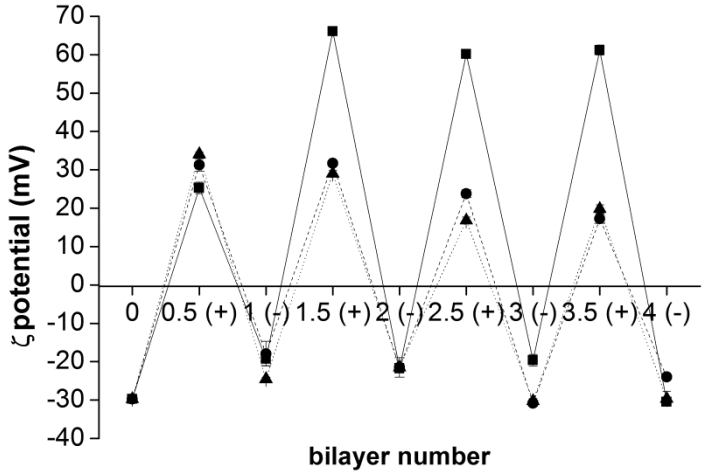


**Figure 3.11** Zeta potential measurements of LbL assembled microgels with increasing bilayer number show particle surface charge reversal upon polyelectrolyte sequential deposition: (■) PP9010/$(PDAC/PSS)_n$; (▲) PP9010/$(PAH/PAA)_n$, and (●) PP9010/$(PLL/PLGA)_n$. The initial point (0) refers to the zeta potential of native PP9010 microgels when dispersed in water (pH ~ 5).

Further indication on the successful assembly of the polyelectrolytes is clearly shown in Figure 3.12 for the PP9010/$(PAH/PAA)_n$ and PP9010/$(PLL/PLGA)_n$ systems using fluorescent-labeled polymers, especially for the dual labeled PP9010/$(PAH\text{-Rhodamine B}/PAA\text{-Cascade Blue})_1$ micrograph. Moreover, for both systems, the polyelectrolytes were able to distribute across the microgel, with higher fluorescence intensity on the microgel shell. This is consistent with the hypotheses of a "core-shell"-like microstructure of the hydrogel and thus polyelectrolytes with higher intrinsic mobility may display more significant outermost bilayer number "odd-even" effect on size and responsive behavior. On the other hand, it may be argued that the polydispersity of the commercial used polyelectrolytes would result in differentiated fluorescence intensities distributions. The flow cytometry analysis of PP9010/$(PLL\text{-FITC}/PLGA)_n$ and PP9010/$(PAH\text{-RhoB}/PAA)_n$ microgels yet offers another indication of sequential polyelectrolyte assembly, showing a successive increase in fluorescence at each polycation deposition step, in an apparently linear regime within the analyzed bilayer number range. Flow cytometry had already been proposed as a method for monitoring polyelectrolyte assembly on colloidal particles; herein it is shown that it can also be easily expanded for the quick and quantitative evaluation of LbL build-up of polyelectrolytes on soft porous particles.[64]

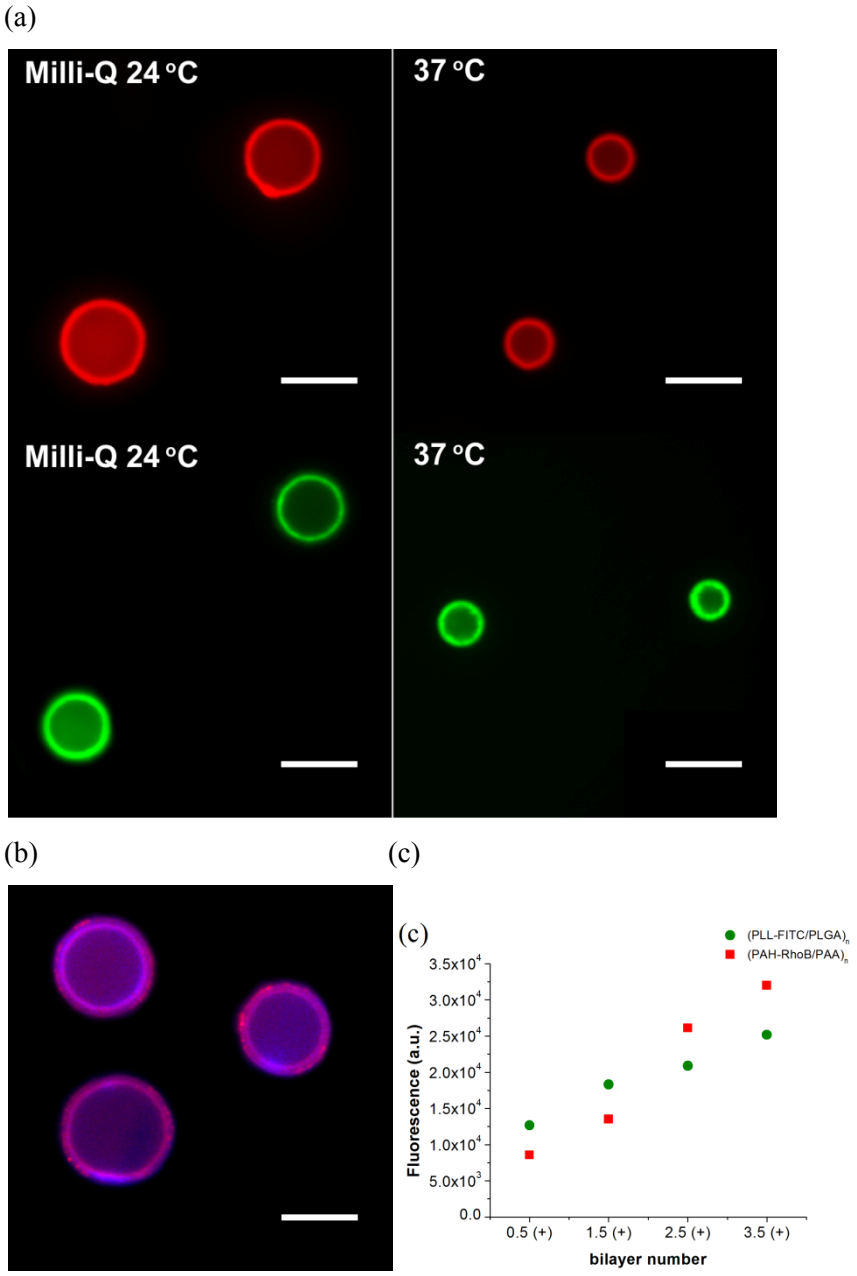


**Figure 3.12** (a) Confocal micrographs of thermoresponsive PP9010 microgels assembled with fluorescent labeled polycations, dispersed in Milli Q water at assembly pH at 24 °C and 37 °C: top PP9010/PAH-RhoB and bottom PP9010/PLL-FITC. (b) Confocal micrographs of PP9010/(PAH-RhoB/PAA-Cascade Blue)$_1$ indicating multilayer build-up. (c) Flow cytometry measurements of the fluorescence of PP9010/(PLL-FITC/PLGA)$_n$ (■) and PP9010/(PAH-RhoB/PAA)$_n$ (●) microgels in 10 mM PBS buffer show an overall linear increase in the amount of polycation with bilayer number.

#### 3.2.2.2 ATR FT-IR spectral analysis of PP9010 assembled microgels

The sequential assembly of the polyelectrolyte pairs used on PP9010 microgels was further inferred from the sequential modifications in the position, intensity and shape of the infrared bands of the dry assembled microgels FT-IR spectra in the wavenumber region between 950 and 1800 $cm^{-1}$ – Figure 3.13. Upon deposition of the first PDAC layer on PP9010 the Amide III band at 1242 $cm^{-1}$ becomes more intense, which was observed as shoulder at 1234 $cm^{-1}$ in the native microgels (PDAC has no infrared bands around this position – Annex II). The sequential assembly of PSS is indicated by the appearance of the characteristic sulfonate ion vibrations at 1008, 1035, 1126 and 1180 $cm^{-1}$.[65] These vibrations decrease when PDAC is subsequently assembled (PP9010/$(PDAC/PSS)_1$PDAC spectra), which may be due to interactions being established between the polyelectrolytes[65,66] or partial stripping of the underlying PSS when the polycation was deposited. Nevertheless there is an overall increase of the sulfonate ion bands intensity with bilayer number. The same tendency was observed on the weak polyelectrolyte pairs deposition. However in both systems the most intense and characteristic bands of the polyelectrolytes overlap with the PP9010 amide vibrations (Annex II). The exact band positions for the polypeptides depend on their conformation (α-helix, β-sheet or random coil), due to vibrational interactions between the peptide groups and the different forms of hydrogen bonding,[67] while for the weak synthetic polyelectrolyte system, the exact peak positions is related to their ionization degree.[41,68] For both polyelectrolyte pairs the Amide region becomes less sharp with increasing layer number and it is possible to observe a modification on the peaks position and relative intensity of the Amide II to Amide I bands. Furthermore, in the high wavenumber region of the spectra the sequential depositon of the PLL/PLGA and PAH/PAA led to an increase in intensity and broadening of the band in the N-H stretching region between 3000-3450 $cm^{-1}$ relative to the isopropyl and alkyl vibrations (2850-3000 $cm^{-1}$), due mainly to the contribution of PLL and PAH νN-H and PLGA and PAA νO-H (Annex II).

From the spectral analysis of the amide region of native and LbL assembled microgels, more information regarding the specific interactions being established can be derived. Firstly, the spectra of the native PP9010 copolymer is dominated by two strong bands at 1641 $cm^{-1}$ and 1531 $cm^{-1}$, corresponding to the Amide I and Amide II vibrations of the PNIPAAm segments, respectively. Both vibrations were slightly shifted to lower energy states in comparison to the amide bands of PNIPAAm homopolymers (1646 and 1533 $cm^{-1}$, respectively), indicating the presence of hydrogen bonding interactions, similar to what has been reported for the Amide I vibration of other acrylamide copolymers.[69] The vibration corresponding to the C=O stretching of unprotonated carboxylic groups of PMAA can be observed as a shoulder at 1707 $cm^{-1}$ (besides a small possible contribution of free C=O groups from PNIPAAm).[70] The stretch vibration of the carboxylate ion has been reported at 1554 $cm^{-1}$ and therefore cannot be distinguished from the strong Amide II vibration of the PNIPAAm segments.[68] Upon spectral deconvolution, two components were identified in the Amide I region at

1637 and 1662 $cm^{-1}$, corresponding to intermolecular and intramolecular H-bonded νC=O vibrations, with the majority involved in intramolecular interactions. In regards to the Amide II vibration, two components can be assigned to free δNH vibrations at 1509 $cm^{-1}$ and H-bonded δNH at 1535 $cm^{-1}$ – *vide* Table 3.3. In both bands, a characteristic component, relative to intermolecular H-bonded νC=O in Amide I and relative to intramolecular H-bonded δNH in Amide II, was absent, which can be an indication of interactions between PNIPAAm amide and PMAA carboxylic groups, similarly to what was observed in other systems involving PNIPAAm.[71]

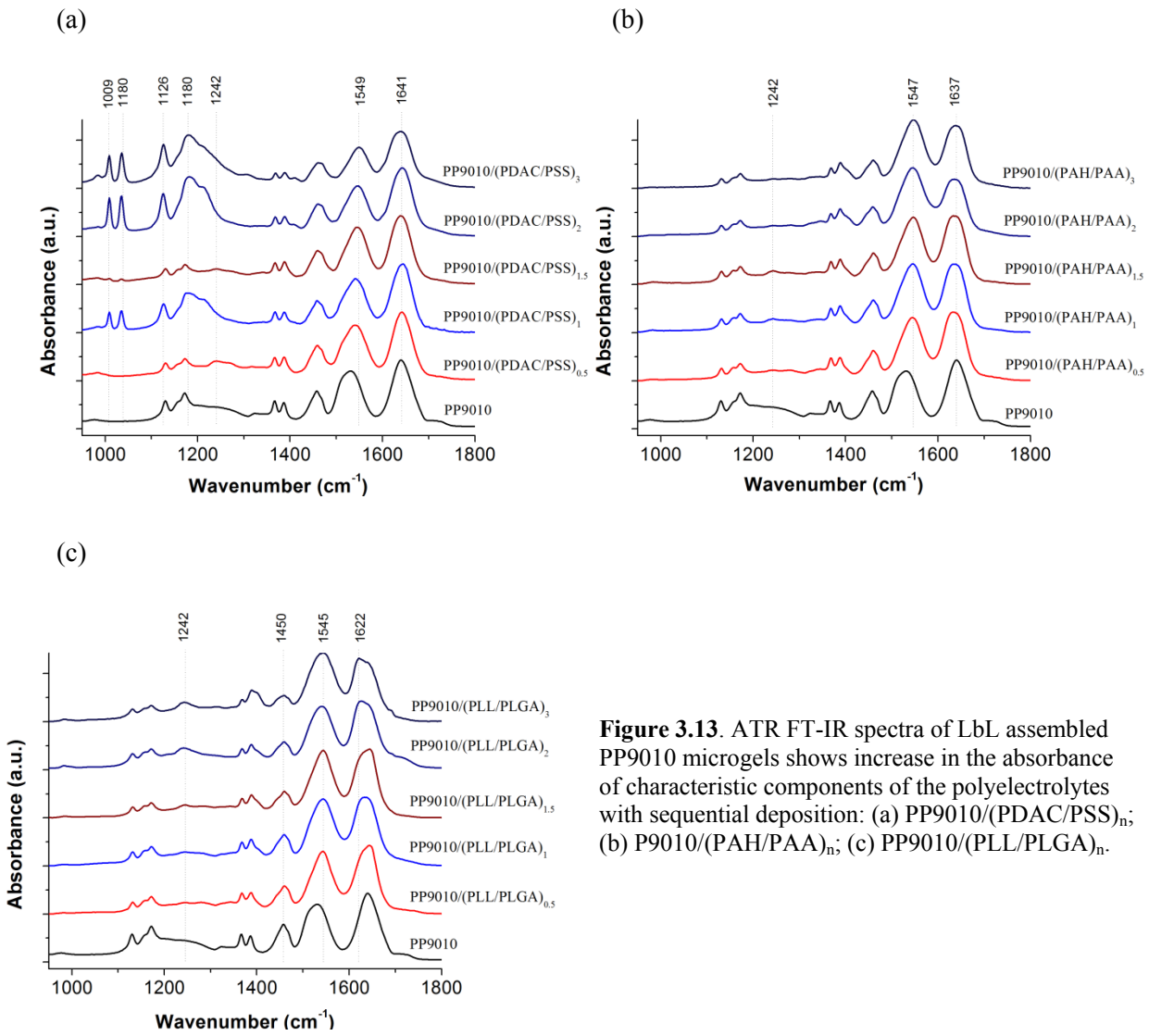


**Figure 3.13**. ATR FT-IR spectra of LbL assembled PP9010 microgels shows increase in the absorbance of characteristic components of the polyelectrolytes with sequential deposition: (a) PP9010/$(PDAC/PSS)_n$; (b) P9010/$(PAH/PAA)_n$; (c) PP9010/$(PLL/PLGA)_n$.

The analysis of the Amide region (1480-1750 $cm^{-1}$) of the LbL assembled microgels revealed some common trends as well as differences across the analyzed polyelectrolyte systems – Table 3.3. The PP9010/$(PDAC/PSS)_n$ samples can be used as a benchmark for the overall spectral analysis as there are no characteristic bands of the polyelectrolytes overlapping with the PP9010 Amide vibrations. In the PP9010/PDAC system, the intensity of the shoulder corresponding to the copolymer carboxylic

groups decreased significantly (1.6 % in area to 0.5 %), indicating that PDAC layering occurs mostly through ionic interactions (spectra in Annex II). The position and relative intensity of the constituent bands of the Amide bands also changed significantly, relatively to the native PP9010. The components relative to H-bonded δNH in the Amide II (1543 $cm^{-1}$), and intramolecular H-bonded νC=O (1644 $cm^{-1}$) and "freer" νC=O (1669 $cm^{-1}$) in the Amide I shifted to higher energy states closer to the characteristic vibrations of cross-linked PNIPAAm homopolymers (in the Amide I overlapping of the carboxylate ion vibration may also contribute for changes in the band composition). These observations are a clear indication that the H-bonding between the composing PNIPAAm and PMAA segments becomes weaker when the polycation is assembled. Probably the interactions established between the PP9010 substrate and PDAC lead to the formation of carboxylate ions on the PMAA segments, and consequently the PNIPAAm segments are "freer". The subsequent assembly of PSS (PP9010/$(PDAC/PSS)_1$) led to a significant shift of the intramolecular H-bonded νC=O (1632 $cm^{-1}$) and "freer" νC=O (1653 $cm^{-1}$) components back to lower wavenumbers, closer to the values found for the native PP9010, and the component relative to intermolecular H-bonded νC=O was not relevant anymore. This transition indicates that as PSS interacts with the underlying polycation layer, PNIPAAm segments are again involved in H-bonding either with water and/or PMAA segments. The intensity of the shoulder relative to free COOH groups remained very low. The sequential deposition of additional strong polyelectrolytes layers did not change the band composition significantly, within the analyzed range and followed assembly conditions.

For the weak polyelectrolyte pairs the same tendency was observed in the Amide bands region when first polycation and then polyanion were assembled. Additionally, a component assigned to a polyelectrolyte specific vibration occurred at 1615-1630 $cm^{-1}$ which may be due to β-sheet infrared bands of PLL in the PP9010/$(PLL/PLGA)_n$ system or the asymmetric $NH_3^+$ bending mode of PAH in PP9010/$(PAH/PAA)_n$. However, these systems differ from the strong polyelectrolyte pair as the weak polycation assembly on the first PP9010/$(PAH/PAA)_1$ and PP9010/$(PLL/PLGA)_1$ bilayer leads again to an Amide bands composition and constituent components intensity similar to the initial PP9010/polycation profile in a quasi-reversible process. The spectral analysis was not performed beyond the second bilayer since the vibrations of the weak polyelectrolytes become predominant over those of the PP9010 substrate. Clearly the spectral analysis correlates well with the observed swelling and thermoresponsive behavior described earlier, suggesting that when polycations are on the outermost layer PNIPAAm segments are freer to undergo the entropy-driven collapse with temperature while in polyanion-terminated microgels the water-amide interactions are stabilized. For PP9010/$(PDAC/PSS)_n$ microgels the initial physical crosslink occuring after the first bilayer prevents any further modification of the water-PNIPAAm interactions upon subsequent deposition.

**Table 3.3** Summary of the deconvolution results obtained for the Amide region of the FT-IR spectra of PNIPAAm homopolymer, PP9010 microgels, and LbL assembled PP9010 microgels with $(PDAC/PSS)_n$, $(PAH/PAA)_n$ and $(PLL/PLGA)_n$. PNIPAAm assignments from the section 3.1 are repeated to facilitate interpretation.

| | **Wavenumber ($cm^{-1}$) (%Area)** | | | | | | | |
|---|---|---|---|---|---|---|---|---|
| **Assignments** | δNH free AmideII | δNH intra HB AmideII | δNH inter HB AmideII | νC=O inter HB Amide I | PE* | νC=O intra HB Amide I | νC=O "freer" Amide I | νC=O free COOH |
| PNIPAAm | 1509 (7.2) | 1529 (16.0) | 1548 (17.7) | 1607 (5.0) | - | 1644 (32.0) | 1669 (9.1) | - |
| PP9010 | 1509 (6.3) | 1535 (31.6) | - | | - | 1637 (36.8) | 1662 (11.8) | 1720 (1.6) |
| **bilayer nr.** | **$PP9010/(PDAC/PSS)_n$ LbL** | | | | | | | |
| 0.5 | 1514 (3.4) | - | 1543 (40.3) | 1623 (6.9) | - | 1644 (43.5) | 1669 (5.4) | 1717 (0.5) |
| 1 | 1514 (3.1) | - | 1543 (37.9) | - | - | 1632 (31.9) | 1653 (26.5) | 1708 (0.6) |
| 1.5 | 1517 (2.4) | - | 1546 (39.6) | - | - | 1630 (32.8) | 1653 (23.3) | 1694 (2.0) |
| 2 | 1519 (2.0) | - | 1547 (34.1) | - | - | 1637 (48.4) | 1657 (11.2) | 1694 (4.4) |
| **bilayer nr.** | **$PP9010/(PAH/PAA)_n$ LbL** | | | | | | | |
| 0.5 | 1515 (3.3) | - | 1545 (41.3) | 1611 (11.6) | 1625 (18.0) | 1648 (21.4) | 1669 (3.6) | 1706 (0.8) |
| 1 | 1514 (2.6) | - | 1546 (46.4) | - | 1624 (8.7) | 1637 (37.9) | 1654 (4.2) | 1715 (0.1) |
| 1.5 | 1516 (6.2) | - | 1547 (39.4) | 1610 (9.1) | 1627 (21.2) | 1650 (19.0) | 1666 (4.3) | 1707 (0.7) |
| 2 | 1514 (3.4) | - | 1545 (47.5) | - | 1619 (19.6) | 1633 (16.3) | 1656 (10.0) | 1696 (3.1) |
| **bilayer nr.** | **$PP9010/(PLL/PLGA)_n$ LbL** | | | | | | | |
| 0.5 | 1512 (4.8) | - | 1542 (34.6) | 1613 (15.6) | 1627 (19.0) | 1649 (18.4) | 1672 (5.0) | 1706 (2.6) |
| 1 | 1515 (2.6) | - | 1544 (44.0) | - | 1620 (1.0) | 1634 (47.3) | 1653 (2.8) | 1702 (2.3) |
| 1.5 | 1511 (2.3) | - | 1543 (42.5) | 1617 (13.2) | 1626 (19.9) | 1650 (18.8) | 1677 (3.1) | 1706 (0.2) |
| 2 | 1515 (5.2) | - | 1544 (37.6) | - | 1617 (3.8) | 1635 (46.8) | 1651 (1.3) | 1707 (5.2) |

* PE: polyelectrolyte characteristic component

### 3.2.3 Conclusions

The LbL sequential complexation of both strong and weak polyelectrolyte pairs was successfully performed on the prepared temperature and pH-sensitive p(NIPAAm-co-MAA) microgels, as shown by surface charge reversal on zeta potential measurements, increased fluorescence in dye-labeled polyelectrolyte assembled microgels, confocal microscopy and FT-IR analysis. LbL assembly may be used not only to modify the microgel surface chemistry, namely through the assembly of potential cell-adhesive films, but also to further tune their responsive behavior and swelling; hence possibly permeability. It was shown by optical microscopy that the microgels swelling and temperature sensitivity at the analyzed solution conditions is dependent on the type of assembled polyelectrolyte pairs as well as on the composition of the outermost layer, being clear that LbL assembly on soft porous microgels is a substrate-dependent process. Overall, polycation-terminated microgels are less swollen and exhibited thermoresponsive behavior, even at a pH above PMAA $pK_a$; while polyanion-terminated assembled microgels are more swollen and do not exhibit significant volume phase transition with temperature. This process is mediated by the interactions between the microgel and the assembled polyelectrolytes that have an impact on the deprotonation of COOH groups, which contribute for the stabilization of the polymer conformation in a solvated state and for the increase on the mobile ions concentration within the microgels. Therefore for higher ionic strengths, these interactions are weakened due to charge shielding and the observed "odd-even" effect of the last complexed layer on microgel swelling and responsiveness is less significant. The FT-IR spectral analysis of the amide region of the assembled microgels has shown that the microbead carboxylic groups are clearly engaged on the initial complexation of the polycation, leading to microgel deswelling. Moreover, when a polycation is present as the outermost layer the PNIPAAm segments are less H-bonded to water and/or PMAA and the microgels become sensitive to temperature stimulus. As a polyanion is assembled, the interaction between the underlying polycation and the microgels weakens and not only PNIPAAm is again involved in H-bonding interactions but also carboxylic groups can deprotonate, contributing for microgel swelling.

The variety of coatings that are amenable to assembly on p(NIPAAm-co-MAA) particles, the cell-like size of the LbL assembled microgels under physiological conditions, and the exceptional tunability of this system prompted further studies on the incorporation of a protease function in this specific system, which will be the subject of the next chapter.

## 3.3 References


1. Akagawa, M. & Suyama, K. Amine oxidase-like activity of polyphenols. *Eur. J. Biochem.* **268**, 1953-1963 (2001).

2. Chung, K.T., Lu, Z. & Chou, M.W. Mechanism of inhibition of tannic acid and related compounds on the growth of intestinal bacteria. *Food Chem. Toxicol.* **36**, 1053-60 (1998).

3. Haslam, E. Natural polyphenols (vegetable tannins) as drugs: possible modes of action. *J. Nat. Prod.* **59**, 205-15 (1996).

4. Edelmann, A. & Lendl, B. Toward the optical tongue: flow-through sensing of tannin-protein interactions based on FTIR spectroscopy. *J. Am. Chem. Soc.* **124**, 14741-7 (2002).

5. Frazier, R. a, Papadopoulou, A., Mueller-Harvey, I., Kissoon, D. & Green, R.J. Probing protein-tannin interactions by isothermal titration microcalorimetry. *J. Agric. Food Chem.* **51**, 5189-95 (2003).

6. Baxter, N.J., Lilley, T.H., Haslam, E. & Williamson, M.P. Multiple interactions between polyphenols and a salivary proline-rich protein repeat result in complexation and precipitation. *Biochemistry* **36**, 5566-77 (1997).

7. Haslam, E., Lilley, T.H., Cai, Y., Martin, R. & Mangnolato, D. Traditional Herbal Medicines - The Role of Polyphenols. *Planta Med.* **55**, 1-8 (1989).

8. Oh, H.I., Hoff, J.E., Armstrong, G.S. & Haff, L. a Hydrophobic interaction in tannin-protein complexes. *J. Agric. Food Chem.* **28**, 394-398 (1980).

9. Shutava, T., Prouty, M., Kommireddy, D. & Lvov, Y. pH Responsive Decomposable Layer-by-Layer Nanofilms and Capsules on the Basis of Tannic Acid. *Macromolecules* **38**, 2850-2858 (2005).

10. Yen, K.-C., Mandal, T.K. & Woo, E.M. Enhancement of bio-compatibility via specific interactions in polyesters modified with a bio-resourceful macromolecular ester containing polyphenol groups. *J Biomed Mater. Res. A* **86**, 701-12 (2008).

11. Erel-Unal, I. & Sukhishvili, S. a Hydrogen-Bonded Multilayers of a Neutral Polymer and a Polyphenol. *Macromolecules* **41**, 3962-3970 (2008).

12. Kozlovskaya, V., Kharlampieva, E., Drachuk, I., Cheng, D. & Tsukruk, V.V. Responsive microcapsule reactors based on hydrogen-bonded tannic acid layer-by-layer assemblies. *Soft Matter* **6**, 3596 (2010).

13. Kim, B.-S., Lee, H.-I., Min, Y., Poon, Z. & Hammond, P.T. Hydrogen-bonded multilayer of pH-responsive polymeric micelles with tannic acid for surface drug delivery. *Chem. Commun.* 4194-6 (2009).

14. Schmidt, D.J. & Hammond, P.T. Electrochemically erasable hydrogen-bonded thin films. *Chem. Commun.* **46**, 7358-60 (2010).

15. Wong, J.E. & Richtering, M. Surface Modification of Thermoresponsive Microgels via Layer-by-Layer Assembly of Polyelectrolyte Multilayers. *Prog. Colloid Polym. Sci.* **133**, 45-51 (2006).

16. Keerl, M., Smirnovas, V., Winter, R. & Richtering, W. Copolymer Microgels from Mono- and Disubstituted Acrylamides: Phase Behavior and Hydrogen Bonds. *Macromolecules* **41**, 6830-6836 (2008).

17. Kosik, K., Wilk, E., Geissler, E. & László, K. Distribution of Phenols in Thermoresponsive Hydrogels. *Macromolecules* **40**, 2141-2147 (2007).

18. Chen, G. *et al.* Phase transition behaviors of poly(*N*-isopropylacrylamide) microgels induced by tannic acid. *J. Colloid Interface Sci.* **343**, 168-75 (2010).

19. Araujo, P.Z., Morando, P.J. & Blesa, M.A. Interaction of catechol and gallic acid with titanium dioxide in aqueous suspensions. 1. Equilibrium studies. *Langmuir* **21**, 3470-4 (2005).

20. Langmuir, I. The Adsorption of Gases on Plane Surfaces of Glass, Mica and Platinum. *J. Am. Chem. Soc.* **40**, 1361-1403 (1918).

21. Kubelka, P. & Munk, F. *Zeitschrift fur technische Physik* **12**, 593-601 (1931).

22. Cowen, S. & Al-Abadleh, H.A. DRIFTS studies on the photodegradation of tannic acid as a model for HULIS in atmospheric aerosols. *Phys. Chem. Chem. Phys.* **11**, 7838-7847 (2009).

23. Jastrzebska, M. *et al.* Tannic acid-stabilized pericardium tissue : IR spectroscopy, atomic force microscopy, and dielectric spectroscopy investigations. *J. Biomed. Mater. Res. A* (2006).

24. Mohammed-Ziegler, I. Vibrational spectroscopic calculations on pyrogallol and gallic acid. *J. Mol. Struct.-THEOCHEM* **618**, 259-265 (2002).

25. Janković, I.A., Saponjić, Z.V., Džunuzović, E.S. & Nedeljković, J.M. New Hybrid Properties of TiO(2) Nanoparticles Surface Modified With Catecholate Type Ligands. *Nanoscale Res. Lett.* **5**, 81-88 (2009).

26. Maeda, Y., Higuchi, T. & Ikeda, I. Change in Hydration State during the Coil-Globule Transition of Aqueous Solutions of Poly(*N*-isopropylacrylamide) as Evidenced by FTIR. *Langmuir* **16,** 7503 - 7509 (2000).

27. Sun, B., Lin, Y. & Wu, P. Structure Analysis of Poly(*N*-isopropylacrylamide) Using Near-Infrared Spectroscopy and Generalized Two-Dimensional Correlation Infrared Spectroscopy. *Appl. Spectrosc.* **61**, (2007).

28. Skrovanek, D.J., Painter, P.C. & Coleman, M.M. Hydrogen bonding in polymers. 2. Infrared temperature studies of nylon 11. *Macromolecules* **19**, 699-705 (1986).

29. Lin, S.-Y., Chen, K.-S. & Liang, R.-C. Thermal micro ATR/FT-IR spectroscopic system for quantitative study of the molecular structure of poly(*N*-isopropylacrylamide) in water. *Polymer* **40**, 2619-2624 (1999).

30. Decher, G. Fuzzy Nanoassemblies: Toward Layered Polymeric Multicomposites. *Science* **277**, 1232-1237 (1997).

31. Stubbe, B.G., Gevaert, K., Derveaux, S., Braeckmans, K., De Geest, B.G., Goethals, M., Vandekerckhove, J., Demeester, J. Evaluation of Encoded Layer-By-Layer Coated Microparticles As Protease Sensors. *Adv. Funct. Mater.* **18**, 1624-1631 (2008).

32. Kang, J., Loew, M., Arbuzova, A., Andreou, I. & Dähne, L. Nucleic acid diagnostic FRET particles based on layer-by-layer technology. *Adv. Mater.* **22**, 3548-52 (2010).

33. Cortez, C., Tomaskovic-Crook, E., Johnston, A.P.R., Radt, B., Cody, S.H., Scott, A.M., Nice, E.C., Heath, J.K. & Caruso, F. Targeting and Uptake of Multilayered Particles to Colorectal Cancer Cells. *Adv. Mater.* **18**, 1998-2003 (2006).

34. Rogach, A. *et al.* Nano- and Microengineering: 3-D Colloidal Photonic Crystals Prepared from Sub-µm-sized Polystyrene Latex Spheres Pre-Coated with Luminescent Polyelectrolyte/Nanocrystal Shells. *Adv. Mater.* **12**, 333-337 (2000).

35. Peyratout, C.S. & Dähne, L. Tailor-made polyelectrolyte microcapsules: from multilayers to smart containers. *Angew. Chem., Int. Ed.* **43**, 3762-83 (2004).

36. Hammond, P.T. Form and Function in Multilayer Assembly: New Applications at the Nanoscale. *Adv. Mater.* **16**, 1271-1293 (2004).

37. Itano, K., Choi, J. & Rubner, M.F. Mechanism of the pH-Induced Discontinuous Swelling / Deswelling Transitions of Poly(allylamine hydrochloride)-Containing Polyelectrolyte Multilayer Films. *Macromolecules* **38**, 3450-3460 (2005).

38. Wong, J.E., Rehfeldt, F., Hänni, P., Tanaka, M. & Klitzing, R.V. Swelling Behavior of Polyelectrolyte Multilayers in Saturated Water Vapor. *Macromolecules* **37**, 7285-7289 (2004).

39. Farhat, T.R. & Schlenoff, J.B. Doping-controlled ion diffusion in polyelectrolyte multilayers: mass transport in reluctant exchangers. *J. Am. Chem. Soc.* **125**, 4627-36 (2003).

40. Farhat, T., Yassin, G., Dubas, S.T. & Schlenoff, J.B. Water and Ion Pairing in Polyelectrolyte Multilayers. *Langmuir* **15**, 6621-6623 (1999).

41. Choi, J. & Rubner, M.F. Influence of the Degree of Ionization on Weak Polyelectrolyte Multilayer Assembly. *Macromolecules* **38**, 116-124 (2005).

42. Mendelsohn, J.D., Yang, S.Y., Hiller, J., Hochbaum, A.I. & Rubner, M.F. Rational design of cytophilic and cytophobic polyelectrolyte multilayer thin films. *Biomacromolecules* **4**, 96-106 (2003).

43. Hiller, J., Mendelsohn, J.D. & Rubner, M.F. Reversibly erasable nanoporous anti-reflection coatings from polyelectrolyte multilayers. *Nat. Mater.* **1**, 59-63 (2002).

44. Chia, K.-K., Cohen, R.E. & Rubner, M.F. Amine-Rich Polyelectrolyte Multilayer Nanoreactors for in Situ Gold Nanoparticle Synthesis. *Chem. Mater.* **20**, 6756-6763 (2008).

45. Richert, L., Lavalle, P., Vautier, D., Senger, B., Stoltz, J.-F., Schaaf, P., Voegel, J.-C., Picart, C. Cell interactions with polyelectrolyte multilayer films. *Biomacromolecules* **3**, 1170-8 (2002).

46. Serizawa, T., Yamaguchi, M. & Akashi, M. Alternating bioactivity of polymeric layer-by-layer assemblies: anticoagulation vs procoagulation of human blood. *Biomacromolecules* **3**, 724-31 (2002).

47. Richert, L., Boulmedais, F., Lavalle, P., Mutterer, J., Ferreux, E., Decher, G., Schaaf, P., Voegel, J.-C. & Picart, C. Improvement of stability and cell adhesion properties of polyelectrolyte multilayer films by chemical cross-linking. *Biomacromolecules* **5**, 284-94 (2004).

48. Picart, C. Polyelectrolyte multilayer films: from physico-chemical properties to the control of cellular processes. *Curr. Med. Chem.* **15**, 685-97 (2008).

49. Jourdainne, L., Lecuyer, S., Arntz, Y., Picart, C., Schaff, P., Senger, B., Voegel, J.-C., Lavalle, P. & Charitat, T. Dynamics of poly(L-lysine) in hyaluronic acid/poly(L-lysine) multilayer films studied by fluorescence recovery after pattern photobleaching. *Langmuir* **24**, 7842-7 (2008).

50. Shenoy, D.B., Antipov, A.A., Sukhorukov, G.B. & Möhwald, H. Layer-by-layer engineering of biocompatible, decomposable core-shell structures. *Biomacromolecules* **4**, 265-72 (2003).

51. Ochs, C., Such, G., Stadler, B. & Caruso, F. Low-Fouling, Biofunctionalized, and Biodegradable Click Capsules. *Biomacromolecules* **9**, 3389-3396 (2008).

52. De Geest, B.G., De Koker, S., Demeester, J., De Smedt, S.C. & Hennink, W.E. Pulsed in vitro release and in vivo behavior of exploding microcapsules. *J. Control. Release* **135**, 268-73 (2009).

53. Kleinen, J., Klee, A. & Richtering, W. Influence of architecture on the interaction of negatively charged multisensitive poly(N-isopropylacrylamide-co-methacrylic acid) microgels with oppositely charged polyelectrolyte: absorption vs adsorption. *Langmuir* **26**, 11258-65 (2010).

54. Díez-Pascual, A.M. & Wong, J.E. Effect of layer-by-layer confinement of polypeptides and polysaccharides onto thermoresponsive microgels: a comparative study. *J. Colloid Interface Sci.* **347**, 79-89 (2010).

55. Wong, J.E., Díez-Pascual, A.M. & Richtering, W. Layer-by-Layer Assembly of Polyelectrolyte Multilayers on Thermoresponsive P(NiPAM-co-MAA) Microgel: Effect of Ionic Strength and Molecular Weight. *Macromolecules* **42**, 1229-1238 (2009).

56. Ibarz, G., Dähne, L., Donath, E. & Möhwald, H. Smart Micro- and Nanocontainers for Storage, Transport, and Release. *Adv. Mater.* **13**, 1324 (2001).

57. Christian, D.A. *et al.* Spotted vesicles, striped micelles and Janus assemblies induced by ligand binding. *Nat. Mater.* **8**, 843-9 (2009).

58. Ohshima, H. Electrokinetics of soft particles. *Colloid Polym. Sci.* **285**, 1411-1421 (2007).

59. Hoare, T. & Pelton, R. Functional group distributions in carboxylic acid containing poly(*N*-isopropylacrylamide) microgels. *Langmuir* **20**, 2123-33 (2004).

60. Jones, C.D. & Lyon, L.A. Shell-Restricted Swelling and Core Compression in Poly(*N*-isopropylacrylamide) Core−Shell Microgels. *Macromolecules* **36**, 1988-1993 (2003).

61. Zhou, S. & Chu, B. Synthesis and Volume Phase Transition of Poly(methacrylic acid-co-*N*-Isopropylacrylamide) Microgel Particles in Water. *J. Phys. Chem. B* **102**, 1364-1371 (1998).

62. Xue, W., Champ, S. & Huglin, M.B. Observations on some copolymerisations involving *N*-isopropylacrylamide. *Polymer* **41**, 7575-7581 (2000).

63. Varga, I., Gilányi, T., Mészáros, R., Filipcsei, G. & Zrínyi, M. Effect of Cross-Link Density on the Internal Structure of Poly(*N*-isopropylacrylamide) Microgels. *J. Phys. Chem. B* **105**, 9071-9076 (2001).

64. Johnston, A.P.R., Zelikin, A.N., Lee, L. & Caruso, F. Approaches to quantifying and visualizing polyelectrolyte multilayer film formation on particles. *Anal. Chem.* **78**, 5913-9 (2006).

65. Fan, X.-D. & Bazuin, C.G. Sulfonated Polystyrene Ionomers Neutralized by Bi- and Multifunctional Organic Cations. 1. An Infrared Spectroscopic Study. *Macromolecules* **28**, 8209-8215 (1995).

66. Gregoriou, V.G., Hapanowicz, R., Clark, S.L. & Hammond, P.T. Infrared Studies of Novel Optically Responsive Materials: Orientation Characteristics of Sulfonated Polystyrene/ Poly(diallyldimethylammonium chloride) Ionic Polymer Multilayers on Patterned Self-Assembled Monolayers. *Appl. Spectrosc.* **51**, 470-476 (1997).

67. Lee, N.H. & Frank, C.W. Surface-Initiated Vapor Polymerization of Various α-Amino Acids. *Langmuir* **19**, 1295-1303 (2003).

68. Sukhishvili, S. a & Granick, S. Layered, Erasable Polymer Multilayers Formed by Hydrogen-Bonded Sequential Self-Assembly. *Macromolecules* **35**, 301-310 (2002).

69. Shibanuma, T. *et al.* Thermosensitive Phase-Separation Behavior of Poly(acrylic acid)-graft-poly(N, N-dimethylacrylamide) Aqueous Solution. *Macromolecules* **33**, 444-450 (2000).

70. Garcia, D. *et al.* Synthesis and characterization of poly(methacrylic acid) hydrogels for metoclopramide delivery. *Eur. Polym. J.* **40**, 1637-1643 (2004).

71. Costa, E., Coelho, M., Ilharco, L.M., Aguiar-Ricardo, A. & Hammond, P.T. Tannic Acid Mediated Suppression of PNIPAAm Microgels Thermoresponsive Behavior. *Macromolecules* **44**, 612-621 (2011).

# CHAPTER 4:

## Development of a Microbead Protease Sensor

# 4 Development of a Microbead Protease Sensor

Matrix metalloproteinases (MMPs) are extracellular endopeptidases generally active near or on the cell surface.[1] MMPs are key regulators of the extracellular microenviroment, being involved in normal physiological processes such as tissue remodeling[2] or inflammation[3]. The dysregulation of the MMPs activity has been associated with a wide range of pathologies, such as cancer[1], arthritis[4] or endometriosis[5]. The detection of MMPs in biological samples may provide important information for diagnosis, prognosis, and therapeutic monitoring of various diseases. Of the existing methods to study MMPs, Förster resonance energy transfer (FRET) based synthetic protease probes have been extensively developed to directly assess activity in a non-invasive and real-time manner.[6,7] However, synthetic protease substrates are generally cleaved by multiple proteases, impairing specificity.[8] Furthermore, no systematic tools are available to provide information on protease activity at the cellular level. The conjugation of protease probes on microparticles may allow (i) the deployment of the sensor in different 2D and 3D cultures; (ii) potential protease activity spatial resolution; (iii) monitoring activity using cell culture analytical tools such confocal laser scanning microscopy; and flow cytometry. Herein, two different approaches for the incorporation of protease sensing function on the synthesized p(NIPAAm-co-MAA) microbeads are described. Previously it was shown that these beads present a "cell-like" size, a theoretical mesh size suitable for biomacromolecules permeation and potentially physiologically relevant mechanical properties. In addition, it was demonstrated that polyelectrolyte multilayers can be assembled on these beads to tune surface chemistry, swelling, charge and responsive behavior. These beads are proposed as supports for the FRET MMP probes under development at the Griffith and Hammond labs.

## 4.1 Introducing Protease Sensing Function on Microbeads by Complexation of Functionalized Polymers

The assembly of macromolecules and high molecular weight polymers on well-defined PNIPAAm-based microparticles, synthesized in $scCO_2$, was described in Chapter 2. Thus, the conjugation of a FRET MMP probe on a polymeric backbone and subsequent polymer complexation on the particles may be possible route to introduce a protease sensing function onto the microbeads. Indeed the LbL coating of microparticles for the development of a protease sensor was proposed in the literature.[9]
Synthetic polypeptides have been thoroughly studied for biological applications as they exhibit physico-chemical properties of natural polypeptidic sequences and are potentially biocompatible.

Conventional solid-phase peptide synthesis is neither useful nor practical for the preparation of large polypeptides (above 100 residues) due to probable deletions and truncations that may arise from incomplete deprotection and coupling steps. The most economical and convenient method for the synthesis of long polypeptide chains is the ring-opening polymerization of α-aminoacid-N-carboxyanhydrides (NCAs).[10,11] NCA polymerizations are traditionally initiated by primary amines or organometallic transition metal-based complexes. Recently, a lot of research has been focused on the improvement of amine-initiated NCA polymerizations for the development of well-defined polypeptides and hybrid block copolymers.[10,11] This synthesis route is especially attractive because, if the polymerization progresses without any chain breaking reactions, the amine initiator becomes the polypeptide C-terminal. Thus, there is the potential to easily introduce specific functionalities on the polypeptide end-group, such as functional groups suitable for click chemistry.

Recently, strategies combining NCA polymerization and click chemistry have been proposed for the preparation of block copolymers[12,13] and modification of polypeptides.[14] Click chemistry refers to a series of highly efficient reactions, including the copper-catalyzed Huisgen 1,3 – dipolar cycloaddition between and alkyne and an azide to form a triazole.[15] It is a versatile method widely used for conjugation, combining mild experimental conditions, functional group tolerance, and high yields.

The preparation of a well-defined α-alkyne terminated poly(L-lysine) (PLL) is described below. The FRET MMP probes being developed in the Griffith and Hammond labs include a terminal azide functional group that could be conjugated to the synthesized PLL. Herein, the complexation of the protease sensing polymeric backbone with the microbeads is evaluated as a potential strategy to the development of a microbead protease sensor.

## 4.1.1 Experimental section

### 4.1.1.1 Materials

$N_\varepsilon$-Z-L-lysine (> 99.0 %; $M_w$ 280.32), triphosgene (> 99.0 %; $M_w$ 296.75), *N*,*N*,*N*′,*N*″,*N*″-Pentamethyldiethylenetriamine (PDMETA; 99.0 %; $M_w$ 173.30), copper bromide (CuBr; 98.0 %, $M_w$ 143.45), hydrobromic acid solution (33 wt % in acetic acid; $M_w$ 80.91), trifluoroacetic acid (TFA), tetrahydrofuran (THF), dimethylformamide (DMF), and diethylether (DEE) were purchased from Sigma. 6-fluorescein-triethyleneglycol-azide (FAM-$N_3$; $M_w$ 576.55) was obtained from Berry & Associates (US). Trypsin 2.5 % (10×), without EDTA or phenol red, and Fetal Bovine Serum (FBS)

was obtained from Invitrogen (USA). Deionized water was purified through a Milli-Q system and had a resistivity greater than 18 MΩ.cm. Poly(NIPAAm-co-MAA) 90:10, PP9010, microbeads were prepared by synthesis in $scCO_2$, as described in Chapter 2.

#### 4.1.1.2 Synthesis of Z-L-lysine N-carboxyanhydride monomer

The protocol developed for the synthesis of ε-carbobenzoxy-L-lysine *N*-carboxyanhydride (Z-L-lysine NCA) was adapted directly from the literature.[16] In short, 3 equivalents of $N_\varepsilon$-Z-L-lysine (1.5 g; 5.3 mmol) were dissolved in 100 mL of anhydrous THF and stirred at 50 °C under $N_2$. Triphosgene (1 eq.; 0.53 g; 1.8 mmol) was dissolved in 10 mL of anhydrous THF and added drop-wise to the $N_\varepsilon$-Z-L-lysine solution. The reaction progressed for 1 hour until a clear solution was obtained, being vented through NaOH pellets to neutralize the hydrochloric acid byproduct. The solution was then filtered and concentrated in a rotary evaporator. The obtained product was further purified by dissolving in cold dry ethyl acetate, followed by washes in cold water, 5 wt % sodium bicarbonate and brine; then dried twice with magnesium sulfate anhydrous. The obtained solution was concentrated in a rotary evaporator and dried under high vacuum to remove any residual solvents. Yield = 55 %.

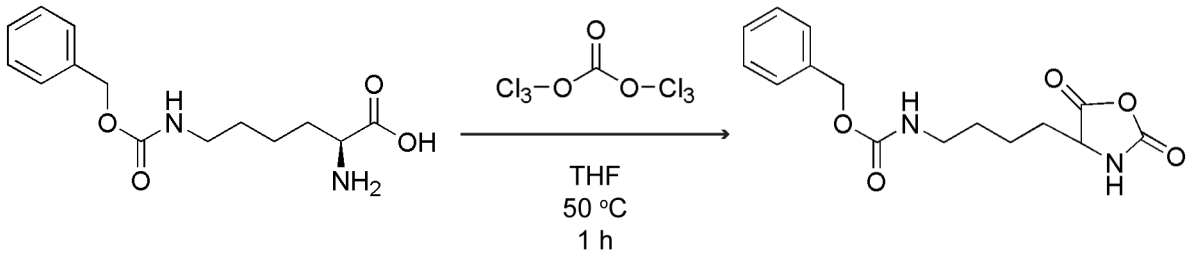


**Figure 4.1** Synthesis of Z-L-Lysine NCA monomer.

#### 4.1.1.3 α-alkyne initiated polymerization of Z-L-lysine N-carboxyanhydride

In order to obtain a polypeptide with a click-functional terminal group, polymerization of Z-L-lysine *N*-carboxyanhydride was initiated using propargylamine, based on a protocol described in the literature[12] – Figure 4.2. For a degree of polymerization of 25, Z-L-lysine NCA (0.5 g; 1.63 mmol) was dissolved in 3 mL of anhydrous DMF. Propargylamine (4.4 μl; 0.065 mmol) dissolved in 3 mL of anhydrous DMF was added to the reaction using air-free techniques. The reaction was performed at room temperature under stirring for 3 days. The obtained poly(Z-L-lysine) (PZLL) solution was concentrated in high vacuum and then precipitated in cold DEE. The precipitate was recovered by centrifugation, washed 3 times in cold DEE and dried under vacuum overnight. $^1$H NMR ($CDCl_3$, δ/ppm): 5.06 (s, 2H, $C_6H_5CH_2$), 4.38 (t, 1H, CH), 3.04 (br, 2H, $CH_2$), 2.17 (t, 1H, C≡CH), and 1.63 (br, 2H, $CH_2$). Degree of polymerization, DP = δCH/δC≡CH = 23; hence $M_w$ ~ 6090. Yield = 73 %.

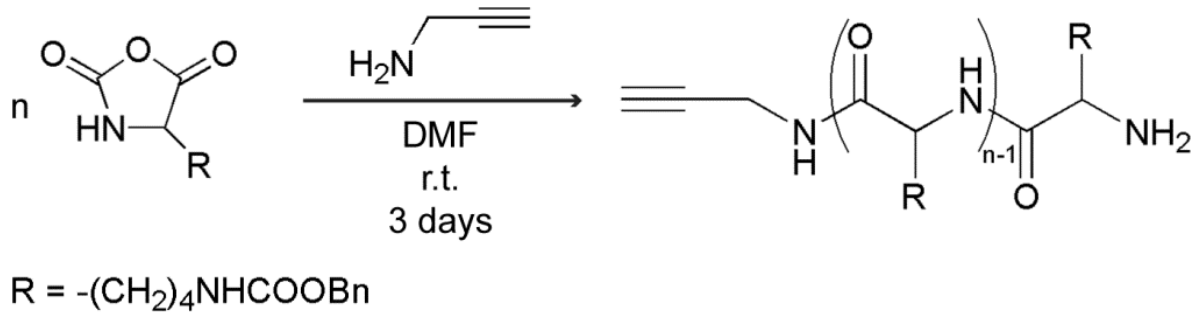


**Figure 4.2** Propargylamine initiated polymerization of Z-L-Lysine NCA monomer.

#### 4.1.1.4 Click cycloaddition of model fluorescein to poly(Z-L-lysine), polymer deprotection and copper removal

α-Alkyne PZLL (1 eq.), FAM-$N_3$ (1.5 eq.) and PMDETA (5 eq.) were dissolved in 3-5 mL DMF. In a schlenk flask under Ar, 5 equivalents of CuBr were added. The reaction was performed overnight at room temperature in the dark. The polymer was precipitated in cold DEE. To remove unreacted fluorescein the product was further washed with DEE and cold water before drying under vacuum. Yield = 91 %.

The amine groups of α-fluorescein PZLL were regenerated by hydrolysis of the Z groups. The polymer was dissolved in TFA at 33 mg/mL concentration. A 4-fold molar excess of HBr solution, relative to the number of L-lysine repeat units, was added. The reaction was performed for 1 hour at room temperature in the dark. The solution was precipitated in cold DEE. After extensive washing the α-fluorescein poly(L-lysine) (FAM-PLL) was recovered by filtration and dried under vacuum. In order to remove excess CuBr and/or PMDETA the product was initially dissolved in water. Pourex M4195 beads were added to the solution and the mixture was stirred for 15 min. The product was filtered and then purified by dialysis at 4 $^{o}$C for 1 day ($M_W CO$ ~ 1000) in the dark. The final FAM-PLL product was then lyophilized until further use. Yield = 66 %.

The final product as well as the synthesized intermediates were characterized by $^{1}$H NMR in $CDCl_3$ with 15 % TFA to promote unfolding of the polymer, recorded on a Bruker spectrometer (400 MHz).

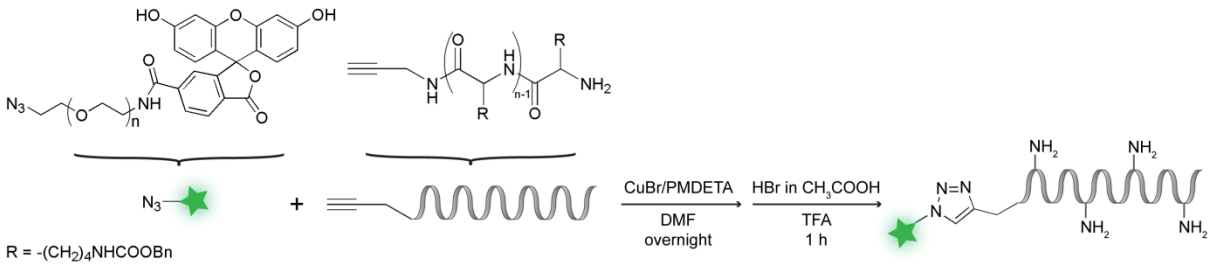


**Figure 4.3** Huisgen's 1,3-dipolar cycloaddition of FAM-$N_3$ and α-alkyne poly Z-L-lysine as a model fluorescent MMP sensing polymer. Amine groups regeneration by hydrolysis of the Z-groups.

#### 4.1.1.5 Complexation of model protease sensing FAM-$PLL_{25}$ on PP9010 microbeads. Protease activity assessment and stability assays.

The synthesized FAM-PLL (with a DP ~ 25; FAM-$PLL_{25}$) was complexed on PP9010 microbeads under the conditions described for the LbL assembly of poly(L-lysine) / poly(L-glutamic acid) multilayers in Chapter 3 – Figure 4.4. Layer-by-layer assembly of PAA/PAH was performed on FAM-$PLL_{25}$ complexed PP9010 microbeads using the experimental conditions described in Chapter 3, except that assembly pH was set to 7.4 for both polyelectrolytes to prevent destabilization of the previously complexed polylysine. All samples were freshly prepared before tryptic digestion.

The degradation of FAM-$PLL_{25}$ complexed on the beads by trypsin, as a model protease, was assessed by mixing $10^6$ particles/mL (determined with a hemocytometer) with 300 mL of 0.25 μg/mL trypsin in PBS and PBS only (controls) and incubating at 37 $^oC$. At specific time points, aliquots of beads were taken, placed immediately on ice and added 10 vol% of FBS to stop trypsin activity. The samples were centrifuged at 13,000 × *g* for 15 min. Trypsin was removed from the supernatants using a Microcon (Millipore, USA) centrifugal filter device ($M_WCO$ ~ 10,000). The concentration of trypsinized polymer was determined by measuring the fluorescence of the supernatant in a SpectraMax M2e plate reader (Molecular Devices, USA; $\lambda_{exc}$ = 495 nm; $\lambda_{em}$ = 514 nm). Tryptic cleavage was also used to determine the relative amount of FAM-$PLL_{25}$ that remains stable in the native and PAA/PAH coated complexes during the LbL assembly, by performing total degradation with 2.5 g/mL Trypsin for 1 day at 37 $^oC$. In addition a qualitative evaluation of the constructs stability under physiological conditions was performed by incubation in PBS for 2 days and determining the fluorescence of the supernatant. Furthermore, for all these assays the beads were observed on a CARV II spinning disk confocal system equipped with an environmental chamber at 37 $^oC$ and a Zeiss inverted microscope.

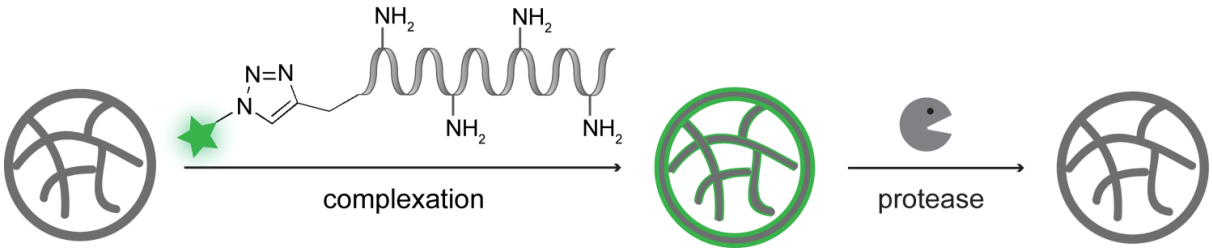


**Figure 4.4** Introducing model MMP sensing into PP9010 beads through functionalized PLL complexation (pH 7.4 and 10 mM in polyelectrolyte). The action of the protease may be detected in this model construct by a decrease in overall bead fluorescence.

### 4.1.2 Results and discussion

#### 4.1.2.1 Preparation and characterization of FAM-PLL$_{25}$

In Chapter 3, the successful assembly of PLL / poly(L-glutamic acid) multilayers on PP9010 microgels was described; hence PLL can be used as a polymeric backbone for the incorporation of a protease sensing function. The FRET-based protease sensors being synthesized at the Griffith lab include terminal groups, such as azides or thiols, which can be efficiently conjugated to any support containing antagonist functionalities with high yields: from polymers to gels. The synthesis approach followed herein is based on a four-step sequence combining (1) the synthesis of Z-L-lysine N-carboxyanhydride monomer; (2) the preparation of α-alkyne terminated PZLL by ring opening polymerization of Z-L-lysine NCA monomer; (3) the Huisgen's 1,3-dipolar cycloaddition (click chemistry) of α-alkyne terminated PZLL and azide functionalized fluorescent molecule (as a model for a MMP sensing construct); and (4) the regeneration of PLL amines by HBr hydrolysis of the protecting Z groups – Figures 4.1 to 4.3.

Z-L-lysine *N*-carboxyanhydride monomer was successfully prepared and subsequently polymerized using propargylamine as an initiator, as can be observed in the $^{1}$H NMR spectrum depicted in Figure 4.5. The spectrum is similar to the literature except that some diethylether peaks (labeled 'dee' in the Figure) were also found as contaminants (solvent used for polymer precipitation)[17]. A α-alkyne terminated PZLL with a degree of polymerization of 23 was obtained, as determined from the relative integration of characteristic protons of the alkyne terminal to protons of the polymer main chain, corresponding to a molecular weight of ~ 6090 Da. In fact the initial monomer to initiator ratio (25:1) closely determined the length of the synthetic polypeptides, emphasizing that well-defined polypetides are readily prepared by NCA polymerization.[10]

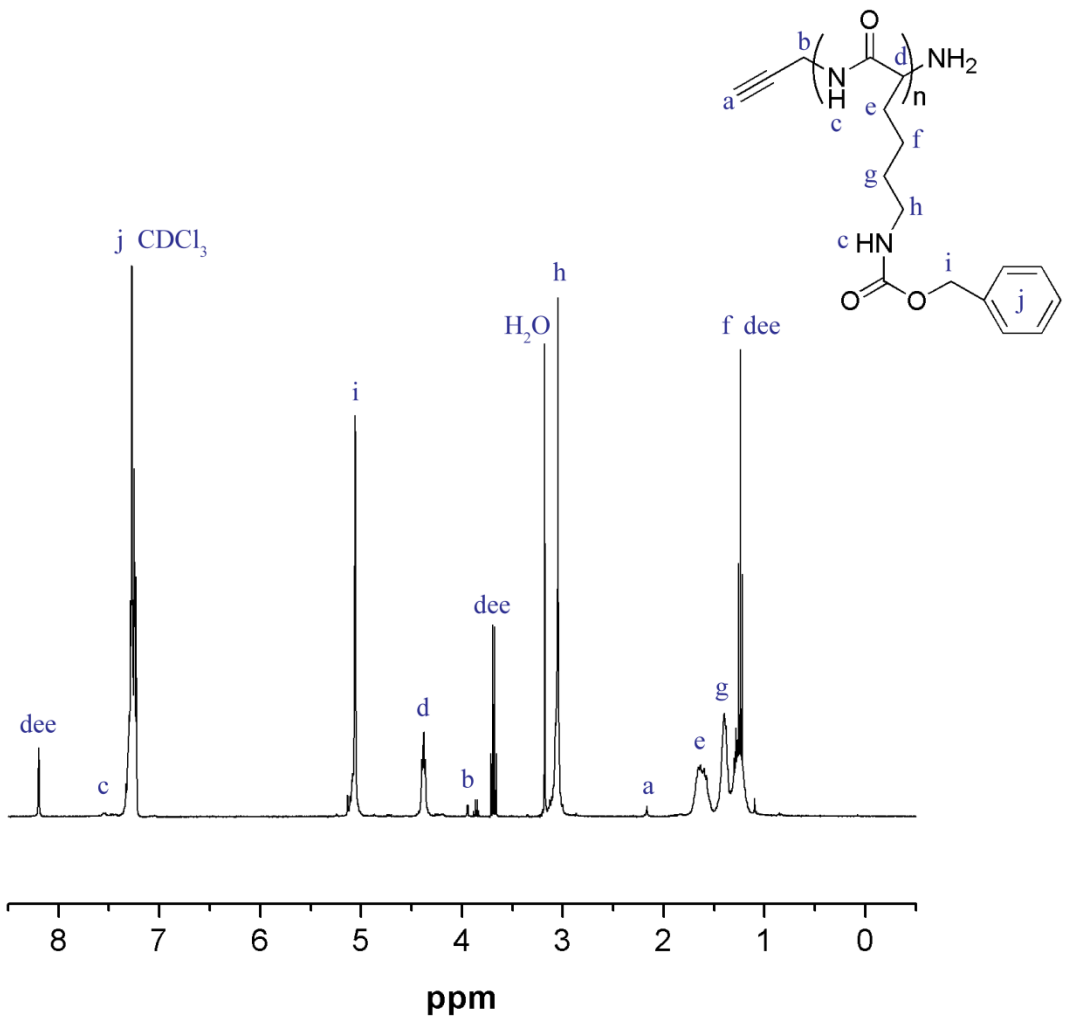


**Figure 4.5** $^{1}$H NMR spectra of propargyl-terminated poly Z-L-lysine in $CDCl_3$ with 15 % TFA (dee: diethyl ether).

A slight excess of 6-fluorescein azide (FAM-$N_3$), 1.5 equivalents, was used for its conjugation to the poly(Z-L-lysine) backbone through click chemistry, in agreement with previous protocols described in the literature.[12] The $^{1}$H NMR spectra demonstrated that the click reaction was complete, as no peaks assigned to the terminal alkyne are observed (data not shown). After deprotection of the polymer Z-groups, a water soluble polymer was obtained which is suitable for applications in aqueous conditions. The HBr hydrolysis was amenable to the maintenance of the polymer fluorescence. These results demonstrate that the combination of NCA polymerization with click chemistry allows the preparation of well-defined polypeptides that could be conjugated with probes bearing matching functionalities in high yields, being a possible synthetic route to prepare protease sensing polymers that can be deployed in microbeads, as coatings, etc.

#### 4.1.2.2 Complexation of FAM-PLL$_{25}$ on PP9010 microbeads

Preliminary experiments performed with short fluorescein-labeled polylysine peptides (with 3, 6, 9, 12 and 15 aminoacids), prepared by solid-phase peptide synthesis, showed that at least 15 lysine residues were necessary to prepare a complex with PP9010 that remains stable under physiological conditions (PBS buffer, 37 $^{o}$C) – data not shown. Indeed, it has been thoroughly shown that polymer length contributes to the formation of more stable interactions among polymers, especially in particle coating.[18] These observations reinforce the selection of the above described synthetic route for the preparation of long functionalized polymers as backbones for a protease sensing moiety.

The prepared FAM-PLL$_{25}$ polymer was successfully loaded onto PP9010 microbeads, following the experimental conditions described for the commercial long $M_w$ PLL used in Chapter 3, as can be observed in the micrographs depicted in Figure 4.6. In order to investigate whether a protease can actually access the complexed PP9010 microbeads and exhibit enzymatic activity, trypsin was used as a model. Trypsin is a serine protease produced in the pancreas and secreted to the small intestine, cleaving peptide bonds on the C-terminal side of arginines and lysines. It has been show to degrade synthetic PLL into 2 and 3 residue segments.[19] Trypsin has a $M_w$ of about 23 kDa and a radius of gyration ($R_g$) around 20 Å, depending on solution conditions,[20] thus having a size within the range of some metalloproteinases (*vide* Introduction). In Chapter 2 it was shown that the native PP9010 microbeads present a theoretical mesh size an order of magnitude higher than trypsin radius of gyration, and trypsin should permeate freely across the bead (unless other interactions interfere, namely ionic). On the other hand, the complexation of polycations decreases the bead swelling (Chapter 3); hence it can be anticipated that the mesh size is smaller for the complexes.

PP9010 microbeads complexed with FAM-PLL$_{25}$ (PP9010-FAM-PLL$_{25}$) were incubated in PBS with 2.5 g/mL of trypsin (1× dilution from the stock trypsin solution) at 37 $^{o}$C for 1 hour, as shown in Figure 4.6. The enzymatic degradation of the fluorescent polymer, and consequent decomplexation from the bead, can be inferred from the decay in fluorescence from the PBS control to the trypsin digested PP9010-FAM-PLL$_{25}$ bead.

Previous assays for tryptic degradation of a fluorescently labeled PLL established that initial velocity conditions were observed for a 0.25 μg/mL trypsin concentration, in which the rate of degradation was constant for about 2 hours. Upon incubation of PP9010-FAM-PLL$_{25}$ beads with that amount of trypsin, the progress of the supernatant fluorescence with time followed a typical enzymatic progression curve. Indeed, the fluorescence of the supernatant increases linearly for the initial time points until reaching a plateau upon substrate consumption, after 5 hours. Furthermore, when comparing with the controls in PBS, it is clear that the increase in fluorescence is not due to simple diffusion of the FAM-PLL$_{25}$ polymer out of the complexes, but is a result of tryptic digestion and consequent release of the complexed polymer from the bead.

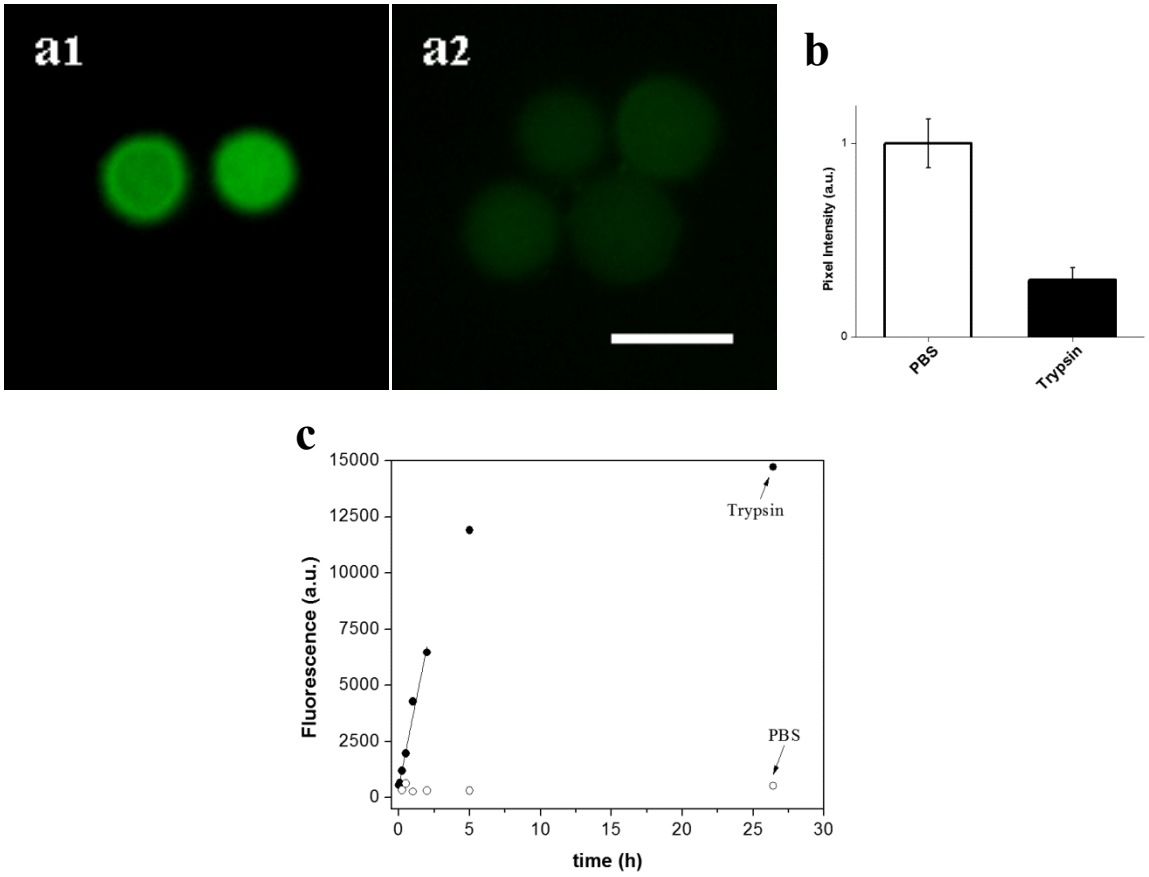


**Figure 4.6** Trypsin cleavage of complexed FAM-$PLL_{25}$ polymer in PP9010 beads: confocal micrographs of PP9010-$PLL_{25}$ beads incubated in PBS (a1) and in 2.5 mg/mL of trypsin in PBS (a2) for 1 hour at 37 $^{o}$C; (b) pixel intensity differences for confocal micrographs of PP9010-$PLL_{25}$ beads incubated in PBS and in 2.5 mg/mL of trypsin in PBS for 1 hour at 37 $^{o}$C, as determined by image analysis; (c) fluorescence of the supernatants for $1\times10^{6}$ beads/mL incubated with 0.25 μg/mL of trypsin in PBS (♦) and only PBS (○) at 37 $^{o}$C, highlighting a linear adjustment at initial velocity conditions.

Observations under a confocal microscope for the trypsin digested beads shown that no significant fluorescence remains on the bead at the end of the assay. These results support that trypsin can actually access and exhibit activity in the PP9010-FAM-$PLL_{25}$ microbeads. Although these observations cannot be extrapolated for MMPs, as their size and charge differs from trypsin and varies significantly among different MMPs, it leaves the possibility open that a target MMP would be able to permeate throughout the beads.

#### 4.1.2.3 Stability of FAM-$PLL_{25}$ complexed PP9010 microbeads

After concluding that trypsin could cleave a complexed polypeptide on the PP9010 microbeads, it would be interesting to assess whether LbL coating of the complex would impact the observed enzymatic activity. Previous studies on protease sensing particles have shown that charge influences the partitioning of enzymes from solution to the particles. Trypsin activity was higher for LbL coated

microbeads with a negatively charged outer layer, which can be explained by a higher affinity of the positively charged trypsin (pI = 8.2).[9]

The LbL assembly of synthetic poly(acrylic acid) / poly(allylamine hydrochloride) (PAA/PAH) polyelectrolytes was performed on the PP9010-FAM-$PLL_{25}$ microbeads at the same conditions as described in Chapter 3, but maintaining the pH constant at 7.4. This pair was chosen since it is not degradable by enzymatic activity. Being the complex positively charged (ζ-potential ~ 4 mV), PAA was assembled first. The stability of the underlying complex was analyzed by measuring the amount of fluorescence released in time relative to the amount of polymer initially complexed during the actual LbL assembly and after incubation for 2 days in PBS – Table 4.1. Despite the error associated to the data below, it becomes clear that there are significant losses of complexed $PLL_{25}$ polymer during LbL assembly of the synthetic polyelectolytes and upon incubation in PBS, which may impair their application as sensor in long term cell cultures.

**Table 4.1** Stability of complexed FAM-$PLL_{25}$ upon LbL assembly of polyelectrolytes and incubation in PBS buffer.

| Sample | FAM-$PLL_{25}$ retained during LbL (%) | FAM-$PLL_{25}$ retained in PBS (%) |
|---|---|---|
| PP9010-$PLL_{25}$ | n.a. | 89 ± 5 |
| PP9010-$PLL_{25}$ /PAA | 88 ± 19 | 85 ± 1 |
| PP9010-$PLL_{25}$ /$(PAA/PAH)_1$ | 62 ± 24 | 94 ± 4 |

Confocal micrographs in Figure 4.7 exemplify that the fluorescence is unequally distributed from the native to the PAA/PAH coated complexes, showing that possibly FAM-$PLL_{25}$, as a diffusible polyelectrolyte, migrates differently throughout the microbead depending on the outermost layer (at the second bilayer the confocal micrographs become similar to the PP9010-FAM-$PLL_{25}$/PAA/PAH micrograph depicted). Experiments with a pH-insensitive dye confirmed that the observed differences in fluorescence among samples are not due to local variations in pH (data not shown), as it is widely known that FAM fluorescence is extremely sensitive to pH.[21] For the above reasons, the bead functionalization approach via complexation with a polymer does not seem a robust method to incorporate a protease due to lack of overall construct stability. Furthermore, comparing the trypsin enzymatic kinetics between the native complexed beads and the LbL coated ones would be quite unreliable as enzymatic degradation rates are dependent on the local concentration of substrate. As alternatives, a backbone polymer that would establish stronger interactions with the PP9010 microbeads could be developed, the molecular weight of the prepared PLL backbone could be

increased or the protease sensing moiety could be covalently attached to the bead itself. The latter strategy was the subject of the next section of this chapter.

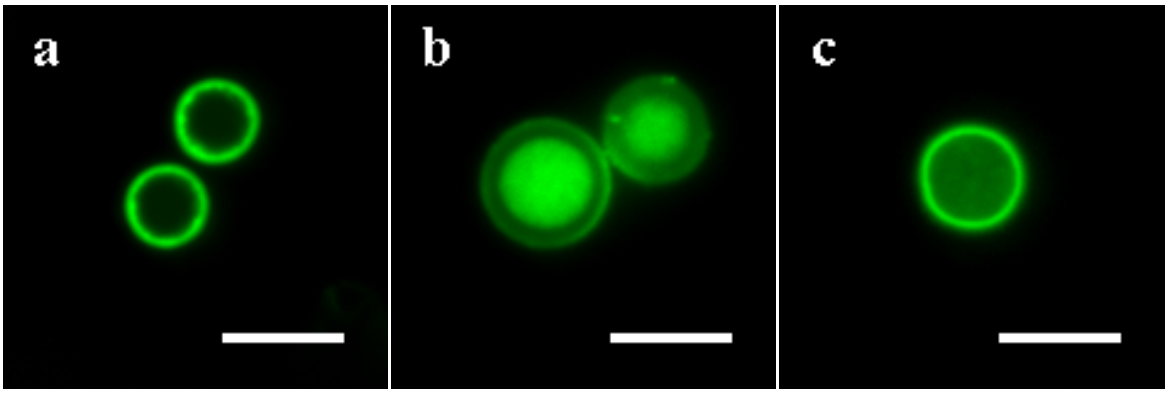


**Figure 4.7** Location of $PLL_{25}$ in complexed beads after PAH/PAA assembly dispersed in water at pH 7.4. Scale bar: 10 μm.

## 4.2 Protease Sensor Conjugation on Microbeads

Another possible route to enable a protease sensing function to the prepared PP9010 microbeads is to directly tether the MMP probe to the beads. The PP9010 microbeads have carboxylic functional groups that are amenable to conjugation through amide linkage formation.[22] Carbodiimides cross-linking agents can be used for activating the carboxylate group for coupling with an amine-containing compound. This approach was followed for the conjugation via amide coupling of FRET protease probes on cross-linked poly(ethylene glycol acrylamide) hydrogel microbeads for the design of elastase sensors.[23] The probe's amine groups were initially Fmoc-protected and regenerated after conjugation. During the chemical modification of the PP9010 beads, no significant diffusion limitations are expected as trypsin was shown to access the microbeads and exhibit enzymatic activity, and the estimated mesh size in aqueous environment is far greater than the expected size of the reagents used, although charge can also influence transport into the bead.

The MMP probes under development at the Hammond and Griffith lab include a terminal (i) azide or (ii) cysteine for further conjugation through (i) click chemistry or (ii) thioether coupling. Recently, a copper-free azide-alkyne cycloaddition strategy was developed by Bertozzi *et al.*, relying on the use of strained cyclooctynes to overcome the need for metal catalysis.[24] This route is especially ideal for macromolecular engineering in biological applications. Besides being a bioorthogonal click reaction, meaning that the components involved are inert to biomacromolecules, the potential cytotoxic effects of the presence of exogeneous metals are avoided. In a pioneer work, the Bertozzi group reported the successful labeling of surface glycoproteins of living cells using the copper-free click chemistry

strategy, without compromising cell viability.[25] As for the second available chemistry on the MMP probes, the thioether coupling is one of most common and well-known routes for conjugation or modification of biomacromolecules, namely antibodies, by taking advantage of available thiol groups in cysteine residues.[22] Different functional groups, such as maleimides, are able to undergo an alkylation reaction preferentially with thiol groups to form stable thioether bonds in aqueous environments.[22] This latter strategy has the major disadvantage that cannot be generalized for the conjugation of MMP probes containing cysteine groups in the enzyme cleavage site.

In this section, a strategy involving the coupling of cyclooctyne or maleimide containing linkers on PP9010 microbeads and further conjugation to azide or thiol terminated model molecules or MMP probes is described. The activation of a microbead conjugated MMP probe is shown upon incubation with trypsin, as a model protease.

## 4.2.1 Experimental section

### 4.2.1.1 Materials

1-ethyl-3-[3-dimethylaminopropyl]carbodiimide hydrochloride (EDC) was purchased at Pierce (USA). 6-fluorescein-amine (FAM-$NH_2$; $\lambda_{ex}/_{em}$ = 494/519 nm; $M_w$ 347.32) was obtained at Aldrich (USA). Fluorescein-polyethyleneglycol-amine (FAM-PEG-$NH_2$; $M_w$ 2000) was purchased from Nanocs (USA). Maleimide-polyethyleneglycol-amine TFA salt linker (Mal-PEG-$NH_2$; $M_w$ 2000) was obtained at JenKem Technology, USA. Dibenzylcyclooctyne-PEG-amine (DBCO-PEG-$NH_2$; $M_w$ 523.62) and carboxyrhodamine 110-PEG-azide (RhoCOOH-PEG-$N_3$; $\lambda_{ex}/_{em}$ = 501/525 nm; $M_w$ 575.59) were purchased from Click Chemistry Tools (Dexter, MI, USA). Collagen I, rat tail, DMEM and Williams E media were purchased from GIBCO, USA. Dimethyl sulfoxide (DMSO) was obtained from Sigma. Deionized water was purified through a Milli-Q system and had a resistivity greater than 18 MΩ.cm. Poly(NIPAAm-co-MAA) 90:10, PP9010, microbeads were prepared by synthesis in $scCO_2$, as described in Chapter 2.

### 4.2.1.2 Preparation of azide/cysteine -terminated MMP fluorogenic peptide probe

MMP peptide probe was prepared by conjugating a resonance energy transfer donor/acceptor pair (fluorescein fluorophore, 5-(6)-carboxyfluorescein ($\lambda_{ex}/_{em}$; 494/519 nm), and 4-(4-dimethylaminophenylazo)benzoic acid, Dabcyl ($\lambda_{abs}$ = 650 nm) to a MMP specific substrate shown in Figure 4.8, wherein the cleavage site was synthesized using standard solid-phase peptide chemistry. The depicted substrate was chosen since it is relatively short (thus easier to prepare) and cleaved by several MMPs.[8] The optimization of the synthesis of the peptide probe as well as further

modifications required for its conjugation were subject of work performed by Caroline Chopko, PhD candidate from the Griffith and Hammond labs, and are beyond the scope of the present thesis.

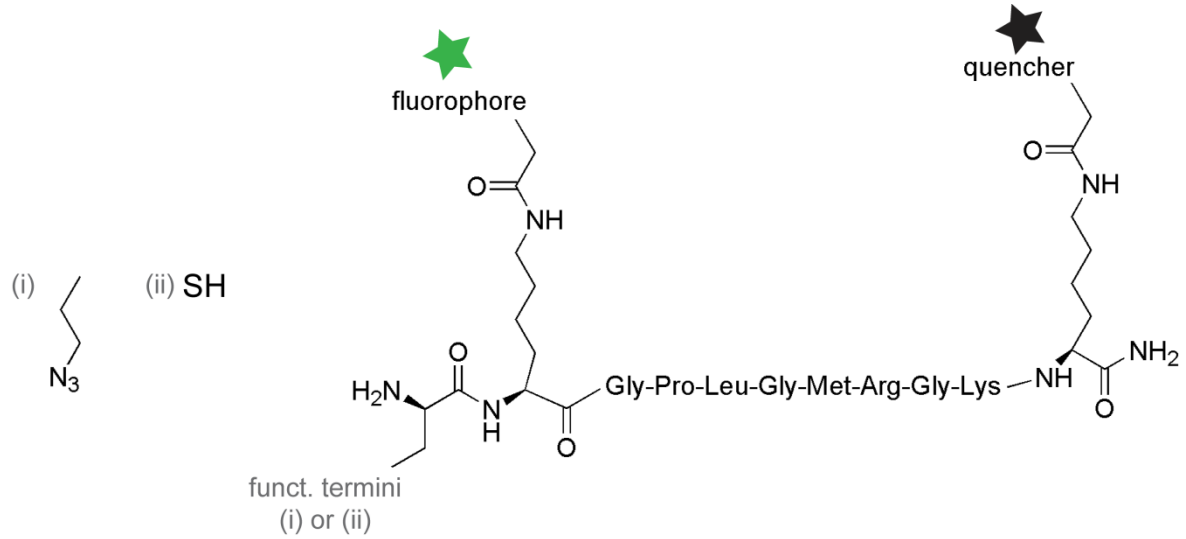


**Figure 4.8** (i) Azide ($N_3$) and (ii) cysteine (-SH) terminated "clickable" MMP FRET probe containing a peptide sequence cleaved by a wide variety of MMPs. In this work 5(6)-carboxyfluorescein (FAM) was used as fluorescence donor and 4-(4-dimethylaminophenylazo)benzoic acid (Dabcyl) as an acceptor (quencher).

#### 4.2.1.3 Preparation of model fluorescent and DBCO / maleimide-modified microbeads

PP9010 microbeads were modified in order to allow their conjugation to the synthesized MMP probe, using EDC carbodiimide chemistry to add either DBCO or maleimide terminal groups – Figure 4.9. Initially, model fluorescent molecules were used to evaluate the efficiency of carbodiimide conjugation strategy and optimize reaction conditions. PP9010 microbeads were dispersed overnight in 10 mM phosphate buffer pH 7.2 at 0.5 mg/mL concentration. FAM-$NH_2$ (0.42 mg; 1.2 μmol) dissolved in DMSO or FAM-PEG-$NH_2$ (2.4 mg; 1.2 μmol) dissolved in the phosphate buffer were mixed with EDC (1 mg; 5.2 μmol) and added to 1 mL of PP9010 microbeads dispersion. The reaction was performed at room temperature in the dark with shaking for 12 hours. Unreacted conjugates were removed by centrifuging the microbeads at 13,000 × *g* for 30 min. The supernatant was discarded and the beads resuspended in 1 mL of 10 mM phosphate buffer pH 7.2. The centrifugation/resuspension cycle was repeated until no fluorescence was detected in the supernatant. For the preparation of DBCO or thiol-modified microbeads, DBCO-PEG-$NH_2$ (2 mg; 3.8 μmol) or Mal-PEG-$NH_2$ (7 mg; 3.5 μmol) were used instead in the EDC conjugation and the resulting microbeads were centrifuged/resuspended three times. The amide coupling of the fluorescent molecules was assessed by confocal laser scanning microscopy (CLSM) using a Zeiss LSM 510 (Germany) at ambient

temperature. Since these modifications were performed on insoluble cross-linked microbeads, the reaction yields could not be quantitatively determined.

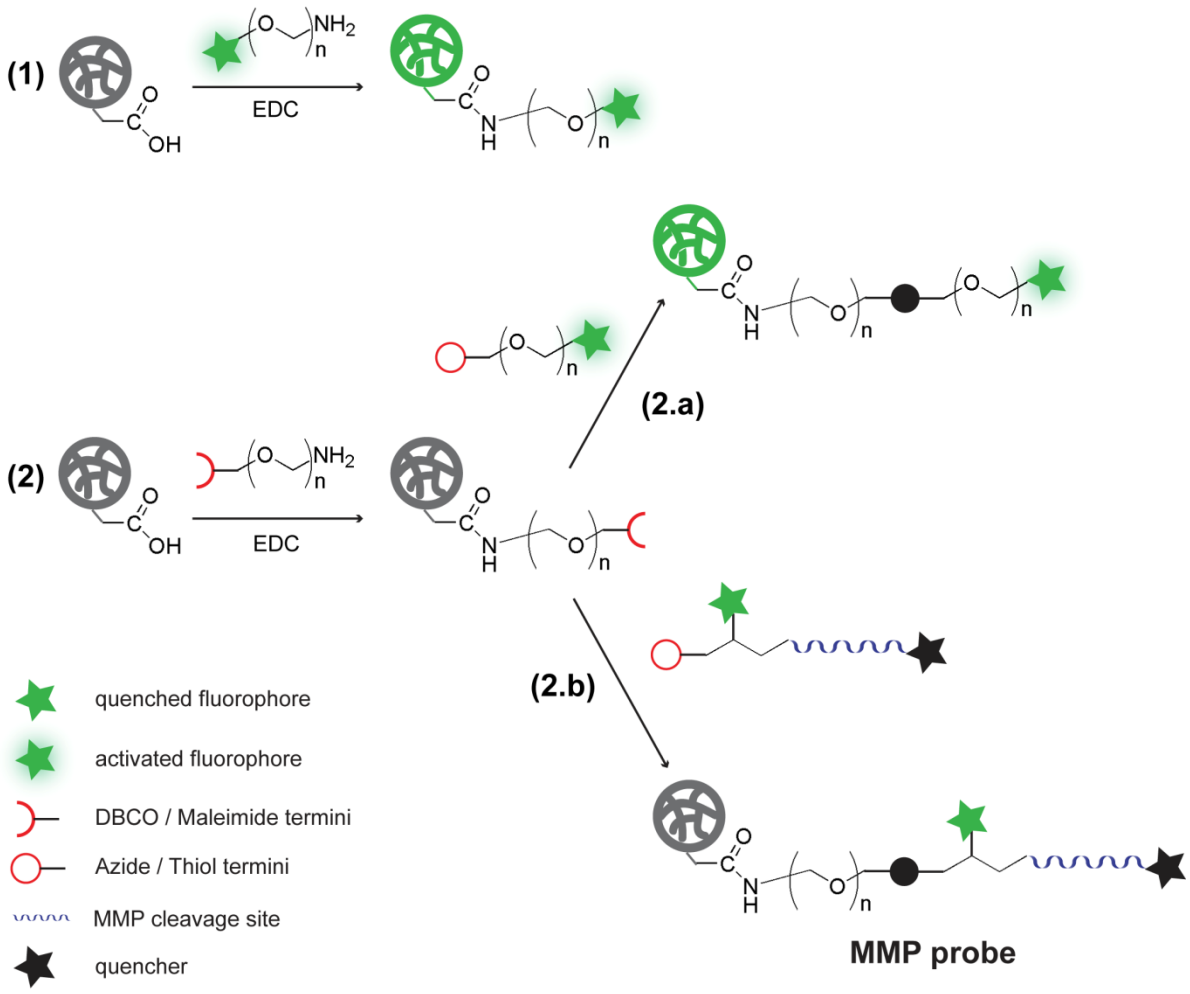


**Figure 4.9**. Combination of amide coupling (reactions 1 and 2) and cycloaddition / thiol-maleimide coupling (reactions 2.a and 2.b) chemistries for tethering model fluorogenic compounds and the MMP probe on PP9010 microbeads. Only the main reactive moieties are depicted, being a schematic representation of the molecules involved.

#### 4.2.1.4 MMP probe or model fluorescent molecules click to DBCO / maleimide -modified beads. MMP probe activation with model protease.

Fluorescent model molecules and the MMP probe were conjugated to the PEG-DBCO or PEG-mal modified microbeads via (i) copper-free click cycloaddition or (ii) condensation with thiol – Figure 4.9, reactions 2.a and 2.b. Both reactions are characterized by high conjugation yields. For the model fluorescent molecules, used to assess the feasibility of such synthesis strategy, 0.5 equivalents of (i) RhoCOOH-PEG-$N_3$ (1.1 mg; 1.8 µmol), relative to the amount used for previous PEG-DBCO linker conjugation, were added to 0.5 mg of DBCO-terminated beads suspended in 0.5 mL of 10 mM

phosphate buffer pH 7.2. For assessing the (ii) thiol-maleimide coupling, a thiol-containing tetramethylrhodamine (TAMRA) dimer was initially prepared following the procedure described in the literature.[26] TAMRA thiol (TAMRA-SH) was obtained by reducing the disulfide bonds in the presence of agarose gel immobilized tris(2-carboxyethyl) phosphine resin: 0.5 eq. of the obtained TAMRA-SH (0.9 mg; 1.8 μmol) were mixed with 0.5 mg of the maleimide-terminated beads suspended in 0.5 mL of 10 mM phosphate buffer pH 7.2. In regards to the probe preparation, only a thiol-terminated MMP probe was used herein (Figure 4.8). However, the peptide probes are not as soluble in water as the model fluorescent molecules. For the probe conjugation 0.5 eq. (~1 mg; 1.8 μmol) were dissolved in DMSO and mixed with 0.5 mg of beads bearing the maleimide linkers suspended in 5 vol% of DMSO, 15 vol% acetonitrile and 80 vol% of the phosphate buffer. All these conjugation reactions progressed for at least 12 hours. Additionally, the MMP probe conjugation was performed in 0.05 wt% sodium azide to prevent microbial growth. The microbeads were purified by centrifuging the microbeads at 13,000 × *g* for 30 min. The supernatant was discarded and the beads resuspended in 1 mL of 10 mM phosphate buffer pH 7.2. The centrifugation/resuspension cycles were repeated until no fluorescence was detected in the supernatant or for three times for the actual MMP probe conjugation. The presence and activity of the MMP probe was assessed by mixing ~ 0.05 mg of conjugated beads with 1 × trypsin in PBS and incubating at 37 $^{o}$C for 2 hours – Figure 4.7. The conjugation of fluorescent molecules was assessed by confocal laser scanning microscopy (CLSM) using a Zeiss LSM 510 (Germany) at ambient temperature and $\lambda_{exc}$ = 488 nm for FAM and RhoCOOH fluorophores and $\lambda_{exc}$ = 540 nm for TAMRA.

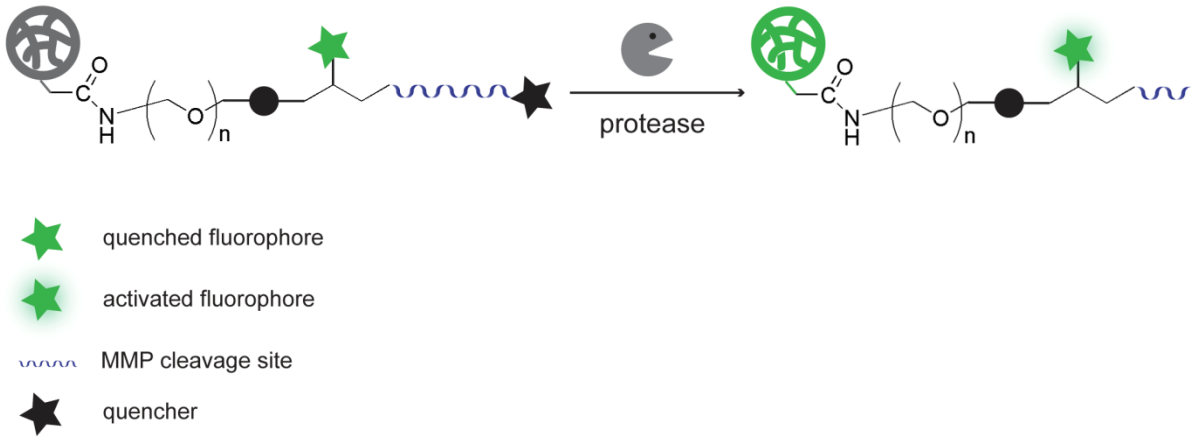


**Figure 4.10** Activation of microbead conjugated MMP probe by proteases. The protease cleaves the peptide sequence and the quencher diffuses away from the fluorophore, resulting in the overall fluorescence of the microbead.

#### 4.2.1.5 Layer-by-Layer assembly of polyelectrolytes on conjugated PP9010 microbeads.

PP9010 beads conjugated with DBCO-PEG-$NH_2$ through EDC carbodiimide coupling and further modified with RhoCOOH-PEG-$N_3$ through click chemistry were prepared as described above and used as a model to assess the possibility of LbL assembly of polyelectrolytes on the modified beads. Rhodamine B labeled poly(allylamine hydrochloride) (PAH-RhoB) was prepared and assembled on the model conjugated beads, according to the conditions already described in Chapter 3. The obtained constructs were observed on a Zeiss LSM 510 (Germany) at ambient temperature and $\lambda_{exc}$ = 488 nm for RhoCOOH and $\lambda_{exc}$ = 543 nm for the RhoB flurophores.

#### 4.2.1.6 Incorporation of tethered microbeads in model cell cultures

Preliminary experiments were performed to assess the deployment of the conjugated microbeads into model 2D and 3D cell cultures. For the 2D assays, mouse primary hepatocytes-enriched populations were obtained using a perfusion procedure similar to methods described in the literature.[27] 75,000 cells/$cm^2$ and 7,500 microbeads/$cm^2$ were mixed in Williams E media and plated in collagen coated polystyrene culture 6-well plates. The media was exchanged before imaging after 6 and 24 hours of incubation. For the collagen gels experiment the concentration of beads per cell was increased to 3,200,000 microbeads/$cm^2$ and mixed with collagen (to a final collagen concentration of 2.7 mg/mL) and immortalized 12-Z[27] endometriotic cells at 5,000 cells/well concentration in DMEM media. 100 μL of the mixture was immediately placed on bovine serum albumin coated tissue culture 96-well plates. After incubating for about 10 min to form the collagen gel, 100 μL of media were placed on each well .Imaging was performed on a CARV II spinning disk confocal system equipped with an environmental chamber at 37 $^oC$ and a Zeiss inverted microscope.

### 4.2.2 Results and discussion

#### 4.2.2.1 Conjugation of model fluorogenic compounds to PP9010 microbeads

As shown in Figure 4.8, the MMP sensor sequences comprise a FRET donor-acceptor pairs of fluorescein-Dabcyl separated by an enzyme-sensitive peptide linker that is specifically cleaved by the protease of interest, and also an azide / terminal cysteine to allow their conjugation to any support in high yields and with the formation of stable bonds in physiological media.[22,24] The approach followed to chemically modify the PP9010 for conjugation with the prepared MMP fluorogenic substrates consists on: (i) conjugation of a PEG linker containing DBCO/maleimide antagonist chemistries by

EDC carbodiimide reaction between native PP9010 carboxylic acid groups and the linker terminal primary amine; (ii) cycloaddition of an azide terminated MMP probe or thioether bond formation with thiol terminated MMP probe, as shown in Figure 4.8. In order to monitor and optimize the chemical modification of PP9010 microbeads, fluorescent model molecules were initially used.

The amide conjugation of fluorescent FAM-$NH_2$ and FAM-PEG-$NH_2$ molecules on PP9010 microbeads was assessed by confocal microscopy as shown in Figure 4.11, clearly showing that EDC chemistry can be used to modify the beads accordingly. Furthermore, conjugation occurred irrespective of the length of the fluorescent molecule PEG spacer. The higher fluorescence intensity on the bead shell may be due to a native higher concentration of carboxylic groups, as discussed in Chapter 3. In terms of bead size it is possible to qualitatively observe that beads exhibit similar diameters in 10 mM phosphate buffer pH 7.2, as both conjugations were performed with same initial molar concentration of conjugate molecule and therefore approximately the same amount of carboxylic groups are expected to be substituted. The presence of a PEG spacer is important for both improving the solubility of the DBCO/maleimide moieties to be conjugated in aqueous environment and improving future enzyme accessibility in physiological conditions.

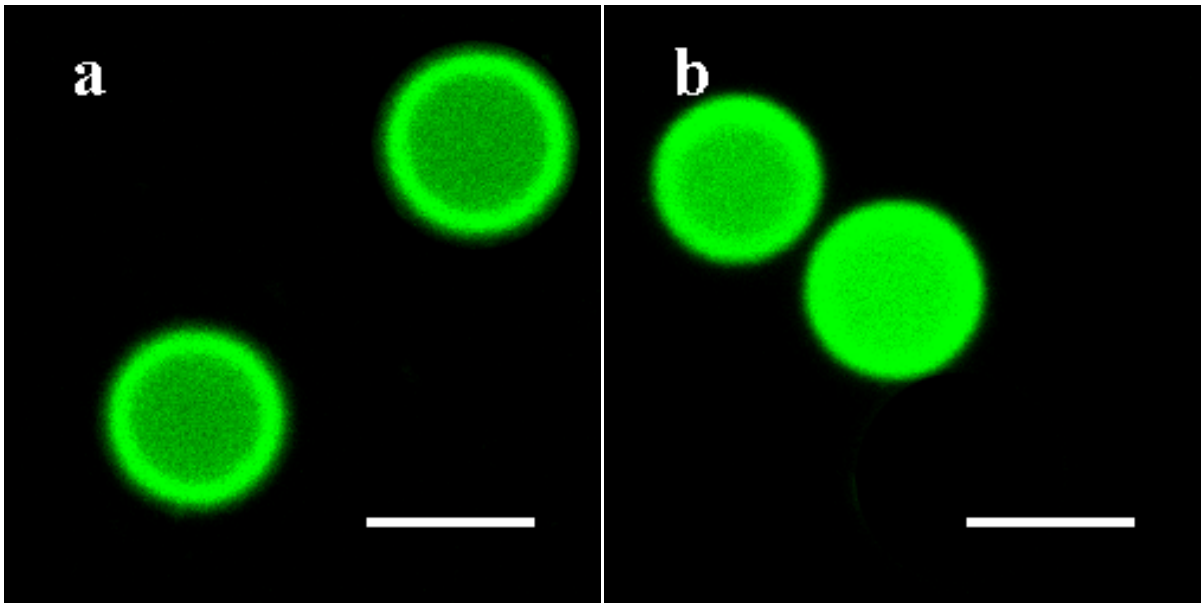


**Figure 4.11** Confocal micrographs of the middle plane of PP9010 microgels conjugated with (a) FAM-$NH_2$ and (b) FAM-PEG-$NH_2$ by EDC carbodiimide chemistry, dispersed in 10 mM phosphate buffer pH 7.4 (with 0.15 M NaCl to simulate physiological salt conditions). Scale bar: 10 μm.

The same experimental conditions as shown for the amide coupling of the model dye-labeled molecules were used for the conjugation of PEG linkers bearing functional groups antagonists to the MMP probe terminal azide/cysteine, namely DBCO-PEG-$NH_2$ / Mal-PEG-$NH_2$. In order to visually determine whether the conjugation of those linkers was successful, subsequent conjugation of azide / thiol terminated dyes was used, as shown in Figure 4.12. Indeed, after extensive washing, both samples exhibited fluorescence. Further controls were performed in which either the initial EDC or

the linkers were not used in the conjugation protocol and beads did not exhibit any fluorescence, confirming that the fluorescence observed is due to dyes effectively tethered on the beads.

Subsequent conjugation of a non-quenched (without Dabcyl) MMP probe showed that beads exhibited fluorescence across the beads. Therefore, similar modifications on PP9010 beads were performed for conjugation of an MMP probe bearing a terminal cysteine. For these experiments, all solutions contained 0.05 wt % sodium azide to prevent bacterial growth, as bacteria produce proteases that are able to cleave the MMP probe peptide sequence. After thiolether bond formation between the MMP probe and maleimide modified PP9010 beads an extremely dim fluorescence was observed. The probe's peptide sequence contains an arginine residue, being a preferential site for cleavage by trypsin. Trypsin can thus be used as a model protease. After trypsin incubation, an increase up to 10-fold in fluorescence, as determined by image analysis, was observed – Figure 4.13.

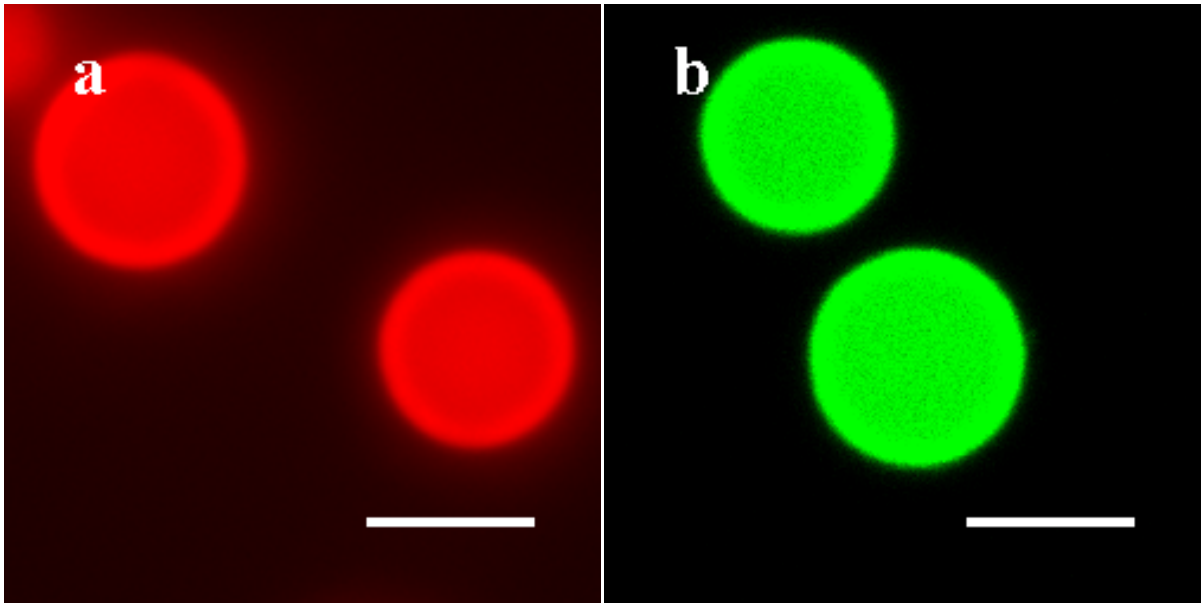


**Figure 4.12** Confocal micrographs of the middle plane of PP9010 microgels conjugated with (a) TAMRA-SH and (b)RhoCOOH-PEG-$N_3$ by click chemistry, dispersed in 10 mM phosphate buffer pH 7.4 (with 0.15 M NaCl to simulate physiological salt conditions). Scale bar: 10 μm.

These are very promising results for immobilized MMP probe activation, being higher than the only literature example for bead conjugated FRET protease sensors.[23] The dynamic range between quenched and activated MMP probe may be further improved by using different FRET donors with higher quantum yields. Currently, assays with specific MMPs are undergoing, using the flow cytometry method outlined in Chapter 3 for microgels with multilayered films of dye-labeled polyelectrolytes.

As referred in previous chapters, the LbL assembly of coatings surrounding the MMP probe tethered microbead may be a way to further improve the sensor specificity by tuning bead charge or permeability according to the target protease and to promote cell adhesion.[9,23] The proposed modification strategy outlined above decreases the amount of available carboxylic groups on the bead,

necessary for the polyelectrolytes multilayer assembly. In order to verify whether polyelectrolytes multilayer could be assembled on the conjugated microbeads, rhodamine B labeled poly(allylamine hydrochloride) (PAH-RhoB) was complexed on model RhoCOOH-PEG-PP9010 modified beads. The confocal micrographs in Figure 4.14 clearly show the presence of PAH-RhoB (red fluorescence) on the modified microbeads, being evidence that there are probably carboxylic groups still available. Further characterization, such as titration or labeling of the carboxylic groups would provide more quantitative information on the extent of modification of the beads. Nevertheless, LbL assembly to tune microbead protease sensitivity still remains an open possibility.

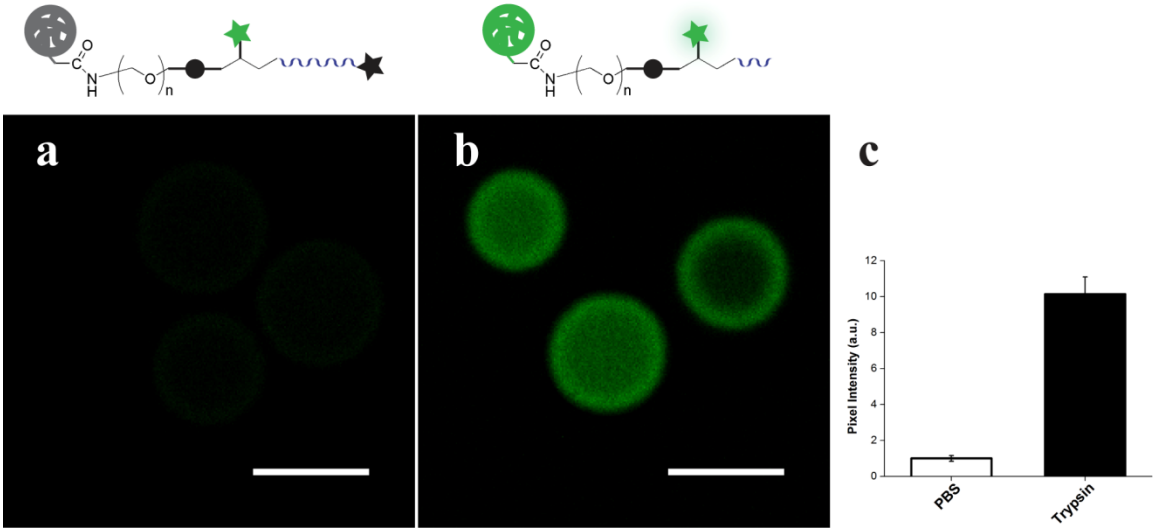


**Figure 4.13** Activation of MMP probe conjugated to PP9010 microbeads upon incubation in PBS buffer with trypsin: (a) in PBS; (b) in 1× trypsin; and (c) normalized pixel intensity of the confocal micrographs as determined by image analysis using Image J software. Scale bar: 10 μm.

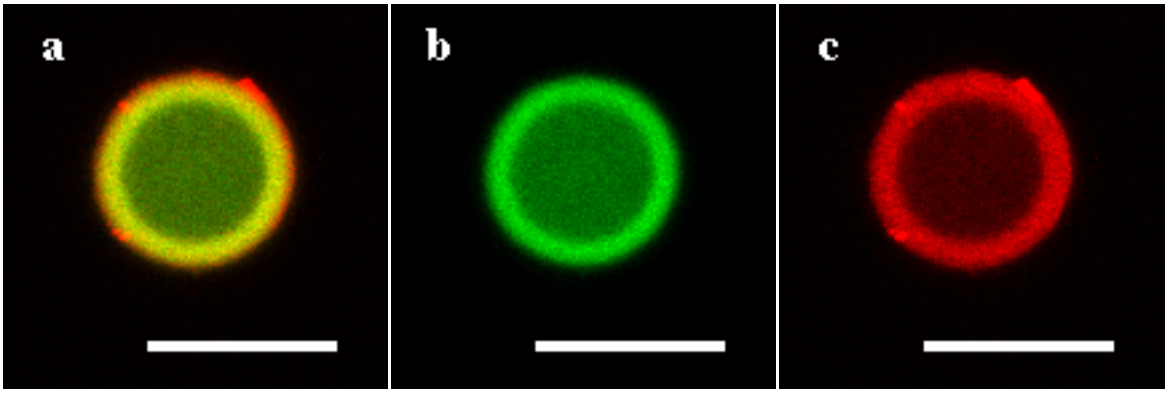


**Figure 4.14** CLSM micrographs of PP9010 RhoCOOH-PEG conjugated microbeads complexed with PAH-Rho in PBS buffer: (a) overlay; (b) fluorescence from the native RhoCOOH-PEG conjugated bead; (c) fluorescence from the complexed PAH-RhoB. Scale bar: 10 μm.

Preliminary experiments on the deployment of the conjugated microbeads into model 2D and 3D cell cultures of interest were performed: primary hepatocytes and immortalized endometriotic epithelial 12-Z cells, respectively – Figure 4.15. MP activity has been associated with several diseased states, namely liver fibrosis[29] and endometriosis.[5] Incorporation of protease sensors in the referred cell

cultures could provide useful insights on the molecular and cellular aspects of these diseases. For the primary 2D cell culture, conjugated PP9010 microbeads were successfully plated along the hepatocytes and remained in culture even after media exchange (micrograph taken after 24 hours of culture – Figure 4.15 (a)). For the 3D cell construct, the conjugated microbeads were simply mixed with 12-Z cells plus collagen for the formation of a 3D tissue. Co-localization of both the microbeads and 12-Z was observed after 24 hours of culture and no significant deformation of the particles occurred, as shown in Figure 4.15 (b). These results are shown just as an example of the incorporation of the microbeads into different cell culture scenarios, being a promising approach for the future use of these sensors for gathering information on the complex behavior of primary cell cultures or on obtaining protease activity profiles during matrix turnover, cell migration, and other processes, by cells cultured in 3D engineered configuration.

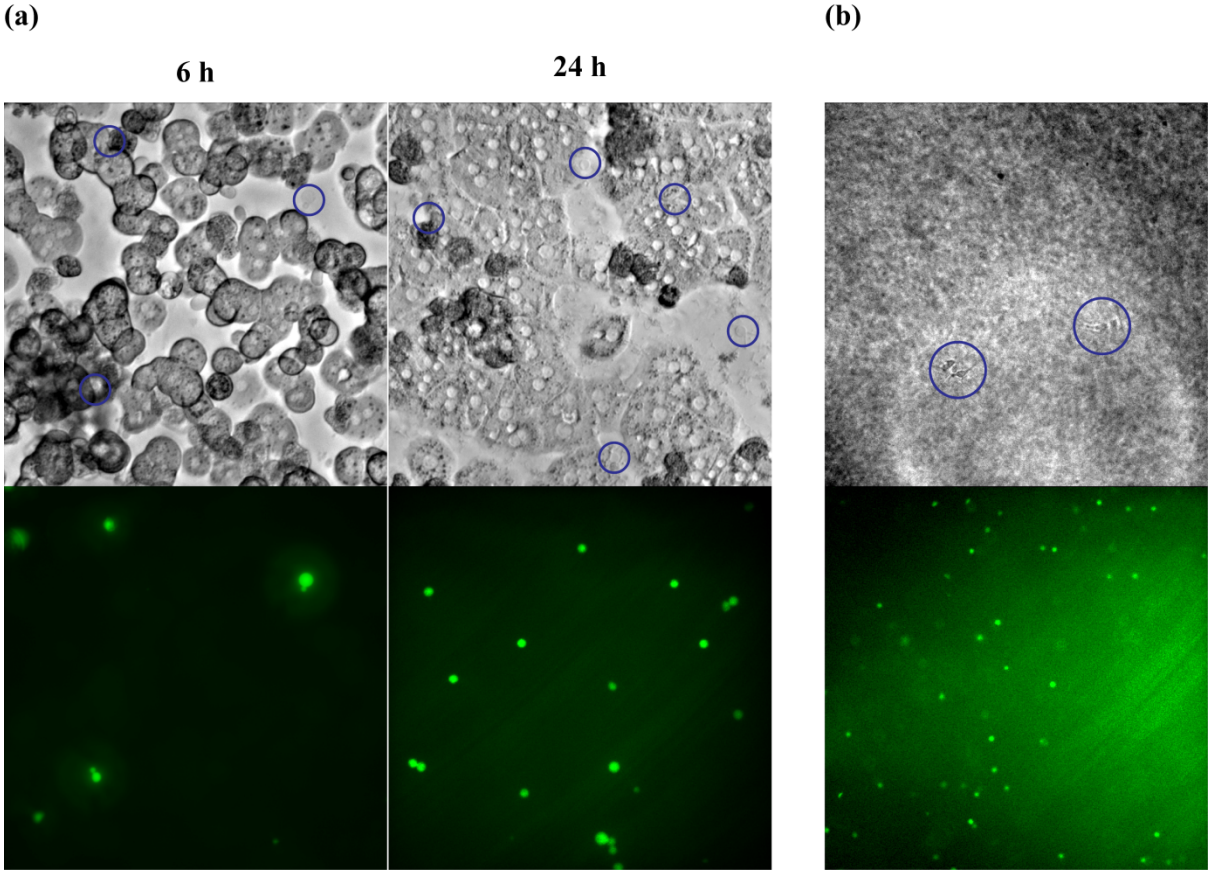


**Figure 4.15** Integration of conjugated microbeads in (a) 2D primary mouse hepatocytes cell cultures (PP9010 coupled to FAM-$NH_2$), magnification 200× (circles highlight beads location); and (b) 12-Z cells cultures in collagen gels after 24 hours (activated PP9010 coupled MMP probe), magnification 100× (circles highlight cells location).

Overall, the above results outline a systematic strategy for conjugation of MMP probes on microbeads and perhaps improving probe sensitivity by tuning microbeads properties via LbL assembly of polyelectrolytes, and may enable a flexible tool to monitor specific protease activity in different long term cell cultures.

## 4.3 Conclusions

Two different strategies were followed for enabling protease sensing function to p(NIPAAm-co-MAA) 90:10 microbeads, initially synthesized in $scCO_2$. The first strategy comprised the preparation of a well-defined polymeric backbone for conjugation of MMP probes in high yields and subsequent complexation with the PP9010 microbeads. The second strategy involved tethering the MMP probe directly on PP9010 microbeads. The MMP probes being developed comprised a FRET donor-acceptor pair, an enzyme-sensitive peptide sequence and a terminal azide/cysteine to enable probe coupling to any support. LbL assembly of different polyelectrolytes could be then performed on these protease sensing microbeads to potentially tailor the construct sensitivity according to the target protease, by manipulating charge and overall accessibility.

For the first strategy, a α-alkyne polypeptidic backbone was prepared by N-carboxyanhdride polymerization, a synthetic route that may allow a fine control over the length of the polymer and a narrow molecular weight distribution. An azide terminated model fluorescein molecule was further added by conjugation with the terminal propargyl group via click chemistry. The obtained polymer was successfully complexed to PP9010 microbeads. Trypsin has been show to degrade synthetic PLL and thus was used to examine whether a small model protease could access the complexed microbead and exhibit enzymatic activity. Indeed enzymatic degradation and consequent loss of bead fluorescence was demonstrated upon incubation with trypsin. However, these complexes did not show enough stability under physiological conditions and upon polyelectrolyte multilayer assembly; hence a more robust approach for MMP sensor incorporation was pursuit, namely by covalently tethering the MMP probe onto the microbeads.

EDC carbodiimide chemistry was used to tether linkers bearing chemistries compatible with conjugation of the developed MMP probes through either click chemistry or thiol-maleimide coupling. Using model fluorescent molecules, the successive microbead modification steps were assessed and optimized. Finally a MMP probe was covalently attached to the microbeads and its successful activation by incubation with trypsin, as a model protease, was observed. The obtained dynamic range between quenched and activated microbead sensor was about 10-fold, being higher than literature. Further analysis using specific MMPs are undergoing. These constructs were also amenable to be further manipulated by LbL assembly of polyelectrolytes and to be potentially incorporated into 2D and 3D cell cultures. As a result, the developed modification route described herein may potentially be applied for the development of a protease activity specific sensor to be deployed for monitoring cell cultures. In addition, both developed strategies may easily be translated to other supports of interest, besides the $scCO_2$-synthesized microbeads, such as macroscopic 3D hydrogels or 2D surfaces.

## 4.4 References


1. Kessenbrock, K., Plaks, V. & Werb, Z. Matrix metalloproteinases: regulators of the tumor microenvironment. *Cell* **141**, 52-67 (2010).

2. Page-McCaw, A., Ewald, A.J. & Werb, Z. Matrix metalloproteinases and the regulation of tissue remodelling. *Nat. Rev. Mol. Cell Biol.* **8**, 221-33 (2007).

3. Parks, W.C., Wilson, C.L. & López-Boado, Y.S. Matrix metalloproteinases as modulators of inflammation and innate immunity. *Nat. Rev. Immunol.* **4**, 617-29 (2004).

4. Huang, K. & Wu, L.D. Aggrecanase and aggrecan degradation in osteoarthritis: a review. *J. Int. Med. Res.* **36**, 1149-60 (2008).

5. Osteen, K.G., Ph, D., Yeaman, G.R. & Bruner-tran, K.L. Matrix Metalloproteinases and Endometriosis. *Semin. Reprod. Med.* **21**, 155-164 (2003).

6. Bremer, C., Tung, C.H. & Weissleder, R. In vivo molecular target assessment of matrix metalloproteinase inhibition. *Nat. Med.* **7**, 743-8 (2001).

7. Ryu, J.H. *et al.* "One-step" detection of matrix metalloproteinase activity using a fluorogenic Peptide probe-immobilized diagnostic kit. *Bioconjug. Chem.* **21**, 1378-84 (2010).

8. Miller, M.A., Barkal, L., Jeng, K., Herrlich, A., Moss, M., Griffith, L.G. & Lauffenburger, D.A. Proteolytic Activity Matrix Analysis (PrAMA) for simultaneous determination of multiple protease activities. *Integr. Biol.***3**, 422-438 (2011).

9. Stubbe, B.G. *et al.* Evaluation of Encoded Layer-By-Layer Coated Microparticles As Protease Sensors. *Adv. Funct. Mater.* **18**, 1624-1631 (2008).

10. Deming, T.J. Polypeptide and Polypeptide Hybrid Copolymer Synthesis via NCA Polymerization. *Adv. Polym. Sci.* **202**, 1-18 (2006).

11. Kricheldorf, H.R. Polypeptides and 100 years of chemistry of alpha-amino acid N-carboxyanhydrides. *Angew. Chem., Int. Ed.* **45**, 5752-84 (2006).

12. Agut, W., Taton, D. & Lecommandoux, S. A Versatile Synthetic Approach to Polypeptide Based Rod−Coil Block Copolymers by Click Chemistry. *Macromolecules* **40**, 5653-5661 (2007).

13. Agut, W., Agnaou, R., Lecommandoux, S. & Taton, D. Synthesis of Block Copolypeptides by Click Chemistry. *Macromolecular Rapid Communications* **29**, 1147-1155 (2008).

14. Engler, A.C., Lee, H.-il & Hammond, P.T. Highly efficient "grafting onto" a polypeptide backbone using click chemistry. *Angew. Chem., Int. Ed.* **48**, 9334-8 (2009).

15. Kolb, H.C., Finn, M.G. & Sharpless, K.B. Click Chemistry: Diverse Chemical Function from a Few Good Reactions. *Angew. Chem., Int. Ed.* **40**, 2004-2021 (2001).

16. Motala-timol, S. *et al.* Amphiphilic Poly(L-lysine-b-caprolactone) Block Copolymers Synthesis, Characterization, and Solution Properties. *Macromolecules* **41**, 5571-5576 (2008).

17. He, X., Zhong, L., Wang, K., Lin, S. & Luo, S. Synthesis of water-soluble ABC triblock copolymers containing polypeptide segments. *React. Funct. Polym.* **69**, 666-672 (2009).

18. Quinn, J.F., Johnston, A.P.R., Such, G.K., Zelikin, A.N. & Caruso, F. Next generation, sequentially assembled ultrathin films: beyond electrostatics. *Chem. Soc. Rev.* **36**, 707-18 (2007).

19. Waley, S.G. & Watson, J. The Action of Trypsin on Polylysine. *Biochemistry* **55**, 328-337 (1953).

20. Caracciolo, G. *et al.* Conformational changes of bovine beta-trypsin and trypsinogen induced by divalent ions: an energy-dispersive X-ray diffraction and functional study. *Arch. Biochem. Biophys.* **449**, 157-63 (2006).

21. Sjöback, R., Nygren, J. & Kubista, M. Absorption and fluorescence properties of fluorescein. *Spectrochimica Acta A* **51**, L7-L21 (1995).

22. Hermanson, G.T. *Bioconjugate Techniques*. (Academic Press: San Diego, California, USA, 1996).

23. Patrick, A.G. & Ulijn, R.V. Hydrogels for the Detection and Management of Protease Levels. *Macromolecular Bioscience* **10**, 1184-1193 (2010).

24. Jewett, J.C. & Bertozzi, C.R. Cu-free click cycloaddition reactions in chemical biology. *Chemical Society Reviews* **39**, 1272-1279 (2010).

25. Agard, N.J., Baskin, J.M., Prescher, J.A., Lo, A. & Bertozzi, C.R.B. A Comparative Study of Bioorthogonal Reactions with Azide. *ACS Chem. Biol.* **1**, 644-648 (2006).

26. Christie, R.J., Tadiello, C.J., Chamberlain, L.M. & Grainger, D.W. Optical properties and application of a reactive and bioreducible thiol-containing tetramethylrhodamine dimer. *Bioconjug. Chem.* **20**, 476-80 (2009).

27. Hwa, A.J. *et al.* Rat liver sinusoidal endothelial cells survive without exogenous VEGF in 3D perfused co-cultures with hepatocytes. *FASEB J.* **21**, 2564-79 (2007).

28. Banu, S.K., Lee, J., Starzinski-Powitz, A. & Arosh, J.A. Gene expression profiles and functional characterization of human immortalized endometriotic epithelial and stromal cells. *Fertil. Steril.* **90**, 972-87 (2008).

29. Benyon, R.C. & Arthur, M.J. Extracellular matrix degradation and the role of hepatic stellate cells. *Semin. Liver Dis.* **21**, 373-84 (2001).

# CHAPTER 5:

## Conclusions and Future Directions

# 5 Conclusions and Future Directions

## 5.1 Conclusions

The present thesis is a result of the combination of different technologies for the development of a microbead protease activity sensor to be easily deployed in different cell cultures. Firstly, supercritical fluid technology was used for the preparation of well-defined hydrogel smart microparticles with cell mimicking properties. Then, complexation of macromolecules or layer-by-layer of polyelectrolytes was proposed as a method to systematically tune microparticle swelling, responsive behavior and overall net charge, being a potential approach to adjust microbead permeability to specific proteases. Polyelectrolytes known to generally promote cell adhesion were successfully assembled on the microbeads. Finally, approaches for the incorporation of a protease sensing function to the microbeads were outlined, namely by the preparation of functionalized polymers for conjugation of protease probes and subsequent complexation on the microbeads; and by directly tethering a fluorogenic MMP probe on the native microbead functional groups.

The keys advantages of using supercritical carbon dioxide for the preparation of polymeric particles for biological applications is the elimination of hazardous and cytotoxic organic solvents during synthesis and purification, and easy removal of any residual monomers or other contaminants, yielding highly pure materials. In addition, an extensive body of literature exists on strategies for the synthesis of particles with well-defined morphology. The synthesis of responsive polymers in supercritical $CO_2$ was successfully optimized to yield large spherical monodisperse beads by following a dispersion polymerization strategy. The microbeads properties, such as size, swelling, responsive and rheological behaviors could be tuned by changing cross-linker species, the cross-linking degree or the co-monomer composition. The preparation of poly(*N*-isopropylacrylamide) (PNIPAAm) particles with carboxylic groups enabled temperature and pH sensitive systems, enlarging their application scope. Under physiological conditions, the deprotonation of the carboxylic groups leads to swollen microbeads with little temperature-induced volume phase transition in the targeted cell-like size range of 10 μm. Furthermore, the carboxylic groups can be chemically modified or interact with other macromolecules through electrostatics, determinant for a stable layer-by-layer assembly. From the rheological data collected for these microparticles, it can be expected that these beads will be compliant with soft human tissues, and therefore will be less likely to trigger non-physiological responses when probing tissue microenvironments.

The assembly of macromolecules on smart microgels may be used not only to modify their surface chemistry, but also their native properties and responsive behavior. Tannic acid (TA), a bioactive

polyphenolic macromolecule, was effectively complexed on PNIPAAm microgels, increasing or even suppressing the thermoresponsive polymer LCST behavior, depending on the experimental conditions. Indeed, above a critical concentration, TA physically cross-links the polymer chains due to extensive hydrogen bonding between PNIPAAm and TA leading to microgel collapse and water displacement. The H-bonding interactions may be reversibly destabilized by increasing pH above TA $pK_a$, leading to the increase in microgel swelling and to the recovery of PNIPAAm native responsive behavior. This case study clearly shows that the performance of PNIPAAm-based smart devices can be clearly modified by the incorporation of other molecules.

The synthesized copolymeric p(NIPAAm-co-MAA) 90:10 particles were amenable to layer-by-layer (LbL) sequential complexation of polyelectrolytes due to its pH-dependent net negative charge, presenting enough colloidal stability during assembly steps, and therefore different polyelectrolytes were explored for their coating, namely weak synthetic polyelectrolytes and polypeptides known to promote cell adhesion as well as a strong polyelectrolyte pair. The microbeads swelling and temperature sensitivity was determined by the type of assembled polyelectrolyte pair and the composition of the outermost layer, although not as significantly under physiological conditions than in water. Polyelectrolytes can indeed penetrate throughout the microgel mesh, recruiting more carboxylic groups if it is a polycation than a polyanion. Thus, polycation-terminated microbeads are less swollen and thermoresponsive, as less free COOH functionalities are available to stabilize the polymer chains conformation in a solvated state and promote swelling. This outermost layer effect had a larger magnitude for polyelectrolyte pairs with higher intrinsic mobility. The LbL assembly of polyelectrolytes may indeed allow the customization of the synthesized microbeads in terms of water content, overall charge and potentially permeability to macromolecules according to their specific size and charge, being a possible route to improve the sensitivity of a protease sensing construct to particular proteases.

For incorporating a protease sensing function on the synthesized p(NIPAAm-co-MAA) 90:10, two different strategies were outlined. Since different polymers were successfully assembled on the microbeads, one first possible strategy would be to functionalize a polymeric backbone with a protease sensor. The second approach would be to directly conjugate the protease probe on the microbeads. Subsequent assembly of LbL multilayers would be used to adjust the overall probe sensitivity to specific protease activity. The MMP probes being developed comprise a Förster resonance energy transfer (FRET) donor-acceptor pair, an enzyme-sensitive peptide sequence and a terminal azide/cysteine to enable probe coupling to any support by click chemistry/thiol coupling. For the first strategy, an alkyne-terminated polypeptide was prepared by N-carboxyanhdride polymerization of a synthesized Z-L-lysine NCA monomer. Although the polymer was efficiently conjugated to a model dye and further complexed on the microbeads, the complexes did not show enough stability under physiological conditions and upon subsequent polyelectrolyte multilayer assembly; hence focus was placed on the other alternative strategy of covalently tethering the MMP

probe onto the microbeads. EDC carbodiimide chemistry was used to tether linkers bearing antagonist chemistries to either click chemistry or thiol-maleimide coupling. Using model fluorescent molecules, the successive microbead modification steps were assessed and optimized. Finally a MMP probe was tethered to the microbeads and its successful activation by incubation with trypsin, as a model protease, was observed. The obtained dynamic range between quenched and activated microbead sensor was about 10-fold, being a promising result. Furthermore, these constructs were suitable for further LbL assembly of polyelectrolytes and to be easily deployed in both 2D and 3D cell cultures relevant for protease biology studies. In addition, both developed strategies may easily be translated to other supports of interest, besides the $scCO_2$-synthesized microbeads, such as macroscopic 3D hydrogels or 2D surfaces.

Overall, the technological basis for the development of a protease probe was set. Microbeads with cell-like size, on which LbL multilayers could be assembled, and that were conjugated to a protease probe were prepared. However, an extensive amount of further characterization and tuning of this microbead-based system would be necessary to develop a fully functional probe to monitor a specific protease in a 3D engineered tissue.

## 5.2 Future Directions

One of the goals of the thesis was the preparation of hydrogel beads with cell-like size and mechanical properties in order to guarantee that the presence of the beads would not trigger any non-physiological response in the cells arising from mechanical stress. However, the mechanical properties of the prepared hydrogel microbeads were only roughly estimated by rheological measurements of the bulk microgels in equilibrium swelling. In order to assess the Young's modulus at the microbead level other methods would be more informative, such as nanoindentation using atomic force microscopy, which has been developed to determine mechanical properties of individual living cells.[1] This is not a straightforward approach for determining mechanical properties and careful optimization is required for each analyzed system in terms of the selection of the appropriate tip geometry and the correct tip-cell contact model for a reliable computation of the mechanical modulus.

The LbL method was hypothesized as a way to potentially tune the microbead probe construct sensitivity to specific proteases, by imposing a selective permeation barrier to proteases through mesh size sieving and/or overall net charge.[2] Indeed, LbL assembly had an impact on microgel swelling and thus on the expected mesh size. Nevertheless permeation experiments using labeled macromolecules with different sizes/charges would provide further insight. In addition, experiments on the impact of LbL assembled coatings on cell adhesion of different soft tissue derived cell lines (with mechanical moduli similar to that of the native particles) needed also to be evaluated.

Another important aspect in validating the approach described herein for the development of a functional protease probe would be to screen bead fluorescence activation using specific MPs and under different cell culture conditions. For the first analysis, flow cytometry could be used as a robust method to assess bead activation, as this analytical method was herein shown to be applicable for monitoring microgel fluorescence. From that initial screen, the best performing microbead probes could be selected for their deployment into cell cultures under conditions that are expected to result in different protease profiles. For example immortalized endometriotic cells lines such as the 12-Z cells were shown to express different protease levels in response to cytokine concentration[3] and could be used as a model.

## 5.3 References

1. Rico, F. *et al.* Probing mechanical properties of living cells by atomic force microscopy with blunted pyramidal cantilever tips. *Phys. Rev. E* **72**, 1-10 (2005).

2. Balabushevitch, N.G., Sukhorukov, G.B., Moroz, N.A., Volodkin, D.V., Larionova, N.I., Donath, E. & Möhwald, H. Encapsulation of proteins by layer-by-layer adsorption of polyelectrolytes onto protein aggregates: factors regulating the protein release. *Biotechnol. Bioeng.* **76**, 207-13 (2001).

3. Banu, S.K., Lee, J., Starzinski-Powitz, A. & Arosh, J.A. Gene expression profiles and functional characterization of human immortalized endometriotic epithelial and stromal cells. *Fertil. Steril.* **90**, 972-87 (2008).

# CHAPTER 6:

## Annexes

# Annex I: DRIFT Spectroscopy Analysis of Tannic Acid Complexation on PNIPAAm microgels

Herein a detailed spectral analysis of tannic acid and PNIPAAm is described as well as the constituent components retrieved from relevant bands upon deconvolution (Figure A1, Figure A2 and Table A2).

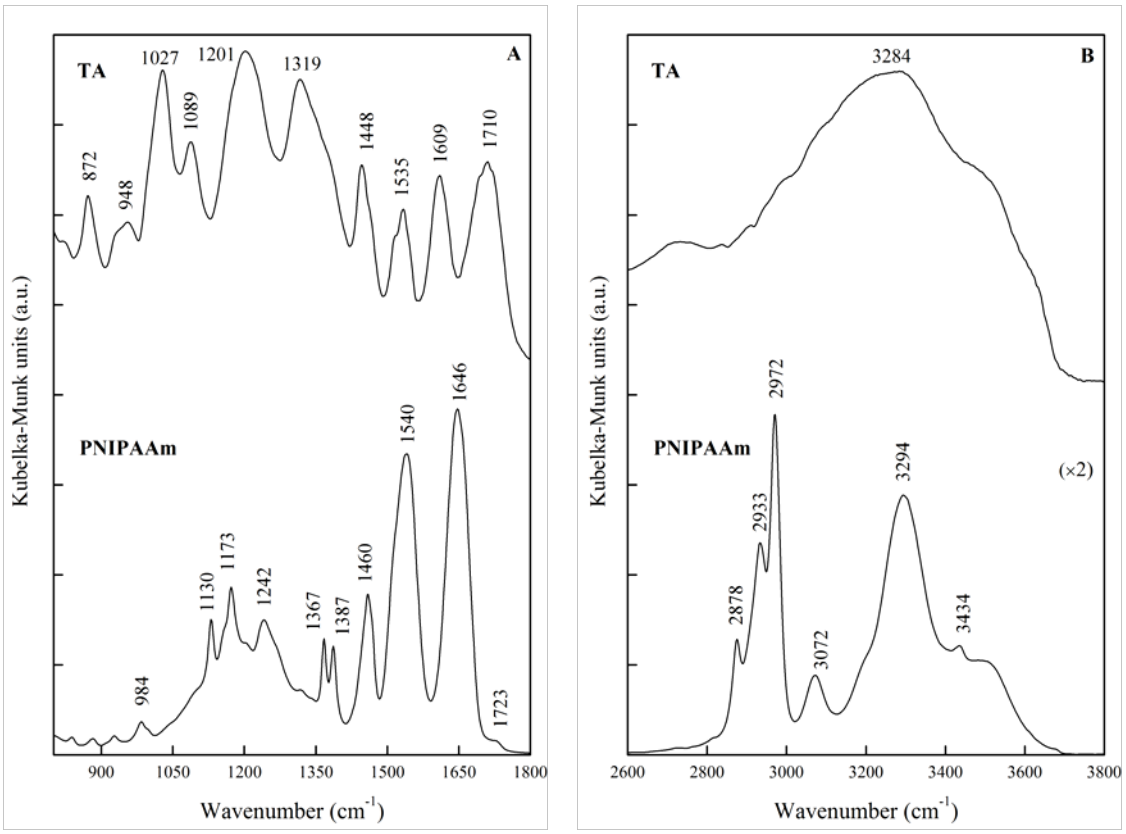


**Figure A1.** DRIFT spectra of TA and PNIPAAm in two wavenumber regions: (A) 800-1800 $cm^{-1}$; (B) 2500-3800 $cm^{-1}$. The scale factors in regions A and B are different for better visualization.

**Tannic Acid.** In TA DRIFT spectra, a broad band in the range 2800-3600 $cm^{-1}$, centered at 3284 $cm^{-1}$ can be observed. This band includes several unresolved components: the O-H stretching modes of free and hydrogen bonded hydroxyl groups (the first as shoulders above 3500 $cm^{-1}$ and the latter as lower wavenumber components), the C-H stretching mode (at ~3050 $cm^{-1}$) and overtones of the C-C stretching modes (at ~2800 $cm^{-1}$). The diversity of hydrogen bonds in which the hydroxyl groups are engaged was well demonstrated by the broadness of the band. H-bonds with the TA hydroxyl group include intra- and intermolecular with other hydroxyl, C=O and/or C-O groups. The structured profile of the νC=O band from the ester groups, centered at 1710 $cm^{-1}$, concurred with this observation as it

may be attributed to different H-bonds in which the carbonyl groups were involved. The strong bands at 1448, 1535 and 1609 $cm^{-1}$ are assigned to the C-C stretching modes of aromatic rings, with possible contribution from the νC=O modes of H-bonded carbonyl groups. The aromatic ring breathing and the in-plane CH deformation modes appeared unresolved as a very strong band at 1319 $cm^{-1}$. Also intense are the bands related to C-O stretching modes, at 1201, 1089, 1027 and 948 $cm^{-1}$. The νC-O in ester links (at 1201 $cm^{-1}$) is particularly broad, which suggested that these oxygen atoms may also act as charge donors in H-bonds with hydroxyl groups.

After deconvolution of pure TA bands in the relevant wavenumber regions, several components were retrieved as can be observed in Figure A2A and A2B. In the region comprised between 900 and 1420 $cm^{-1}$, the components retrieved for the phenolic νC-OH modes (at 932 and 957 $cm^{-1}$ plus the major band at 1027 $cm^{-1}$) and νC-O of ester links (at 1175 and 1208 $cm^{-1}$) demonstrate the diversity of H-bonding in which these groups are involved. A component at 1373 $cm^{-1}$ was recovered, which has been reported as due to coupling of the νC-O with δC-OH modes. In the region between 1420 and 1800 cm-1 (Figure A2B), apart from adjustments in the maxima positions, some new components were revealed: two small ones at 1469 and 1512 $cm^{-1}$ provide evidence of yet other types of C-C bonds in the aromatic rings, which is not surprising given their large number and the possibility of π interactions between them. The three identified νC=O components confirm the diversity of carbonyl groups: a small proportion of free groups (1728 $cm^{-1}$) and most of them H-bonded (1701 and 1629 $cm^{-1}$). The more strongly bonded (1629 $cm^{-1}$) contribute to the band at 1609 $cm^{-1}$, as anticipated. Along with spectral analysis, deconvolution showed that in pure TA the predominant interactions are OH…OH bonds (both intra and inter molecular), OH···O-C (ester links) and OH···O=C, with a fraction of carbonyl groups remaining free. There are also π interactions between the aromatic moieties of the gallic substituents. The star-like structure of the molecule is suitable for the interpenetration of branches from different molecules, favoring the observed H-bonding.

**Poly(*N*-Isopropylacrylamide).** In regards to PNIPAAm, the dominant bands in the spectrum, at 1646 and 1540 $cm^{-1}$, were assigned to Amide I and Amide II vibrations, respectively. The main contribution to the Amide I band is the carbonyl stretching mode, whereas the Amide II is mainly due to the in-plane N-H bending.[1] Since both C=O and N-H may establish H-bonds, these two bands are expected to include components assignable to free, as well as intra and intermolecular H-bonded groups.[2] The very weak band at 1723 $cm^{-1}$ may be assigned to a very small proportion of free carbonyl groups. The 2600-3800 $cm^{-1}$ spectral region included the strong N-H stretching modes (as a broad band with maximum at 3294 $cm^{-1}$ and shoulders at higher wavenumbers, consistent with H-bonded and free NH groups, respectively), the C-H stretching modes of the methyl groups ($\nu_{as}CH_3$ at 2972 cm-1 and $\nu_{s}CH_3$ at 2878 $cm^{-1}$), and of the backbone methylene groups ($\nu_{as}CH_2$, at 2933 $cm^{-1}$). The weak band at 3072 $cm^{-1}$ has been assigned to the Amide B, which resulted from Fermi resonance between the first

overtone of Amide II and the N-H stretching mode; the shoulder at ~3183 $cm^{-1}$ was attributed to Amide I and Amide II overtone.[3] The isopropyl deformation and rocking modes appear at 1460 cm-1 ($\delta_{as}CH_3$), 1387 $cm^{-1}$ ($\delta_sCH_3$), and 1130 $cm^{-1}$ ($\rho CH_3$).[4] A contribution of in-phase skeletal C-C stretching to the last band is also possible.[3] The scissor and rocking modes of the methylene groups in the main chain correspond to the bands at 1367 $cm^{-1}$ ($\delta_{sc}CH_2$) and 984 $cm^{-1}$ ($\rho CH_2$). The strong band at 1242 $cm^{-1}$ has been assigned to the Amide III mode, which results from coupling between N-C stretching and N-H in plane deformation.[5] The N-C (isopropyl) stretching mode was assigned to the band at 1173 $cm^{-1}$. The spectral deconvolution in the Amide I band (Figure A2C and Table A2) revealed the presence of three components at 1607, 1644 and 1669 $cm^{-1}$ that were assigned to intermolecular, intramolecular H-bonded and free or freer C=O groups, respectively, with the majority involved in intramolecular interactions. Similarly, in the Amide II band, hydrogen bonded NH groups originated the components at 1529 and 1548 $cm^{-1}$ (intra and intermolecularly, respectively),[6] with similar relative intensities, plus a minority of free or freer NH groups appearing at 1509 $cm^{-1}$. A small $\delta CH_2$ band of gauche conformers was retrieved at 1446 $cm^{-1}$. In the stretching region (Figure S2D), besides the well defined νC-H modes, the overtone of Amide I and Amide II was recovered as a small band at 3208 cm-1, as well as a number of N-H stretching components (at 3294, 3366, 3429 and 3494 $cm^{-1}$). The relative areas of the higher wavenumber components and the absence of bands above 3500 $cm^{-1}$ confirmed the small fraction of free or less H-bonded NH groups in PNIPAAm. From the above results, we may conclude that in PNIPAAm there are significant intramolecular C=O···H-N bonds, and a small fraction of free or freer carbonyl and NH groups. It is also clear that the NH groups must also be involved in intermolecular N-H···N-H bonds. The existence of significant intramolecular hydrogen bonding between CO and NH groups, in conjunction with the $\delta CH_2$ mode of *gauche* conformers, provided a valuable indication on the coiled structure of PNIPAAm in the solid phase.

**Table A1.** Assignments of the DRIFT spectra of pure TA and PNIPAAm.

| TA | | PNIPAAm | |
|---|---|---|---|
| **Wavenumber ($cm^{-1}$)** | **Assignment** | **Wavenumber ($cm^{-1}$)** | **Assignment** |
| $872_{(m)}$ | γCH | $984_{(vw)}$ | $\rho CH_2$ |
| $948_{(m)}$ | νC-OH (phenolic) | $1130_{(S)}$ | $\rho CH_3$ / νC-C (skeletal, in phase) |
| $1027_{(VS)}$ | νC-OH (phenolic) | $1173_{(S)}$ | νN-C(isopropyl)- |
| $1089_{(S)}$ | νC-OC (carbohydrate moiety) | $1242_{(S)}$ | Amide III (coupled νN-C and δN-H) |
| $1201_{(VS)}$ | νC-OC (ester links) | $1367_{(m)}$ | $\delta_{sc}CH_2$ |
| $1319_{(VS)}$ | δCH (in plane and aromatic ring breathing | $1387_{(m)}$ | $\delta_sCH_3$ |
| $1448_{(S)}$ | νC-C (aromatic rings) | $1460_{(S)}$ | $\delta_{as}CH_3$ |
| $1535_{(S)}$ | νC-C (aromatic rings) | $1540_{(VS)}$ | Amide II (δNH) |
| $1609_{(S)}$ | νC-C (aromatic rings) | $1646_{(VS)}$ | Amide I (νC=O) |
| $1710_{(S)}$ | νC=O | $1723_{(vw)}$ | νC=O (free) |
| $\sim 3284_{(S, br)}$ | νO-H (H-bonded) | $2878_{(w)}$ | $\nu_sCH_3$ |
| | | $2933_{(m)}$ | $\nu_{as}CH_2$ |
| | | $2972_{(S)}$ | $\nu_{as}CH_3$ |
| | | $3072_{(w)}$ | Amide B |
| | | $3294_{(S, br)}$ | νN-H (H-bonded) |
| | | $3434_{(sh)}$ | νN-H |

VS, very strong; S, strong; m, medium; w, weak; vw, very weak; sh, shoulder; sc, scissors; br; broad

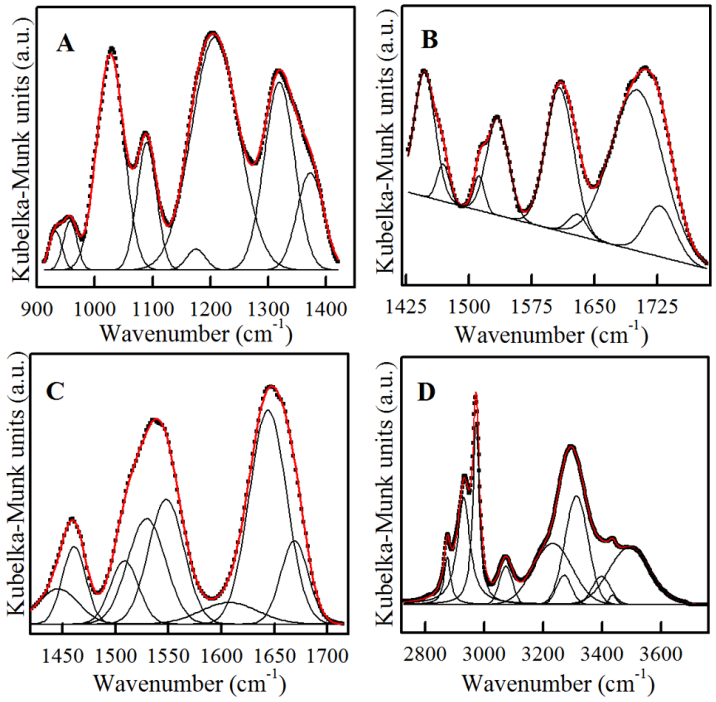


**Figure A2.** Deconvolution of the DRIFT spectra of pure TA (A and B) and PNIPAAm (C and D) in relevant wavenumber regions.

**Table A2.** Summary of the deconvolution results (positions and relative areas of the components) obtained for relevant regions of the DRIFT spectra of pure TA and pure PNIPAAm.

| | **Wavenumber ($cm^{-1}$)** **(%Area)** | | | | | | | | |
|---|---|---|---|---|---|---|---|---|---|
| TA assignments | 932 (1.7) | 957 (2.3) | 1027 (19.9) | 1090 (8.6) | 1175 (1.4) | 1208 (37.7) | 1319 (19.5) | 1373 (8.9) | |
| | νC-OH (phenolic) | | | νC-OC (carbohy) | νC-OC (ester) | | δCH | νC-O / δCOH | |
| | 1447 (12.7) | 1469 (2.3) | 1512 (1.9) | 1534 (10.8) | 1608 (20.2) | 1629 (2.0) | 1701 (42.4) | 1728 (7.7) | |
| | νC-C (aromatic) | | | | νC=O (H bonded) | | | νC=O (free) | |
| PNIPAAm assignments | 1446 (5.7) | 1461 (7.3) | 1509 (7.2) | 1529 (16.0) | 1548 (17.7) | 1607 (5.0) | 1644 (32.0) | 1669 (9.1) | |
| | $\delta CH_2$ (*gauche*) | $\delta_{as}CH_3$ | δNH (free) | δNH (intra HB) | δNH (inter HB) | νC=O (inter HB) | νC=O (intra HB) | νC=O (freer) | |
| | 2875 (3.6) | 2930 (15.0) | 2972 (13.4) | 3073 (4.0) | 3208 (12.5) | 3294 (24.1) | 3366 (8.7) | 3429 (1.3) | 3494 (17.5) |
| | $\nu_s CH_3$ | $\nu_{as}CH_2$ | $\nu_{as}CH_3$ | Amide B | Overtone | νN-H (inter HB) | νN-H (intra HB) | | νN-H (freer) |

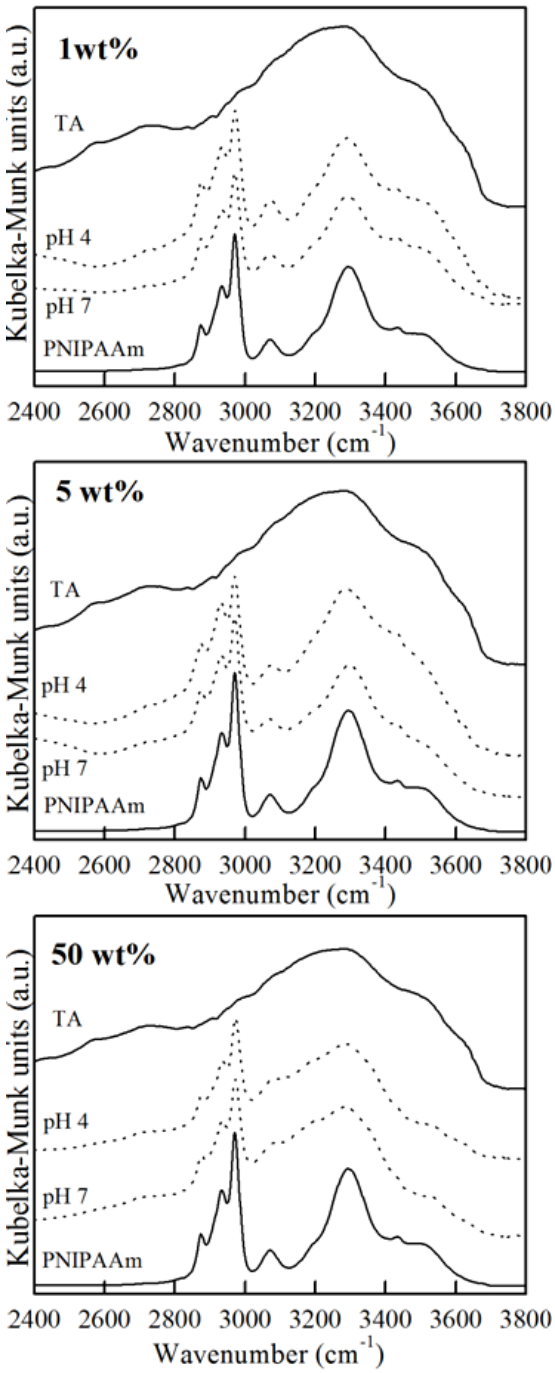


**Figure A3.** DRIFT spectra (2400-3800 $cm^{-1}$) of TA, PNIPAAm-TA complexes and PNIPAAm.

# References

1. Harris, P.I. & Chapman, D. Does Fourier-transform infrared spectroscopy provide useful information on protein structures? *Trends Biochem. Sci.* **17**, 328-333 (1992).

2. Skrovanek, D.J., Painter, P.C. & Coleman, M.M. Hydrogen bonding in polymers. 2. Infrared temperature studies of nylon 11. *Macromolecules* **19**, 699-705 (1986).

3. Kurz, V., Grunze, M. & Koelsch, P. In situ characterization of thermo-responsive poly(*N*-isopropylacrylamide) films with sum-frequency generation spectroscopy. *Chemphyschem* **11**, 1425-9 (2010).

4. Sun, B., Lin, Y. & Wu, P. Structure Analysis of Poly(N-isopropylacrylamide) Using Near-Infrared Spectroscopy and Generalized Two-Dimensional Correlation Infrared Spectroscopy. *Appl. Spectrosc.* **61**, (2007).

5. Katsumoto, Y., Tanaka, T., Sato, H. & Ozaki, Y. Conformational change of poly(N-isopropylacrylamide) during the coil-globule transition investigated by attenuated total reflection/infrared spectroscopy and density functional theory calculation. *J. Phys. Chem. A* **106**, 3429-3435 (2002).

6. Lin, S.-Y., Chen, K.-S. & Liang, R.-C. Thermal micro ATR/FT-IR spectroscopic system for quantitative study of the molecular structure of poly(*N*-isopropylacrylamide) in water. *Polymer* **40**, 2619-2624 (1999).

# Annex II: ATR-FTIR Analysis of LbL Assembled poly(NIPAAm-co-MAA) 90:10 microgels

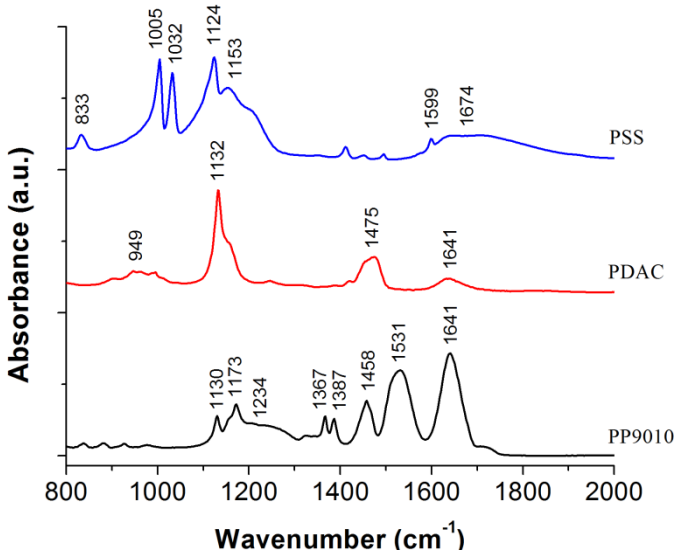


**Figure A4.** ATR-FTIR spectra of the pure PP9010, PDAC and PSS in the 800-2000 $cm^{-1}$ wavenumber region.

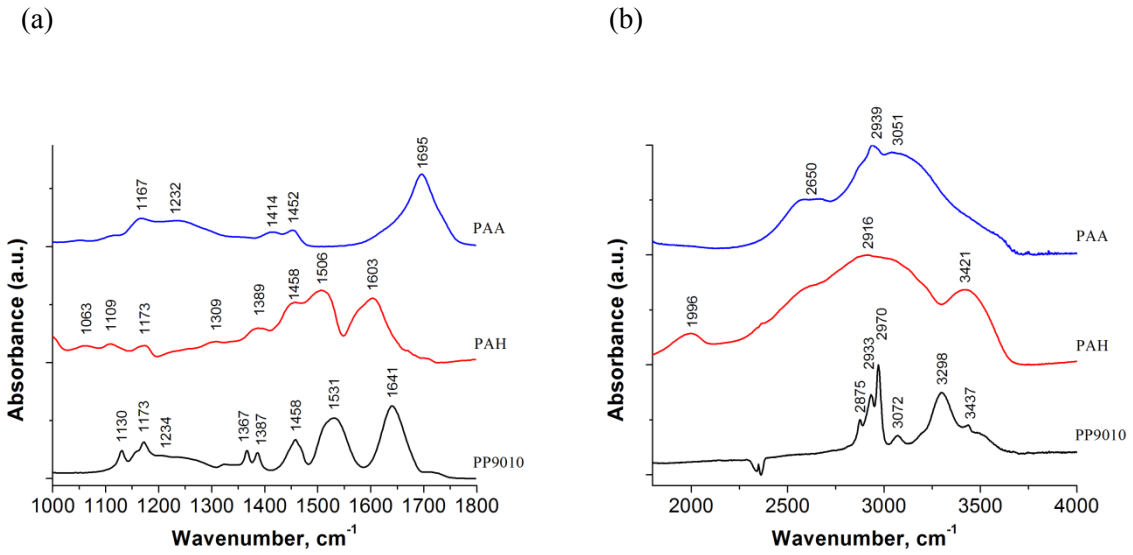


**Figure A5.** ATR-FTIR spectra of the pure PP9010, PAH and PAA in two wavenumber regions: (a) 1000-1800 $cm^{-1}$ and (b) 1750-4000 $cm^{-1}$.

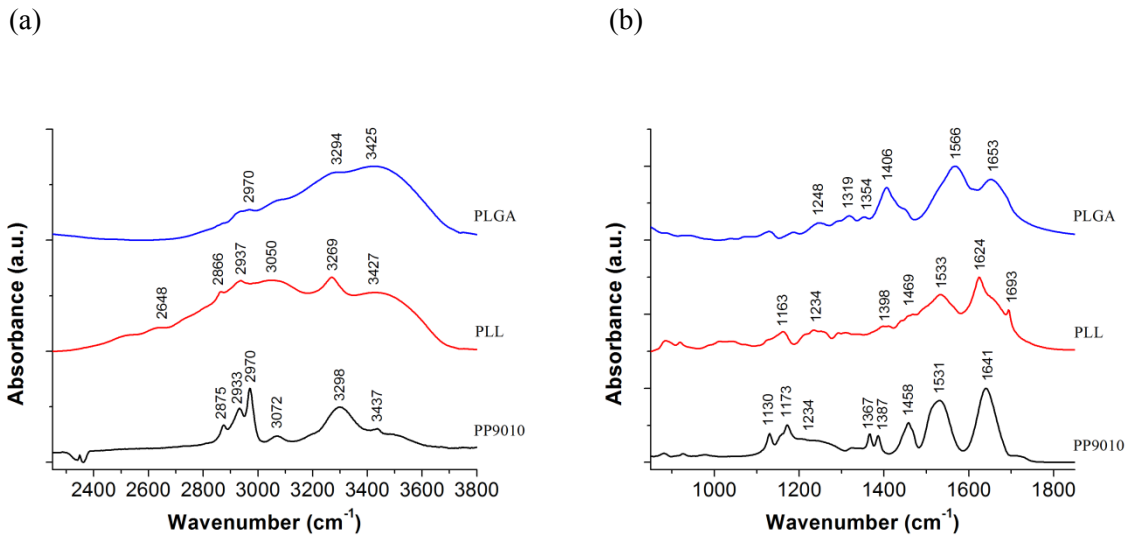


**Figure A6.** ATR-FTIR spectra of the pure PP9010, PLL and PLGA in two wavenumber regions: (a) 850-1850 $cm^{-1}$ and (b) 1750-4000 $cm^{-1}$.

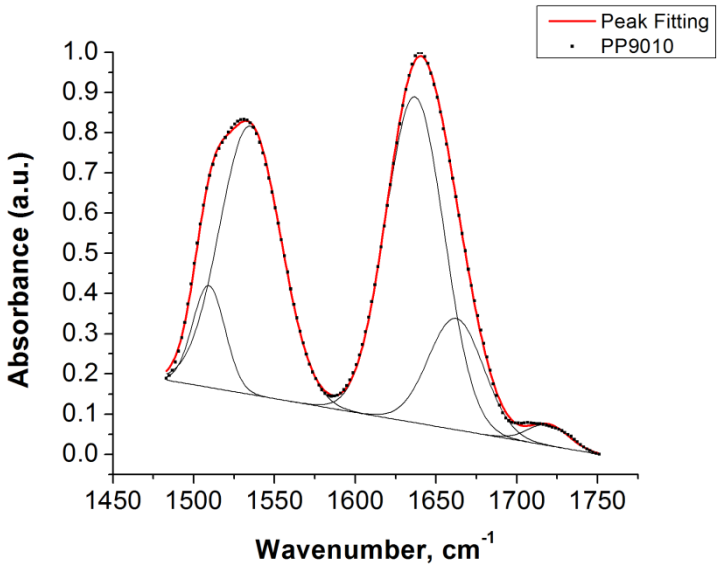


**Figure A7.** The deconvoluted Amide region of the PP9010 microgels ATR FT-IR spectra.

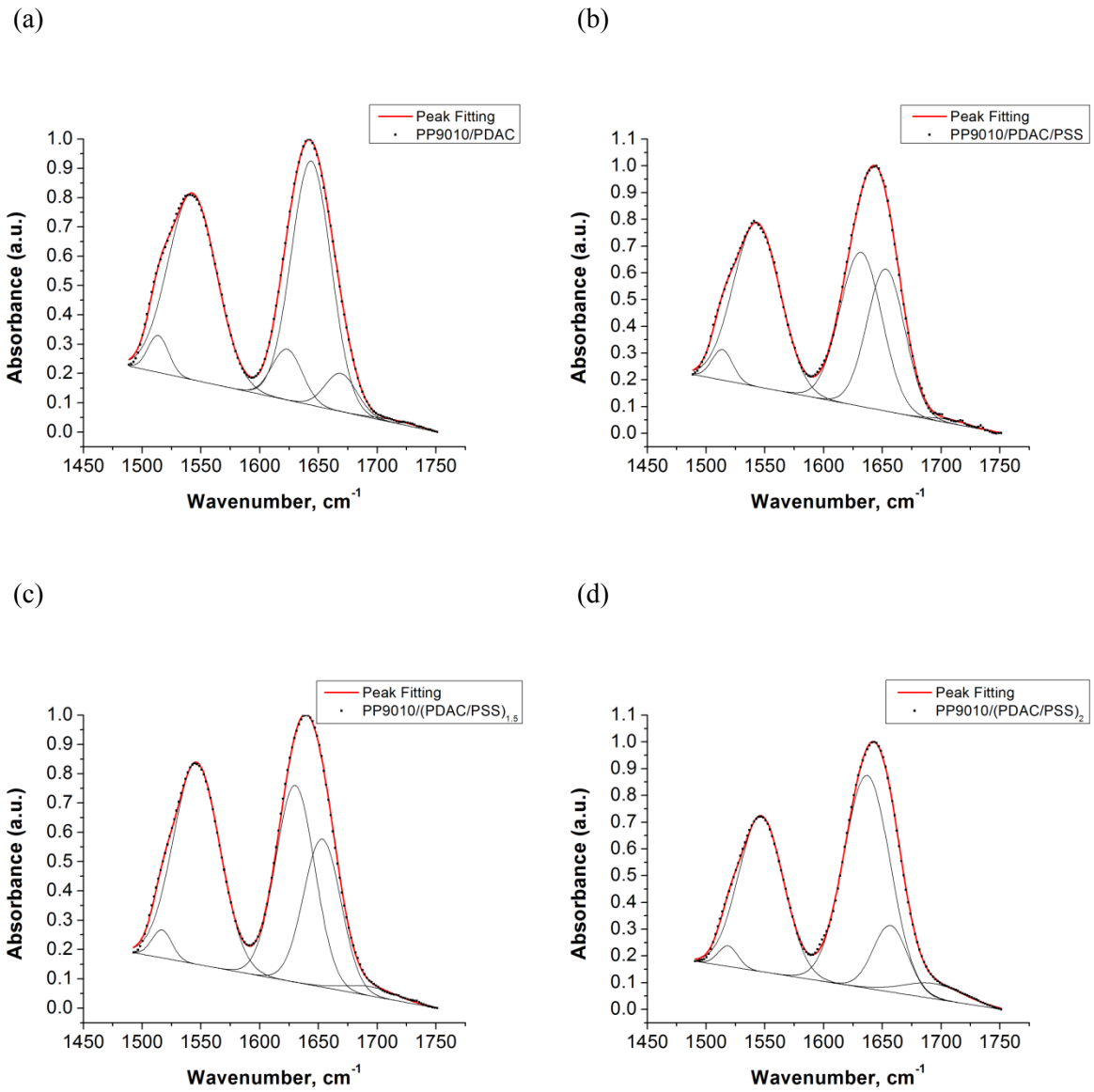


**Figure A8.** The deconvoluted Amide region of the PP9010 microgels assembled with strong polyelectrolytes ATR FT-IR spectra: (a) PP9010/$(PDAC/PSS)_{0.5}$, (b) PP9010/$(PDAC/PSS)_1$, (c) PP9010/$(PDAC/PSS)_{1.5}$, and (d) PP9010/$(PDAC/PSS)_2$.

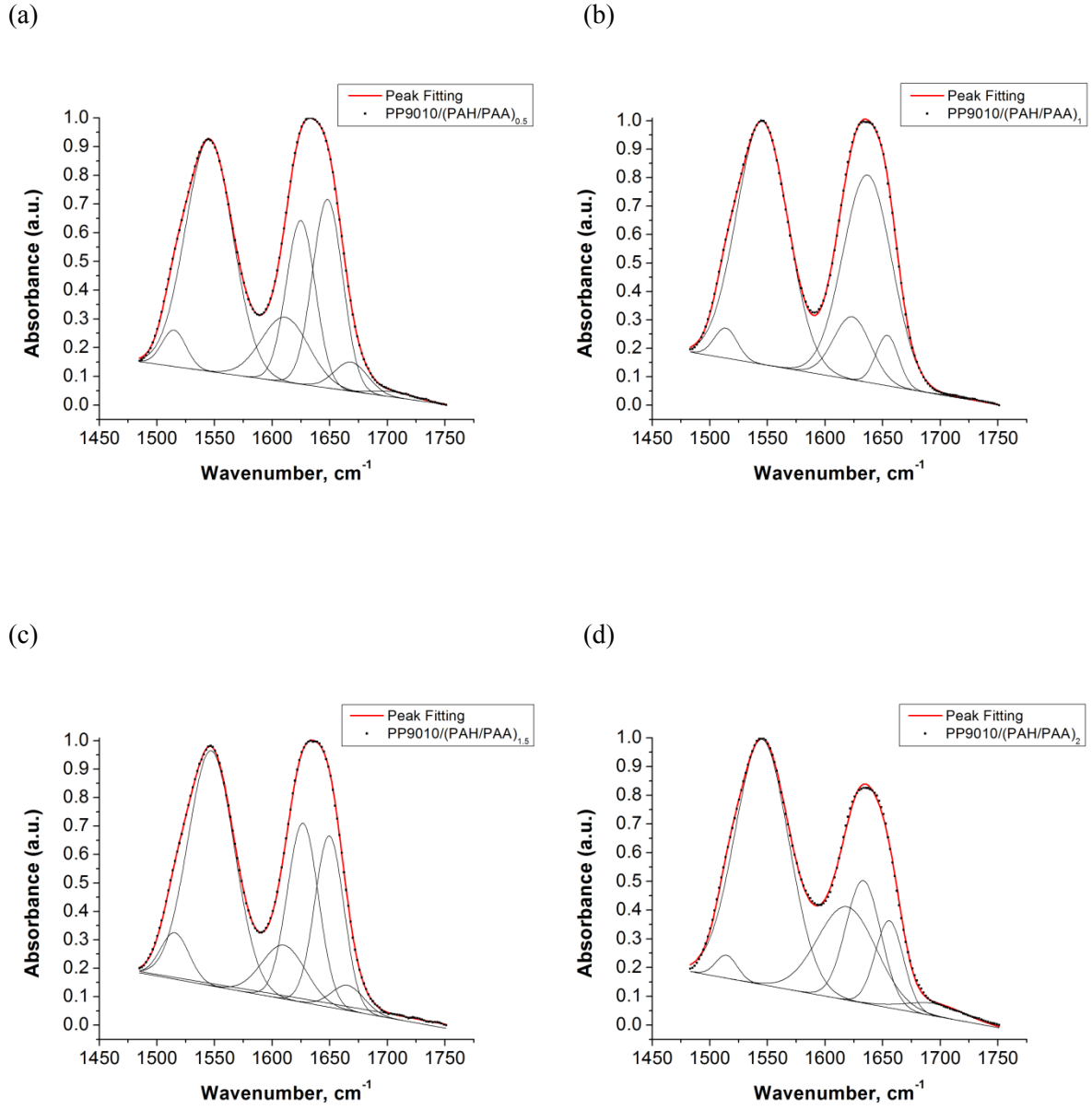


**Figure A9.** The deconvoluted Amide region of the LbL assembled PP9010 microgels ATR FT-IR spectra: (a) PP9010/(PAH/PAA)$_{0.5}$, (b) PP9010/(PAH/PAA)$_1$, (c) PP9010/(PAH/PAA)$_{1.5}$, and (d) PP9010/(PAH/PAA)$_2$.

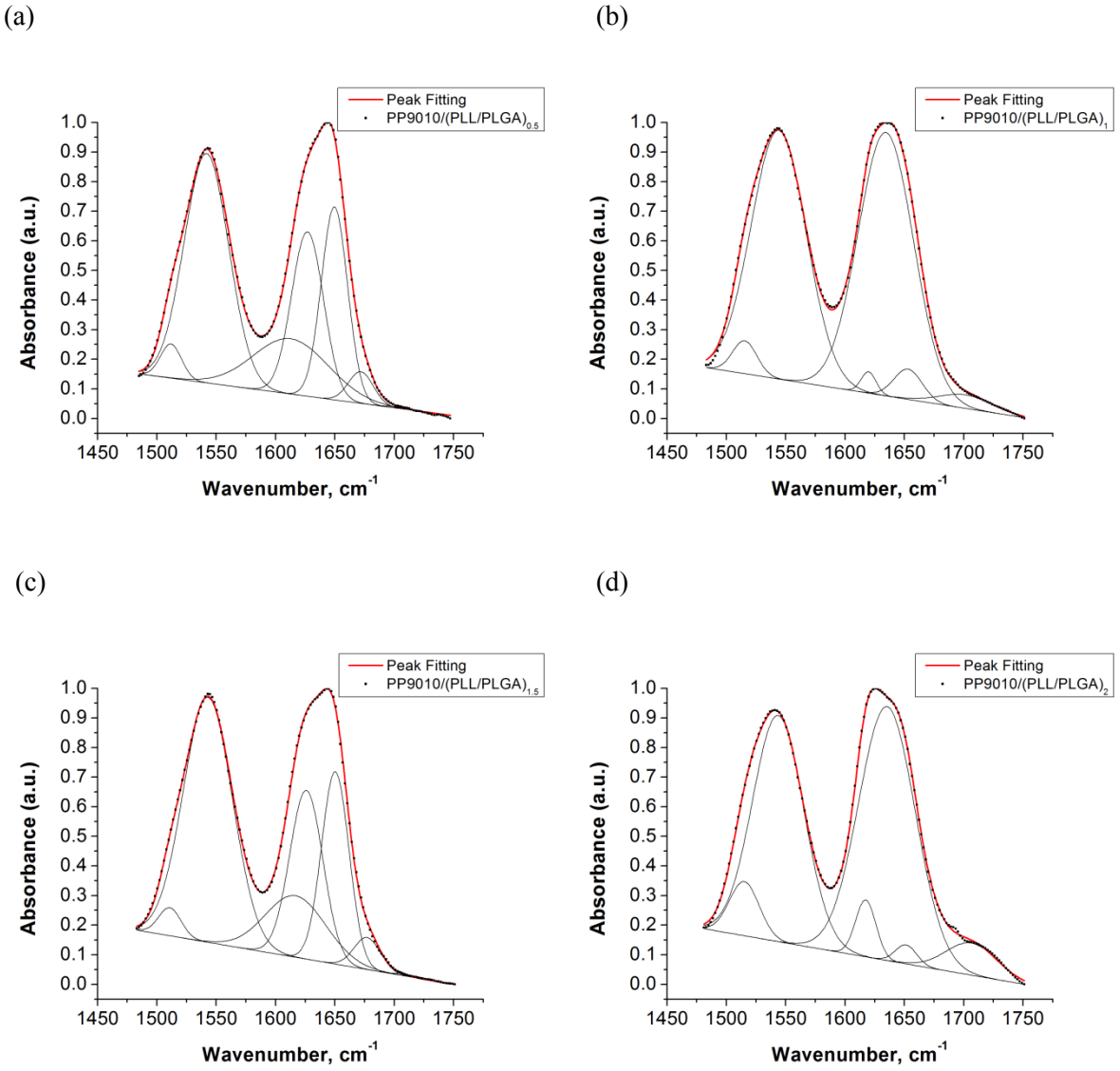


**Figure A10.** The deconvoluted Amide region of the LbL assembled PP9010 microgels ATR FT-IR spectra: (a) PP9010/(PLL/PLGA)$_{0.5}$, (b) PP9010/(PLL/PLGA)$_1$, (c) PP9010/(PLL/PLGA)$_{1.5}$, and (d) PP9010/(PLL/PLGA)$_2$.